Diagnostic and Analysis of Long-term Transient Pressure Data from Permanent Down-hole Gauges (PDG)

Fuyong Wang

Submitted for the degree of Doctor of Philosophy

Heriot-Watt University

Institute of Petroleum Engineering

December 2012

Abstract

Permanent Down-hole Gauge (PDG) is the down-hole measuring device installed during the well completion. It can provide the continuous down-hole transient pressure in real-time. Since 1980s, PDG has been widely applied in oilfields. The wide field applications have demonstrated that the long-term pressure monitoring with PDG is useful for production optimization, reservoir description and model calibration.

Analysing the long-term, noisy and large volume of PDG pressure data and extracting useful reservoir information are very challenging. Although lots of achievement has been made in PDG data processing, such as denoising, outlier removal and transient identification, analysis of long-term transient pressure from PDG is still difficult due to several challenging problems. The first problem is the dynamic changes in reservoir-well properties, which can cause the linearity assumption for pressure-transient analysis invalid, also the reservoir model needs calibration to match the field performance. The second problem is unknown or incomplete flow rate history. These problems together make it a very challenging task for engineer to interpret long-term transient pressure from PDG.

This study investigates novel methods to analyse the long-term transient pressure from PDG with Wavelet Transform (WT). Firstly, a new diagnostic function named as Unit Reservoir System Response A_{urc} has been developed, and it can effectively diagnose the nonlinearities from PDG pressure due to the changes in reservoir-well properties. The nonlinearity diagnostic and evaluation is an important procedure before pressure analysis. Secondly, a model-independent method of reconstructing unknown rate history has been developed. This method has wide applications, considering the effects of skin, wellbore storage, reservoir heterogeneity and multiphase flow. Thirdly, based on the nonlinearity diagnostic result, sliding window technique is proposed to analyse long-term pressure with nonlinearities and update reservoir model with time-dependent reservoir properties.

The synthetic cases and field data application have demonstrated that the developed methods can reveal more useful reservoir information from PDG pressure and realize the potential of PDG as the tool of reservoir management.

Acknowledgement

Firstly, I will give my deepest gratitude to my primary supervisor Prof. Shiyi Zheng for providing me this opportunity to carry out this Ph. D study in Institute of Petroleum Engineering at Heriot-Watt University. The work would not have come into fruition without his constant guidance, advice, and encouragement, and these will be wealthy of my lifetime.

I want to thank my examiners Dr. Arfan Ali and Prof. Yanghua Wang for reading my thesis and giving lots of useful comments and recommendations.

I would also thanks to BG Group, Wintershall AG, EPS Weatherford and PetroChina for their financial support.

I would like to express great appreciations to the staff, secretaries, and librarian who gave me lots of help and support during my study. Many thank my colleagues in PRIME group members and all my friends in Edinburgh. Their support, help and encouragement are gratefully appreciated.

I am especially thankful to my parents and brothers, for their unconditional support and love.

ACADEMIC REGISTRY
Research Thesis Submission

Name*:*	Fuyong Wang		
School/PGI:	Institute of Petroleum Engineering (IPE)		
Version: *(i.e. First, Resubmission, Final)*	Final	Degree Sought (Award **and** Subject area)	Ph. D in Petroleum Engineering

Declaration

In accordance with the appropriate regulations I hereby submit my thesis and I declare that:

1) the thesis embodies the results of my own work and has been composed by myself
2) where appropriate, I have made acknowledgement of the work of others and have made reference to work carried out in collaboration with other persons
3) the thesis is the correct version of the thesis for submission and is the same version as any electronic versions submitted*.
4) my thesis for the award referred to, deposited in the Heriot-Watt University Library, should be made available for loan or photocopying and be available via the Institutional Repository, subject to such conditions as the Librarian may require
5) I understand that as a student of the University I am required to abide by the Regulations of the University and to conform to its discipline.

* *Please note that it is the responsibility of the candidate to ensure that the correct version of the thesis is submitted.*

Signature of Candidate*:*		Date:	

Submission

Submitted By *(name in capitals):*	
Signature of Individual Submitting:	
Date Submitted:	

For Completion in the Student Service Centre (SSC)

Received in the SSC by *(name in capitals):*			
1.1 Method of Submission *(Handed in to SSC; posted through internal/external mail):*			
1.2 E-thesis Submitted (**mandatory for final theses)**			
Signature:		Date:	

Table of contents

Chapter 1 Introduction 1

1.1 Background 1

1.1.1 Permanent Down-hole Gauge (PDG) 1

1.1.2 The applications of PDG in reservoir development 3

1.2 Problem statement 4

1.2.1 Nonlinear problems for pressure-transient analysis 5

1.2.2 Changes in reservoir properties and well conditions 7

1.2.3 Unknown flow rate history 8

1.2.4 Reservoir management with PDG 9

1.3 Research objective 9

1.4 Thesis outline 10

Chapter 2 Wavelet Theory and Literature Review 11

2.1 Introduction 11

2.2 Wavelet theory 11

2.2.1 Wavelet history and application 11

2.2.2 Wavelet Transform (WT) 12

2.2.3 Mother wavelet selection 19

2.2.4 Scale parameter s selection 19

2.3 Literature review of PDG pressure data processing and interpretation 21

2.3.1 Review of PDG pressure data processing 22

2.3.2 Review of PDG pressure data interpretation 26

2.4 Literature review of diagnostic of the change in reservoir properties and well conditions 30

2.5 Literature review of unknown flow rate history reconstruction 32

2.6 Chapter summary 34

Chapter 3 Diagnostic of Nonlinearity from Transient Pressure Data 35

3.1 Introduction 35

3.2 Theory description of the novel nonlinearity diagnostic method 35

3.3 Base case and sensitivity study 38

3.4 Cases study 49

3.4.1 Permeability and skin factor change case 49

3.4.2 Real gas flow 51

3.4.3 Non-Darcy flow 54
3.4.4 Oil and gas two-phase flow after gas out of solution 57
3.4.5 Oil and water two-phase flow after water breakthrough 61
3.4.6 The interference between production wells 67
3.5 Discussion 69
3.5.1 Time interval 69
3.5.2 Radius of investigation 70
3.5.3 Flow rate 71
3.6 New procedures of long-term transient pressure analysis 71
3.7 Chapter conclusions 72
Chapter 4 Reconstructing Unknown Flow Rate History from Transient Pressure Data . 74
4.1 Introduction 74
4.2 Theory description 74
4.3 Flow rate history reconstruction in single oil phase reservoir 76
4.3.1 Base case study 76
4.3.2 Sensitivity study 79
4.4 Flow rate history reconstruction for the case initial flow rate q_1 is unknown . 89
4.4.1 Algorithm development 89
4.4.2 Case study 91
4.5 Flow rate history reconstruction for multi-wells 94
4.5.1 Reconstruction algorithm for multi-wells 94
4.5.2 Case study 95
4.6 Flow rate history reconstruction in oil and water two-phase reservoir 99
4.6.1 Oil and water two-phase flow with constant water cut case 100
4.6.2 Oil and water two-phase reservoir with increasing water cut 105
4.7 Flow rate history reconstruction in gas reservoir and gas condensate reservoir 109
4.7.1 Real gas reservoir 109
4.7.2 Gas condensate reservoir 113
4.7.3 Gas out of solution 114
4.8 Chapter conclusions 117
Chapter 5 Sliding Window Technique for Long-term Transient Pressure Analysis and Reservoir Model Calibration 118
5.1 Introduction 118
5.2 Theory description 119

5.2.1 Deconvolution 119
5.2.2 Sliding window technique 120
5.2.3 Reservoir model calibration with updating Near Wellbore Model (NWM) 123
5.3 Analysis of transient pressure with nonlinearity using sliding window technique and deconvolution 124
5.3.1 Time-dependent skin case 124
5.3.2 Time-dependent permeability-thickness case 128
5.4 Reservoir model calibration with sliding window technique 131
5.4.1 Reservoir model description 131
5.4.2 Nonlinearity diagnostic with wavelet transform 132
5.4.3 Sliding time window selection 134
5.4.4 Pressure-transient analysis for time-dependent parameter interpretation 136
5.4.5 Near Wellbore Model (NWM) selection and update 138
5.5 Chapter conclusions 140
Chapter 6 Field Data Application 141
6.1 Introduction 141
6.2 PDG pressure data processing 142
6.3 Reconstructing rate history from PDG pressure data 144
6.3.1 Window selection 144
6.3.2 Rate calculation with wavelet transform 145
6.4 Diagnostic of time-dependent reservoir-well properties 156
6.4.1 Frequency diagnostic analysis 156
6.4.2 Transitional well test analysis 158
6.5 Chapter conclusions 162
Chapter 7 Conclusions and Recommendations 163
7.1 General conclusions 163
7.2 Recommendations for future work 165
References 166

List of Figures

Figure 1-1: The technical evolution of electronic PDG (Baker et al, 1995) 2

Figure 2-1: Different frequency analysis methods. Wavelet transform is multi-resolution frequency analysis method (Source: Matlab/wavelet toolbox user's guide). 14

Figure 2-2: Different kinds of mother wavelet..... 16

Figure 2-3: Discrete Wavelet Transform (DWT) (source: Matlab/wavelet toolbox user's guide)..... 17

Figure 2-4: Wavelet decomposition tree. The signal is decomposed into several detailed signals D and approximations A..... 17

Figure 2-5: The wavelet decomposition tree of the pressure signal at level 3. 18

Figure 2-6: Signal decomposition and reconstruction with wavelet transform (source: Matlab/wavelet toolbox user's guide)..... 18

Figure 2-7: Transient pressure data is processed with CWT on scale 2 using the Haar, db5, coif5, sym8, Morlet and Meyer wavelet. 19

Figure 2-8: Pressure data is processed by the Haar wavelet using CWT with different scale parameter s. 20

Figure 2-9: The noisy pressure data is processed by the Haar wavelet using CWT with different scale parameters s..... 21

Figure 2-10: Identification of spike outlier and step outlier with wavelet transform 23

Figure 2-11: Noisy pressure data and wavelet transform with the Haar wavelet. 25

Figure 2-12: Denoised pressure data with the removed noise compared with the original pressure data. 25

Figure 2-13: Well PI diagnostic plot for Field Case 3 in Unnrland et al. (1998) paper. 31

Figure 2-14: The "4D" pressure and pressure-derivative diagnostic plot in the paper of Haddad et al. (2004). 32

Figure 3-1: The impulse response of reservoir system $g(t)$in the first 1hour and zoom in. Its value is largest at first but it declines fast with time. 60s after it declines to 2.83%, and 2 minute after, it is 0.8% of the initial value. 37

Figure 3-2: The transient pressure is processed by WT using the Haar wavelet. 39

Figure 3-3: Impact of skin change on A_{urc} function..... 43

Figure 3-4: A_{urc} declines with increasing permeability k 43

Figure 3-5: A_{urc} changes almost linearly with $1/k$ 44

Figure 3-6: A_{urc} changes linearly with the reciprocal of formation thickness h 44

Figure 3-7: A_{urc} changes logarithmically with porosity $\emptyset$..... 45

Figure 3-8: A_{urc} increases linearly with the increasing viscosity μ, and viscosity has big effect on A_{urc} 45

Figure 3-9: A_{urc} increases linearly with the increasing oil FVF B_o 46

Figure 3-10: A_{urc} declines with the increasing total compressibility, but the change is small. 46

Figure 3-11: A_{urc} declines logarithmically with the increasing wellbore size. 47

Figure 3-12: Fluid density has no effect on A_{urc} 47

Figure 3-13: A_{urc} declines with the increasing wellbore storage coefficient Cs 48

Figure 3-14: The impact of different parameters change on URSR A_{urc} 49

Figure 3-15: The reservoir model with time-varying skin factor and permeability.....50

Figure 3-16: Skin factor and permeability change with time during the production history.....51

Figure 3-17: After pressure data is processed by Haar wavelet, URSR A_{urc} is calculated and it is time-varying due to in the changes in skin factor and permeability.51

Figure 3-18: Production history in the gas reservoir case.....53

Figure 3-19: The calculated A_{urc} is time-varying due to the pressure-dependent gas properties.....53

Figure 3-20: URSR A_{urc} increases a lot due to the depletion in the real gas reservoir.54

Figure 3-21: URSR A_{urc} for gas reservoir at different non-Darcy flow conditions. The larger the non-Darcy flow coefficient is, the lager changes in A_{urc} will be. 55

Figure 3-22: The A_{urc} function for the uncompressible fluid flow at different non-Darcy flow conditions. The larger non-Darcy flow coefficient, the lager change in A_{urc} will be. 56

Figure 3-23: Modified isochronal test for gas reservoir.....57

Figure 3-24: URSR A_{urc} of modified isochronal test. 57

Figure 3-25: Production history for the oil reservoir with dissolved gas.....59

Figure 3-26: URSR A_{urc} changes sharply when gas is out solution. 60

Figure 3-27: When wellbore storage is considered, URSR A_{urc} performs differently due to the phase segregation effect in the wellbore. 60

Figure 3-28: The heterogeneous oil and water two-phase reservoir model. 61

Figure 3-29: Down-hole pressure and water cut history.....63

Figure 3-30: URSR A_{urc} increases in the case of water breakthrough and changes with water cut. 63

Figure 3-31: Oil and water saturation function and total mobility. 64

Figure 3-32: URSR A_{urc} and $1/\lambda_t$ for the same water cut f_w 65

Figure 3-33: URSR A_{urc} increases at first but declines later when oil viscosity is 1.2 cp. 66

Figure 3-34: URSR A_{urc} and $1/\lambda_t$ when μ_o=1.2 cp. 66

Figure 3-35: URSR A_{urc} and water cut f_w at the down-hole when μ_o=1.5 cp. 67

Figure 3-36: URSR A_{urc} and $1/\lambda_t$ when μ_o=1.5 cp. 67

Figure 3-37: The reservoir model with two production wells.....68

Figure 3-38: Production history and URSR A_{urc} for two interference wells. 68

Figure 3-39: The URSR A_{urc} is different for the pressure data with different time steps. 69

Figure 3-40: URSR A_{urc} has logarithmic relationship with time step. 70

Figure 3-41: New procedures of long-term transient pressure analysis 72

Figure 4-1: Pressure history in base case. 77

Figure 4-2: Down-hole pressure data in base case is processed with CWT using the Haar wavelet 78

Figure 4-3: The impulse response function $g(t)$ with different wellbore storage coefficient. 81

Figure 4-4: WT detailed signal with different wellbore storage coefficient. 82

Figure 4-5: Zoom-in of WT detailed signal with different wellbore storage coefficient. 82

Figure 4-6: The impulse response function $g(t)$ with different skin factor. 83

Figure 4-7: WT detailed signal with different skin factor. 83

Figure 4-8: Zoom in of WT detailed signal with different skin factor. 84

Figure 4-9: Flow history with flow events happened closely. 85

Figure 4-10: WT detailed signal and zoom in on closely happening flow events 85

Figure 4-11: Artificial noise is added to the pressure data. 88

Figure 4-12: Noisy pressure is processed with wavelet transform. 88

Figure 4-13: The trial-and-error algorithm for flow rate history reconstruction with unknown initial flow rate q_1. 91

Figure 4-14: A heterogeneous oil reservoir model with a single producer. 92

Figure 4-15: The noisy pressure data is processed with WT. 93

Figure 4-16: A heterogeneous reservoir model with two producers. Total production for two wells is measured. 96

Figure 4-17: Down-hole pressure history for two wells. The total production of two wells is measured together. 98

Figure 4-18: The calculated flow rate for two wells is very close to the real flow rate, and the error is less 1%. 99

Figure 4-19: Dispersed flow with uniform saturation and segregated flow (from Xu, W. 2010) 101

Figure 4-20: The segregated flow reservoir model. 102

Figure 4-21: Down-hole flow pressure and water cut history in the segregated flow reservoir 102

Figure 4-22: The pressure of segregated flow is processed with Haar wavelet. 103

Figure 4-23: The reconstructed total liquid flow rate history. 103

Figure 4-24: The real flow rate and reconstructed flow rate history of oil and water. 104

Figure 4-25: Nonlinearity diagnostic result in the segregated flow model. 104

Figure 4-26: Oil and water two-phase reservoir with increasing water cut. 105

Figure 4-27: The reconstructed oil flow rate history in the first window. 106

Figure 4-28: Pressure data in the second window is processed by Haar wavelet. 107

Figure 4-29: The reconstructed total liquid flow rate history. 107

Figure 4-30: The diagnostic result in the second window. URSR A_{urc} is almost constant, and indicates the system can be treated as linear in this time window. 108

Figure 4-31: The reconstructed oil and water flow rate history in the second window. 108

Figure 4-32: Down-hole pressure history from real gas reservoir 110

Figure 4-33: Normalized pseudo-pressure and WT 112

Figure 4-34: The down-hole pressure and GOR history from a gas condensate reservoir. 113

Figure 4-35: The calculated oil and gas rate is near to the real rate. 114

Figure 4-36: Two time windows are selected to reconstruct flow rate history. 115

Figure 4-37: The calculated flow rate for gas and oil phase in the first time window. 115

Figure 4-38: The reconstructed flow rate history in the second time window. 116

Figure 4-39: The reconstructed flow rate history in the second time window when wellbore storage is considered. 116

Figure 5-1: The simulated test data from a heterogeneous closed reservoir model. 119

Figure 5-2: Comparison of pressure derivative from PU1 with the response from deconvolution. 120

Figure 5-3: Sliding window technique. The pressure data is grouped into different windows, and in each window pressure data is interpreted separately. 121

Figure 5-4: Calculated model parameters in different time windows (Athichanagorn 1999). 122

Figure 5-5: The workflow of window selection based on URSR A_{urc} function. 123

Figure 5-6: Model calibration with updating near wellbore model. 124

Figure 5-7: The production and skin factor history in a heterogeneous reservoir. 124

Figure 5-8: Deconvolved response obtained from the whole pressure data in Figure 5-7 with changing skin factor. 125

Figure 5-9: The convolved pressure doesn't match the real pressure. 126

Figure 5-10: Nonlinearity diagnostic and sliding window selection. 126

Figure 5-11: Comparison of the drawdown response derived from the deconvolution of pressure data in two time windows. 127

Figure 5-12: Comparison of convolved pressure calculated from deconvolution with the real pressure data in two time windows. 127

Figure 5-13: Pressure and rate history with changing permeability. 128

Figure 5-14: Deconvolution of the whole pressure data with changing permeability. 129

Figure 5-15: The convolved pressure data doesn't match the pressure data due to changing permeability. 129

Figure 5-16: Nonlinearity diagnostic result and sliding window selection. The nonlinear system is divided into two linear systems. 130

Figure 5-17: Comparison of unit response p_u and p_u derivative in two windows. 130

Figure 5-18: Reservoir model for model calibration case study. 132

Figure 5-19: Production history for three wells. 132

Figure 5-20: WT is applied to process transient pressure data of three wells. 133

Figure 5-21: URSR A_{urc} for three wells. It is constant for PROD2 well, but it is time-dependent for well1 and well3. 133

Figure 5-22: The pressure from simulated model with constant reservoir properties cannot match the real pressure performance. 134

Figure 5-23: The window selection for PROD1 well in URSR A_{urc} function plot 135

Figure 5-24: The window selection for PROD1 well in pressure history 135

Figure 5-25: The window selection for PROD3 well in URSR A_{urc} function plot 136

Figure 5-26: The window selection for PROD3 well in pressure history 136

Figure 5-27: Pressure BU of PROD1 well in the second time window is analysed. ... 137

Figure 5-28: Near wellbore model selection for PROD3 139

Figure 5-29: The pressure performance after NWM update can match the real pressure of PROD1 and PROD3 well 140

Figure 6-1: PDG pressure data and measured daily rate history from an oil reservoir. 141

Figure 6-2: The noisy PDG pressure data in the first 530 hours and zoom-in plot. 143

Figure 6-3: Processed PDG pressure data in the first 530 hours and zoom in plot. 144

Figure 6-4: The pressure data between two build-ups are selected in one window. 145

Figure 6-5: The PDG pressure data in window 3 is processed with WT, and rate history is calculated. 146

Figure 6-6: Wavelet transform processing pressure data and calculated rate history in window 2. 147

Figure 6-7: Calculated rate history in the window 1 from the 0 hour to the 227 hour. 148

Figure 6-8: Calculated rate history from the 970 hour to the 1070 hour. 148

Figure 6-9: Calculated rate history from the 1070 hour to the 1336 hour. 149

Figure 6-10: Calculated rate history from the 1557 hour to the 2375 hour 150

Figure 6-11: Calculated rate history from the 2500 hour to the 3418 hour. 150

Figure 6-12: Calculated rate history from the 3418 hour to the 3619 hour. 151

Figure 6-13: Calculated rate history from the 3925 hour to the 4000 hour. 151

Figure 6-14: Calculated rate history from the 4090.19 hour to the 4385h. 152

Figure 6-15: Calculated rate history from the 4395 hour to the 4995 hour. 152

Figure 6-16: Calculated rate history from the 5015 hour to the 5785 hour. 153

Figure 6-17: Calculated rate history from the 5820 hour to the 6710 hour. 153

Figure 6-18: Calculated rate history from the 6781 hour to the 7163 hour. 154

Figure 6-19: Calculated rate history from the 7180 hour to the 8400 hour. 154

Figure 6-20: Calculated rate history from the 8500 hour to the 9040 hour. 155

Figure 6-21: Calculated rate history from the 9066 hour to the 9400 hour. 155

Figure 6-22: The reconstructed whole rate history from PDG pressure data.....156

Figure 6-23: The diagnostic function A_{urc} changes with time and three time windows are selected for model calibration. 157

Figure 6-24: The reservoir model needs update around 4000 hours, and another calibration may need around 9000 hours. 158

Figure 6-25: Several build-ups are selected to analyse in log-log plot. 159

Figure 6-26: Build-up 1 and 3 are analysed in the log-log plot. 160

Figure 6-27: Build-up 4 and 11 are analysed in the log-log plot. 160

Figure 6-28: Build-up 11 and 16 are analysed in the log-log plot. 161

List of Tables

Table 3-1: Reservoir properties of a simulated reservoir model 37
Table 3-2: Reservoir properties in the single oil phase reservoir 39
Table 3-3: The A_{urc} function in the single oil phase reservoir is almost same. 40
Table 3-4: PVT properties in the real gas reservoir 52
Table 3-5: Some reservoir properties of oil with dissolved gas reservoir 58
Table 3-6: Live oil PVT properties (with dissolved gas) 59
Table 3-7: The distribution of permeability and porosity in the oil and water two-phase reservoir 62
Table 3-8: Other reservoir-well parameters in the model 62
Table 4-1: The reservoir model parameters 77
Table 4-2: Identification of flow event time 78
Table 4-3: The reconstructed flow rate history in the base case 79
Table 4-4: The impulse response function $g(t)$declines with time for different wellbore storage coefficient. 81
Table 4-5: The impulse response function $g(t)$declines with time for different skin factor. 83
Table 4-6: The proportional coefficients b for every flow event. 86
Table 4-7: The errors of calculated flow rate are small 87
Table 4-8: The calculated rate history from the noisy pressure data. 89
Table 4-9: Model parameters in the case study. 92
Table 4-10: The errors of calculated flow rate are nearly less than 5%. 94
Table 4-11: The permeability and porosity for different layer. 97
Table 4-12: The parameters for the two-well reservoir model. 97
Table 4-13: The real gas PVT properties. 111
Table 4-14: The calculated flow rate with gas pressure data. 111
Table 4-15: The flow rate calculation using pseudo-pressure. 112
Table 5-1: The parameters for reservoir model 131
Table 5-2: Pressure-transient analysis result in each time window for PROD1 137
Table 5-3: Pressure-transient analysis result in each time window for PROD3 138
Table 5-4: The size of NWM for PROD3 well calculated from the radius of investigation equation. 139

Nomenclature

A = Amplitude of WT coefficient

A_{urc} = Unit Reservoir System Response (URSR)

b= The proportional coefficient of WT amplitude and change in rate

B = Formation volume factor, rb/STB

B_o = Oil formation volume factor, rb/STB

C = Complementary transform operator

C_g = Gas compressibility, 1/psi

C_f = Rock compressibility, 1/psi

C_o = Oil compressibility, 1/psi

C_s = Wellbore storage coefficient, bbl/psi

C_t = Total compressibility, 1/psi

C_w = Water compressibility, 1/psi

D= Non-Darcy coefficient

$\boldsymbol{D}$= Matrix in curvature measure

Δd= Change in choke size

E= Objective function

e^{ix} = Euler's formula

$f(t)$= Function processed by WT

$\hat{f}(\omega)$= Fourier transform of $f(t)$

f_w = Water cut

$g(t)$= Impulse function of the system, psi/(STB/day)

$g(t)$= Window function in Short-Time Fourier Transform (STFT)

h= Reservoir thickness, ft

i= Imaginary unit

k= Permeability, mD

$\boldsymbol{k}$=Vector of curvature measure

k_{ro} = Oil relative permeability

k_{rw} = Water relative permeability

l= Flow event numbers

m = Well numbers

$m(p)$= Pseudo-pressure, psia^2/cp

$m_n(p)$= Normalized pseudo-pressure, psi

n= Time period of total production measurement

p_0= Initial pressure, psi

p_i= Reference pressure, psi

p_u= Rate-normalized constant-rate pressure response, psi/ (STB/day)

p_{wf} = Bottom-hole flow pressure, psi

$\boldsymbol{p}_m$ = Vector of measured down-hole pressure, psi

Δp_{wf} = Bottom-hole flow pressure change, psi

q= Flow rate, STB/day

$\boldsymbol{q}_m$ = Vector of measured flow rate, STB/day

q_o= Oil flow rate, STB/day

$q_{up\,(t)}$= Normalized constant-pressure rate response, psi/STB

q_w = Water flow rate, STB/day

Δq= Flow rate change STB/day

Q= Accumulative production, STB

r_{inv} = Radius of investigation, ft

r_w = Wellbore radius, ft

R= Reservoir length, ft

s = WT scale factor

S= Skin factor

S' = Rate-dependent skin factor

S_w = Water saturation

t= Time, hours

Δt= Time period, hours

u= WT translation factor

v = Flow velocity

V_w = Wellbore storage volume, cu ft

W= Wavelet transform operator

x= X direction

y=Y direction

$\boldsymbol{y}$= Vector of calculated flow rate, STB/day

z= Z direction

z = Response function defined in deconvolution algorithm

$\boldsymbol{z}$= (Vector of) response coefficients

Z= Real gas deviation factor

Greek letters

β= Non-Darcy flow coefficient

ρ= Fluid density, lb/ cu ft

λ= Relative error weight for curvature

λ_t= Total mobility

ς= Error bounds

τ= Time, integration variable

μ= Viscosity, cp

μ_o= Oil viscosity, cp

μ_w= Water viscosity, cp

υ= Relative error weight for flow rate

$\emptyset$= Porosity

$\emptyset(t)$ = Scale function

$\psi(t)$= Wavelet function

η_j = Hydraulic diffusivity in j direction

σ= Natural logarithm of time

ω= Frequency, hertz

Subscripts

f = Rock

g= Gas

i= Initial, flow event index

j= Flow event index in multi-well algorithm

k= Well index

n= Flow rate index

o= Oil

t= Total

w= Well

Name

BU: pressure Build-up

CWT: Continuous Wavelet Transform

DD: pressure Drawdown

DTS: Distributed Temperature Sensing

DWT: Discrete Wavelet Transform

FFM: Full Field Model

FT: Fourier Transform

FVF: Formation Volume Factor

LGR: Local Grid Refinement

NWM: Near Wellbore Model

PDG: Permanent Down-hole Gauge

PI: Production Index

PTA: Pressure-Transient Analysis

STFT: Short-Time Fourier Transform

URSR: Unit Reservoir System Response

WT: Wavelet Transform

Chapter 1 Introduction

1.1 Background

The demand for oil and gas is increasing with the development of global economy, but petroleum resources are limited. Most conventional reservoirs have been discovered in the last century and many of them have become mature reservoirs. The exploration of new reservoir becomes more difficult. How to produce enough hydrocarbons to satisfy the increasing demand in the future is challenging. Maximizing the ultimate oil and gas recovery is one of the most promising solutions, which requires the reservoir is developed with the optimal development plan. The accurate reservoir model is the key for reservoir development and management, as many complex decisions are made based on the future forecasting from reservoir modelling.

The creation and calibration of reservoir model need lots of accurate reservoir information including geological data, seismic data, well logging and core data, and the dynamic production information. Many measuring tools have been applied in oilfields, and one of them is Permanent Down-hole Gauge (PDG). PDG is the down-hole measuring equipment installed during well completion and provides real-time and continuous pressure, temperature and sometime flow-rate information throughout the lifetime of the well. The real-time and long-term down-hole monitoring is useful for production monitoring and optimization, reservoir description, reservoir model calibration and future forecasting of reservoir and well performance.

1.1.1 Permanent Down-hole Gauge (PDG)

The installation of PDG was traced back to 1960's, when the pressure data acquired from PDG was used for production monitoring during secondary recovery project (Nestlerode, 1963). During the late time of 1970's, PDG began to be installed in subsea wells. The first subsea well with PDG was performed in the Cappos Basin in 1977 (Bezerra et al. 1992), followed by another subsea installations in the Offshore West Africa and North Sea in 1978 and 1979 respectively (Lilley 1988, Hansen 2010). However, the industry-wide application of PDG began in 1980's. The main reason was the poor reliability at the early time of PDG application. Many failures were caused by damaging during the installation or gauge-cable connection problems in later time (Baker et al. 1995). With the newly designed structure (**Figure 1-1**) and improved

down-hole cable, the reliability of PDG had been improved a lot (Frota and Destro, 2006). van Gisbergen and Vandeweijer (2001) evaluated 952 PDGs installed since 1987 and found that 5-year survival probability improved from 40% in the period of 1987-1988 to 75% during the period of 1991-1992. Meanwhile, the fiber-optic sensing has developed a lot recently and provides a reliable alternative to the conventional electronic gauge (Flecker et al. 2000, Kragas et al. 2004, Izgec et al. 2007). Without down-hole electronics, fiber-optic sensing system tends to have higher reliability, especially in the high temperature environment (Omotosho 2004). To Chorneyko (2006), the total number of PDG installations worldwide was in excess of 10,000 according. New technologies have improved the reliability of PDG a lot, and with the valuable information it provides, PDG application has become common worldwide.

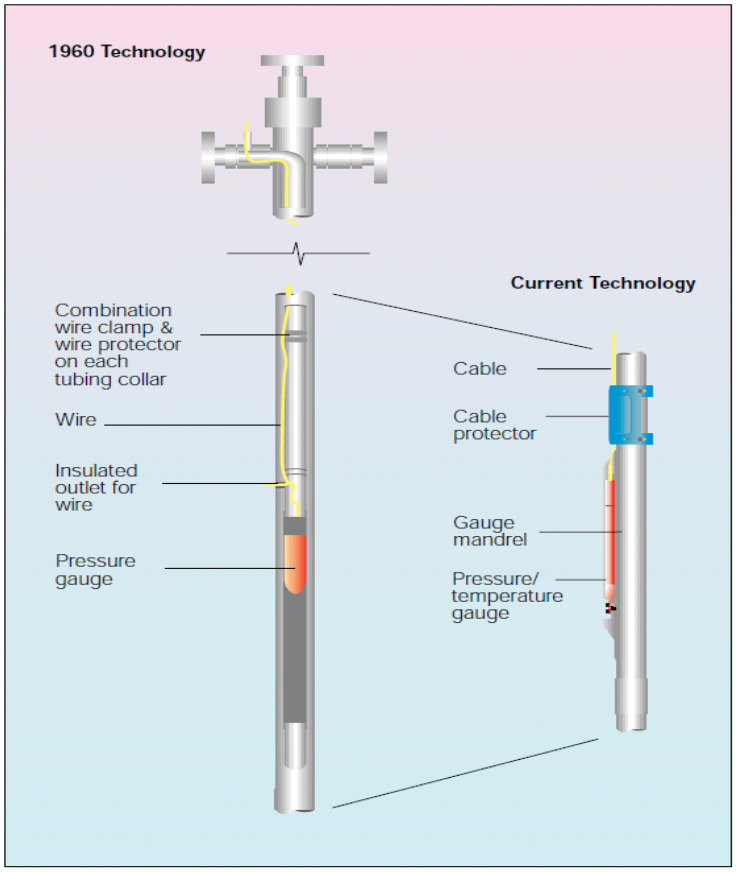

Figure 1-1: The technical evolution of electronic PDG (Baker et al, 1995)

The PDG system is built of several standard components which are carefully chosen to fit reservoir requirements. Usually the electronic PDG system includes pressure gauge, gauge mandrel, cable, connectors, acquisition systems, software and power supply (Baker et al. 1995). For the fiber-optic PDG system, the basic components consist of surface instrumentation, wellhead outlet, in-well cable and connectors, and sensor

assembly (Kragas et al. 2001). Coating technology (Kluth et al. 2000) can protect fiber-optic sensors in high temperature and high pressure environment, and avoid the problem of drifting. The accuracy of pressure measurement for both two kinds of PDG can reach 0.001 psi. By contrast, flow rate measurement is not satisfying compared with the pressure measurement. Although some improvements for down-hole flow rate monitoring have been made recently (Jalali et al. 1998, Tibolad et al. 2000, Kragas et al. 2003, Webster et al. 2006), the real-time flow rate information usually is unavailable due to the high expense and low reliability of rate measurements.

1.1.2 The applications of PDG in reservoir development

High quality data relating to the reservoir is the key to effective reservoir management. Data acquisition is an important procedure in the field development. Traditional data acquisition from short periods of logging and testing usually cause production intervention, which leads to production loss and increases risk. In contract, PDG can provide continuous down-hole production information without production intervention, and has been widely applied in oilfield.

Initially, the pressure data from PDG was mainly used for production monitoring, such as pump pressure observation, surface and subsurface equipment monitoring, and lifting problem identification (Nestlerode, 1963). With the improved reliability and wide applications, PDG has been proven to be cost-effective through providing valuable information for reservoir management. Bezerra et al. (1992) summarized 14 year experience concerning PDG installation in the Campos Basin oilfield, and demonstrated that PDG can increase production and reduce operation cost. Shepherd et al. (1991) discussed the application of PDG for continuous reservoir monitoring and extended well tests in Balmoral Field in UK. Bigno et al. (1997) presented the role of PDG pressure monitoring as the one of main reservoir management tools for Dunbar Field. In 1990s, several case studies discussing the application of PDG in reservoir management from North Sea were reported (Unneland and Haugland 1994, Unneland et al. 1998).

Many applications of PDG have been reported from the industry (Baker et al. 1995, Nyhavn et al. 2000, Queipo et al. 2002, Ouyang and Kikani 2002, Haddad et al. 2004, Chorneyko, 2006). These applications can be classified into three categories: reservoir description, reservoir modelling and production monitoring.

The applications of PDG in reservoir description are shown as below:

1. Estimate reservoir parameters such as permeability, thickness and distance to boundaries/contacts through traditional well test analysis on unscheduled build-ups.
2. Reduce ambiguity and uncertainties in pressure interpretation.
3. Monitor the change in reservoir properties, well conditions and drive mechanism with time.
4. Estimate communications between wells through interference testing.

For the reservoir modelling purpose, PDG can be used to:

1. Reconstruct unknown flow rate history.
2. Provide data for history matching and reservoir model calibration.

For production monitoring purpose, PDG can be used to:

1. Identify well problems quickly.
2. Monitor pump pressure and other equipments.
3. Evaluate the performance of stimulation or well workover jobs.
4. Diagnose formation damage and wax deposition.
5. Determine when production or injection rates in wells can be adjusted.
6. Distinguish and track well and reservoir performance over time.

1.2 Problem statement

Analysing the long-term, noisy and large volume of PDG pressure data and converting the data into useful information and economic value is very challenging. Usually, the pressure is measured at several second intervals lasting for several years, and millions of data consisting of hundreds of flow events are collected. Furthermore, PDG pressure data is collected under an uncontrolled environment, and therefore noise, outliers and other types of errors are always accompanying with pressure data.

Data processing is necessary before interpreting PDG pressure data, including outlier removal, denoising, transient identification, data reduction and etc. Many effective methods and algorithms related to pressure data processing and interpretation have been proposed and applied in practice with good performance. The literature review is provided in Chapter 2.

Although lots of achievements have been made in PDG pressure data processing and interpretation, there are several challenging problems need to be solved.

1.2.1 Nonlinear problems for pressure-transient analysis

The main assumption of well-test analysis is the linearity of the problem, which underlies the principle of superposition in time and space (Houzé, 2009). If the reservoir with production well is treated as a system, flow-rate and down-hole pressure are the system input signal and output signal. The down-hole pressure $p(t)$ due to the time-varying flow-rate $q(t)$ can be described with Duhamel's integral (van Everdingen and Hurst 1949):

$$p(t) = p_0 - \int_0^t q(\tau) g(t-\tau) d\tau \tag{1.1}$$

where p_0 is the initial reservoir pressure; $g(t)$ is the impulse response of the system. It depends on the system parameters and $g(t) = \frac{dp_u}{dt}$, where p_u is the rate-normalized constant-rate pressure response. When calculating p_u with the measured down-hole pressure $p(t)$ and flow-rate $q(t)$, this is pressure-rate deconvolution.

Mathematically, Eq. 1.1 is an expression of superposition principle and theoretically it is only valid in linear systems, which satisfy both of the following properties:

1. Additivity: if both x and y is the solution, $x + y$ is also a solution;
2. Homogeneity: if x is the solution, cx is also the solution and c is the constant.

For the reservoir, if it is a linear system, the pressure diffusivity equation governing fluid flow in porous media should be linear. The diffusivity equation is derived from the continuity equation, Darcy flow equation and the equation of state, and it is a second order partial differential equation:

$$\frac{\partial}{\partial x}\left(\frac{\rho k_x}{\mu}\frac{\partial p}{\partial x}\right) + \frac{\partial}{\partial y}\left(\frac{\rho k_y}{\mu}\frac{\partial p}{\partial y}\right) + \frac{\partial}{\partial z}\left(\frac{\rho k_z}{\mu}\frac{\partial p}{\partial z}\right) = \rho \emptyset C_t \frac{\partial p}{\partial t} \tag{1.2}$$

With the properly defined assumption for the application to the slightly compressible single phase flow, the Eq. 1.2 can be linearized:

$$\eta_x \frac{\partial^2 p}{\partial x^2} + \eta_y \frac{\partial^2 p}{\partial y^2} + \eta_z \frac{\partial^2 p}{\partial z^2} = \frac{\partial p}{\partial t} \tag{1.3}$$

where η_j is the hydraulic diffusivity:

$$\eta_j = \frac{k_j}{\phi \mu C_t}, \quad j = x, y, z \tag{1.4}$$

The linear diffusivity equation of Eq. 1.3 ensures superposition principle is valid. For example, a single phase flow of slightly compressible fluid in porous media with constant reservoir-well parameters is a linear system. In addition, some systems can be pseudo-linear with appropriate parameter transforms. For instance, in the case of single gas reservoir, pseudo-pressure or pseudo-time is used to linearize the nonlinear diffusivity equation (Al-Hussainy et al. 1966, Lee and Holditch 1982, Agarwal 1979, Meunier et al. 1987).

The superposition principle is the fundamental theory of pressure-transient analysis (PTA). Many PTA methods are based on this theory, such as Horner analysis, pressure derivative and deconvolution.

In practice, many reservoir behaviours can make the diffusivity equation nonlinear and superposition principle invalid, such as time-dependent skin and permeability, multiphase flow, non-Darcy flow, variable wellbore storage coefficient and etc.

Levitan (2005) demonstrated that deconvolution failed for the changes of wellbore storage and skin case, and it also was verified by Houzé et al. (2010). Ilk et al. (2010) discussed several scenarios where deconvolution is invalid, such as gas flow, multiphase flow, non-Darcy flow, etc. These nonlinearities usually are caused by the changes in reservoir properties and well conditions. Kuchuk et al. (2005) pointed out that any changes in reservoir model can make deconvolution nonlinear. Without nonlinearity diagnostic, superposition principle and related PTA methods may be erroneously applied and wrong or misleading results will be derived.

However, there are no effective methods for nonlinearity diagnostic (Houzé, 2009). Many methods such as pressure-derivative in log-log plot are based on the superposition function and derived from the linear equations. A novel and effective nonlinearity diagnostic method needs to be developed.

1.2.2 Changes in reservoir properties and well conditions

For the short time traditional well-testing, reservoir properties and well conditions unusually are assumed to be constant, but it is not trustworthy for the long-term PDG pressure data.

In practice, skin and effective permeability may change due to formation compaction, subsidence and fine migration, which are especially common for the unconsolidated depositions (Saputelli, 2010). For instance, Holicek et al. (2008) presented a deepwater field case in the Gulf of Mexico, where there were reduction in permeability-height and increasing skin due to formation damage. Besides, stimulation treatments sometimes are applied to improve the production conditions near the wellbore, such as acidizing and fracturing, and reservoir-well parameters change significantly in a short time. Furthermore, there are high possibilities that flow conditions around/in the wellbore may change, such as the multiphase flow due to water breakthrough and gas out of solution. Multiphase flow is much complex than the single phase flow due to the changes in relative permeability of each fluid phase, and relative permeability is function of saturation, which also changes with time and space. For the real gas reservoir, although pseudo-pressure and pseudo-time transforms can linearize the diffusivity equation, non-Darcy flow near the wellbore and PVT change due to high reservoir depletion are challenging as well.

The changes in reservoir properties and well conditions bring challenges for long-term PDG pressure interpretation. As discussed before, they cause nonlinearities and the PTA methods based on the superposition principle are invalid.

The changes in reservoir parameters and well conditions also cause production problems. For instance, significant Production Index (PI) losses have been observed in deep offshore Gulf of Mexico reservoirs due to compaction near the wellbore, increasing skin, or relative permeability changes due to water production (Saputelli et al. 2010). Early water breakthrough and gas out solution are important events and need attention. Diagnostic of these production events and making remedy responses to them is the key to production optimization.

The changes in reservoir properties and well conditions also bring difficulties for reservoir modelling. Reliable reservoir model can enable reservoir engineers understanding the past performance of oilfields, and make future forecasting and

provide guidelines for planning new wells. Field studies illustrated that the analytical models traditionally used for conventional well test interpretation may be too simple for PDG data analysis (de Oliveira Silva and Kato 2004, Horne 2007), and the variation of reservoir properties and well conditions make the constant-property modelling cannot match the long-term pressure history. Therefore, the reservoir model should be calibrated continuously with the new reservoir-well parameters to match the real field performance.

1.2.3 Unknown flow rate history

Production rate information is important for reservoir surveillance and management. For instance, production rate is the key for pressure-transient analysis to obtain reservoir and well parameters. Haddad et al. (2004) pointed out that flow rate is critical for the recognition of time-dependent as well as rate-dependent parameters, such as time-dependent skin and rate-dependent skin. Besides, history-matching rate and volume data is essential for the development of reliable reservoir model, based on which lots of investment decisions can be made (McCracken and Chorneyko 2006, Ibrahim 2008). Furthermore, inaccurate volume information can lead to financial consequences between different owners and tax regimes (Cramer et al. 2011).

However, flow rate metering is not satisfying in practice. Although many measurements have been developed and applied to collect flow rate data, such as production-logging tools, surface and down-hole flow meters, and flow rate metering is less-satisfying compared with pressure and temperature measurement. Production logs intervenes normal productions, and only provides flow information as a function of depth instead of time. Surface multiphase flow meters may have problems when GOR is high, and also are limited by the space and expense. Although permanent down-hole multiphase flow meters have been developed a lot in the recent years, the applications are not popular due to the high expense and low reliability. Also accessibilities for maintenance are difficult as it is equipped at the down-hole.

The common practice is several wells are measured together through manifolds, and daily, monthly rates or total cumulative production is measured with surface separation equipments. The flow rate details for each individual well are unavailable. Rate allocation is utilized to assign flow rate for each well from total production, based on the separation test on the surface. The test frequency varies differently for different

wells, from weekly to monthly. For the well with rapidly changing conditions, test with weekly intervals is necessary. However, as many producers sharing one gathering and separation equipments, the high test frequency for each well is not possible. Generally, the allocation result is not very satisfying, due to the variable flow conditions and low test frequency (Bergren 1997, Udofia et al. 2012).

1.2.4 Reservoir management with PDG

The real-time down-hole information recorded by PDG has the substantial potential to benefit reservoir management through production monitoring and optimization. Unfortunately, lots of valuable information is left in the real-time PDG pressure data without discovery in time, such as down-hole equipment failure, early time water breakthrough and gas out of solution. Diagnosing this information and make remedy response is the key to real-time reservoir management.

1.3 Research objective

It has been noted that the long-term PDG transient pressure data analysis is not satisfying to provide enough valuable information for reservoir management. In summary, the research objective of this study is realizing the potential of PDG as the tool of reservoir management through developing new algorithms for PDG pressure processing and analysis. To achieve this objective, the following works need performed:

1. Developing a novel method of diagnosing nonlinearities from pressure data to correctly apply PTA methods which are based on the linearity assumption.
2. Analysing long-term pressure data with nonlinearities;
3. Diagnosing production problems and events for production monitoring and optimization.
4. Reconstructing unknown rate history from pressure data in the single phase and multi-phase reservoir, considering the effect of wellbore storage, skin factor, reservoir heterogeneity and well interference.
5. Diagnosing the changes in reservoir properties and well conditions and updating reservoir model continuously using time-dependent reservoir-well parameters derived from PDG pressure data.

1.4 Thesis Outline

The thesis is organized as follows:

Chapter 2 discusses the theory and application of wavelet transform. The literatures related to the study in this thesis are reviewed, including the PDG pressure data processing and analysis, diagnostic of the changes in reservoir-well properties and methods of reconstructing unknown flow rate history.

Chapter 3 presents a novel method for nonlinearity diagnostic. Different kinds of nonlinearities due to the changes in reservoir properties and well conditions are diagnosed from the transient pressure data with the wavelet transform.

Chapter 4 proposes the method of reconstructing flow rate history from the transient pressure data using wavelet transform. The effects of skin, wellbore storage, data noise, reservoir heterogeneity, well interference, compressible gas flow and multiphase flow are researched.

Chapter 5 illustrates the sliding window technique for long-term transient pressure data analysis and reservoir model calibration. The time-dependent reservoir-well parameters are diagnosed and analysed, and used for update near wellbore model.

Chapter 6 uses the field PDG pressure data to valid the developed algorithms in this thesis, including (1) reconstructing flow rate history from the PDG pressure data and daily rate; (2) diagnosing time-dependent reservoir-well parameters for model calibration with sliding window technique .

Chapter 7 concludes major results in the thesis and gives suggestions for the future work based on the current experience.

Chapter 2 Wavelet Theory and Literature Review

2.1 Introduction

In this chapter, the theory of wavelet transform is introduced and literatures related to the study in this thesis are reviewed.

Section 2.2 briefly introduces the theory of wavelet transform. Wavelet transform is a multi-resolution frequency analysis method, and has been widely applied in petroleum industry. The study carried out in this thesis is based on wavelet transform. The selection of mother wavelet and scale parameter s is researched. Section 2.3 gives the literature review related to PDG pressure data processing and interpretation. Section 2.4 presents the review of the methods of diagnosing the changes in reservoir properties and well conditions. The methods of reconstructing unknown flow rate history are reviewed in section 2.5.

2.2 Wavelet theory

2.2.1 Wavelet history and application

Although the first literature related to wavelet was as early as 1910 when Haar wavelet was proposed, the wide development and application of wavelet started in 1980s from seismic signal processing area by Morlet (1982). Grossman and Morlet invented the term wavelet in 1984, and the concept of multi-resolution was proposed in 1988 by Mallat and Meyer. The relationship between quadrature mirror filters and orthogonal wavelet bases was discovered and multi-resolution analysis method provided a powerful tool in digital signal processing. In the same year, Daubechies developed a series of compact support orthogonal wavelet functions. Since then, wavelet transform has been widely applied in many disciplines of science and engineering (Daubechies 1988, Mallat 1989, Mallat 1998).

Guan et al. (2004) provides a review of wavelet application in petroleum industry, such as reservoir model characterization, geological model upscaling, data denoising and solving partial differential equations.

Panda et al. (1996) applied wavelet transform to upscale heterogeneous permeability remove white noise and identify local discontinuities. Jansen and Kelkar (1998) used

wavelet analysis to upscale fine geological models, and the accuracy and computational efficiency are improved. Lu and Horne (2000), Sahni and Horne (2005) also demonstrated multi-resolution wavelet analysis is effective in reservoir characterization, such as estimating reservoir parameters and their distribution. Soliman et al. (2003) applied Daubechies wavelet to analyse transient pressure data to determine wellbore anomalies, boundary effects and etc. Moridis et al (1996) used wavelet to solve the nonlinear partial differential equation of the oil and water two-phase flow.

The first application of wavelet analysis in PDG pressure data processing was proposed by Kikani and He (1998) and Athichanagorn et al. (1999). They found that wavelet is effective in processing PDG pressure data, outlier removal, deniosing, transient identification and etc. Since then dozens of paper have been published, and the performance of wavelet in PDG pressure data processing and analysis has been improved a lot (Ouyang et al. 2002, Viberti et al. 2007, Zheng et al. 2007, Ribeiro et al. 2008).

2.2.2 Wavelet Transform (WT)

A large amount of information carried by a signal may be hidden in time-domain, but it can be revealed in frequency-domain with a mathematical transform. The most popular frequency analysis method is Fourier Transform (FT). A signal is considered to be constructed by a superposition of sine and cosine waves with different frequencies in FT:

$$f(t) = \frac{1}{\sqrt{2\pi}} \int_{-\infty}^{\infty} \hat{f}\,(\omega) e^{-i\omega t}\, d\omega \qquad (2.1)$$

where $\hat{f}(\omega)$ is Fourier coefficients, representing the spectral component of $f(t)$ at the certain frequency:

$$\hat{f}(\omega) = \frac{1}{\sqrt{2\pi}} \int_{-\infty}^{\infty} f\,(t) e^{-i\omega t}\, dt \qquad (2.2)$$

The disadvantage is that FT loses the time information of certain frequency content, and only gives the average information on the signal as the whole. Therefore, FT has disadvantage for analysing non-stationary signal, as the frequency contents change over time.

To overcome this deficiency, Short-Time Fourier Transform (STFT) is proposed (Gabor 1946):

$$STFT\{f(t)\}(\omega,\tau) = \int_{-\infty}^{\infty} f(t)g(t-\tau)e^{-i\omega t}\,dt \quad (2.3)$$

where $g(t)$ is the window function, which ensures STFT can provide some information about both when and at what frequency a signal event happens. The drawback is the window size is fixed and the same window is used for the analysis of the whole signal. In fact, flexible window sizes are recommended to analyse non-stationary signal, i.e. the large window for low frequency information and small window for high frequency information.

Wavelet transform is a multi-resolution frequency analysis method, and can utilize different window size to analyse the signal with variable frequency contents, i.e. long-time window analysing low-frequency information and short-time window analysing high-frequency information. **Figure 2-1** depicts the comparison of FT, STFT and WT three different kinds of frequency analysis method. Wavelet transform is the most suitable frequency analysis method for analysing non-stationary signal, such as long-term transient pressure data from PDG.

Wavelet $\psi(t)$ refers to the oscillatory function like a wave and has an average value of zero:

$$\int_{-\infty}^{\infty} \psi(t) = 0 \quad (2.4)$$

where $\psi(t)$ is the mother wavelet function, and is shifted by translation parameter u and dilated by scale parameter s:

$$\psi_{u,s} = \frac{1}{\sqrt{s}}\int_{-\infty}^{\infty} \psi(\frac{t-u}{s})\,dt, \text{ while } s > 0 \quad (2.5)$$

The wavelet transform of signal $f(t)$ at scale s and position u is computed by correlating signal $f(t)$ with wavelet $\psi_{u,s}$:

$$Wf(u,s) = \int_{-\infty}^{+\infty} f(t)\frac{1}{\sqrt{s}}\psi\left(\frac{t-u}{s}\right)dt \quad (2.6)$$

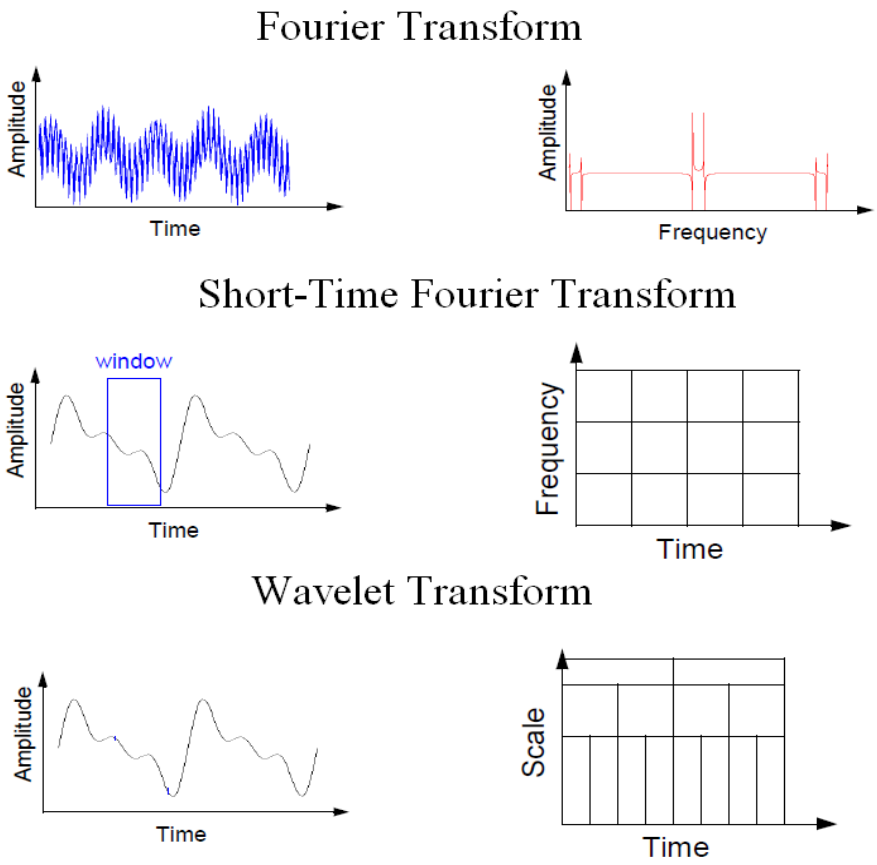

Figure 2-1: Different frequency analysis methods. Wavelet transform is multi-resolution frequency analysis method (Source: Matlab/wavelet toolbox user's guide).

When a small scale parameter s is selected, high frequency information of signal can be analysed, which also gives the detailed information of the signal. For the large scale parameter s, low frequency information and coarse approximation of signal can be analyzed. With this multi-resolution character, wavelet transform is more efficient to analyse non-stationary signals.

The WT coefficients $Wf(u,s)$ contain information on the difference between two approximations of signal $f(t)$ on two successive scales. The approximation of signal $f(t)$ can be calculated from the complementary transform:

$$Cf(u,s) = \int_{-\infty}^{+\infty} f(t) \frac{1}{\sqrt{s}} \emptyset\left(\frac{t-u}{s}\right) dt \qquad (2.7)$$

where $\emptyset(t)$ is scale function, and it is orthogonal to $\psi(t)$:

$$\int_{-\infty}^{\infty} \emptyset(t) = 1 \qquad (2.8)$$

Wavelet function $\psi(t)$ defines a high-pass filter and scale function $\emptyset(t)$ defines a low-pass filter. The original signal $f(t)$ is decomposed into two components: the details $Wf(u,s)$ derived from wavelet transform and the approximation $Cf(u,s)$ calculated from complementary transform.

There are dozens of types of mother wavelet. Haar wavelet is the simplest and most widely applied one. It is discontinuous and the most compactly supported wavelet of all the orthogonal family of wavelets. The definition of Haar wavelet is:

$$\psi(t) = \begin{cases} 1, & 0 \le t < \frac{1}{2} \\ -1 & \frac{1}{2} \le t < 1 \\ 0, & otherwise \end{cases} \tag{2.9}$$

Its scale function is:

$$\emptyset(t) = \begin{cases} 1, & 0 \le t < 1 \\ 0, & otherwise \end{cases} \tag{2.10}$$

Many other groups of wavelets are also widely applied, as shown in **Figure 2-2**, including:

- Daubechies family of wavelets
- Meyer wavelet
- Morlet wavelet
- Mexican hat wavelet
- Coiflet family of wavelets
- Symlet family of wavelets

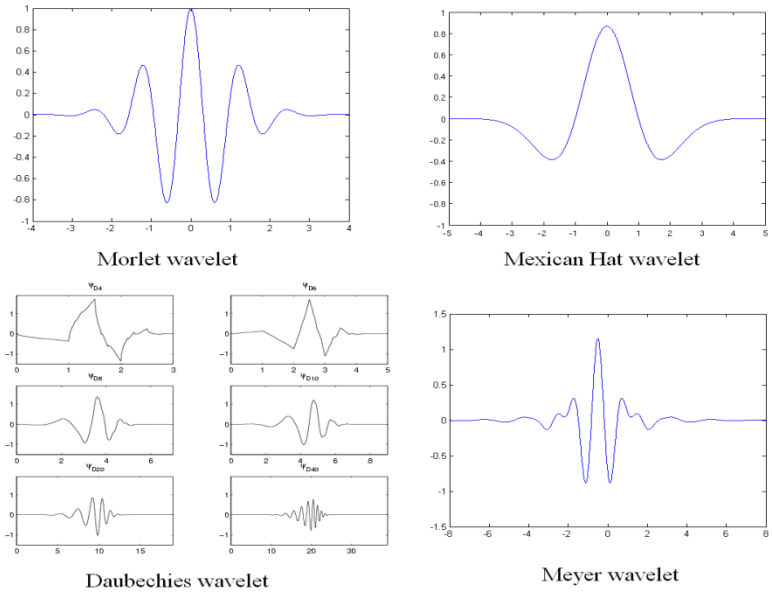

Figure 2-2: Different kinds of mother wavelet.

There are two kinds of wavelet transform: Continuous Wavelet Transform (CWT) and Discrete Wavelet Transform (DWT).

CWT is continuously changing scale parameter s and translation parameter u to perform WT at very scale and very location of the signal $f(t)$. Lots of information is obtained but too much space is occupied. To overcome this drawback, CWT can perform on some suitable scale parameter s instead of all the scale parameters. By selecting different scale factors s, the detailed information on different levels can be obtained.

DWT performs wavelet transform on partial scale and position. Dyadic wavelet transform, which chooses the scale and position based on powers of two, can make the amount of work smaller. The most efficient way to process DWT is Mallat algorithm. In fact, it is two-channel sub-band coder in signal processing. **Figure 2-3** shows with DWT the signal is decomposed into two parts. The first part is the detailed signal, which includes the high frequency information. The second part is the approximation signal, which contains low frequency information of the signal. During this procedure, the data number reduces to the half due to down-sampling.

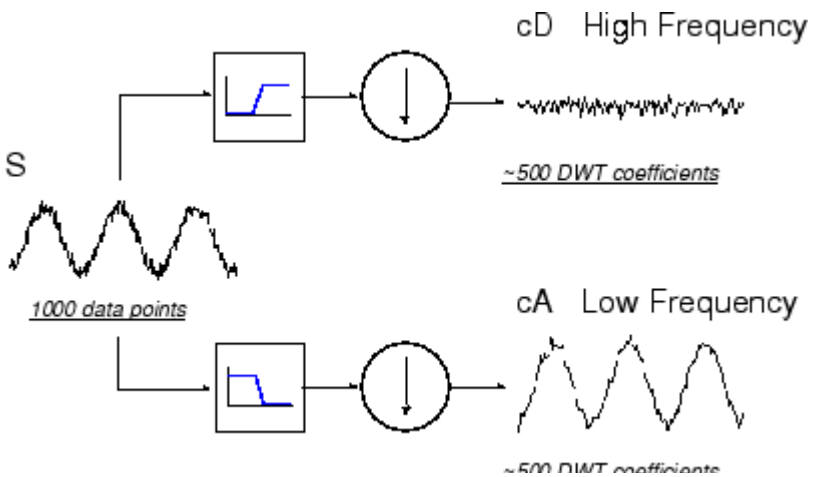

Figure 2-3: Discrete Wavelet Transform (DWT) (source: Matlab/wavelet toolbox user's guide)

Iterate the decomposition process by decomposing the approximation signal, and the signal is divided into many lower-resolution components. This is called wavelet decomposition tree, as shown in **Figure 2-4**. **Figure 2-5** presents the wavelet decomposition tree of the pressure signal at level 3, including the detail signal D1 at level 1, detail signal D2 at level 2, detail signal D3 and approximation A3 at level 3. The data number is reduced due to down-sampling.

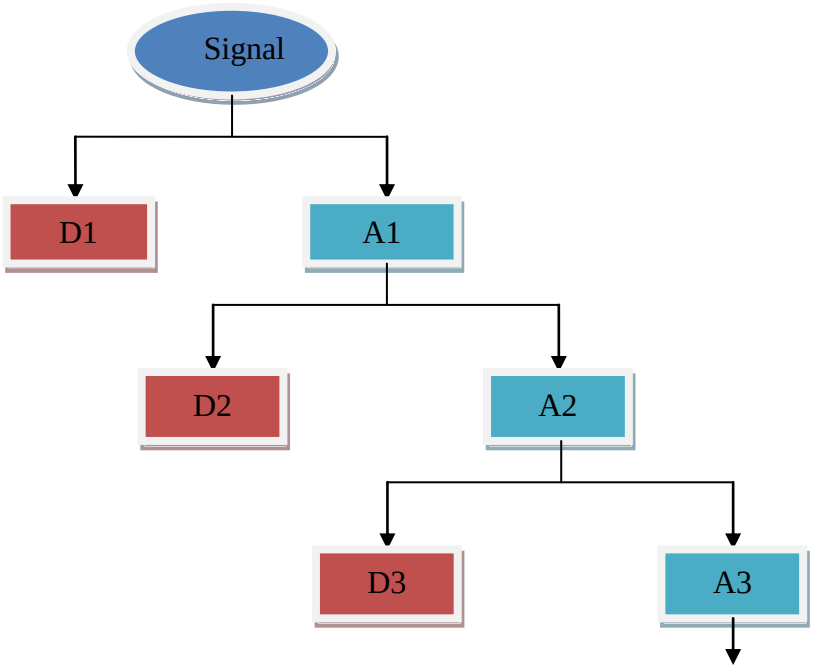

Figure 2-4: Wavelet decomposition tree. The signal is decomposed into several detailed signals D and approximations A.

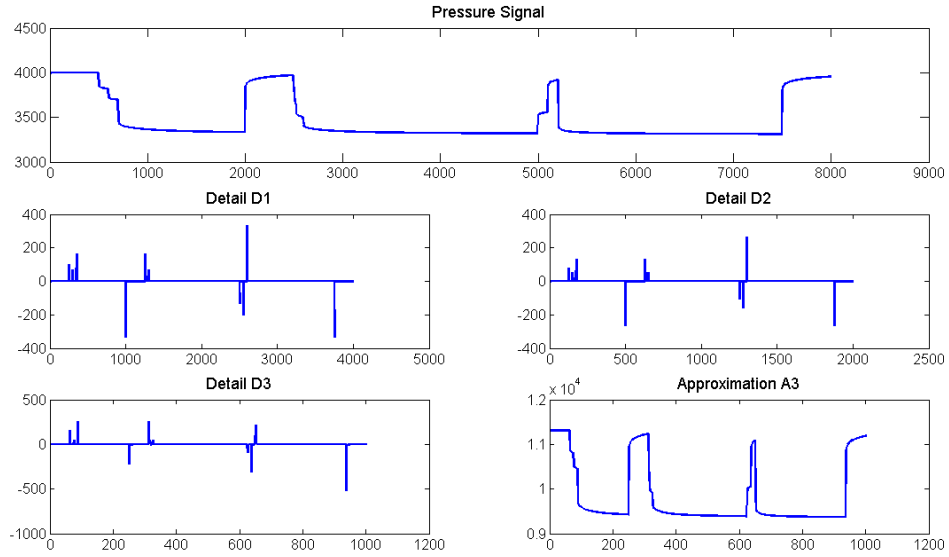

Figure 2-5: The wavelet decomposition tree of the pressure signal at level 3.

Figure 2-6 shows the signal decomposition and reconstruction process with wavelet. This can be used for signal filtering, such as data denoising. It includes three procedures, signal decomposition with DWT, redefining wavelet coefficients and signal reconstruction. Initially, signal is decomposed to several detailed signals and approximations. Then some wavelet coefficients are modified to denoise. The value of wavelet coefficients $Wf(u,s)$ is above the threshold is kept and otherwise it is redefined. Finally, the signal is reconstructed from the modified wavelet coefficients.

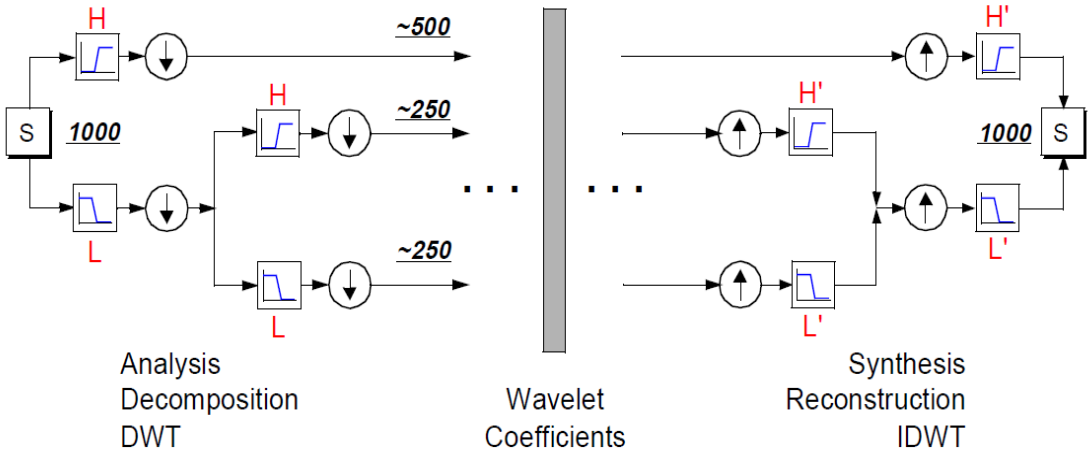

Figure 2-6: Signal decomposition and reconstruction with wavelet transform (source: Matlab/wavelet toolbox user's guide)

2.2.3 Mother wavelet selection

As discussed before, there are dozens of mother wavelets. **Figure 2-7** shows six different kinds of mother wavelet is used to processing transient pressure data, including Haar, Daubechies 5, coif5, sym8, Morlet, and Meyer wavelet. All wavelets are sensitive to the flow event in pressure data due to the change in flow rate. There are amplitudes of WT coefficients for the time of flow events in pressure. For the Haar wavelet, only one direction of amplitudes of WT coefficients appears. That is positive amplitudes for pressure DD and negative amplitudes for pressure BU. Pressure BU and DD can be identified and distinguished with Haar wavelet. But for other kinds of wavelets, when there are flow events double directions of WT amplitude will appear. Besides, the resolution of flow event identification is lower than Haar wavelet, especially when flow events happen closely. The reason is that Haar wavelet is the most compactly supported wavelet and also it is discontinuous, which is good for transient identification.

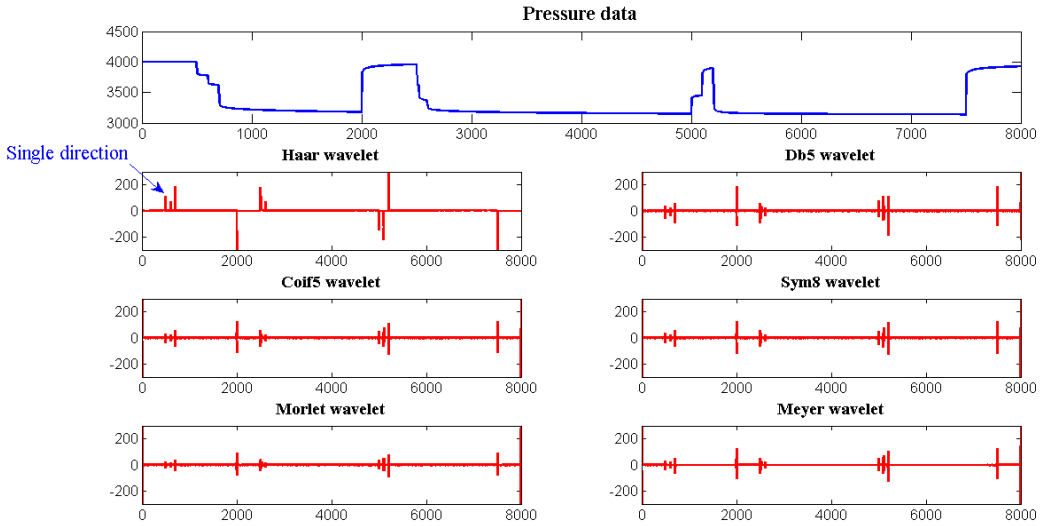

Figure 2-7: Transient pressure data is processed with CWT on scale 2 using the Haar, db5, coif5, sym8, Morlet and Meyer wavelet.

2.2.4 Scale parameter *s* selection

CWT performing on selected scale parameter *s* is used in this study. Selecting the most suitable scale parameter *s* is a problem. There are two factors that need to be considered: identification resolution and pressure data noise.

Identification resolution

When selecting the small scale parameter s, high frequency information for the pressure data can be analysed. This is very useful for transient identification, as flow events are the high frequency information in pressure data. When large scale parameters s are used, the approximate information of pressure data can be analysed.

Figure 2-8 shows a part of transient pressure data is processed by the Haar wavelet with CWT with different scale parameters s. There are three flow events from the time 2.5 day to 2.52 day, which is nearly 30 minutes. When the scale 2 is selected to process CWT, three amplitudes appear in the WT coefficients plot at the same time when flow events happen. Therefore, flow events can be identified from the WT coefficients plot. When scale parameter $s = 8$, time resolution becomes lower, but there are still three amplitudes representing three flow events. When scale parameter $s = 16$, only two amplitudes are left. The small flow event in the middle is merged by the two bigger flow events beside. That means the small flow event is missed when using scale parameter $s = 16$ to identify flow events. When $s = 32$, only the biggest flow event can be identified and two smaller flow events are missed for identification. In this regard, it is better to choose a smaller scale parameter s to identify all flow events.

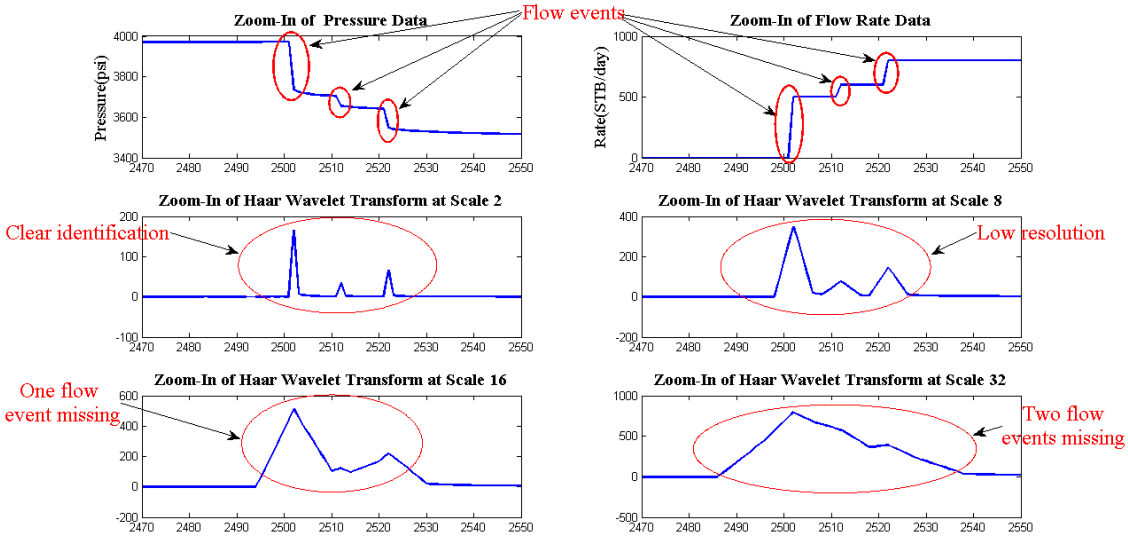

Figure 2-8: Pressure data is processed by the Haar wavelet using CWT with different scale parameter s.

Noise influence

Noise is a group of data scattering around the true signal, and it is very common in PDG pressure data. It can affect flow event identification, because it also is the high

frequency information. **Figure 2-9** shows the noisy pressure data is processed with CWT with different scale parameter s. It is difficult to distinguish flow events from the noise on the WT coefficients plot when a small scale parameter s is used. For the larger scale parameter s, the difference between flow events and noise becomes clear and can be distinguished.

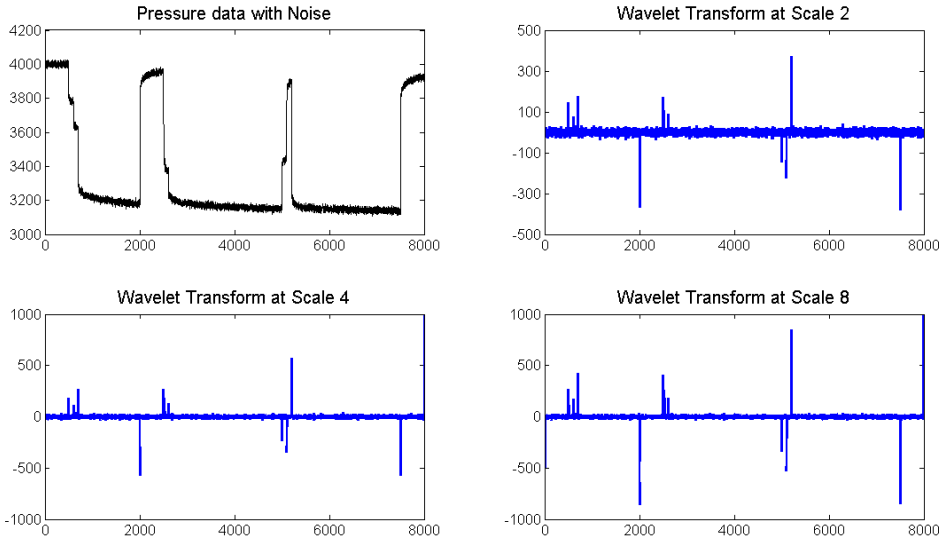

Figure 2-9: The noisy pressure data is processed by the Haar wavelet using CWT with different scale parameters s.

From the noise point of view, it is better to select a larger scale factor to avoid the noise effect. However, as discussed before, a large scale factor may miss small flow events. To reduce the uncertainties, the pressure data with noise is recommended to be processed at first, including denoising, outlier removal and etc. Then the clean pressure data can be processed with CWT with small scale parameters s to identify all the flow events. The methods of pressure data processing are reviewed in section 2.3.

2.3 Literature review of PDG pressure data processing and interpretation

Several workflows for long-term PDG pressure data processing and interpretation have been proposed. Athichanagorn et al. (1999) presented the seven-step procedure to analyse the long-term data, including outlier removal, denoising, transient identification, data reduction, flow-history reconstruction, behavioural filtering and moving window analysis. Wavelet-based algorithm was applied in the initial four steps for data processing with good performance. Nonlinear regression and moving window method

were used for reconstructing unknown flow history and calculating the reservoir parameters which change with time.

Olsen and Nordtvedt (2005a, 2005b, and 2006) proposed two-module procedure involving an automated filter and an automated regression well test module. The first module consisted of several elements including outlier removal, denoising, compression, transient detection, slug detection and continuous noise estimation. The well test module used regression analysis to calculate reservoir parameters with defined confidence interval.

Li (2009) improved the workflow based on the two workflows illustrated above. New workflow for PDG data processing was proposed, including data pre-processing, outlier removal, flow event detection, identification of BU and DD, denoising, data reduction and identifying abnormal events. After data processing, short transients were analysed with conventional well test methods and long-term transients were analysed with numerical well testing for reservoir model calibration. Meanwhile, deconvolution was applied to extend flow event time but before that the identification of nonlinearity for the complex reservoir system was necessary.

2.3.1 Review of PDG pressure data processing

Data processing aims to improve the data quality for better pressure data interpretation. Generally it consists of data pre-processing, outlier removal, transient identification, denoising and data reduction. Each element is briefly reviewed as follows.

Data pre-processing

This procedure was introduced by Li (2009), includes removing the negative values and repetitive values, converting time and pressure format, shifting datum and etc. Data interpolation may be needed to ensure the dataset has equal time intervals, which is required by wavelet algorithm. However, outliers may be introduced during the data interpolation (Athichanagorn, 1999).

Outlier removal

As PDG pressure data is collected in the uncontrolled environment, large disturbances at the down-hole and temporary sensor/transmitter failure can cause outliers. There are two types of outliers: spike outlier and step outlier (Khong, 2001). The spike outlier is

one or two data are away from the trend of data, and the step outlier is a group of data are away from the true value, such as some zero or large negative or positive numbers due to the failure of pressure gauges. Wavelet-based method (Athichanagorn et al. 1999, Ribeiro et al. 2008) can identify spike outliers in detail signal after wavelet decomposition.

As shown in **Figure 2-10**, the spike outlier in pressure data causes two consecutive singularities. In the detailed wavelet signal, spike outliers can be identified by two large WT coefficients with two opposite directions. However, this method fails to remove step outliers and manual removal was suggested by Khong (2001). Olsen and Nordtvedt (2005a) showed that the median filter with accurate noise estimation to remove spike outliers is more efficient than a purely wavelet based method.

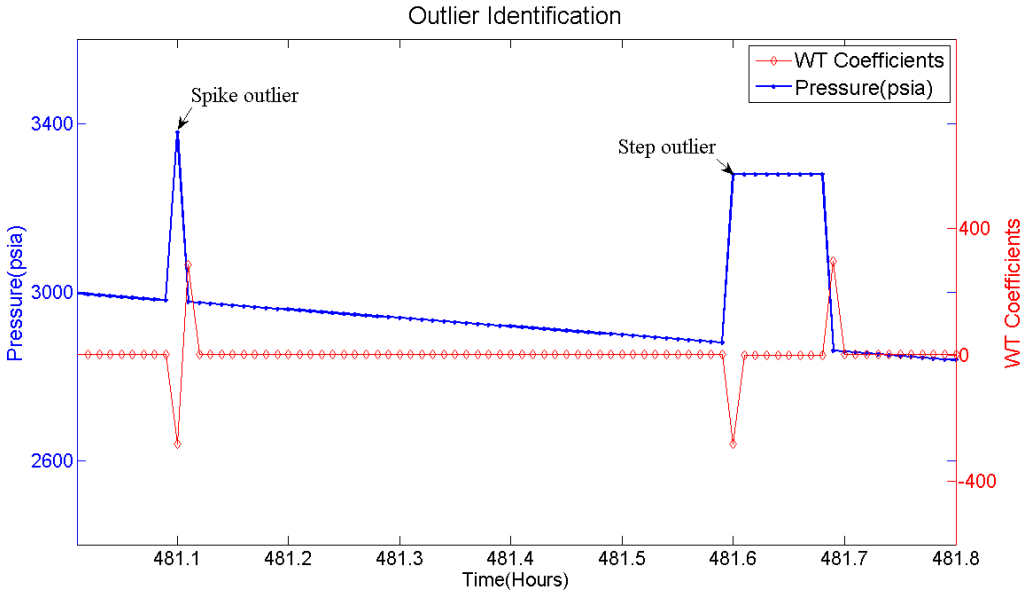

Figure 2-10: Identification of spike outlier and step outlier with wavelet transform.

Transient identification

PDG pressure history consists of hundreds of transient events. Identification of the exact beginning time of transient event is critical for transient pressure interpretation. Wavelet modulus maxima method was initially proposed by Kikani and He (1998), and it was improved by Athichanagorn et al. (1999). However, wavelet modulus maxima method does not always provides satisfactory result. Depending on the threshold, some break points may be missed and false break points may be detected. Rai and Horne (2007) illustrated that the wavelet algorithm had some limitations in transient identification, and they presented two non-wavelet approaches: the Savitzky-Golay (S-

G) polynomial smoothing filter algorithm and a novel pattern recognition approach called the Segmentation Method. Thomas (2002) and Olsen and Nordtvedt (2005a) applied pattern recognition for transient detection. Ouyang and Kiknai (2002) and Ribeiro et al. (2008) utilized the pressure slop approach for automatic transient detection, but the transient threshold value need to be set and adjusted by users with a trail-and-error procedure. Suzuki and Chorneyko (2009) proposed the filter convolution method to automatically detect pressure BU intervals from PDG pressure data.

Data denoising

Denoising is reducing the fluctuations and scatterings to extract the main feature of the data. Wavelet thresholding method is the most effective approach. After wavelet decomposition, small fluctuation in detail signal caused by noise is suppressed, and denoised data can be reconstructed with smoother sub-signals. Haar wavelet combined with soft-thresholding was recommended by Kikani and He (1998). Athichanagorn et al. (1999) proposed a hybrid threshold method. For this method, the soft thresholding criterion is used in continuous data, and the hard thresholding criterion is applied to the vicinity of discontinuities.

Noise level estimation is crucial for denoising. Khong (2001) estimated the noise level with least square error straight line fit, however the assumption that pressure varies linearly with time is not valid for most of the time according to Ouyang and Kiknai (2002), so they improved this algorithm using the polytope nonlinear regression approach. Olsen and Nordtvedt (2005a), Ribeiro et al. (2008) and Ortiz et al. (2009) used the Median Absolute Deviation (MAD) to estimate the noise level, and the median is taken over the details at the first wavelet decomposition.

A simple denoising case using wavelet decomposition and reconstruction theory is presented to illustrate the workflow. **Figure 2-11** presents a part of pressure data with noise and the detailed signal of wavelet transform with Haar wavelet. Noise and flow events are the high frequency information of the pressure signal, but the difference between noise and flow events is the value of WT coefficients. The WT coefficients of noise are small and are round zero, and WT coefficients of flow events are large. Noise threshold can be set to separate the noise and flow events. The WT coefficients due to noise which are small than the threshold will be redefined to be zero and WT coefficients due to flow events which are large than the threshold is kept:

$$\begin{cases} |Wf(t)| > THR, & Wf'(t) = Wf(t) \\ |Wf(t)| \leq THR, & Wf'(t) = 0 \end{cases} \tag{2.11}$$

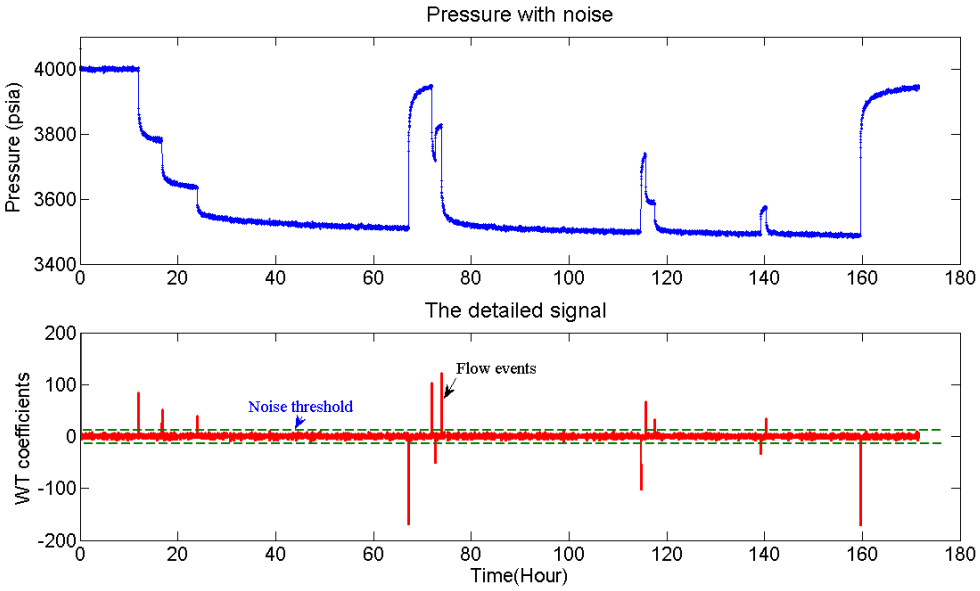

Figure 2-11: Noisy pressure data and wavelet transform with the Haar wavelet.

The redefined WT coefficients $Wf'(t)$ instead of original WT coefficients $Wf(t)$ are used for signal reconstruction. In this way, noises are removed from the original signal. **Figure 2-12** presents the denoised pressure data and the removed noise compared with the original pressure data. The denoised pressure data is smooth and clean, and is better for pressure-transient analysis.

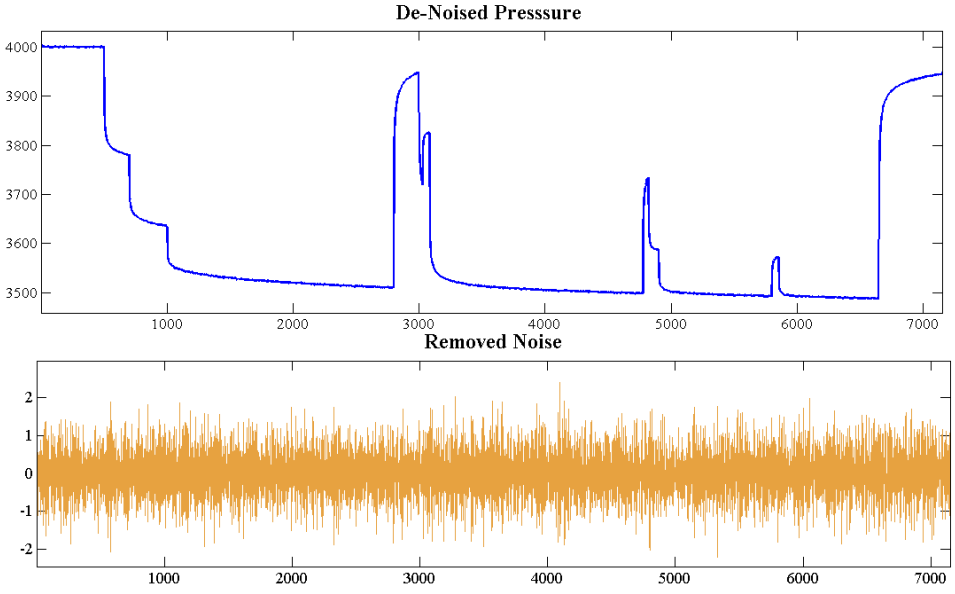

Figure 2-12: Denoised pressure data with the removed noise compared with the original pressure data.

Data reduction

As PDG collects pressure data with high frequency, enormous data size causes inconveniencies for data storage, visualization, processing and interpretation. Reducing data size but keeping the representative data feature is necessary. One of the methods is the pressure thresholding combined with time thresholding method (Athichanagorn et al., 1999). The pressure data will be recorded when the pressure change is higher than the pressure threshold and whenever the time span between samples is higher than the time threshold.

2.3.2 Review of PDG pressure data interpretation

It is well known that the long-term PDG pressure data has the potential to provide more reservoir information than the short time tradition well testing (Horne 2007). PDG pressure data is inherent combination of short-term transient and long-term characters. The short-term transient character can be utilized for reservoir description with conventional well test analysis methods, and the long-term character provides a new time dimension for reservoir description and production monitoring.

Interpreting PDG pressure data to reveal significant amount of reservoir and well information is challenging. The methods of PDG pressure data interpretation is reviewed in this section.

Conventional well test methods

PDG pressure data consists of hundreds of pressure BUs and DDs. The common interpretation procedure for the industry is separating pressure BUs and DDs through transient identification, and flow events are analysed separately. As flow rate information is unknown for majority and flow rate is unstable, only pressure BU data has the quality for pressure-transient analysis with traditional well test methods.

Initially well test techniques come from water hydrology, such as semilog straight line and type-curve matching. Before 1980s, well testing was limited to estimate well conditions and provide little reservoir information with early interpretation methods (straight line analysis, type-cure and log-log pressure plot). Considering the nature of inverse problem for well testing, the ambiguity and non-uniqueness problem was huge at that time. With the pressure derivative technique introduced by Bourdet et al. (1983)

and the development of complex interpretation models, well testing become a powerful tool in reservoir characterization (Gringarten, 2007).

Generally well testing is made up of several flow regimes, from wellbore storage and near wellbore conditions to the late time boundary effect. Log-log pressure derivative can effectively identify different flow regimes, and also is an effective diagnosis tool for interpretation reservoir model selection. For each flow regime, straight line analysis methods such as Horner plot are applied to obtain corresponding well or reservoir parameters.

Nonlinear regression

Nonlinear regression is a well-established technique for well test interpretation. Initially, it was introduced in 1970s for automatic well test analysis to replace the type-curve analysis technique (Earlougher and Kersch 1972, Rosa and Horne 1983, Rosa and Horne 1996). Reservoir parameters are estimated by minimizing the sum of the squares of the differences between the observed pressure/pressure-derivative and the calculated value based on the reservoir model (Horne 1994, Anraku and Horne 1995, Onur and Reynolds 2002).

For PDG pressure data analysis, Athichanagorn et al. (1999) used nonlinear regression to estimate unknown flow rate history and reservoir parameters. Olsen and Nordtvedt (2006) applied automated regression well test module to detect changes or calculate average reservoir parameters with confidence intervals.

Deconvolution

Deconvolution transforms variable-rate pressure data into an equivalent constant-rate pressure response, and the deconvolved response can have a substantially larger radius of investigation than that from a single flow period. In a linear system, the well pressure during a variable-rate test is given by the convolution integral (van Everdingen and Hurst 1949):

$$p(t) = p_0 - \int_0^t q(\tau) \frac{dp_u(t-\tau)}{dt} d\tau \qquad (2.12)$$

At here, p_0 is the initial reservoir pressure, $q(\tau)$ is the flow rate, $p(t)$ is down-hole pressure, and $p_u(t)$ is the rate normalized constant rate pressure response, assuming the

reservoir is in equipment with uniform pressure. Eq. 2.12 is pressure-rate deconvolution, which aims to reconstruct unit constant-rate pressure response $p_u(t)$. Another kind of deconvolution is rate-pressure deconvolution, which aims to reconstruct the pressure normalized constant-pressure rate response $q_{up\,(t)}$:

$$q(t) = \int_0^t q_{up}\,(t-\tau)\frac{d\Delta p(\tau)}{d\tau}d\tau \tag{2.13}$$

Deconvolution is not a new interpretation method. Many papers related to deconvolution algorithm have been published, and these algorithms can be classified into two groups: spectral method and time domain method. Although lots of deconvolution algorithms have been proposed, few of them are robust enough for field application. Deconvolution is an ill-posed inverse problem, which means small errors of input can lead to large change in output. Deconvolution hadn't been applied widely in the industry until the publication of the stable algorithm using nonlinear total least squares method (von Schroeter et al. 2001 and 2004).

In von Schoroeter method, Eq. 2.12 is solved not for the unit constant-rate pressure response $p_u(t)$, but for the function $z(\sigma)$. $z(\sigma)$ is based on the derivative of $p_u(t)$ with respect to the natural logarithm of time:

$$z(\sigma) = ln\left[\frac{d\,p_u(t)}{dln\,(t)}\right] = ln\left[\frac{d\,p_u(\sigma)}{d\sigma}\right] \tag{2.14}$$

where $\sigma = ln(t)$. Eq. 2.14 can ensure $\frac{d\,p_u(t)}{dln\,(t)}$ is positive. The convolution integral of Eq. 5.1 becomes a nonlinear convention equation:

$$p(\sigma) = p_0 - \int_{-\infty}^{\ln t} q(\tau - e^{\sigma})e^{z(\sigma)}d\sigma \tag{2.15}$$

Besides, the curvature of $z(\sigma)$ is regularized to enforce the smooth of the solution of$z(\sigma)$. Considering the error of pressure, rate and regularization curvature constraints, deconvolution is formulated as the unconstrained nonlinear minimization. The objective function is defined as follow:

$$E(p_0, \boldsymbol{z}, \boldsymbol{y}) = \|p_0\boldsymbol{e} - \boldsymbol{p}_m - \boldsymbol{C}(\boldsymbol{z})\boldsymbol{y}\|_2^2 + \upsilon\|\boldsymbol{y} - \boldsymbol{q}_m\|_2^2 + \lambda\|\boldsymbol{D}\boldsymbol{z} - \boldsymbol{k}\|_2^2 \tag{2.16}$$

In Eq. 2.16, $\boldsymbol{p}_m$ and $\boldsymbol{q}_m$ is measured down-hole pressure and flow rate; $\boldsymbol{y}$ is calculated flow rate; $\boldsymbol{k}$ is curvature measure; $\boldsymbol{z}$ is the response coefficient. The υ and λ is the

relative error weight and regularization parameter, and von Schoroeter et al. recommend the default values of these two parameters based on error analysis with Gaussian statistics.

Based on von Schoroeter method, Levitan (2005) and Levitan et al. (2006) made some improvements with practical considerations. Firstly, the assumption unit-slope in wellbore storage before the first node is removed. The first node t_1 is very small and Eq. 2.12 becomes:

$$p(\sigma) = p_0 - q(t_i)p_u(t_1) - \int_{-\infty}^{\ln t} q(\tau - e^{\sigma})e^{z(\sigma)}d\sigma \qquad (2.17)$$

Besides, the objective function is an unconstrained and nonlinear weighted least-squares function and including the sum of mismatch terms for pressure, rate and curvature:

$$E(p_0, p_u(t_1), \boldsymbol{z}, \boldsymbol{y}) = \frac{1}{2}\left\|\frac{p_0\boldsymbol{e} - \boldsymbol{p}_m - p_u(t_1)\tilde{\boldsymbol{y}} - \tilde{C}(z)\boldsymbol{y}}{\varsigma_p}\right\|_2^2 + \frac{1}{2}\left\|\frac{\boldsymbol{y} - \boldsymbol{q}_m}{\varsigma_q}\right\|_2^2 + \frac{1}{2}\left\|\frac{\boldsymbol{D}\boldsymbol{z}}{\varsigma_c}\right\|_2^2 \qquad (2.18)$$

ς_p , ς_q and ς_c is error bounds for the pressure, rate and curvature constrains.

The unit constant-rate pressure response $p_u(t)$ can be reconstructed from the $z(\sigma)$ function:

$$p_u(t) = p_u(t_1) + \int_{\tau_1}^{lnt} e^{z(\tau)}d\tau \qquad (2.19)$$

Ilk et al. (2005 and 2006) presented B-Spline deconvolution and applied this algorithm on gas well testing.

With the installation of permanent down-hole pressure and rate measure systems, deconvolution becomes more important as it can process pressure and rate data simultaneously and obtain the underlying reservoir properties which change with time (Onur et al. 2008). Using the stable algorithm, deconvolution has been applied to analyse the long-term PDG pressure data to identify reservoir compartments connectivity, diagnose production problems and with practice applications (von Schroeter et al. 2002, Gringarten et al. 2003, Gringarten 2005 and 2010).

Decline curve analysis

Decline curve analysis is the most widely used method for the long-term production data analysis. The constant-pressure rate data is analysed for reservoir estimation and production forecasting for a reservoir under depletion. PDG can provide long-term pressure and rate data during the pseudo-steady state or depletion, and the rate-pressure deconvolution can convert the production data with varying pressure data into constant-pressure rate data, so the decline curve analysis method has the potential to provide valuable reservoir information.

Unneland et al. (1998) presented three field case studies about analysing PDG pressure and rate data using decline curve analysis, and the production data variable down-hole flowing pressure was processed by rate convolution. With the stable rate-pressure deconvolution algorithm and decline curves, Kuchuk et al. (2005) proposed a methodology for monitoring well production index, forecasting production and estimating reservoir. Meanwhile, decline curve also was utilized as a diagnostic tool for production problems (Anderson and Mattar 2004, Ilk et al. 2010).

2.4 Literature review of diagnostic of the change in reservoir properties and well conditions

As discussion above, the diagnostic of changes in reservoir parameters and well conditions is important for long-term pressure analysis, production monitoring and reservoir model calibration. Many diagnostic methods have been proposed.

PI is a straightforward and simple method of monitoring the well performance, and it is defined as:

$$\mathrm{PI} = \frac{q_m(t)}{[\overline{p}(t) - p_m(t)]} \tag{2.20}$$

Here $\overline{p}$ is the average reservoir pressure, q_m and p_m is the measured flow rate and down-hole pressure. Unneland et al. (1998) used PI for production monitoring and diagnostic. **Figure 2-13** shows the PI reduction after 200 days and PI increased substantially as the result of fracturing operation. Kuchuk et al. (2005) used the PI to check the changes in near wellbore reservoir parameters, before applying constant-pressure rate response (deconvolved rate from rate-pressure deconvolution) for production optimization and prediction, and they mentioned that the deconvolution can't be carried out during the entire production history with the changes in near wellbore reservoir parameters. However, PI should be estimated during the steady-state

or pseudo-steady state period, and average pressure $\overline{p}$ should be updated continuously due to reservoir depletion. This means PI can't be a real-time diagnostic tool.

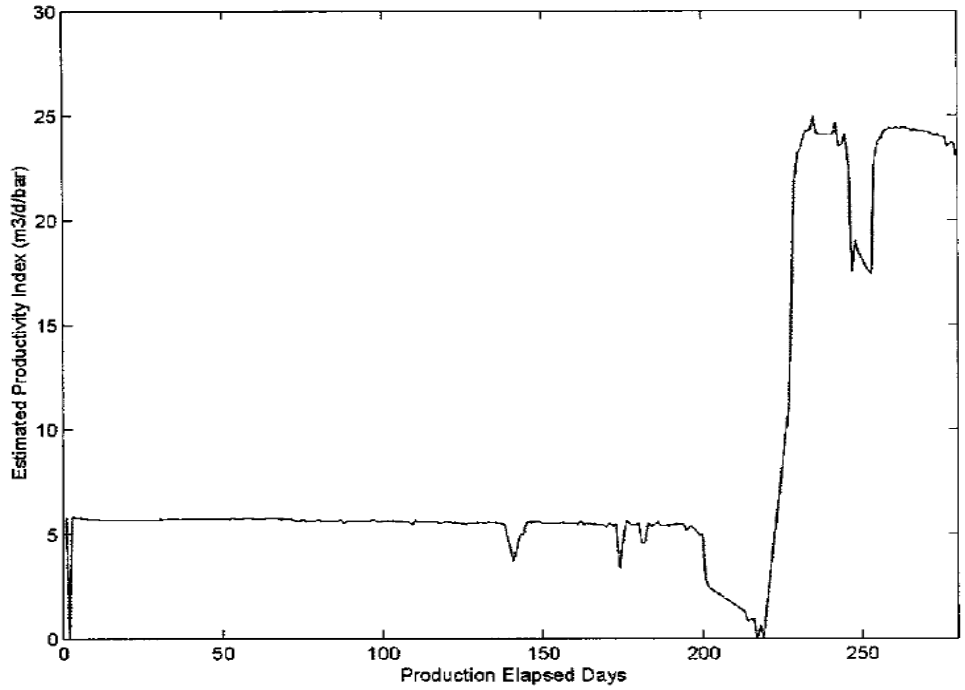

Figure 2-13: Well PI diagnostic plot for Field Case 3 in Unnrland et al. (1998) paper.

Decline curve analysis with type-curve is another method for diagnosing production problems. Anderson et al. (2004) applied this method to identify liquid loading and changing wellbore skin, detect a shift in well productivity and diagnose external pressure support and interference. For this method, changes in overall well productivity can be identified for the discontinuities in the data from a type-curve match (Anderson et al. 2004, Kuchuk et al. 2005, and Ilk et al. 2010). However, a suitable reservoir model providing adequate reservoir/well descriptions needs to be selected at first, and the production should be long enough that the reservoir is in depletion. Besides, production data should be equivalent constant-pressure rate data.

Deconvolution has received much attention in the last 10 years. Ilk et al. (2010) and Li et al. (2011) used the deconvolution to diagnose the nonlinearity in the reservoir, under which conditions superposition principle is invalid. Gringarten et al. (2003) applied deconvolution to diagnose production problems from PDG data, such as the change in relative permeability and water invasion. However, there are theory uncertainties when applying deconvolution in complex systems without nonlinearity diagnostic at first, and some nonlinearity can be covered up by the optimization algorithm, such as nonlinear total least squares.

The "4D" pressure and pressure-derivative analysis in log-log plot is the most widely used method. In this method, the rate-normalized pressure and its derivative from all pressure build-ups are plot in the same log-log plot, and the changes in reservoir-well parameters can be diagnosed in the log-log diagnostic plot (Haddad et al. 2004, Gringarten et al. 2003, Houzé et al. 2010). **Figure 2-14** shows log-log plot of pressure and pressure derivative on BU periods in the paper of Haddad et al. (2004). The changes in pressure and pressure derivative indicate the increasing skin, decreasing kh and gas reservoir depletion. As the data quality from pressure DD is poor for analysis, only data from pressure BU is analysed. However, few pressure build-ups are available, and nonlinearities can't be diagnosed in real-time.

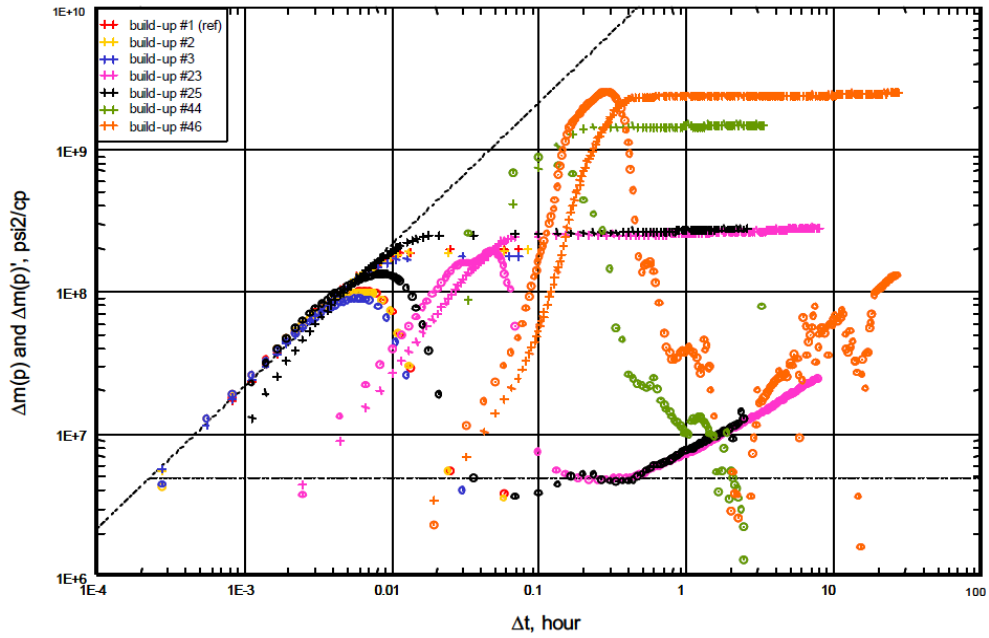

Figure 2-14: The "4D" pressure and pressure-derivative diagnostic plot in the paper of Haddad et al. (2004).

2.5 Literature review of unknown flow rate history reconstruction

Many methods have been proposed to reconstruct unknown flow rate history. The most sample method is using production index (PI), but this method only can be used in pseudo-steady state or steady state. Detailed flow events cannot be reconstructed and the changing PI due to changes in parameters also causes problems. Athichanagorn et al. (1999) used nonlinear regression method to solve the unknown flow rate by treating it as an unknown parameter to match the simulated model response. This method is based on the developed reservoir model, and this is difficult when the reservoir model is

unknown, especially for a new reservoir. Besides, errors may be introduced due to the uncertainties of reservoir model. Haugen et al. (2001) made down-hole production allocation using the passive acoustic listening method. With the measured acoustic noise and established empirical model, flow rates of gas, water and oil can be predicted. However, for different reservoir models the empirical model is different, and also the empirical model needs calibration continuously when there are changes in environment. McCracken and Chorneyko (2005) made rate allocation using pressure data from permanent down-hole gauge. With a created simple reservoir model, flow rate was adjusted as the input parameter of the simple model until the pressure response from model matching the pressure data from permanent down-hole gauge. The result may be limited by the simple and incorrect reservoir model.

Temperature information attracts more and more attentions in oilfields in recent years, with the popularity of distributed temperature sensing (DTS) and permanent down-hole temperature measurement. The temperature change is closely associated with the flow rate behaviour, which provides another opportunity to reconstruct flow rate history (Duru et al. 2008). Sun et al. (2006) predicted and allocated multiphase production in a multiple zone intelligent well system using down-hole real time pressure and temperature data. An improved multiphase choke model has been derived based on the earlier multiphase choke modelling work. Izgec et al. (2009) estimated the flow rate from wellhead pressure and temperature, and two methods were proposed. For the entire-wellbore approach, thermal properties of fluid, tubular and formation are needed, and this approach also relies on modelling. By contrast, the single-point method requires few input parameters and was recommended by authors. Wellbore fluid and thermal effects have not been considered, but for low kh reservoirs, the error may be large. Muradov et al. (2009) made zone rate allocation based on measured down-hole pressure and temperature data in intelligent wells. This approach appears to be based on steady-state modelling. Lorentzen et al. (2010) made improvement by combining a transient well flow model and the ensemble Kalman filter with the high frequency measurements of pressure and temperature data. Only two simple cases were studied and more work needs to validate this method.

Zheng and Li (2009) applied wavelet transform to recover flow rate history using the PDG transient pressure data and accumulative production. The exact timing of rate change is identified through wavelet frequency analysis. With the proportional relationship between the rate and the frequency amplitude of transient pressure, flow

rate history can be reconstructed with daily rate or total cumulative production data. However, many problems still need to be solved for field applications. Firstly, this method is based on the assumption that reservoir system is linear, but how to diagnose nonlinearities in the reservoir is a problem. Then, their theory was based on the homogeneous reservoir model. The effects of data noise, wellbore storage, skin, reservoir heterogeneity and multi-well interference have not been considered, and the algorithm only can be used in the single phase oil reservoir. The pressure-dependent fluid properties for gas reservoir and the total mobility changes in multiphase flowing reservoir raise many problems for rate calculation.

2.6 Chapter summary

In this chapter the wavelet theory is introduced and the literature related to this study is reviewed. Several conclusions can be summarized as follows:

1. Wavelet transform is a multi-resolution frequency analysis method and it is more suitable for analysing the non-stationary signal such as PDG pressure data compared with Fourier Transform and Short-Time Fourier Transform.
2. The Haar wavelet can effectively identify the transient events in PDG pressure data using continuous wavelet transform. When selecting scale parameter s, the resolution of transient identification and noise effect must be considered at same time.
3. For PDG pressure data processing and interpretation, effective methods and algorithms have been developed, but for diagnosing the changes in reservoir-well parameters and reconstructing unknown rate history, more research work needs to be done.

Chapter 3 Diagnostic of Nonlinearity from Transient Pressure Data

3.1 Introduction

In this chapter, a novel nonlinearity diagnostic method based on wavelet transform has been developed. The nonlinearities due to the changes in reservoir properties and well conditions, such as time-dependent skin factor and permeability, water breakthrough and gas out of solution are diagnosed from the transient pressure data. This novel diagnostic method can ensure the PTA methods based on the linearity assumption can be correctly applied, and reduce the uncertainties for pressure analysis. The diagnostic result also is useful for production monitoring and reservoir model calibration.

3.2 Theory description of the novel nonlinearity diagnostic method

PDG pressure history consists of hundreds of flow events. The changes in rate cause the changes in pressure data. If the rate change is treated as input signal, the corresponding pressure change is output response. The pressure change caused by the unit change in rate can reflect the properties of reservoir-well systems.

For a simple case, in a linear system the well produces at constant flow rate q_1 for t_1, then followed by rate change q_2 for a very small impulse time Δt. The bottom-hole pressure p_{wf1} at the time t_1:

$$p_{wf1} = p_0 - q_1 \int_0^{t_1} g(\tau) d\tau \tag{3.1}$$

According to superposition principle, bottom-hole pressure p_{wf2} at the time $t_1 + \Delta t$ is:

$$p_{wf2} = p_0 - q_1 \int_0^{t_1+\Delta t} g(\tau) d\tau - (q_2 - q_1) \int_0^{\Delta t} g(\tau) d\tau \tag{3.2}$$

Eq. 3.1 minus Eq. 3.2, the down-hole pressure change during the impulse time Δt is:

$$p_{wf1} - p_{wf2} = (q_2 - q_1) \int_0^{\Delta t} g(\tau) d\tau + q_1 \int_{t1}^{t_1+\Delta t} g(\tau) d\tau \tag{3.3}$$

In Eq. 3.3, $(q_2 - q_1) \int_0^{\Delta t} g(\tau) d\tau$ is flow-rate change effect, and $q_1 \int_{t1}^{t_1+\Delta t} g(\tau) d\tau$ is production history effect.

Similarly, for n different flow periods, the pressure change during the last impulse time Δt is:

$$p_{wfn} - p_{wfn+1} = (q_{n+1} - q_n) \int_0^{\Delta t} g(\tau) d\tau + \sum_{i=1}^{n} (q_i - q_{i-1}) \int_{t_n - t_{i-1}}^{t_n - t_{i-1} + \Delta t} g(\tau) d\tau \quad (3.4)$$

As Eq. 3.3 and Eq. 3.4 show, the pressure change during the time Δt is not only caused by the flow rate change $(q_{n+1} - q_n) \int_0^{\Delta t} g(\tau) d\tau$, but also is affected by the production history $\sum_{i=1}^{n} (q_i - q_{i-1}) \int_{t_n - t_{i-1}}^{t_n - t_{i-1} + \Delta t} g(\tau) d\tau$.

With the Haar wavelet processing transient pressure data, pressure changes between two successive flow periods can be clearly identified by the amplitude of WT coefficients. The WT amplitude is positive for drawdown and negative for build-up, and the height of amplitude depends on the pressure change. Mathematically, WT is a linear operation, so the WT amplitude A is proportional to the pressure change Δp_{wf}:

$$A \propto \Delta p_{wf} \quad (3.5)$$

Submit Eq. 3.4 into Eq. 3.5:

$$A \propto (q_{n+1} - q_n) \int_0^{\Delta t} g(\tau) d\tau + \sum_{i=1}^{n} (q_i - q_{i-1}) \int_{t_n - t_{i-1}}^{t_n - t_{i-1} + \Delta t} g(\tau) d\tau \quad (3.6)$$

For the infinite homogenous reservoir, the impulse response of the system function $g(t)$ can be calculated, according to the unit constant-rate drawdown solution of the diffusivity equation, $g(t)$ can be expressed:

$$g(t) = \frac{dp_u}{dt} = \frac{d\left\{\frac{70.6\mu B}{kh}\left[-E_i\left(-\frac{\phi \mu C_t r_w^2}{0.00105\, k \Delta t}\right)\right]\right\}}{dt} \quad (3.7)$$

To better understand the character of $g(t)$ function, a simulated reservoir model is taken for research. The reservoir properties are shown as **Table 3-1**. The calculated impulse response function $g(t)$ of the system is shown in **Figure 3-1**. Its value is the largest at the beginning and declines very quickly with time. The reason is $g(t)$ equals the time derivative of unit-rate pressure drawdown response p_u, and the down-hole pressure decline quickly at the beginning of production.

For instance, if q_1 =500 STB/day, q_2=1000 STB/day, the production history time t_1 =1 hour, the impulse time $\Delta t = 1$ second, and then production history effect

$q_1 \int_{t1}^{t_1+\Delta t} g(\tau)d\tau$ =0.0041 psi, rate change effect $(q_2 - q_1) \int_0^{\Delta t} g(\tau)d\tau$ =21.7967 psi. Rate change effect is much larger than production history effect. Even t_1 =1 minute, impulse time Δt =1 second, history production effect is just the 2.58% of rate change effect.

Table 3-1: Reservoir properties of a simulated reservoir model

Initial pressure, p_0	4000 psia
Reservoir radius, R	10000 ft
Thickness, h	30 ft
Oil Formation Volume Factor, B_o	1.2 rb/STB
Permeability, k	$k_x = k_y$ =100 mD, k_z =10 mD
Porosity, ϕ	0.25
Viscosity, μ_o	1 cp
Total compressibility, C_t	6e-6 1/psi
Well radius, r_w	0.2083 ft
Skin factor, S	6
Well bore storage coefficient, C_s	2.9e-4 bbl/psi

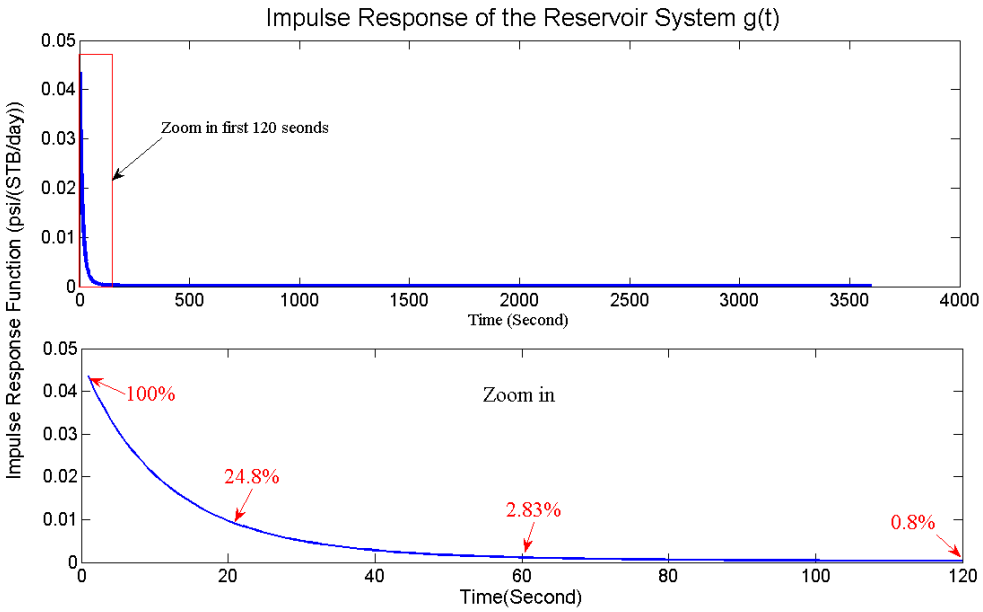

Figure 3-1: The impulse response of reservoir system $g(t)$in the first 1hour and zoom in. Its value is largest at first but it declines fast with time. 60s after it declines to 2.83%, and 2 minute after, it is 0.8% of the initial value.

When the impulse time Δt is very small and the production history time is large, $\int_0^{\Delta t} g(\tau)d\tau$ is much larger than $\int_{t_n-t_{i-1}}^{t_n-t_{i-1}+\Delta t} g(\tau)d\tau$, and therefore the production history effect in Eq. 3.6 can be neglected. The WT amplitude is only caused by flow-rate change:

$$A \propto (q_{n+1} - q_n) \int_0^{\Delta t} g(\tau)d\tau \tag{3.8}$$

Then, the amplitude of WT coefficients A caused by unit-rate-change $A_{urc} = A/(q_{n+1} - q_n)$ is proportional to $\int_0^{\Delta t} g(\tau)d\tau$, shown as Eq. 3.9. The subscript urc stands for unit-rate-change.

$$A_{urc} \propto \int_0^{\Delta t} g(\tau)d\tau \tag{3.9}$$

As $g(\tau)$ depends on reservoir-well parameters, any changes in well conditions and reservoir properties in/around the wellbore can be diagnosed with the A_{urc} function, according to Eq. 3.9. For linear systems, as reservoir-well parameters are constant, A_{urc} is constant with time. When there are nonlinearities near the wellbore, A_{urc} is time-varying. The A_{urc} function is used as a nonlinearity diagnostic function in this thesis and named as Unit Reservoir System Response (URSR).

3.3 Base case and sensitivity study

As discussed above, the single-phase flow of slightly compressible fluid in porous media with constant reservoir-well parameters is a linear system. According to this, a single oil phase homogeneous reservoir is researched. The reservoir properties are shown in **Table 3-2**. **Figure 3-2** shows production history and pressure data is processed with Haar wavelet. Pressure change between successive flow periods (flow events) can be identified by the amplitude of WT coefficients. The amplitude caused by unit-rate-change (URSR A_{urc}) is calculated using $A_{urc} = A/\Delta q$. As shown in **Table 3-3**, URSR A_{urc} is constant with time, verifying that the reservoir properties and well conditions are constant with time.

Table 3-2: Reservoir properties in the single oil phase reservoir.

Initial pressure, p_i	4000 psia
Reservoir radius, R	10000 ft
Thickness, h	30 ft
Oil formation volume factor, B_o	1.2 rb/STB
Permeability, k	100 mD
Porosity, ϕ	0.25
Viscosity, μ_o	1 cp
Oil compressibility, C_o	3e-6 1/psi
rock compressibility, C_f	3e-6 1/psi
Well radius, r_w	0.208 ft
Skin factor, S	6
Well bore storage coefficient, C_s	2.9e-4 bbl/psi

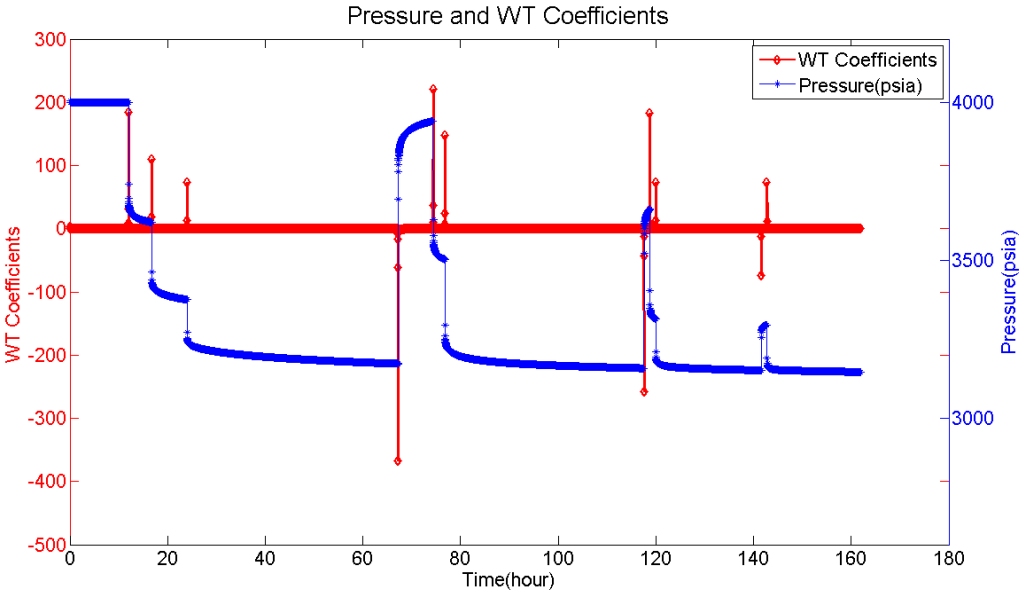

Figure 3-2: The transient pressure is processed by WT using the Haar wavelet.

Table 3-3: The A_{urc} function in the single oil phase reservoir is almost same.

Time (Hour) t	Rate (STB/day) q	Rate change (STB/day) Δq	WT amplitude A	URSR $A_{urc} = A/\Delta q$
0	0			
12	500	500	183.6187	0.3672
16.8	800	300	110.3014	0.3677
24	1000	200	73.5773	0.3679
67.2	0	-1000	-367.678	0.3677
74.4	600	600	220.3397	0.3672
76.8	1000	400	147.1281	0.3678
117.6	300	-700	-257.417	0.3677
118.8	800	500	183.4948	0.3669
120	1000	200	73.6184	0.3680
141.6	800	-200	-73.5602	0.3678
142.8	1000	200	73.4804	0.3674

In this case, how A_{urc} performs with the changes of different reservoir-well parameters will be researched. The reservoir properties include skin factor, permeability, reservoir thickness, wellbore storage, wellbore size, fluid viscosity, reservoir heterogeneity and etc.

As $\int_0^{\Delta t} g(\tau)d\tau = \Delta p_u(\Delta t)$, for the homogeneous infinite reservoir, the pressure drop due to unit constant-rate is:

$$\int_0^{\Delta t} g(\tau)d\tau = \Delta p_u(\Delta t) = \frac{70.6uB}{kh}\left[-E_i\left(-\frac{\emptyset\mu C_t r_w^2}{0.00105\,k\Delta t}\right) + 2S\right] \tag{3.10}$$

Here S is the skin factor. When$\frac{\emptyset\mu C_t r_w^2}{0.00105\,k\Delta t} < 0.01$, Eq. 3.10 can be simplified:

$$\int_0^{\Delta t} g(\tau)d\tau = \frac{70.6uB}{kh}\left[\ln\Delta t + \ln\frac{k}{\emptyset\mu C_t r_w^2} - 7.43173 + 2S\right] \tag{3.11}$$

Then Eq. 3.11 becomes:

$$A_{urc} \propto \frac{70.6uB}{kh}\left[\ln\Delta t + \ln\frac{k}{\emptyset\mu C_t r_w^2} - 7.43173 + 2S\right] \tag{3.12}$$

Eq. 3.12 shows the relationship between different reservoir-well parameters and URSR function A_{urc}. To verify Eq. 3.12, the base case reservoir model with changing parameters is simulated and corresponding A_{urc} is calculated.

Skin factor: According to Eq. 3.12, A_{urc} changes linearly with skin factor S. The larger skin factor causes more pressure drop near the wellbore, and makes the larger WT amplitude for the same rate change. The simulated result for different skin factors is shown in **Figure 3-3**. There is linear relation between skin factor S and URSR A_{urc}, and verifies the theory analysis using Eq. 3.12.

Permeability: There are two parts related to permeability k in Eq. 3.12, $\frac{70.6uB}{kh}$ and $\ln\frac{k}{\emptyset\mu C_t r_w^2}$. Mathematically, the effect of $\frac{70.6uB}{kh}$ is much larger than that of $\ln\frac{k}{\emptyset\mu C_t r_w^2}$, so A_{urc} declines with increasing permeability k, and A_{urc} changes almost linearly with $1/k$. The simulation results are shown in **Figures 3-4 and 3-5**.

Formation thickness: In theory, the A_{urc} function changes linearly with the reciprocal of formation thickness h according to Eq. 3.12, and it is verified by the simulation result, as shown in **Figure 3-6**.

Porosity: As Eq. 3.12 shows, A_{urc} changes linearly with $ln\frac{1}{\emptyset}$. Therefore the relationship between A_{urc} and porosity $\emptyset$ is logarithmic, and it is verified by the simulation result, as shown in **Figure 3-7**. URSR A_{urc} decreases as porosity $\emptyset$ increases, but the change is little compared with the effects of changes in skin factor and permeability.

Viscosity: Similar with permeability k, there are two parts related to viscosity μ in Eq. 3.12, $\frac{70.6uB}{kh}$ and $\ln\frac{k}{\emptyset\mu C_t r_w^2}$. As the effect of $\frac{70.6uB}{kh}$ is much larger, A_{urc} increases almost linearly with the increasing viscosity μ, and it is verified by the simulation result, as shown in **Figure 3-8.**

Formation volume factor (FVF): According to Eq. 3.12, A_{urc} has linear relationship with formation volume factor B_o, and it is identical to the simulation result, shown in **Figure 3-9**.

Compressibility: As Eq. 3.12 shows, unit reservoir system response A_{urc} decreases as the total compressibility c_t increases. The total compressibility c_t is:

$$c_t = c_f + c_w S_w + c_o(1 - S_w) \tag{3.13}$$

Here S_w is water saturation, and c_o, c_w, c_f is compressibility of oil, water and rock respectively. In theory, URSR A_{urc} has linear relationship with $\ln\frac{1}{c_t}$, and logarithmic relationship with total compressibility c_t, which are confirmed by the simulation result (**Figure 3-10)**.

Wellbore size: In theory A_{urc} has linear relationship with $\ln\frac{1}{r_w^2}$, and logarithmic relationship with wellbore size r_w. It is confirmed by the simulation result (**Figure 3-11**). The smaller wellbore size leads to larger A_{urc} compared with the larger wellbore size.

Fluid density: Fluid density has no effect on A_{urc} in theory, and this is confirmed by simulation result (**Figure 3-12**).

Wellbore storage coefficient: Wellbore storage is caused by the compressibility of fluid in the wellbore, and it extends the time of pressure response. In theory, the larger the wellbore storage coefficient is, the smaller URSR A_{urc} it will be, as shown in **Figure 3-13**.

Reservoir heterogeneity*:* As Eq. 3.9 shows, A_{urc} is constant for the reservoir with constant reservoir-well parameters, and the properties variation in space has no effect on A_{urc}. Besides, this novel diagnostic method is independent of reservoir model and only transient pressure data and rate information are used, so this diagnostic method works well in heterogeneous reservoirs.

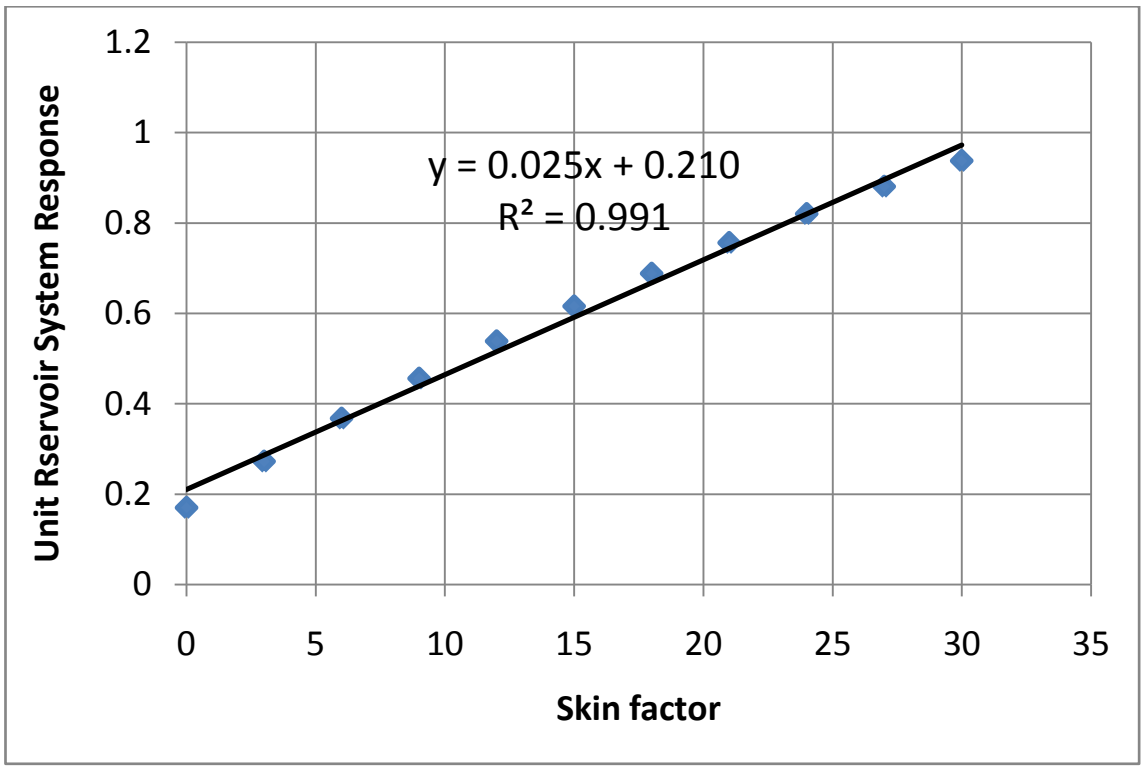

Figure 3-3: Impact of skin change on A_{urc} function.

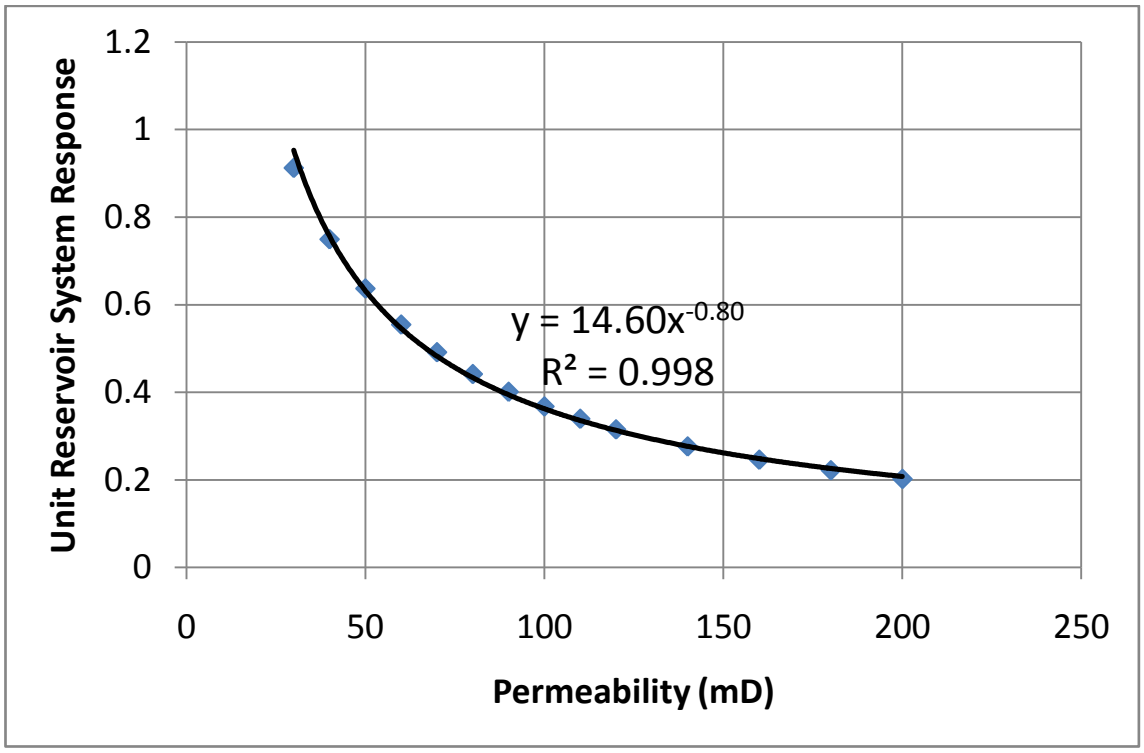

Figure 3-4: A_{urc} declines with increasing permeability$k$.

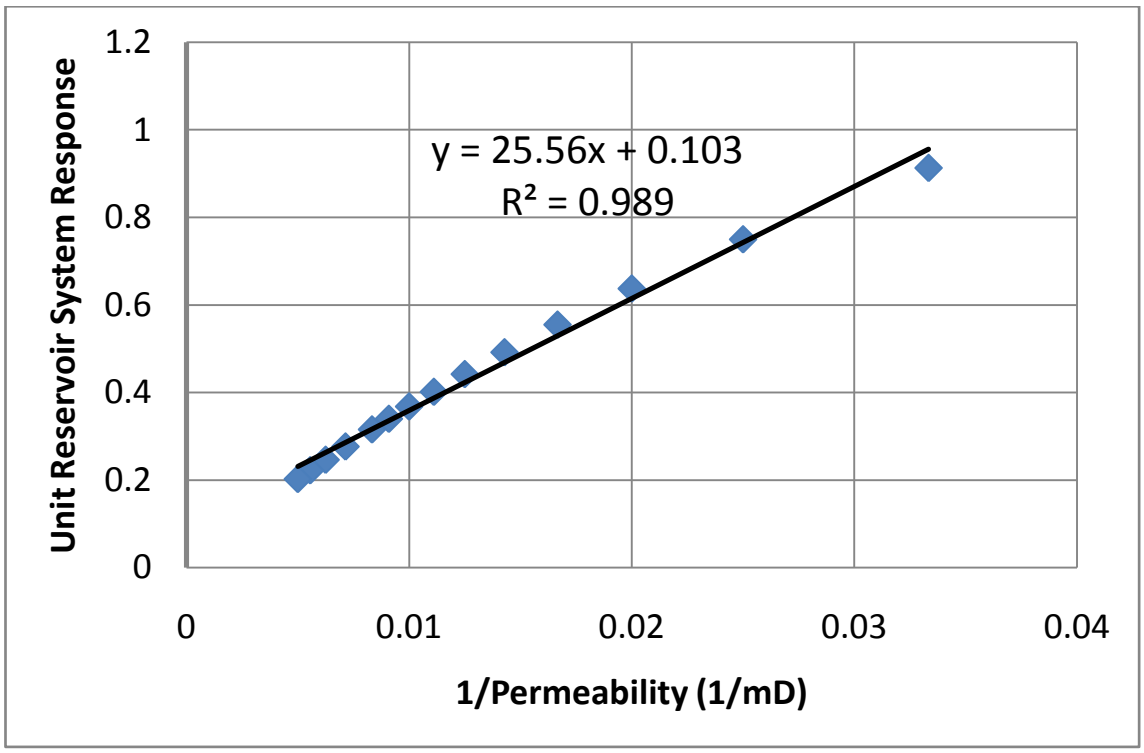

Figure 3-5: A_{urc} changes almost linearly with $\frac{1}{k}$.

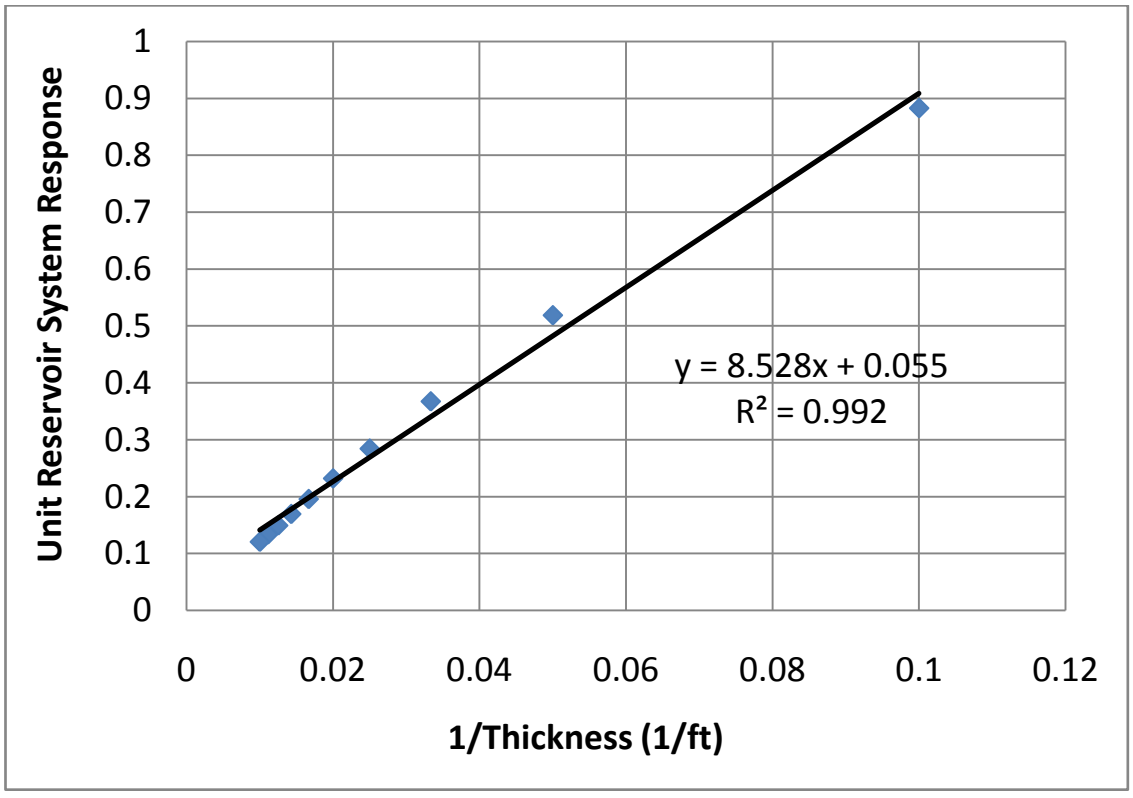

Figure 3-6: A_{urc} changes linearly with the reciprocal of formation thickness h.

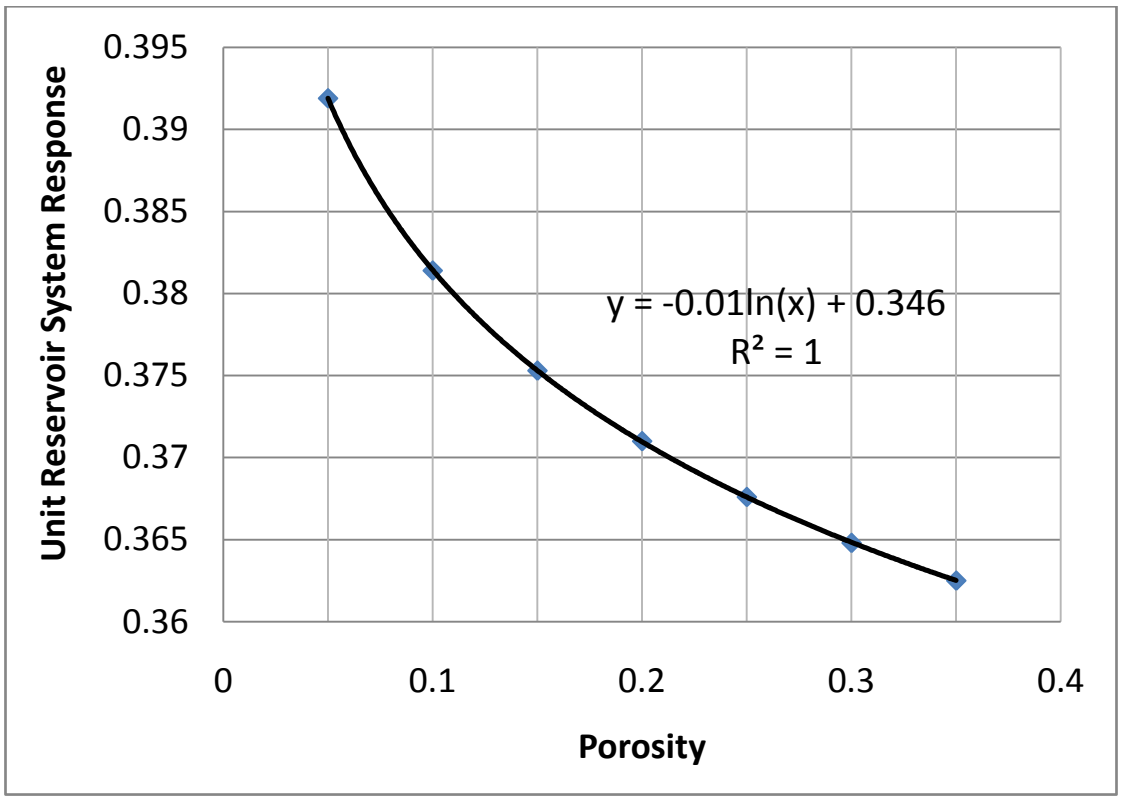

Figure 3-7: A_{urc} changes logarithmically with porosity ∅.

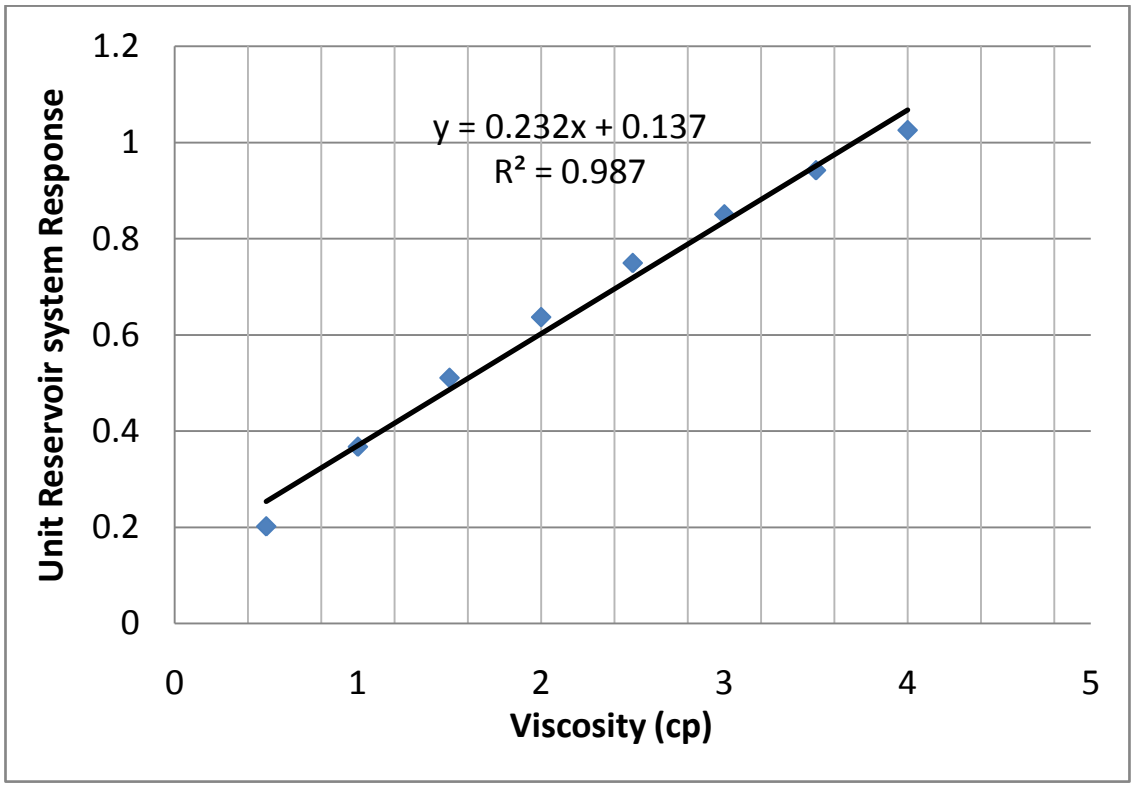

Figure 3-8: A_{urc} increases linearly with the increasing viscosity μ, and viscosity has big effect on A_{urc} .

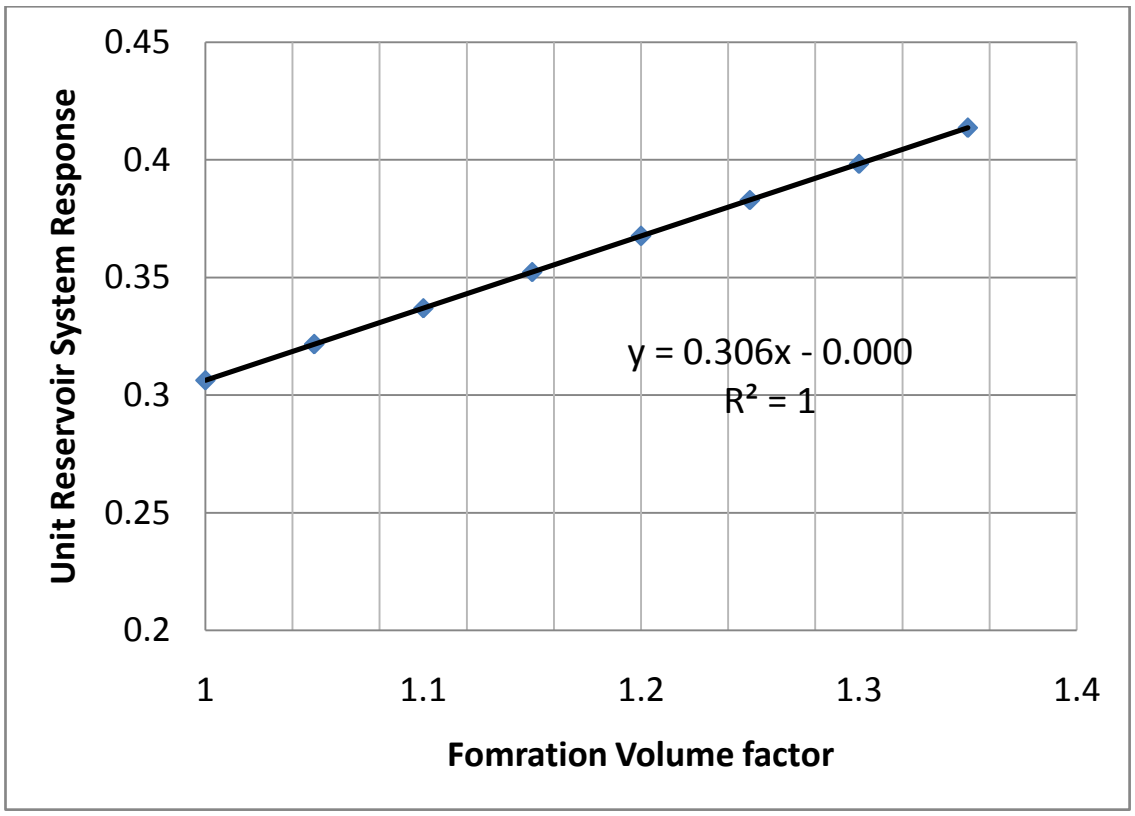

Figure 3-9: A_{urc} increases linearly with the increasing oil FVF B_o.

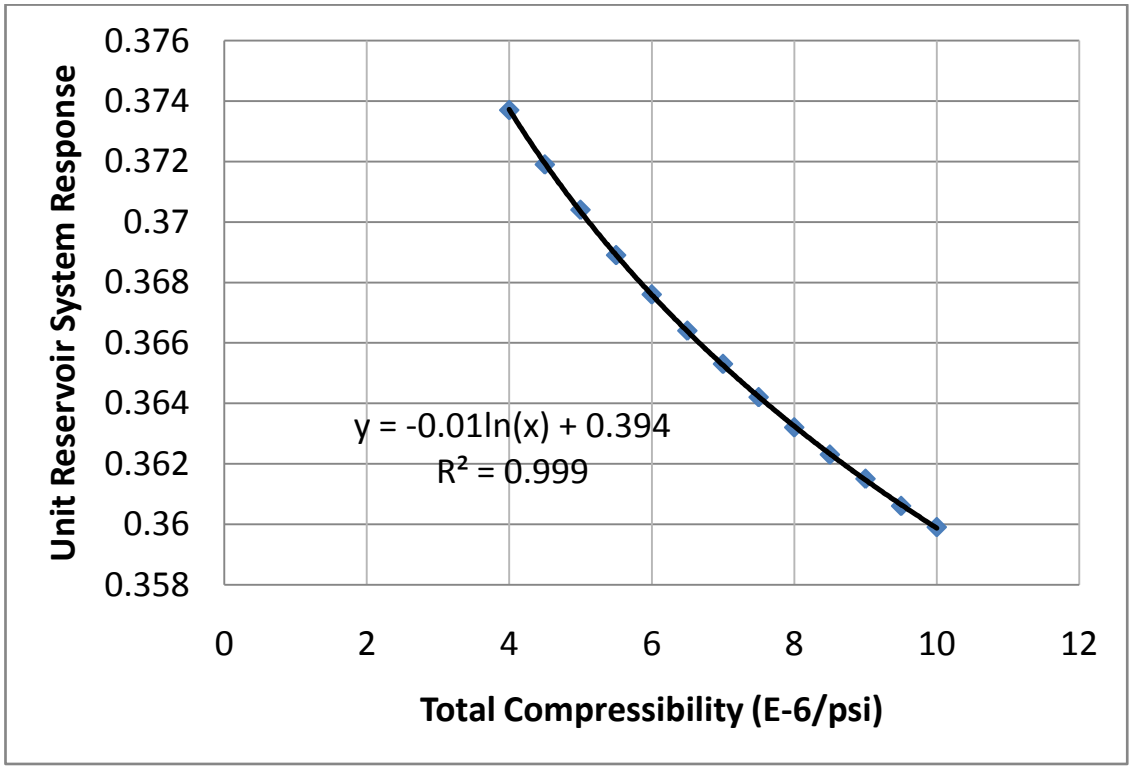

Figure 3-10: A_{urc} declines with the increasing total compressibility, but the change is small.

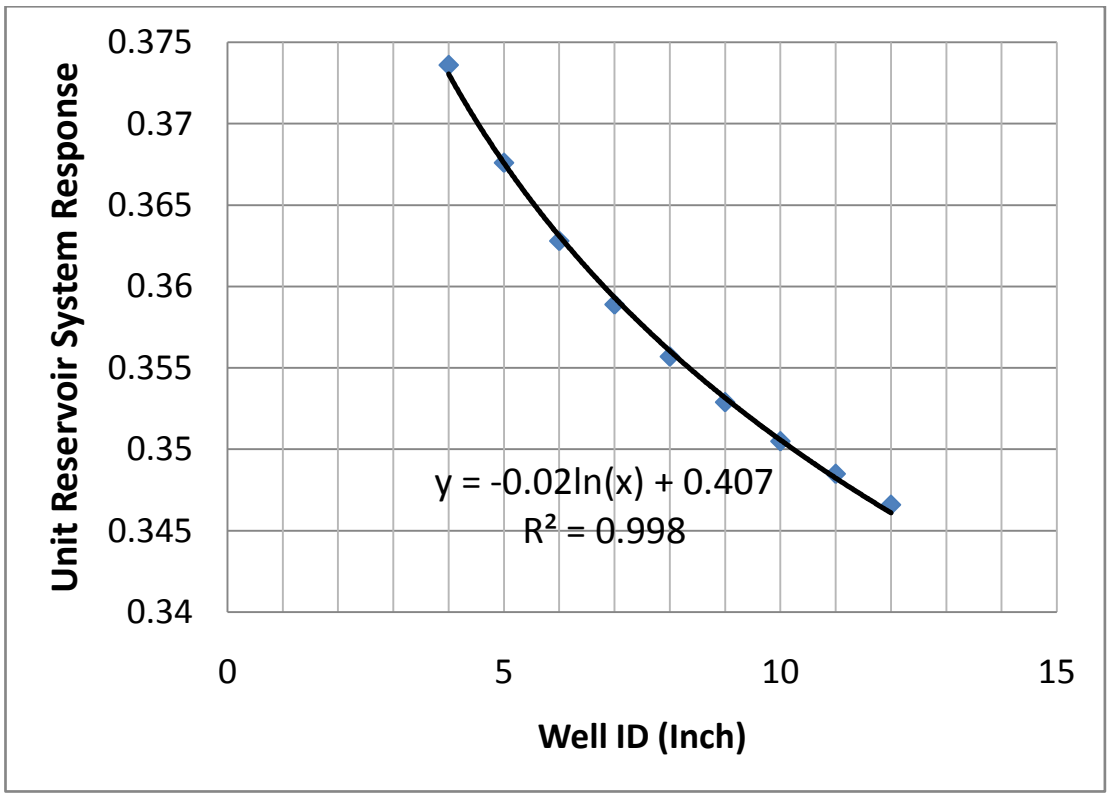

Figure 3-11: A_{urc} declines logarithmically with the increasing wellbore size.

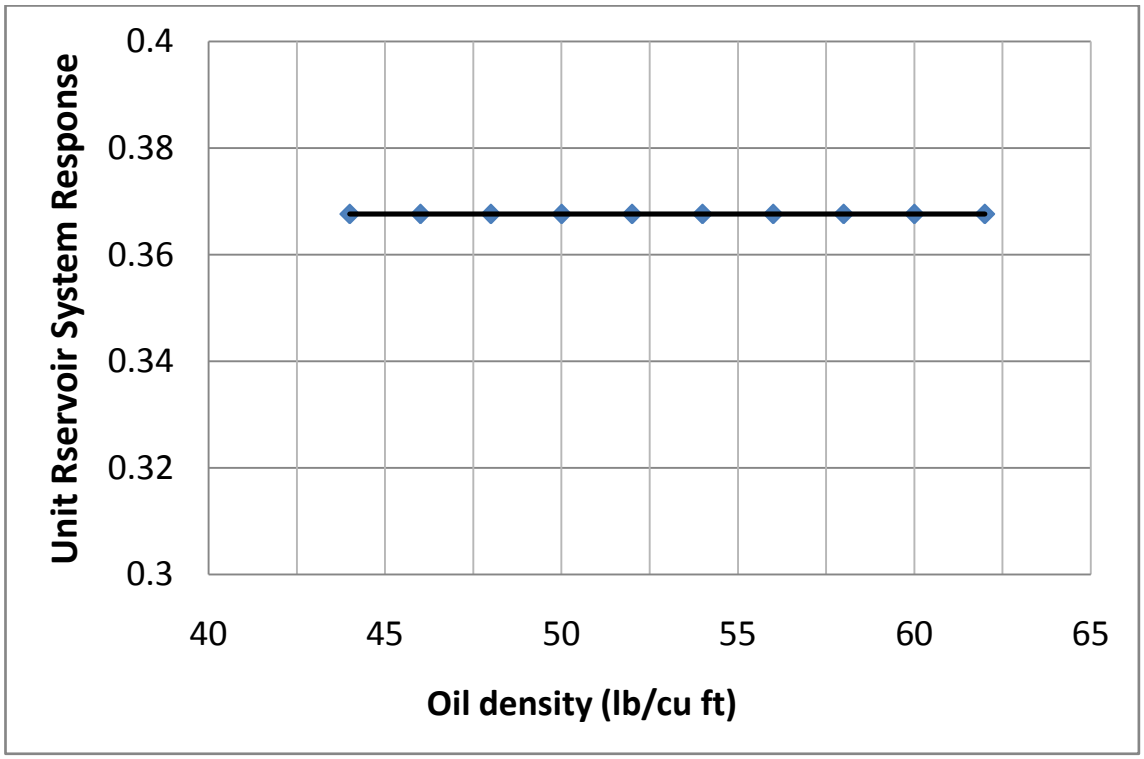

Figure 3-12: Fluid density has no effect on A_{urc} .

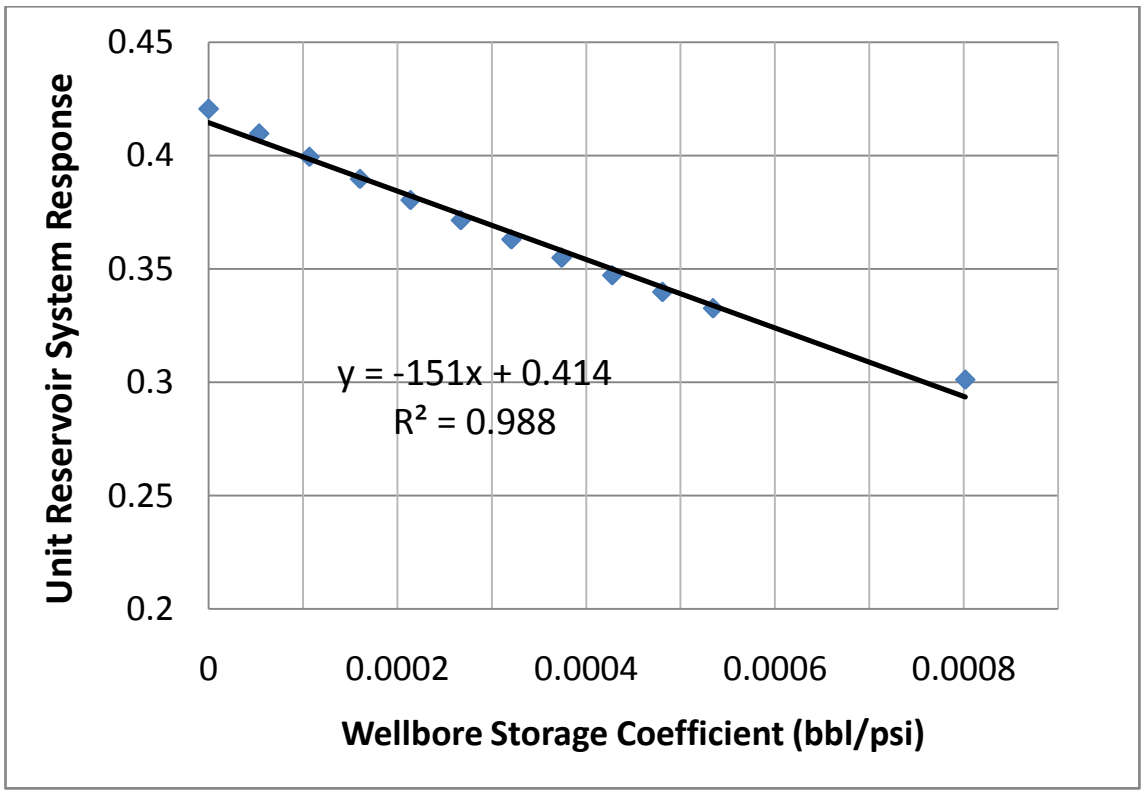

Figure 3-13: A_{urc} declines with the increasing wellbore storage coefficient C_s .

Figure 3-14 shows the effects of different reservoir-well parameters on URSR A_{urc} function. The label in horizontal direction is the change percent of each parameter compared with the value in the base case (shown in **Table 3-2**), and the label in the vertical direction is URSR A_{urc}. As the figure shows, the change in oil density doesn't affect on URSR A_{urc}, and changes in porosity, well ID, wellbore storage coefficient and total compressibility have small negative effect on URSR A_{urc}. However, changes in permeability, formation thickness, viscosity and skin factor have significant impact on URSR A_{urc}. For skin factor and viscosity, their relationships with URSR A_{urc} are positive and almost linear. In contract, URSR A_{urc} declines with the increasing permeability and formation thickness, and their relationships are nearly logarithmic.

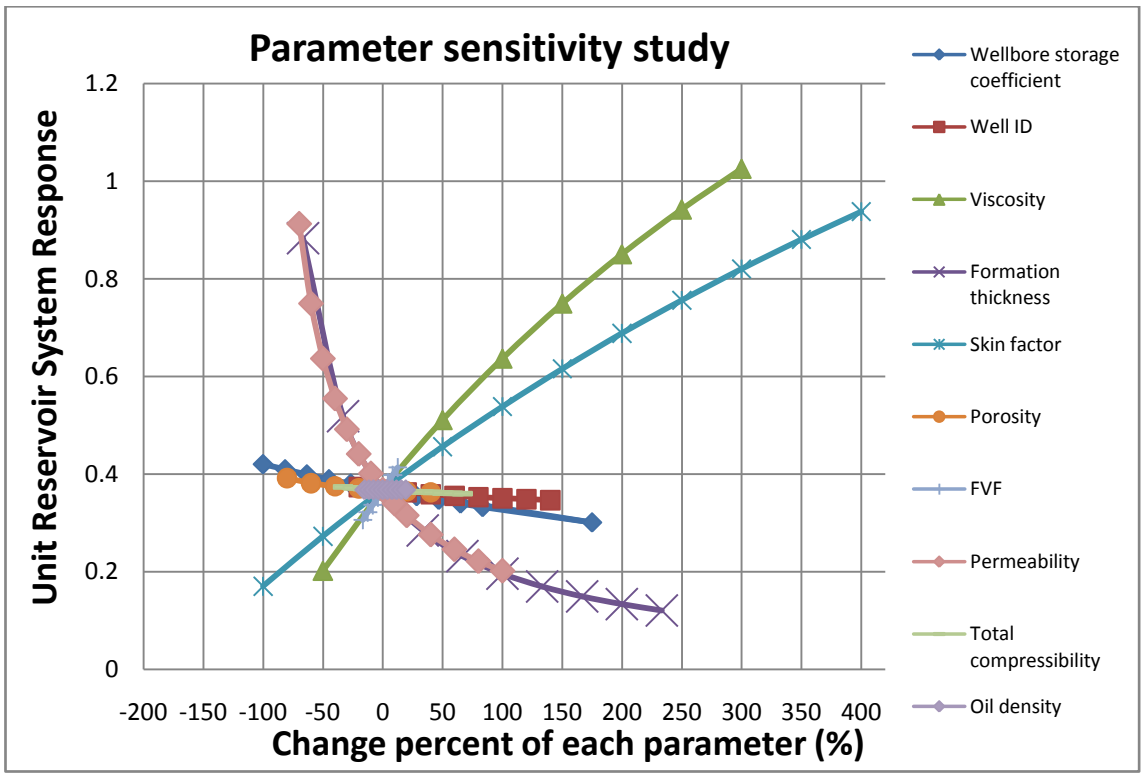

Figure 3-14: The impact of different parameter change on URSR A_{urc} .

In practice, the changes in fluid viscosity in the reservoir are so little that usually they can be neglected. But there are high possibilities that skin factor and permeability (or relative permeability under multiphase flow condition) may change during the long-term production, especially for the area near the wellbore. These changes can be diagnosed from transient pressure with URSR A_{urc} .

3.4 Cases study

Several cases are researched to illustrate how to diagnose different kinds of nonlinearities using this novel diagnostic method.

3.4.1 Permeability and skin factor change case

As discussion above, considering the effect of formation compaction, subsidence or damage during the long production, reservoir properties and well conditions near/in the wellbore such as permeability-thickness kh and skin factor S may change with time.

In this case, a single oil phase reservoir model is researched, shown in **Figure 3-15**. As shown in **Figure 3-16**, reservoir permeability declines from 50 mD to 38 mD and skin factor increases from 6 to 12 during 10 days production. **Figure 3-17** presents the WT of pressure data and the calculated URSR A_{urc} . The changes in transient pressure

between two successive flow events are identified with amplitudes of WT coefficients. According to the novel diagnostic method, URSR A_{urc} is calculated through $A_{urc} = A/\Delta q$. URSR A_{urc} rises sharply from 0.9 to 1.8, compared with the constant value in the linear system, and verifies that there are nonlinearities in the reservoir due to changes in reservoir properties and well conditions.

The increasing URSR A_{urc} indicates the declining Production Index (PI) and the production condition near the wellbore becoming worse. Especially, the sharply increasing A_{urc} needs more attention for production monitoring, and remedy operations may be needed, such as fracturing, acidizing to improve well conditions.

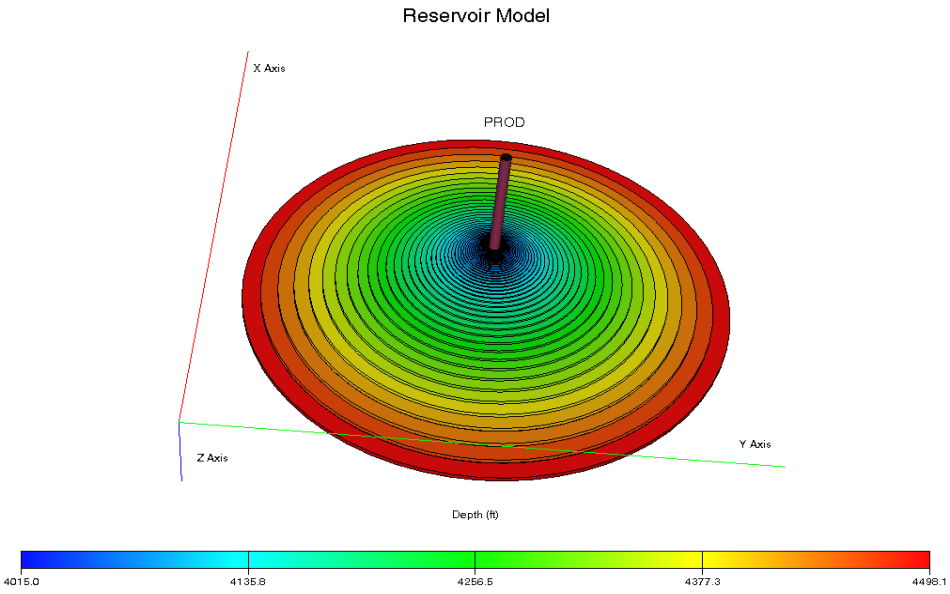

Figure 3-15: The reservoir model with time-varying skin factor and permeability.

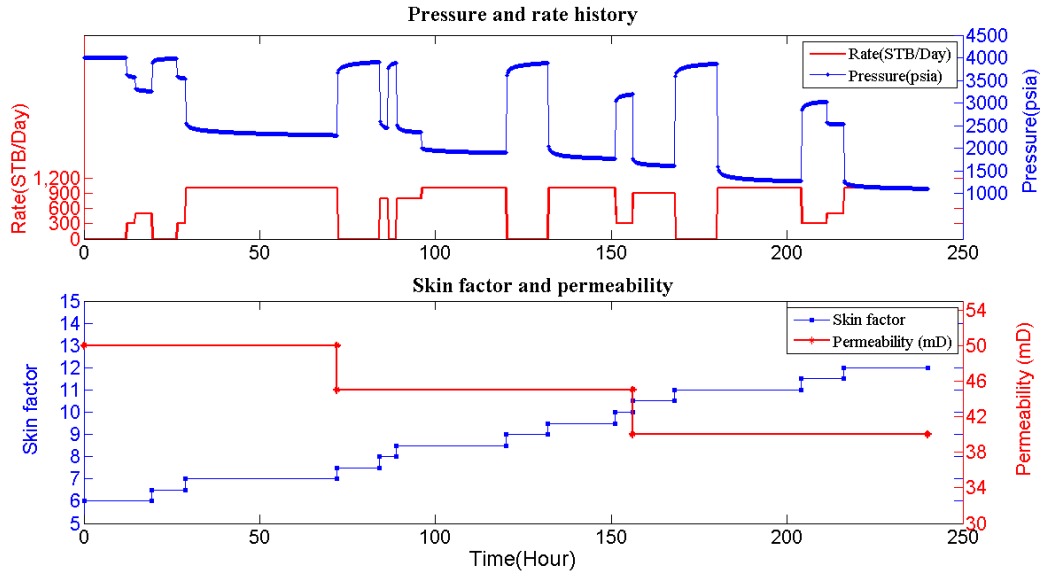

Figure 3-16: Skin factor and permeability change with time during the production history.

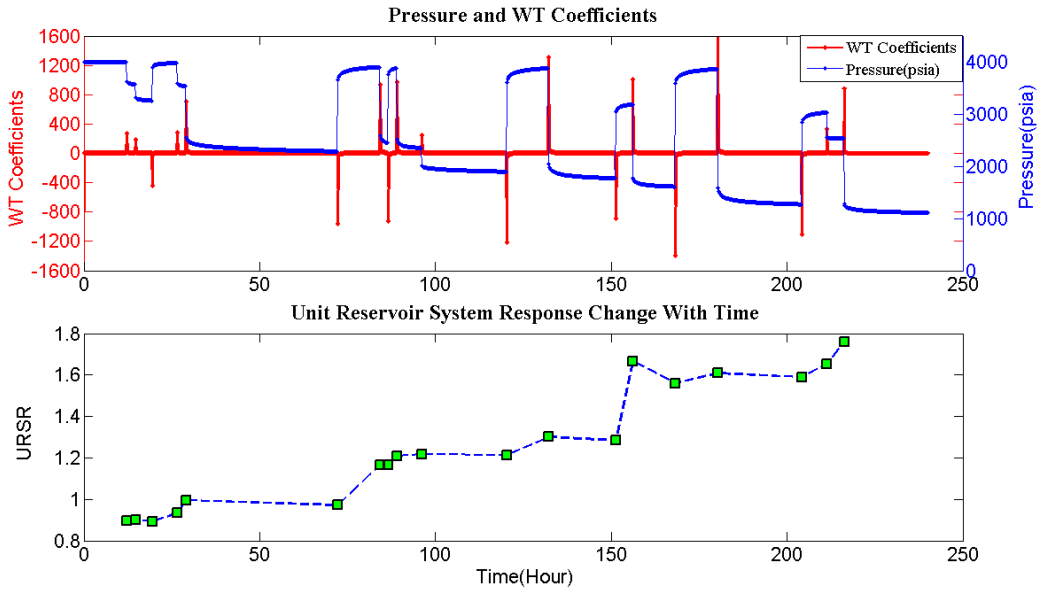

Figure 3-17: After pressure data is processed by Haar wavelet, URSR A_{urc} is calculated and it is time-varying due to in the changes in skin factor and permeability.

3.4.2 Real gas flow

The pressure-dependent gas properties make the flowing behaviour high complex than that in the liquid flow system. This nonlinearity causes superposition principle and related methods invalid, and pseudo-pressure or pseudo-time should be used to linearize the diffusivity equation.

The production history of gas reservoir is shown in **Figure 3-18**, and the gas PVT properties are shown in **Table 3-4**. The gas formation volume factor (FVF) and viscosity vary a lot with the pressure especially when the pressure is low. After the pressure data processed with WT, URSR A_{urc} is calculated, as shown in **Figure 2-19**. Different from the constant value in linear systems, in the gas reservoir A_{urc} function changes with time, due to pressure-dependent gas properties. In addition, the larger the production rate is, the larger changes in down-hole pressure will be, which leads to larger variations in URSR A_{urc}.

Table 3-4: PVT properties in the real gas reservoir

Pressure (psia)	FVF (rb /Mscf)	Viscosity (cp)
50	65.740507	0.012857
205.26316	15.854459	0.012965
360.52632	8.9411518	0.01314
515.78947	6.1938316	0.013333
671.05263	4.7210394	0.013637
826.31579	3.8044907	0.013949
981.57895	3.1803585	0.014198
1136.8421	2.7289377	0.014397
1292.1053	2.3880366	0.014657
1447.3684	2.1221428	0.014936
1602.6316	1.9094889	0.015244
1757.8947	1.7359831	0.015551
1913.1579	1.592094	0.015859
2068.4211	1.4711396	0.016169
2223.6842	1.3682964	0.016568
2378.9474	1.2799878	0.016967
2534.2105	1.203506	0.017366
2689.4737	1.1367658	0.017765
2844.7368	1.0781317	0.01819
3000	1.0263033	0.018632

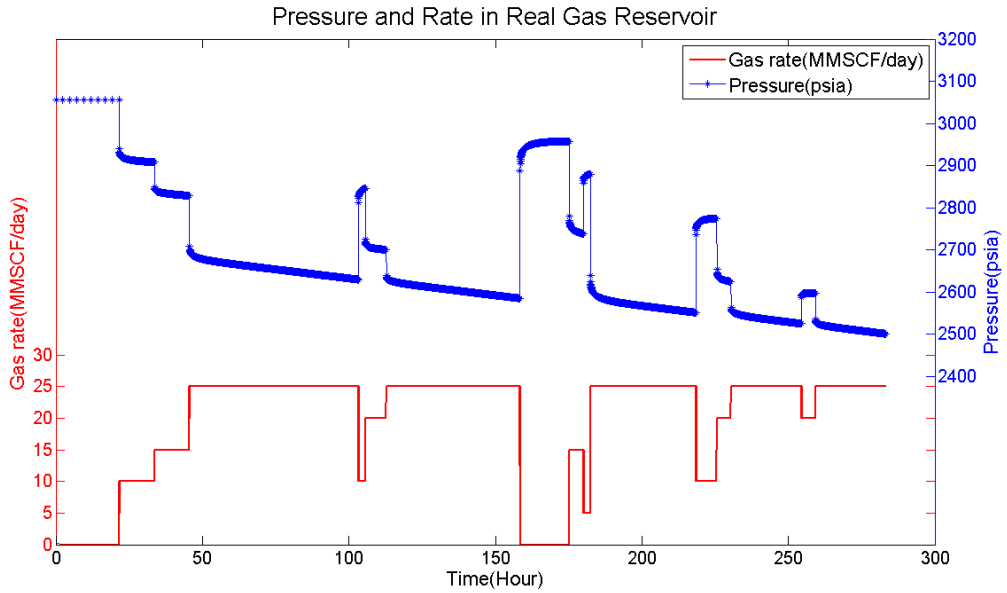

Figure 3-18: Production history in the gas reservoir case

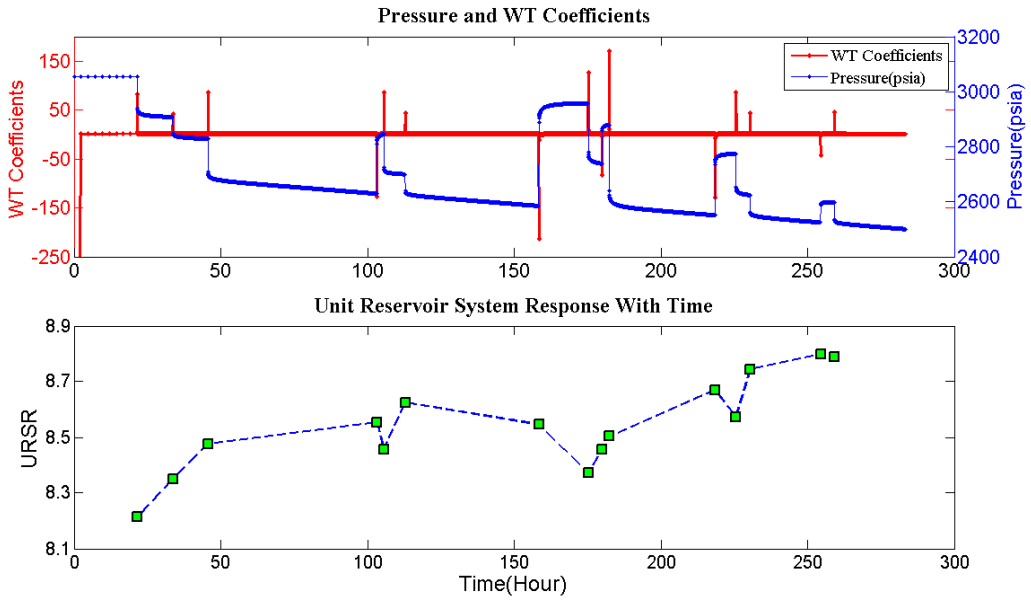

Figure 3-19: The calculated A_{urc} is time-varying due to the pressure-dependent gas properties.

For the long-term production, gas reservoir may come into depletion period. The decreasing average formation pressure causes more changes in gas properties. **Figure 3-20** shows the production history with 800 hours. The reservoir comes into pseudo-steady state and average pressure declines nearly 500 psi. With wavelet transform, URSR A_{urc} is calculated. The increasing URSR A_{urc} indicates the large changes in gas PVT properties due to reservoir depletion.

When there is significant depletion, pseudo-pressure does not correct the changes in gas compressibility. Material balance should be applied to make correction.

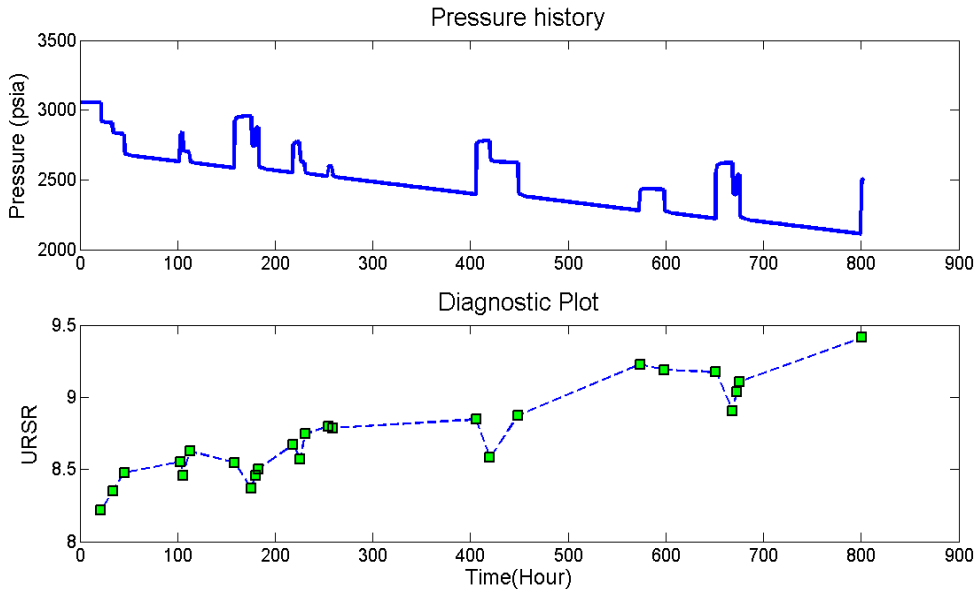

Figure 3-20: URSR A_{urc} increases a lot due to the depletion in the real gas reservoir.

3.4.3 Non-Darcy flow

In the vicinity of the production well, very high velocity of fluid can change the flow from laminar to turbulent, which causes additional pressure drop by the inertial effect. Therefore, equation of Darcy flow is inapplicable and a new accurate equation is needed. To overcome the deficiency, Forchheimer (1901) modified Darcy flow equation by adding inertial effect:

$$-\frac{dp}{dr} = \frac{\mu}{k}v + \beta\rho v^2 \tag{3.14}$$

Here ρ is fluid density, v is flow velocity and $\beta$is non-Darcy flow coefficient. In Eq. 3.14, the relationship between pressure drop and flow rate is nonlinear. The larger the non-Darcy flow coefficient β is, the high nonlinear the flow equation will be. Turbulent flow effect near the wellbore leads to rate-dependent skin which changes for different flow periods.

Figure 3-21 shows the diagnostic result when non-Darcy flow considered for the dry gas reservoir case. The larger non-Darcy flow coefficients β, the larger changes in A_{urc} will be. In fact, the non-Darcy flow not only breaks the linear relationship between flow rate and pressure drop, but also causes additional pressure drop, which

leads to more changes in gas PVT properties. These two factors make the large change in A_{urc}, which means high nonlinearities in the reservoir.

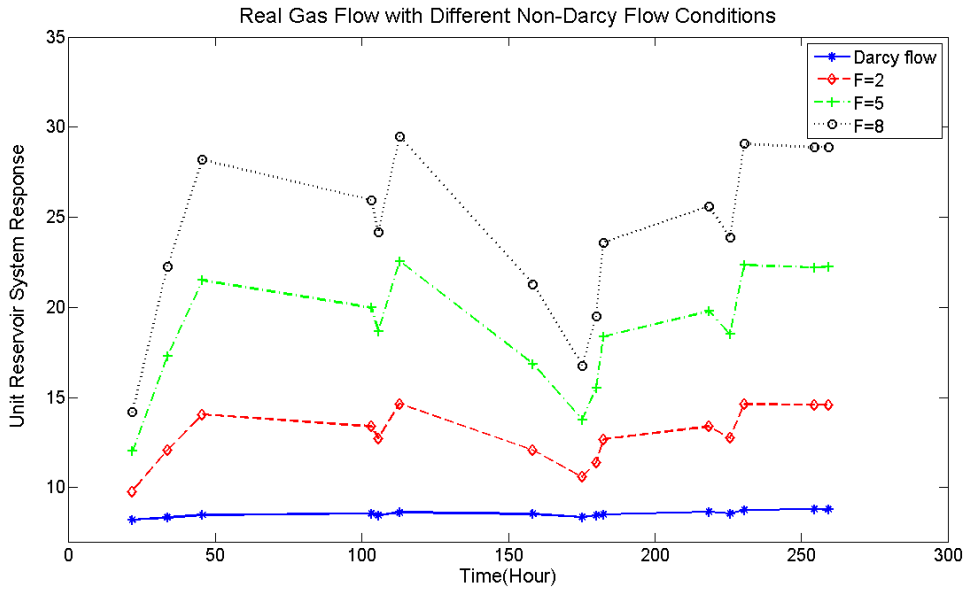

Figure 3-21: URSR A_{urc} for gas reservoir at different non-Darcy flow conditions. The larger the non-Darcy flow coefficient is, the lager changes in A_{urc} will be.

If there were a kind of uncompressible fluid could produce as large flow rate as gas, the pure effect of non-Darcy flow can be investigated. Numerical experiment can realize that by setting constant fluid properties and large production rate with turbulent flow near the wellbore. As **Figure 3-22** shows, A_{urc} is constant for Darcy flow but it changes with time for non-Darcy flow. The larger the non-Darcy flow coefficient β is the larger change in A_{urc} will be. As fluid properties are constant, the reason of A_{urc} change is non-Darcy flow, which breaks linear relation between pressure change and flow rate.

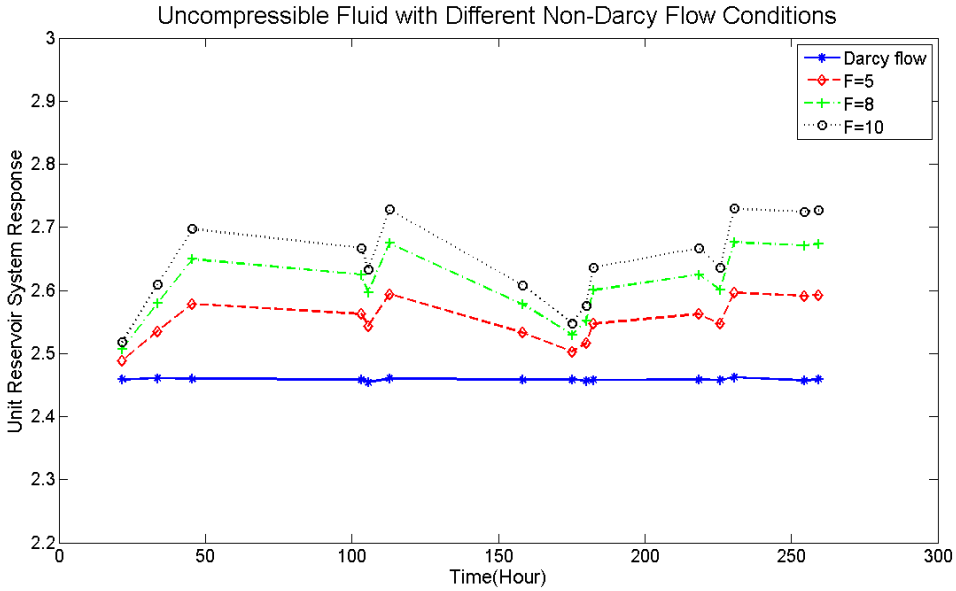

Figure 3-22: The A_{urc} function for the uncompressible fluid flow at different non-Darcy flow conditions. The larger non-Darcy flow coefficient, the lager change in A_{urc} will be.

Modified isochronal test is usually used for deliverability tests in gas reservoir, to determine the gas production rate at a certain back pressure. During this test, the time of producing and shut-in is equal with increasing DD and BU sequences. **Figure 3-23** shows a case of modified isochronal test.

Modified isochronal test also can provides non-Darcy flow analysis. Non-Darcy flow causes rate-dependent skin near the wellbore, and the total skin in gas reservoir is:

$$S' = S + Dq_{sc} \qquad (3.15)$$

where D is called non-Darcy coefficient. Total skin factor S' has to be evaluated at different rate.

In frequency domain, the non-Darcy flow can be diagnosed. The pressure history is simulated with different non-Darcy flow coefficients. URSR A_{urc} is calculated and plotted with corresponding flow rate, as shown in **Figure 3-24**. When there is no non-Darcy flow, URSR is almost constant. The larger the non-Darcy flow coefficient is, the larger the slop will be.

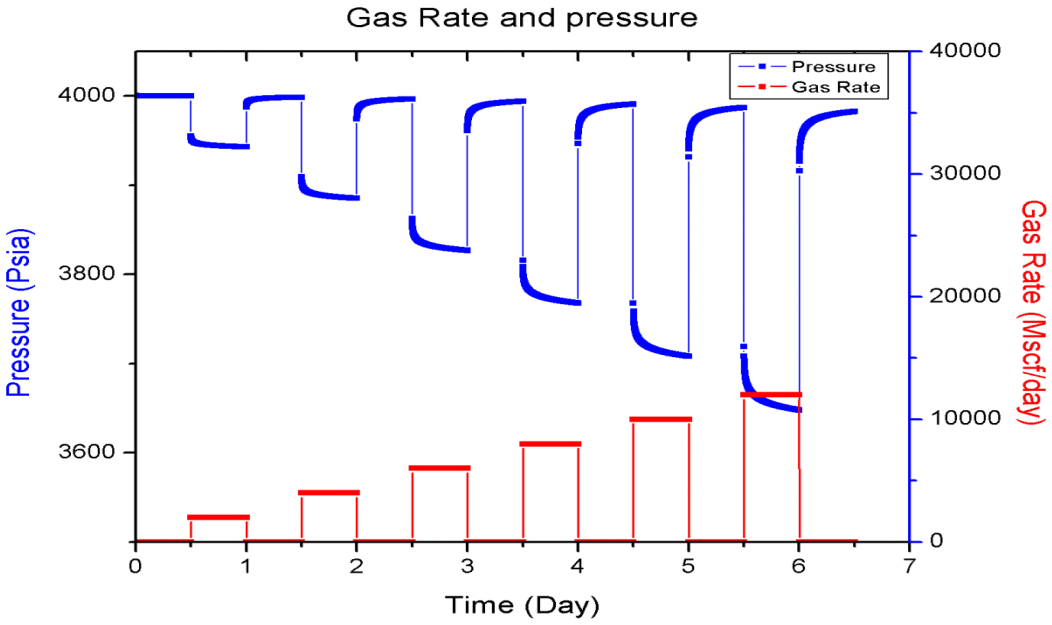

Figure 3-23: Modified isochronal test for gas reservoir

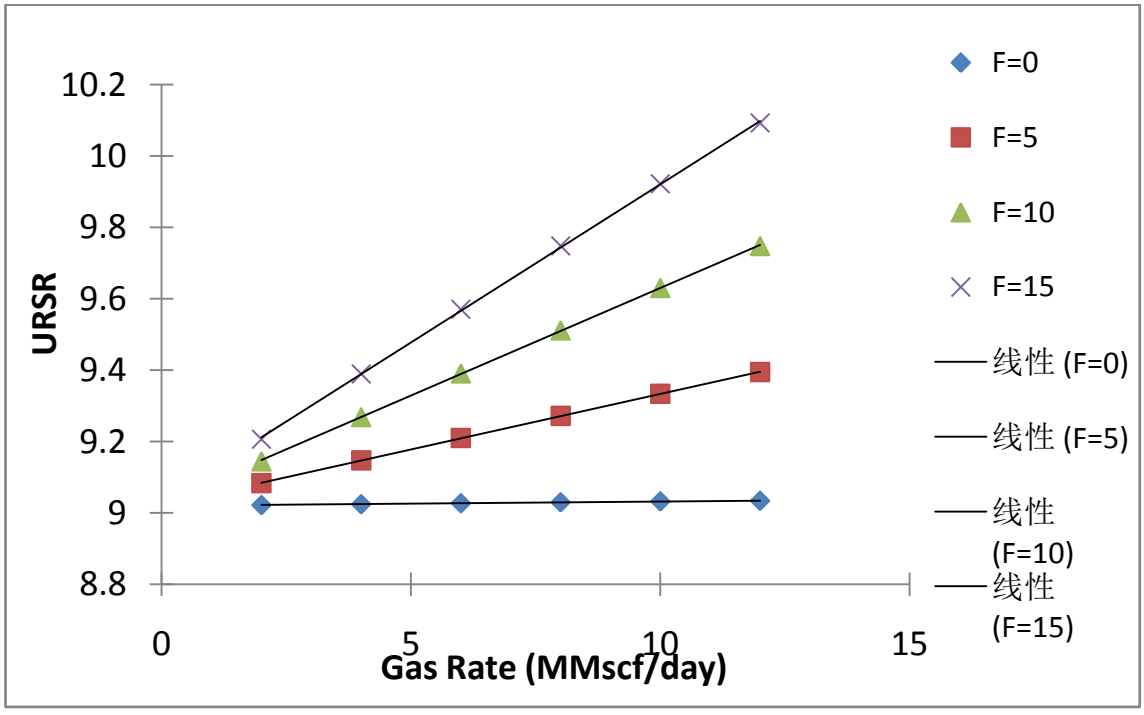

Figure 3-24: URSR A_{urc} of modified isochronal test.

3.4.4 Oil and gas two-phase flow after gas out of solution

When the down-hole pressure drops below the bubble point pressure, dissolved gas is out of solution and flow changes to gas and oil two-phase flow. When several phases flow in the reservoir at same time, the flow ability of certain phase is affected by other phases. The high gas saturation near the wellbore reduces the relative permeability of oil phase, and the flow ability of each fluid is the function of saturation, which changes

with time and space. The dynamic changes in relative permeability of each phase due to saturation change and pressure-dependent gas properties make the system highly nonlinear.

Figure 3-25 shows production history of a simulated oil reservoir with dissolved gas. Reservoir properties are shown in **Table 3-5**, and the PVT properties of live oil are shown in **Table 3-6.** The bubble point is 4000 psi. At the beginning of production history, the production rate is small and down-hole pressure is above the bubble point. After that, down-hole pressure drops below the bubble point and dissolved gas is out of solution. With WT processing transient pressure data, URSR A_{urc} is calculated and shown as **Figure 3-26**. Initially, URSR A_{urc} is constant as only single oil phase is flowing in the reservoir, and therefore the reservoir is a linear system. For the time when the dissolved gas is out of solution, URSR A_{urc} is increases immediately. The reason is there are oil and gas two-phase flow near the wellbore and the flow abilities are reduced due to the total mobility change. Then URSR A_{urc} is time-varying and it fluctuates with time due to the pressure-dependent gas properties.

Table 3- 5: Some reservoir properties of oil with dissolved gas reservoir

Initial pressure, p_0	4000 psia
Reservoir radius, R	10000 ft
Thickness, h	50 ft
Permeability, k	50 mD
Porosity, ϕ	0.25
Viscosity, μ_o	1 cp
rock compressibility, C_f	3e-6 1/psi
Well radius, r_w	0.208 ft
Skin factor, S	3
Wellbore storage volume, V_w	0

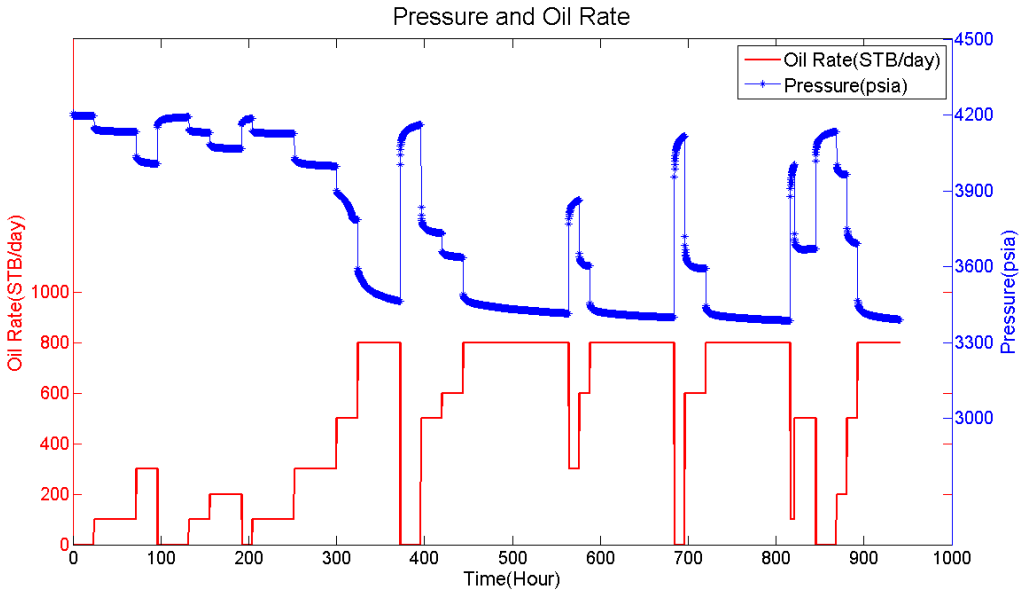

Figure 3-25: Production history for the oil reservoir with dissolved gas

Table 3-6: Live oil PVT properties (with dissolved gas)

Rs (Mscf /STB)	Pbub (psia)	FVF (rb /STB)	Visc (cp)
0.165	400	1.012	1.17
0.335	800	1.0255	1.14
0.5	1200	1.038	1.11
0.665	1600	1.051	1.08
0.828	2000	1.063	1.06
0.985	2400	1.075	1.03
1.13	2800	1.087	1
1.27	3200	1.0985	0.98
1.39	3600	1.11	0.95
1.5	4000	1.12	0.92
	4400	1.1155	0.92
	4800	1.111	0.92
	5200	1.108	0.92

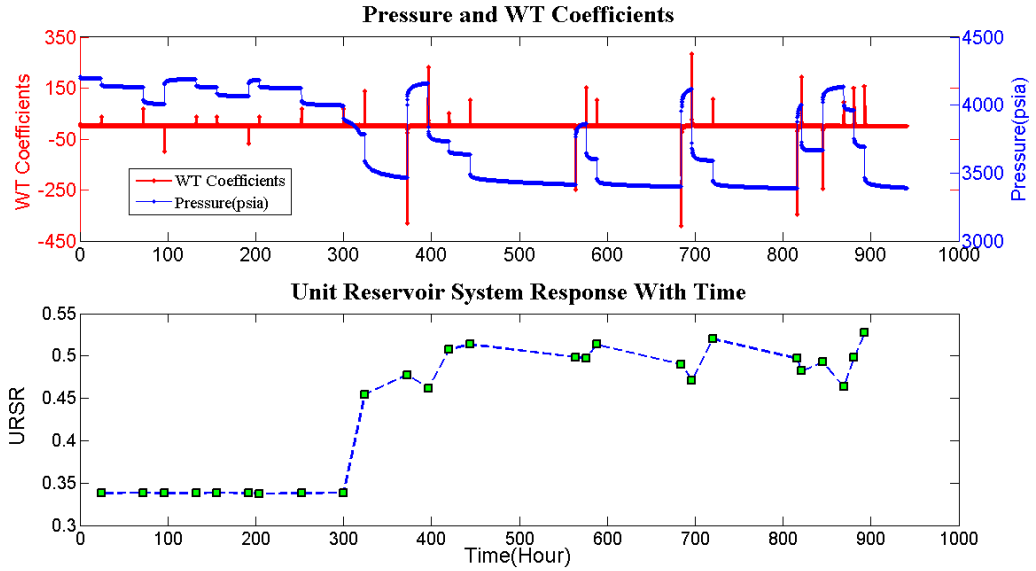

Figure 3-26: URSR A_{urc} changes sharply when gas is out solution.

When the wellbore storage effect is considered, diagnostic result is a little different, as **Figure 3-27** shows. Before gas out of solution, URSR A_{urc} is constant. However, URSR A_{urc} declines sharply when gas is out solution and A_{urc} rises after well shut-in. This phenomenon is due to phase segregation effect in the wellbore. During well shut-in period, due to difference in density, gas rises into the top of wellbore and oil accumulates at the bottom. The phase segregation phenomenon creates a variable wellbore storage as a function of time, which causes the variation of A_{urc} function.

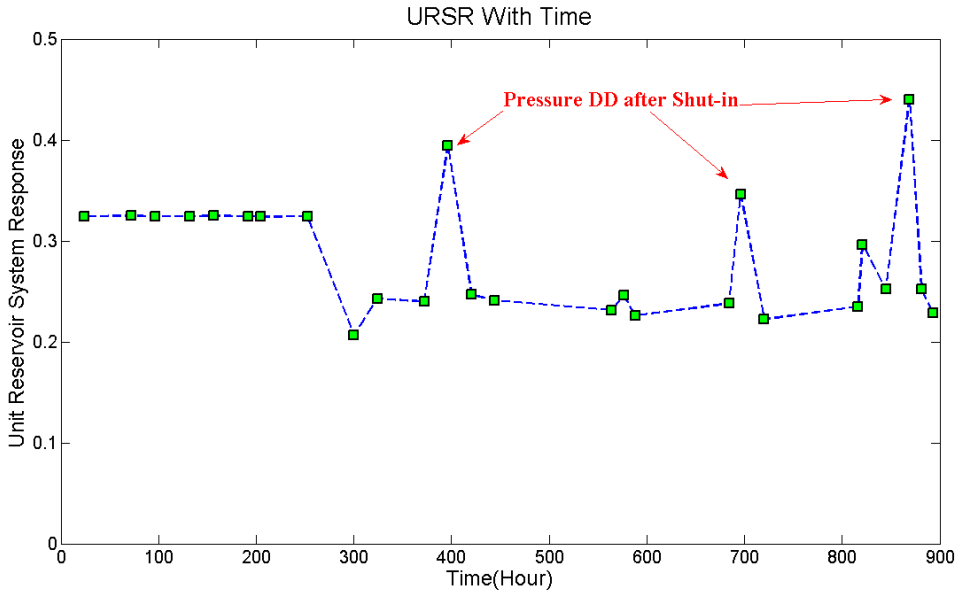

Figure 3-27: When wellbore storage is considered, URSR A_{urc} performs differently due to the phase segregation effect in the wellbore.

3.4.5 Oil and water two-phase flow after water breakthrough

Similar to the gas and oil two-phase flow, the oil and water two-phase flow after water breakthrough is also complex and causes high nonlinearity for the reservoir system. From the production point of view, water production after water breakthrough may cause many problems for productions system, such as hydrate, corrosion and scale. Diagnose the time of water breakthrough and make production optimization is an important task for reservoir engineers.

A heterogeneous oil and water two-phase flowing reservoir is taken as an example (**Figure 3-28**). This reservoir model is very heterogeneous with log normal distribution of permeability and normal distribution of porosity, as shown in **Table 3-7**. Other reservoir-well parameters are shown in **Table 3-8**. The grids near the wellbore are refined to reduce numerical dispersion.

Down-hole pressure and water cut history are shown in **Figure 3-29**, and water breaks through after 10 days production. After that, water cut increases continuously with production time.

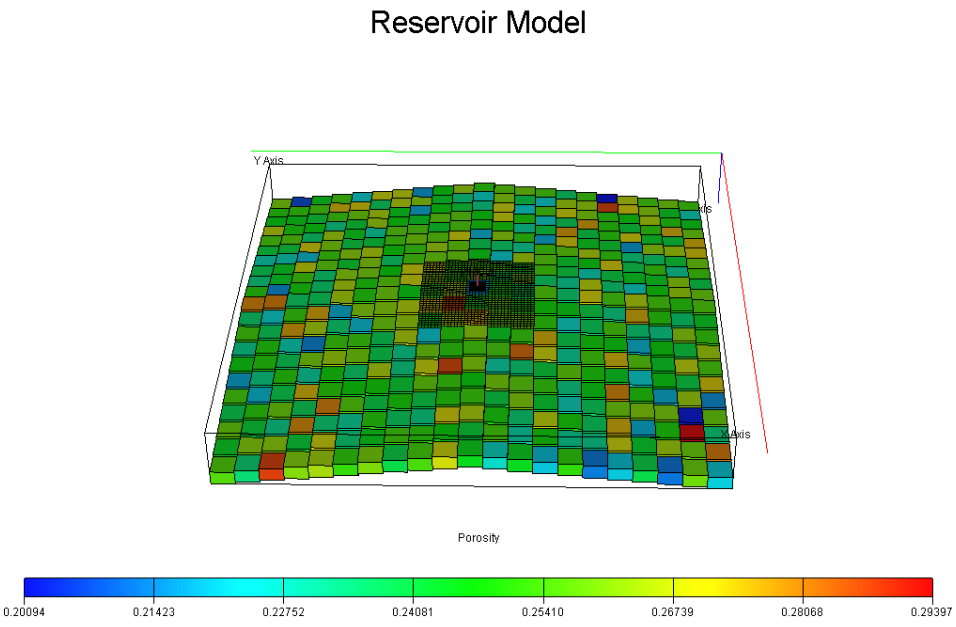

Figure 3-28: The heterogeneous oil and water two-phase reservoir model.

Table 3-7: The distribution of permeability and porosity in the oil and water two-phase reservoir

Property	Direction	Distribution	Average	Maximum	Minimum
Permeability k (mD)	x	Log normal	200	471.94	79.515
	y	Log normal	150	320.5	61.17
	z	Log normal	20	75.83	5
Porosity $\emptyset$		Normal	0.25	0.294	0.2

Table 3-8: Other reservoir-well parameters in the reservoir model.

Initial pressure, p_0	5000 psia
Reservoir length and width, L	2100 ft
Thickness, h	60 ft
Oil FVF,B_o	1.2 rb/STB
Oil compressibility, C_o	3E-6/psi
Oil viscosity, μ_o	0.7 cp
Water FVF, B_w	1 rb/STB
Water compressibility, C_w	3E-6/psi
Water viscosity, μ_w	0.3 cp
Rock compressibility, C_f	3.6E-6/psi
Well radius, r_w	0.167 ft
Skin factor, S	5
Wellbore storage volume, V_w	545.398 cu ft

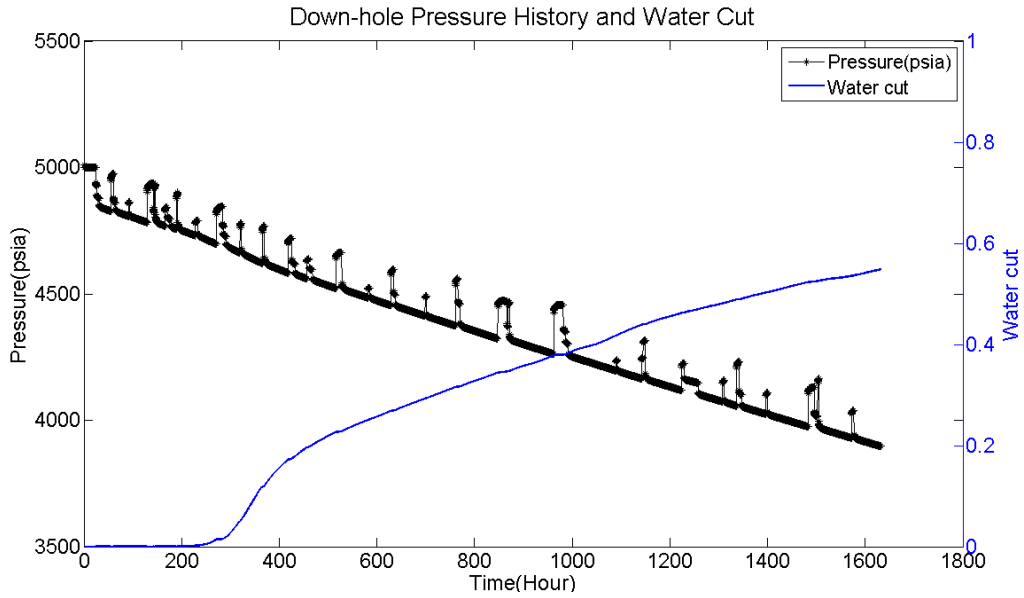

Figure 3-29: Down-hole pressure and water cut history.

With the Haar wavelet processing transient pressure data, URSR A_{urc} is calculated and shown in **Figure 3-30**. Before water breakthrough, URSR A_{urc} is constant as there is only oil flowing in the reservoir and the reservoir system is linear. In case of water breakthrough, URSR A_{urc} increases at the same time and then it changes with the increasing water cut.

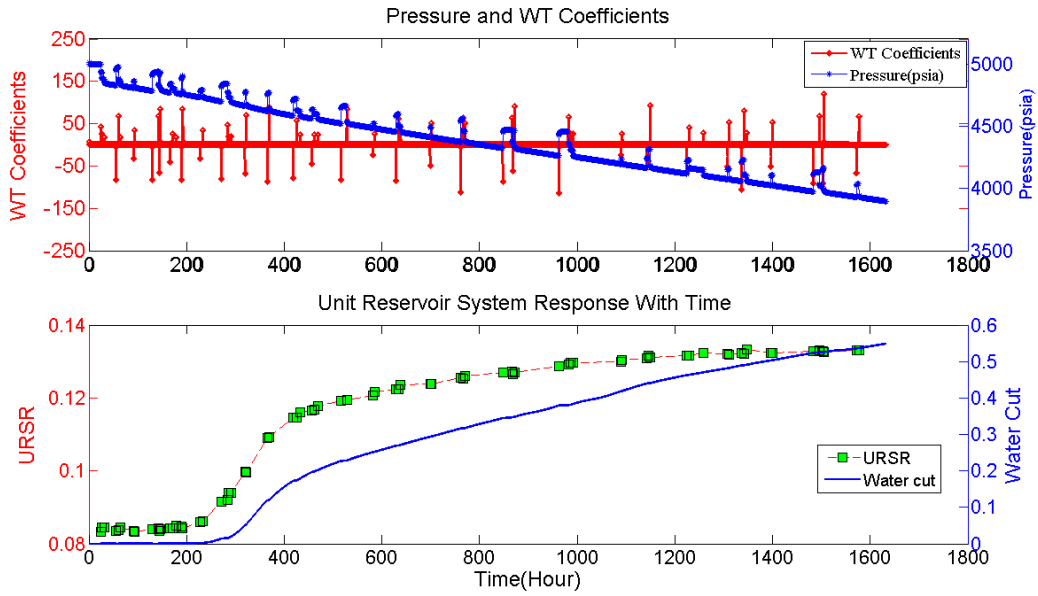

Figure 3-30: URSR A_{urc} increases in the case of water breakthrough and changes with water cut.

The reason is that after water breakthrough, the relative permeability of each phase changes with water saturation and the total mobility of fluids declines, as shown in **Figure 3-31**.

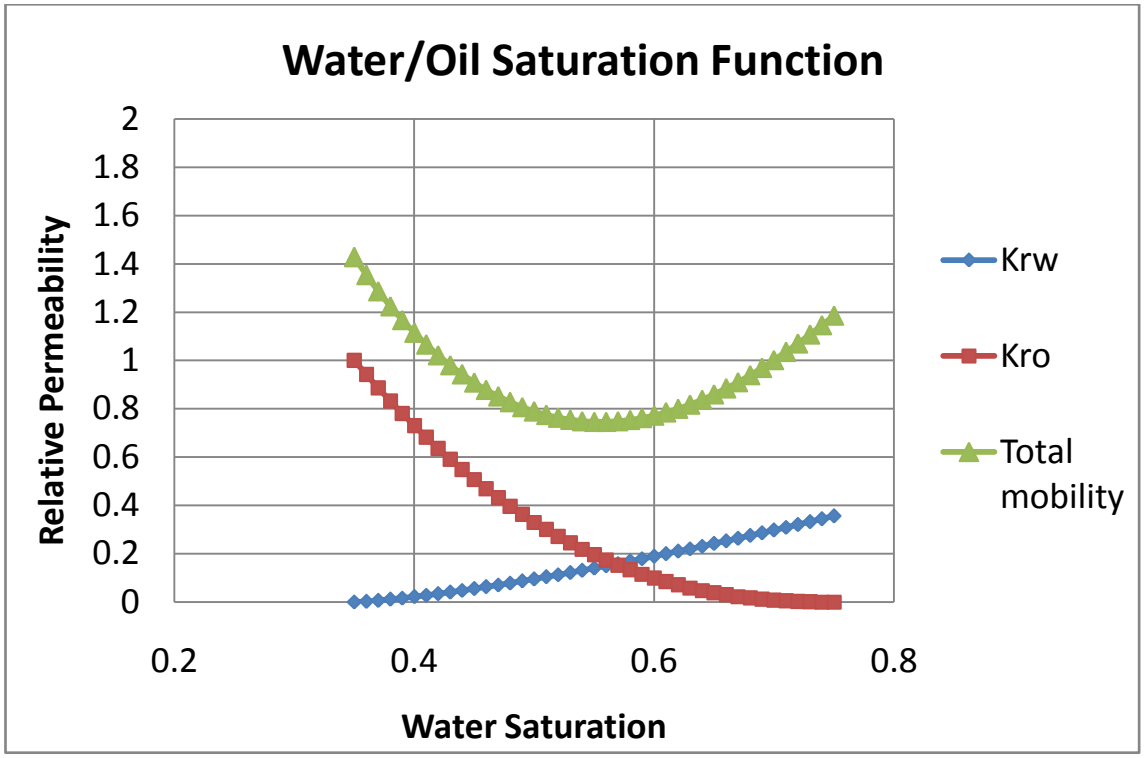

Figure 3-31: Oil and water saturation function and total mobility.

In theory, Perrine (1956) presented an approach, using an equivalent liquid flow with average properties to simplify the problem of multiphase flow. For the oil and water two-phase flow, the total mobility of the equivalent fluid is:

$$\lambda_t = \frac{k_{ro}}{\mu_o} + \frac{k_{rw}}{\mu_w} \tag{3.16}$$

Then, the fluid properties in Eq. 3.12 can be replaced by the total mobility:

$$A_{urc} \propto \frac{70.6B}{\lambda_t kh}\left[\ln t + \ln\frac{\lambda_t k}{\emptyset C_t r_w^2} - 7.43173 + 2S\right] \tag{3.17}$$

As the impact of $ln\frac{\lambda_t}{\emptyset C_t r_w^2}$ is small compared with $\frac{70.6B}{\lambda_t h}$, the relationship between URSR A_{urc} and $\frac{1}{\lambda_t}$ nearly is linear. URSR A_{urc} increases when total mobility decreases.

Water cut in the down-hole can be calculated with oil and water fraction flow theory:

$$f_w = \frac{q_w}{q_w+q_o} = \frac{\frac{k_{rw}}{\mu_w}}{\frac{k_{rw}}{\mu_w}+\frac{k_{ro}}{\mu_o}} = \frac{\frac{k_{rw}}{\mu_w}}{\lambda_t} \tag{3.18}$$

For the same water cut, the reciprocal of total mobility $\frac{1}{\lambda_t}$ and URSR A_{urc} are plotted in the same figure, as shown in **Figure 3-32**. As the figure shows, URSR A_{urc} increases proportionally with the increasing $\frac{1}{\lambda_t}$.

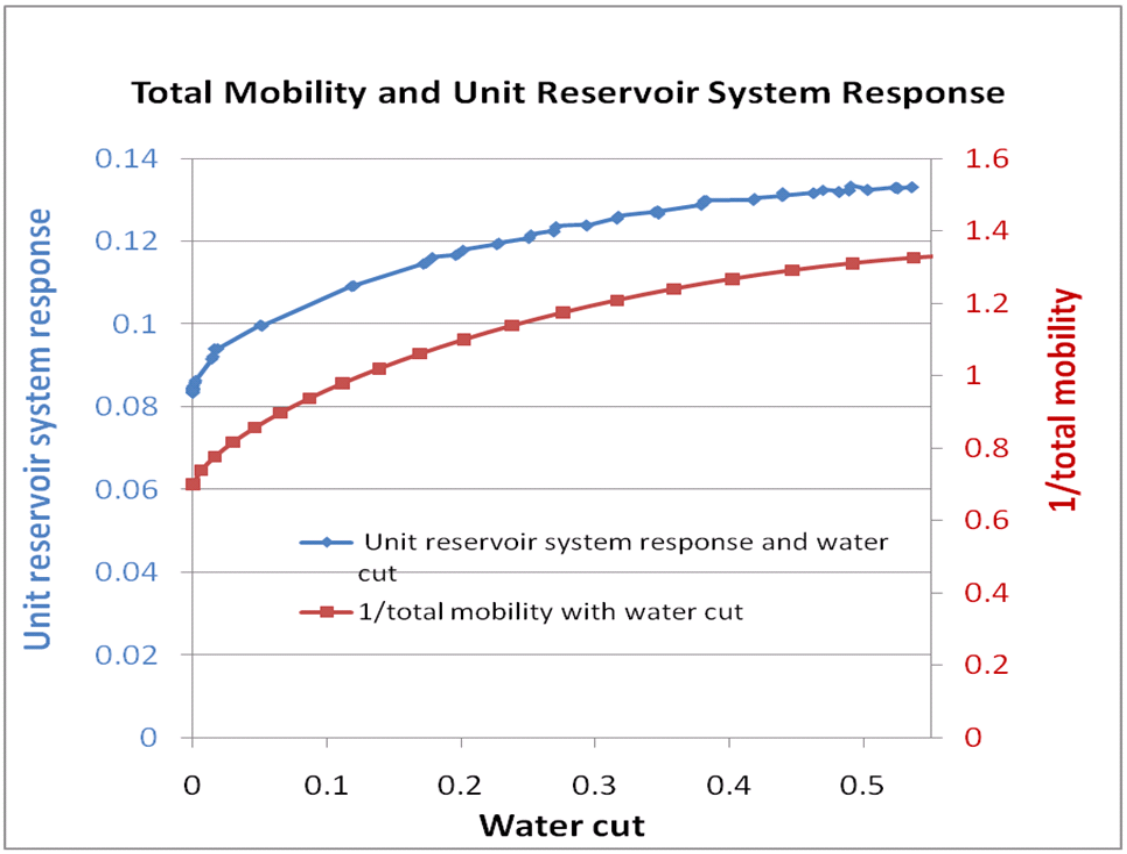

Figure 3-32: URSR A_{urc} and $\frac{1}{\lambda_t}$ for the same water cut f_w.

As well known, the larger the oil viscosity is, the earlier water will break through. **Figure 3-33** shows when oil viscosity $\mu_o = 1.2$ cp, the time of water breakthrough is earlier than that when oil viscosity $\mu_o = 0.7$ cp, and URSR A_{urc} also performs differently. URSR A_{urc} increases sharply due to water breakthrough, however, it declines slightly later though the water cut still is increasing. The reason is total mobility declines at first, but increases later with the increasing water cut, as **Figure 3-34** shows. The reciprocal of total mobility $\frac{1}{\lambda_t}$ increases at first and declines later, and leads to the same performance of URSR A_{urc}, verifying that Eq. 3.17 is correct. When oil viscosity μ_o is 1.5 cp, these phenomena become clearer, shown in **Figure 3-35**. The water breakthrough happens earlier, and URSR A_{urc} increases at the time of water

breakthrough but declines later due to the change in total mobility, shown in **Figure 3-36**.

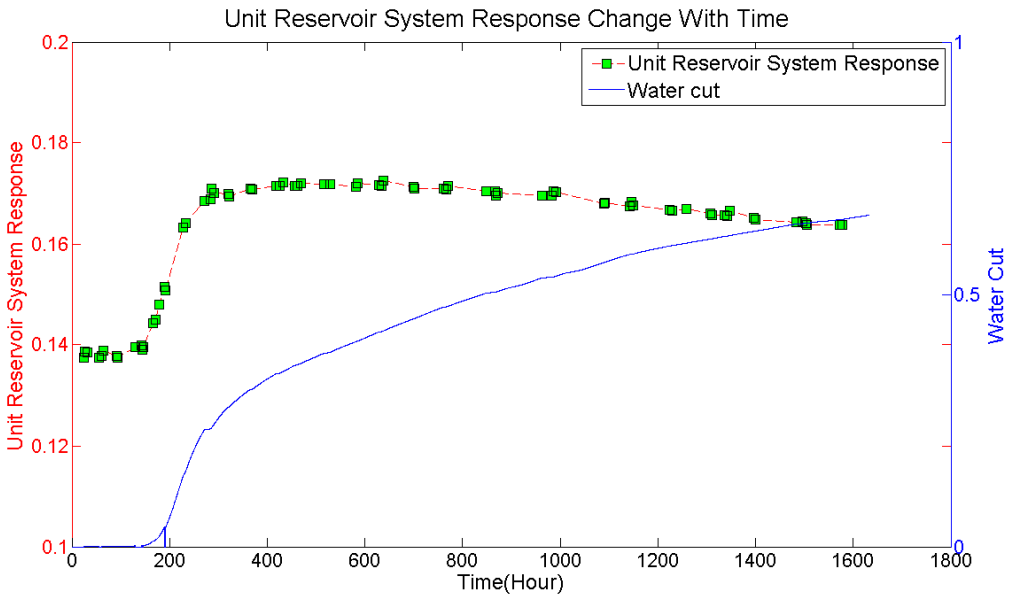

Figure 3-33: URSR A_{urc} increases at first but declines later when oil viscosity is 1.2 cp.

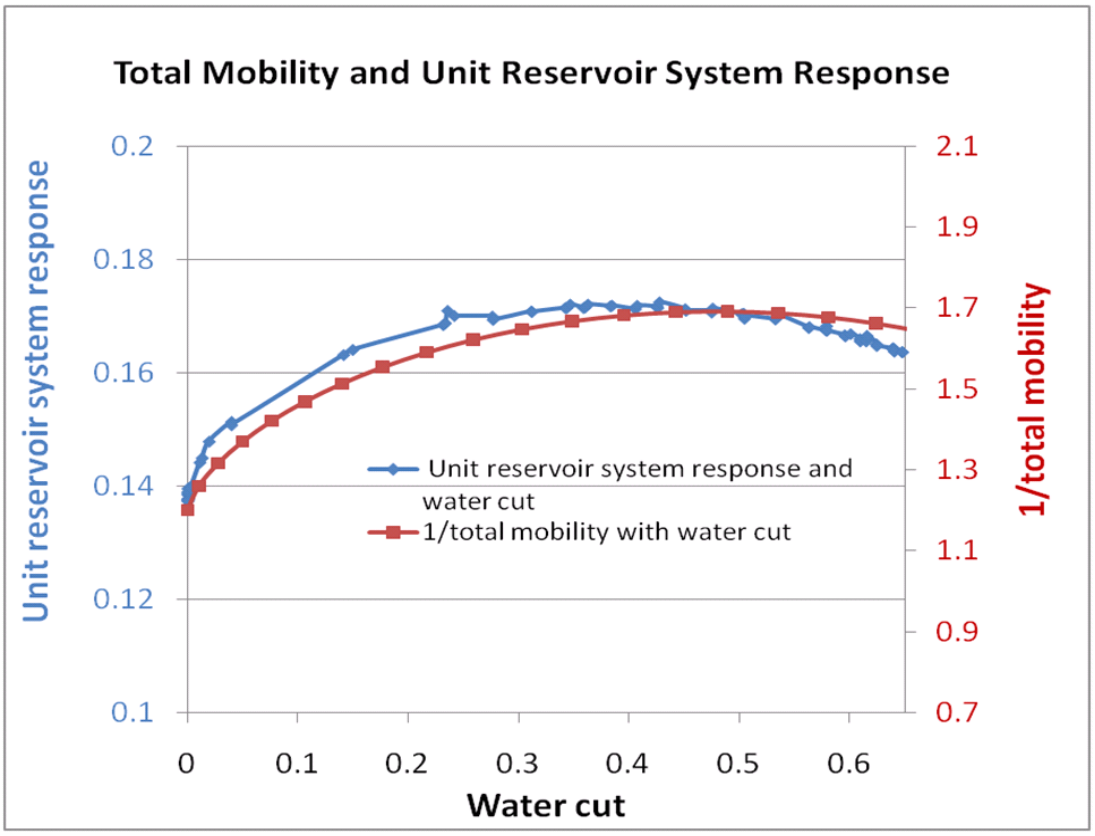

Figure 3-34: URSR A_{urc} and $\frac{1}{\lambda_t}$ when μ_o=1.2 cp.

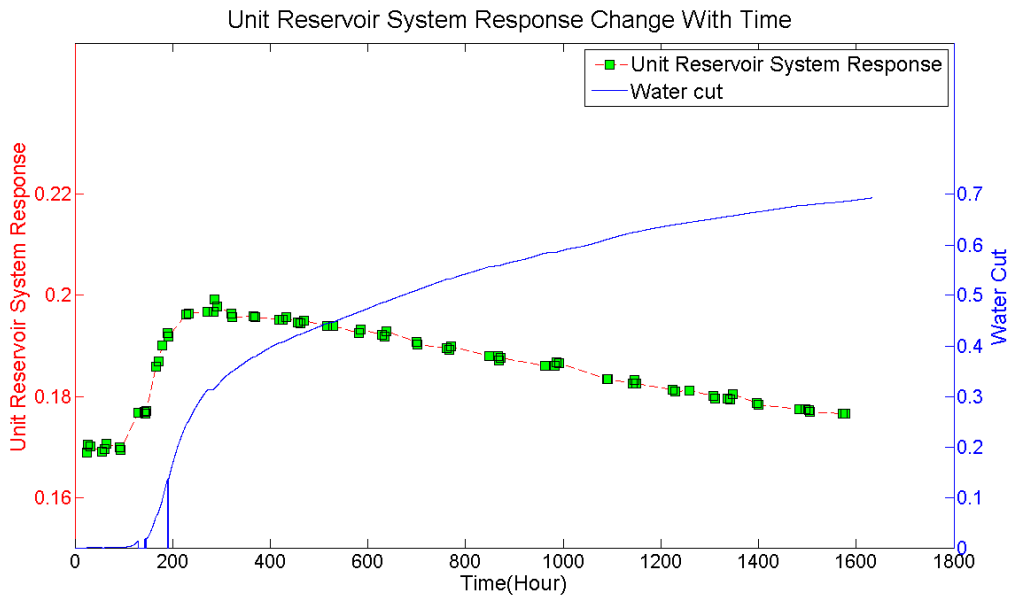

Figure 3-35: URSR A_{urc} and water cut f_w at the down-hole when μ_o=1.5 cp.

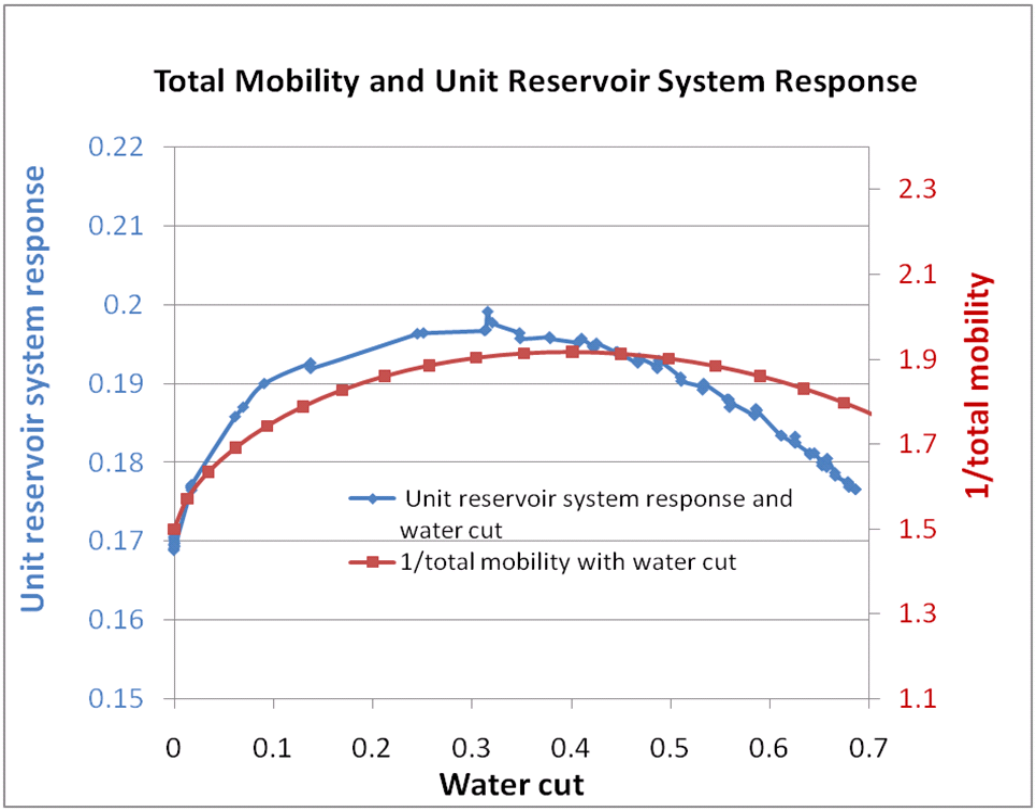

Figure 3-36: URSR A_{urc} and $\frac{1}{\lambda_t}$ when μ_o=1.5 cp.

3.4.6 The interference between production wells

For the reservoir with more than one production well, production interference is common. **Figure 3-37** shows a heterogeneous reservoir model with two interference wells. The production history and URSR A_{urc} of two wells are shown in **Figure 3-38**.

After 75 days production the interference between wells has already formed, but the diagnostic function URSR A_{urc} is constant with time for each well even there is interference effect.

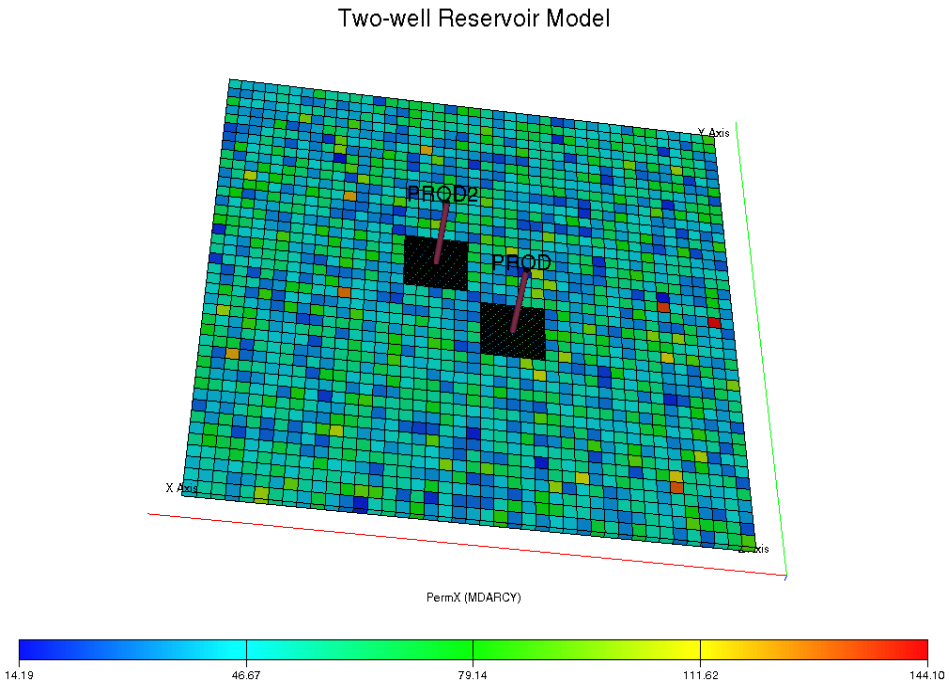

Figure 3-37: The reservoir model with two production wells.

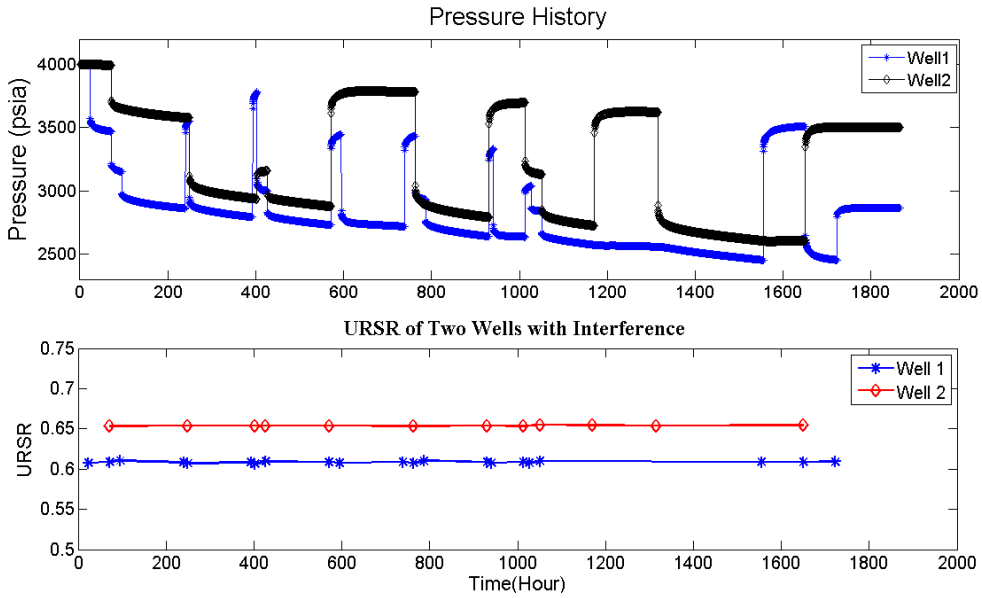

Figure 3-38: Production history and URSR A_{urc} for two interference wells.

Although well interference is not nonlinearity, analysing the transient pressure data with interference is challenging. The measured down-hole pressure of one well contains not only self production response, but also includes pressure response from another

interference wells. As a result, deconvolution can't be applied directly and multi-well deconvolution algorithm is needed (Levitan 2007, Wang 2010).

3.5 Discussion

3.5.1 Time interval

Before applying this novel diagnostic method, transient pressure data should have the equal time interval, which is required by the wavelet algorithm. For the same reservoir system, different values of URSR A_{urc} are obtained if the time intervals of pressure data are different. The small time step tends to have small A_{urc} value but the accuracy is higher. Even there is no nonlinearity in the reservoir, the value of A_{urc} changes if the pressure data has un-uniform time steps, as shown in **Figure 3-39**. In fact, URSR A_{urc} has logarithmic relationship with time step, as shown in **Figure 3-40**.

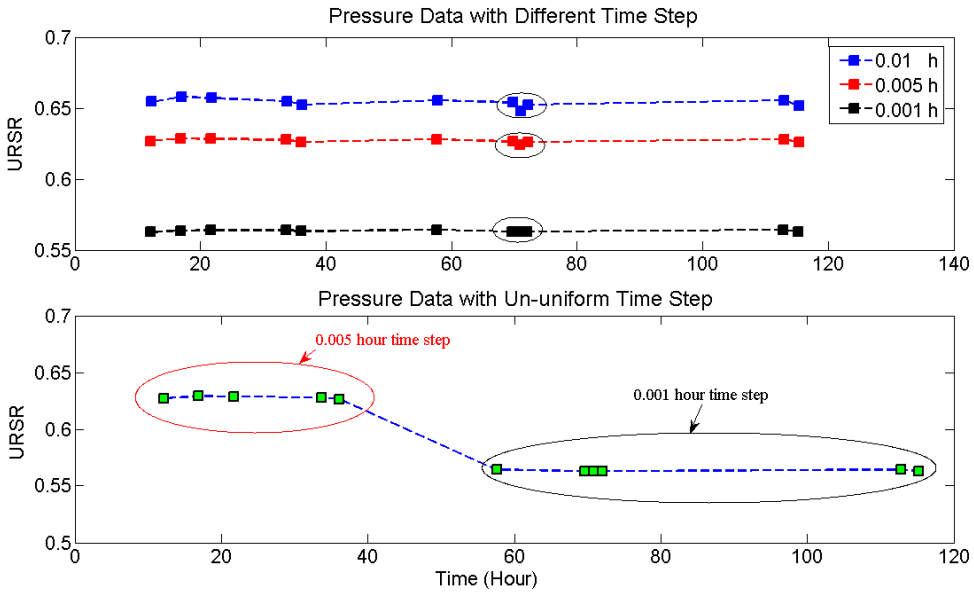

Figure 3-39: The URSR A_{urc} is different for the pressure data with different time steps.

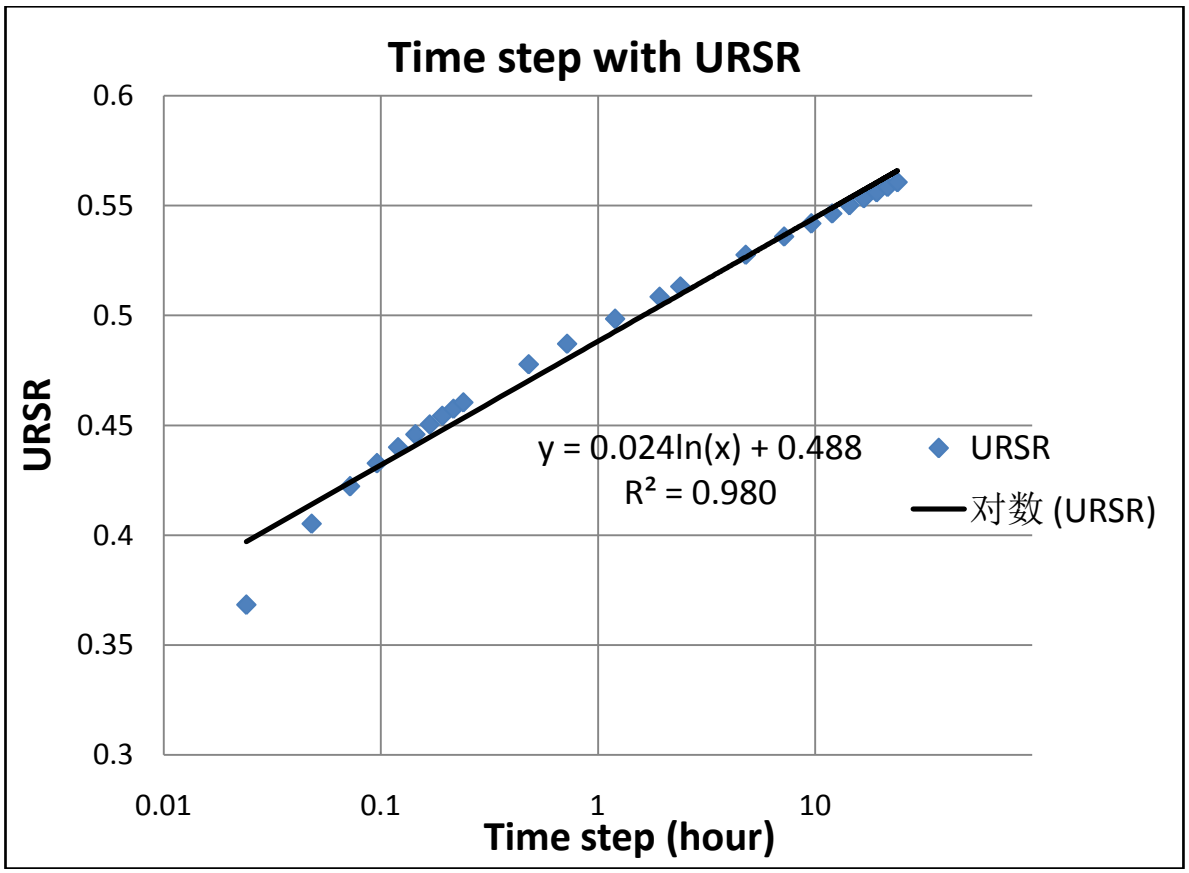

Figure 3-40: URSR A_{urc} has logarithmic relationship with time step.

3.5.2 Radius of investigation

As the time of pressure change between two successive flow events is short, the diagnostic radius is limited according to the equation of radius of investigation:

$$r_{inv} = 0.029\sqrt{\frac{k\Delta t}{\phi\mu c_t}} \tag{3.19}$$

The diagnostic radius is nearly dozens of feet around the wellbore. However, reservoir conditions near the wellbore are curial for productions, as the pressure drop mainly is around the wellbore.

The diagnostic method can benefit production monitoring. Changes in reservoir properties and flow conditions near the wellbore can be diagnosed with URSR A_{urc}. Abnormal changes in URSR A_{urc} indicate production problems in/near the wellbore, and remedy operations should be taken to optimize the production. Furthermore, the near wellbore model needs update to match the field performance.

3.5.3 Flow rate

URSR A_{urc} is a relative function, and the value doesn't have meaningful information. The change of URSR A_{urc} is very useful instead, as it provides the information related to whether or not there is change in reservoir properties and well conditions and how much of the change.

Flow rate information is need when calculating URSR A_{urc}. Unfortunately, rate information is not always available in field practice. As flow rate is the key for pressure-transient analysis, reconstructing unknown flow rate is important. Flow rate history reconstruction is discussed in Chapter 4.

3.6 New procedures of long-term transient pressure analysis

As discussed before, nonlinearity diagnostic is a crucial procedure in long-term transient pressure data analysis. **Figure 3-41** presents the novel workflow of long-term transient pressure data analysis is proposed, and this workflow can be divided into four major steps: pressure data processing, nonlinearity diagnostic and evaluation, pressure data analysis, reservoir management and mode calibration.

Pressure data processing In this procedure, pressure data is collected and processed before analysis, including data interpretation, denoising, outlier removal, transient identification, data reduction and etc.

Nonlinearity diagnostic and evaluation Nonlinearities which cause superposition principle invalid in the reservoir system are diagnosed with the novel diagnostic method using URSR A_{urc}. These nonlinearities include multiphase flow, non-Darcy flow and time-dependent reservoir-well parameters. If the reservoir system is nonlinear, the degree of nonlinearity is evaluated.

Pressure-transient analysis (PTA) For the pressure without nonlinearity, conventional pressure-transient analysis (PTA) methods which are based on the linear assumption are valid, such as Horner analysis, pressure derivative analysis and deconvolution, but it is more complex to analyse the pressure with nonlinearity. Some nonlinearity can be linearized with suitable transforms, such as pseudo-pressure for real gas. If the nonlinearity is low in a certain time, the reservoir system can be approximated to be linear. With the nonlinearity diagnostic and evaluation result, uncertainties due to

nonlinearities can be controlled. For the pressure data with high nonlinearities, numerical methods are the better way.

Reservoir management and model calibration The derived reservoir information can be used for production monitoring, real-time reservoir management, reservoir model calibration and future forecasting.

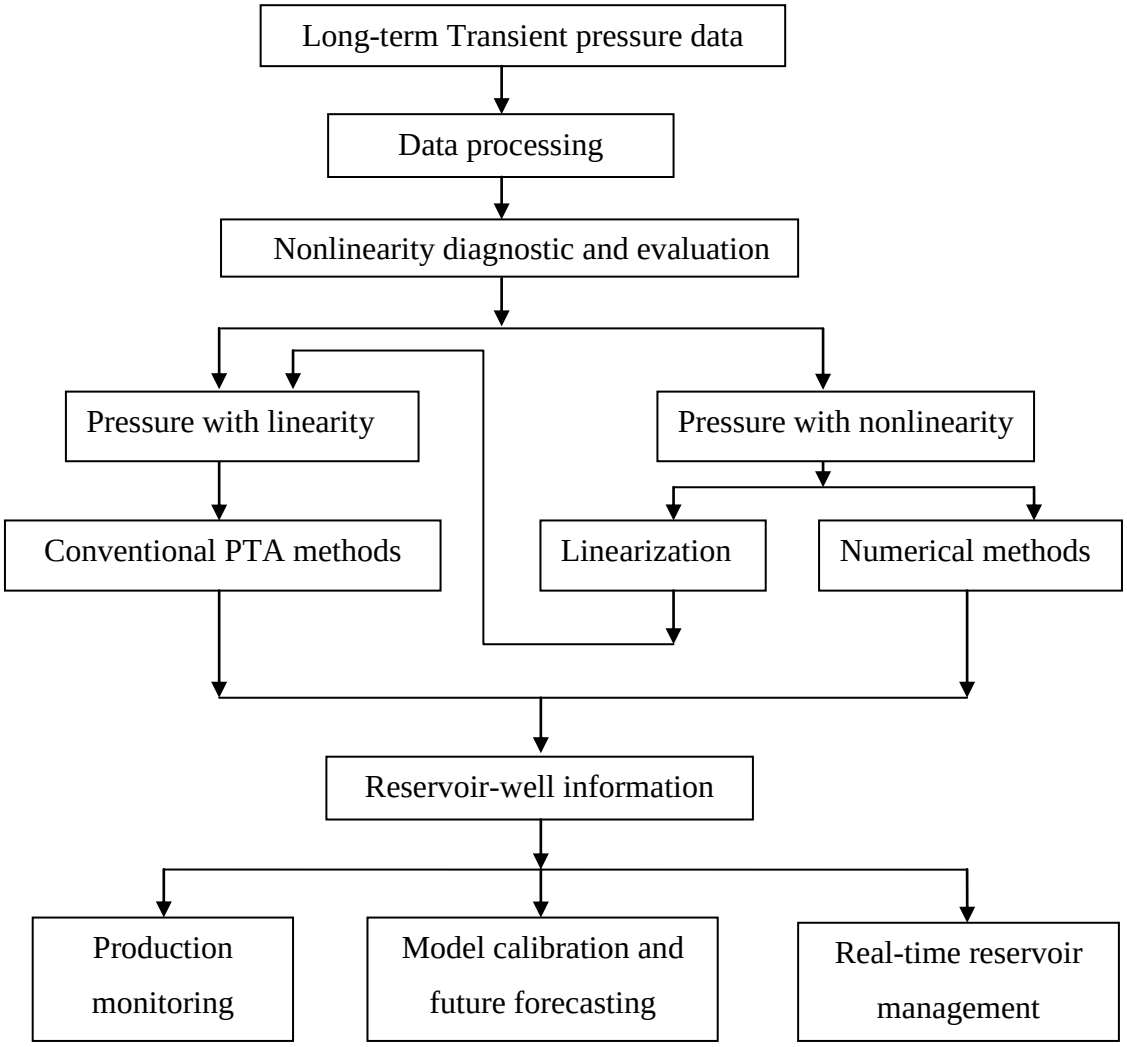

Figure 3-41: New procedures of long-term transient pressure analysis

3.7 Chapter conclusions

With Wavelet Transform (WT), a novel nonlinearity diagnostic method has been developed. This method can effectively diagnose nonlinearities from transient pressure, which are due to the changes in reservoir properties and flow conditions near the wellbore. This method is model- independent, and only pressure data and flow-rate information is used. Through the process of theory development and cases studies, the following conclusions can be drawn:

1. URSR A_{urc} is an effective function to diagnose nonlinearities. For the linear systems, where reservoir-well parameters are constant, URSR A_{urc} is constant with time. When there are nonlinearities near the wellbore, URSR A_{urc} is time-varying.
2. The large changes in URSR A_{urc} mean high nonlinearities, due to large changes in reservoir properties and flow conditions. Therefore, the nonlinearities can be evaluated quantitatively.
3. When URSR A_{urc} is time-varying, the reservoir system is nonlinear and analysis of transient pressure data using the methods based on superposition principle may lead to misleading results.
4. URSR A_{urc} is more sensitive to the changes in skin factor and (effective) permeability than other reservoir-well parameters.
5. Pressure-dependent PVT properties, reservoir depletion and non-Darcy flow in the gas reservoir can be diagnosed with the URSR A_{urc}.
6. For the oil reservoir with dissolved gas, before gas out of solution, URSR A_{urc} is constant. After that, URSR A_{urc} is time varying due to total mobility change, phase segregation in the wellbore and pressure-dependent gas properties.
7. Water breakthrough can be detected with the sudden increasing URSR A_{urc}. After water breakthrough, URSR A_{urc} changes with the total mobility change.
8. URSR A_{urc} can be utilized as a production monitoring tool. Abnormal increasing URSR A_{urc} indicates the reduction in production index (PI) for the production wells, and special cautions and remedy responses are needed to optimize the production.
9. New procedures of long-term PDG pressure data analysis have been proposed. Nonlinearity diagnostic and evaluation is a crucial procedure before PTA, as it can makes sure that suitable PTA methods are selected and reduce analysis uncertainties.

Chapter 4 Reconstructing Unknown Flow Rate History from Transient Pressure Data

4.1 Introduction

Flow rate history is important for pressure-transient analysis, production monitoring, history-matching model simulation and etc. The down-hole flow metering measurements haven't been widely applied in the fields due to the high expense and low reliability. The common practice is dozens of producers are measured together with surface separation equipments. Flow rate history of individual well calculated from back allocation is not accurate due to low test frequency, and the detail flow events are unavailable.

Many methods of reconstructing flow rate history illustrated in Chapter 2 are dependent on reservoir models. As building the accurate reservoir model is difficult, lots of uncertainties and errors may be introduced. According to the convolution integral, transient pressure is directly related to flow rate. In theory, flow rate history can be reconstructed from pressure data directly.

In this chapter, unknown flow rate history is reconstructed from transient pressure and cumulative production data using wavelet transform. This method is model-independent and therefore has wide applications in different kinds of reservoirs.

4.2 Theory description

Flow rate history consists of many different flow periods, and down-hole pressure performs correspondingly according to the convolution integral:

$$p(t) = p_0 - \int_0^t q(\tau)g(t-\tau)d\tau \qquad (4.1)$$

As illustrated in Chapter 3, the pressure change during two successive flow events is not only caused by the rate change, but also affected by the production history:

$$p_{wfn} - p_{wfn+1} = (q_{n+1} - q_n)\int_0^{\Delta t} g(\tau)d\tau + \sum_{i=1}^{n}(q_i - q_{i-1})\int_{t_n - t_{i-1}}^{t_n - t_{i-1} + \Delta t} g(\tau)d\tau \qquad (4.2)$$

With the Haar wavelet processing transient pressure, the time of flow event can be identified in the wavelet detailed signal. When the impulse time Δt is very small and

production history time t is large, the amplitude of WT coefficients is proportional to the pressure change due to the flow rate change (Eq. 3. 8 in Chapter 3):

$$A \propto (q_{n+1} - q_n) \int_0^{\Delta t} g(\tau) d\tau \quad (4.3)$$

For the reservoir with constant reservoir properties and flow conditions (linear systems), $\int_0^{\Delta t} g(\tau) d\tau$ is constant for the same impulse time Δt. The impulse time Δt is a certain constant value when performing WT algorithm and it is decided by the WT scale factor s and time step of pressure data. Therefore the amplitude of WT coefficients A is proportional to rate change Δq. When b is defined as the proportional coefficient, Eq. 4.3 becomes:

$$A = \Delta q \times b \quad (4.4)$$

Here $b = A/\Delta q$, and it equals URSR A_{urc}. According to the research in Chapter 3, URSR A_{urc} is constant in the linear system, where reservoir-well parameters are constant, and Eq. 4.4 is correct. The linear relationship between A and Δq indicates the relationship between flow rate change and corresponding transient pressure response. With the cumulative production Q and Eq. 4.4, the algorithm of flow rate history reconstruction can be developed.

Assuming that initial flow rate is q_1, according to Eq. 4.4, the first flow rate change $q_2 - q_1$ is proportional to the first amplitude of WT coefficients A_1:

$$A_1 = (q_2 - q_1) \times b \quad (4.5)$$

Then q_2 can be expressed with q_1 :

$$q_2 = q_1 + \frac{A_1}{b} \quad (4.6)$$

According to Eq. 4.4, for the second flow event:

$$A_2 = (q_3 - q_2) \times b \quad (4.7)$$

With Eq. 4.6 and Eq. 4.7, q_3 can be expressed with q_1 :

$$q_3 = q_1 + \frac{(A_1 + A_2)}{b} \quad (4.8)$$

Similarly, for the $(i-1)$ *th* flow event, q_i can be expressed with q_1 :

$$q_i = q_1 + \frac{\sum_{j=1}^{i-1} A_j}{b} \tag{4.9}$$

Assuming the flow time for flow rate q_i is t_i, and total cumulative production Q, according to material balance:

$$Q = q_1 t_1 + q_2 t_2 + \cdots q_n t_n = \sum_{i=1}^{n} q_i t_i \tag{4.10}$$

Submit Eq. 4.9 into Eq. 4. 10:

$$Q = \sum_{i=1}^{n} (q_1 + \frac{\sum_{j=1}^{i-1} A_j}{b}) t_i \tag{4.11}$$

The proportional coefficient b can be calculated:

$$b = \frac{\sum_{i=1}^{n} t_i \sum_{j=1}^{i-1} A_j}{Q - q_1 \sum_{i=1}^{n} t_i} \tag{4.12}$$

With the calculated b, flow rate history can be reconstructed. The reconstructed flow rate q_i at time period t_i is:

$$q_i = q_1 + \sum_{j=1}^{i-1} A_j \Big/ \frac{\sum_{i=1}^{n} t_i \sum_{j=1}^{i-1} A_j}{Q - q_1 \sum_{i=1}^{n} t_i} \tag{4.13}$$

To reconstruct flow rate history, not only the value of flow rate needs calculating, but also the time of flow events needs to be identified. With the Haar wavelet processing transient pressure data, the time of flow events t_i can be identified from WT detailed signal, and the amplitude of WT coefficients for each flow events A_j can be determined. Then using Eq. 4.12 and Eq. 4.13, flow rate history can be reconstructed.

4.3 Flow rate history reconstruction in single oil phase reservoir

4.3.1 Base case study

In this case a homogenous and single phase oil reservoir is modelled using Eclipse. The parameters of the model are shown in **Table 4-1**, and skin factor and wellbore storage are considered. Pressure history in the first 8 days is shown in **Figure 4-1**, and the cumulative production during this time is 6212.167 STB.

Table 4-1: The reservoir model parameters

Initial pressure, p_i	4000 psia
Reservoir radial, R	10000 ft
Thickness, h	30 ft
Permeability,k	$k_x = k_y$ =100 mD, k_z =10 mD
Porosity, ϕ	0.25
Oil formation volume factor, B_o	1.2 rb/STB
Total compressibility, c_t	6E-6/psi
Oil viscosity, μ_o	1 cp
Well radius, r_w	0.2083 ft
Skin factor, S	6
Wellbore storage coefficient, C_s	C_s=2.9128e-4 bbl/psi

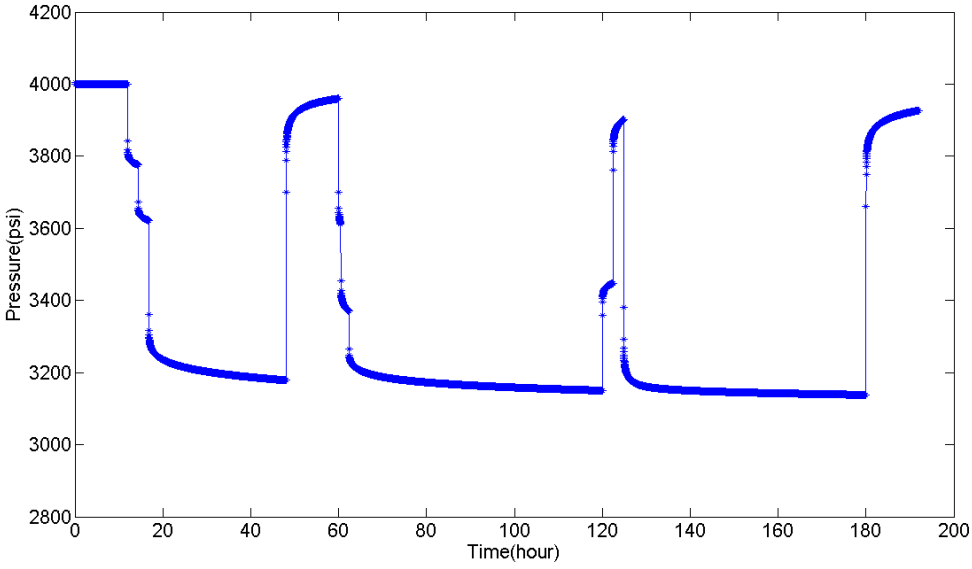

Figure 4-1: Pressure history in base case.

In this case, flow rate history will be reconstructed from the down-hole pressure and cumulative production data. Firstly, pressure data is processed with CWT using the Haar wavelet. As **Figure 4-2** shows, the time of flow events can be identified with the amplitude of WT coefficients in the WT detailed signal. The time of each flow period t_i and amplitude of WT coefficient A_i are shown in **Table 4-2**.

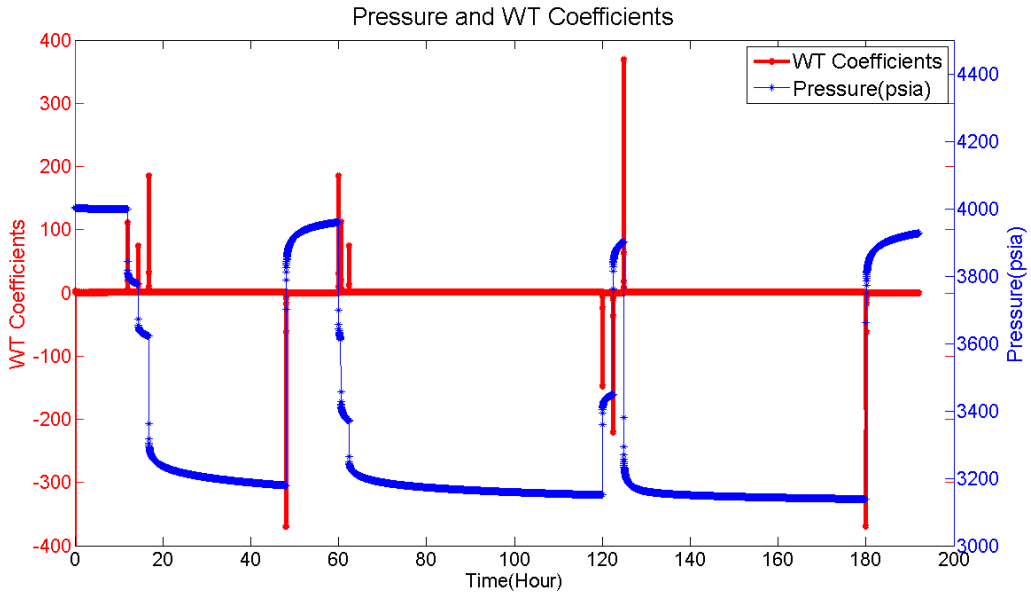

Figure 4-2: Down-hole pressure data in base case is processed with CWT using the Haar wavelet.

Table 4-2: Identification of flow event time

Flow event beginning time (hour)	Flow event ending time (hour)	Flow event time period (hour) t_i	Amplitude of WT coefficients A_j
0	12	12	
12	14.4	2.4	110.4395
14.4	16.8	2.4	73.7991
16.8	48	31.2	184.6843
48	60	12	-369.4933
60	60.48	0.48	184.0257
60.48	62.4	1.92	111.1445
62.4	120	57.6	74.0667
120	122.4	2.4	-147.9488
122.4	124.8	2.4	-221.4461
124.8	180	55.2	368.1030
180	192	12	-369.5476

The initial flow rate $q_1 = 0$, according to Eq. 3.12, the average proportional coefficient b can be calculated, and $b = 0.3681$. Then flow history can be reconstructed with Eq. 4.13, as shown in **Table 4-3**, and error is less than 1%.

Table 4-3: The reconstructed flow rate history in the base case

Beginning (hour)	Ending (hour)	Real rate (STB/day)	Calculated rate (STB/day)	Adjusted rate (STB/day)	Error (%)
0	12	0	0	0	0
12	14.4	300	300	300	0
14.4	16.8	500	500.5	500.5	0.1
16.8	48	1000	1002.2	1002.2	0.22
48	60	0	-1.5	0	0
60	60.48	500	498.4	498.4	-0.32
60.48	62.4	800	800.3	800.3	0.038
62.4	120	1000	1001.5	1001.5	0.15
120	122.4	600	599.6	599.6	-0.067
122.4	124.8	0	-2	0	0
124.8	180	1000	998	998	-0.2
180	192	0	-5.9	0	0

4.3.2 Sensitivity study

4.3.2.1 Wellbore storage

The wellbore storage coefficient defines the rate of pressure change in the pure wellbore storage regime. For the single phase oil reservoir, the wellbore storage is represented by the oil compressibility term:

$$C_s = -\frac{\Delta V}{\Delta p} = c_o V_w \tag{4.14}$$

Here c_o is oil compressibility and V_w is wellbore volume.

When wellbore storage is considered, surface flow rate is reconstructed. The sand face flow rate is different from the surface flow rate due to the wellbore storage effect.

With the recovered surface rate q_s, bottom-hole pressure p_{wf} and wellbore storage coefficient C_s, the sand face flow rate q_{sf} could be calculated as well. For the constant wellbore storage model, the material balance is:

$$q_{sf}B - q_s B = C_s \frac{dp_{wf}}{dt} \tag{4.15}$$

Rearranged, the sand face flow rate q_{sf} may be recovered as following:

$$q_{sf} = q_s + \frac{C_s}{B}\frac{dp_{wf}}{dt} \tag{4.16}$$

The linear system requires that wellbore storage coefficient is constant. However, the wellbore storage coefficient may change in field practice. For naturally flowing oil wells, as pressure decreases when oil rising along the wellbore, pressure may drop below the bubble point pressure and then gas is out of solution. The variable compressibility of gas makes the wellbore storage coefficient is not constant. Particularly when well is shut-in, the phase segregation and changing liquid level may take place in the wellbore, which leads to high nonlinearities in the reservoir system. This case is discussed in **Section 3.4.4**. To simplify the question, constant wellbore storage is considered here.

Wellbore storage has significant impact on the impulse function of the reservoir system $g(t)$. **Figure 4-3** depicts impulse function $g(t)$ with different wellbore storage coefficients in the base case. When there is no well bore storage, the pressure changes promptly and decreases sharply in short time. The larger the wellbore storage is, the small response will be, and the longer time it takes to decrease, shown in **Table 4-4**.

According to Eq. 4.2, for large wellbore storage effect, the pressure change due to history production $\sum_{i=1}^{n}(q_i - q_{i-1})\int_{t_n - t_{i-1}}^{t_n - t_{i-1}+\Delta t} g(\tau)d\tau$ tends to larger than that with small wellbore storage effect, and also the identification of flow events become difficult, as shown in **Figures 4-4 and 4-5**. For the larger wellbore storage coefficient, the amplitude of WT coefficient and the resolution of flow event identification become lower. Therefore, the accuracy of reconstructed flow rate history in the reservoir with small wellbore storage tends to be higher than that in the reservoir with the large wellbore storage effect.

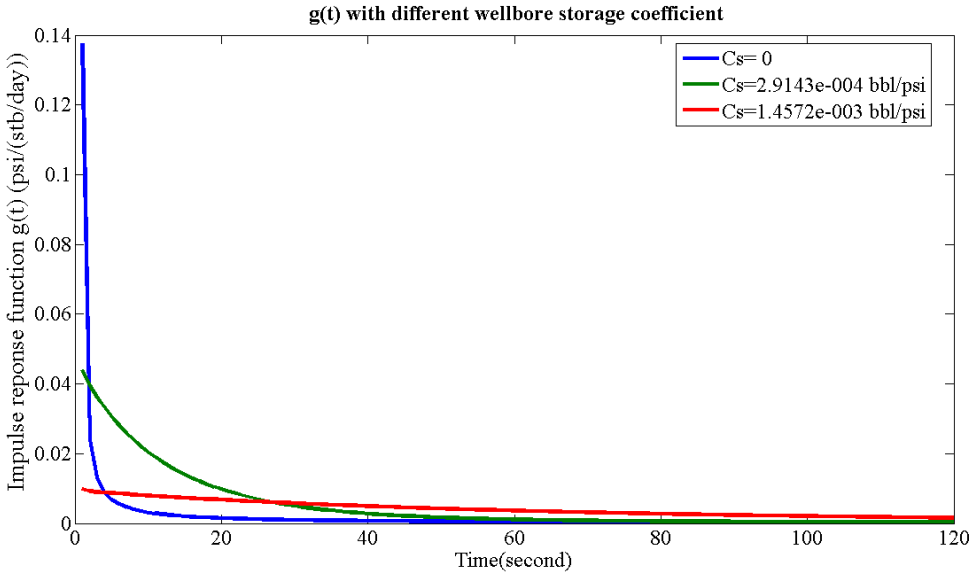

Figure 4-3: The impulse response function $g(t)$ with different wellbore storage coefficient.

Table 4-4: The impulse response function $g(t)$ declines with time for different wellbore storage coefficient.

Wellbore storage coefficient (bbl/psi)	$g(t)$ value at first second (psi/(STB/day))	Percent after 30 seconds	Percent after 1 minute	Percent after 2 minutes
0	0.1376	0.7099%	0.3499%	0.1736%
2.9143e-004	0.0436	11.4669%	2.5846%	0.7325%
1.4572e-003	0.0099	58.3072%	36.9721%	16.06%

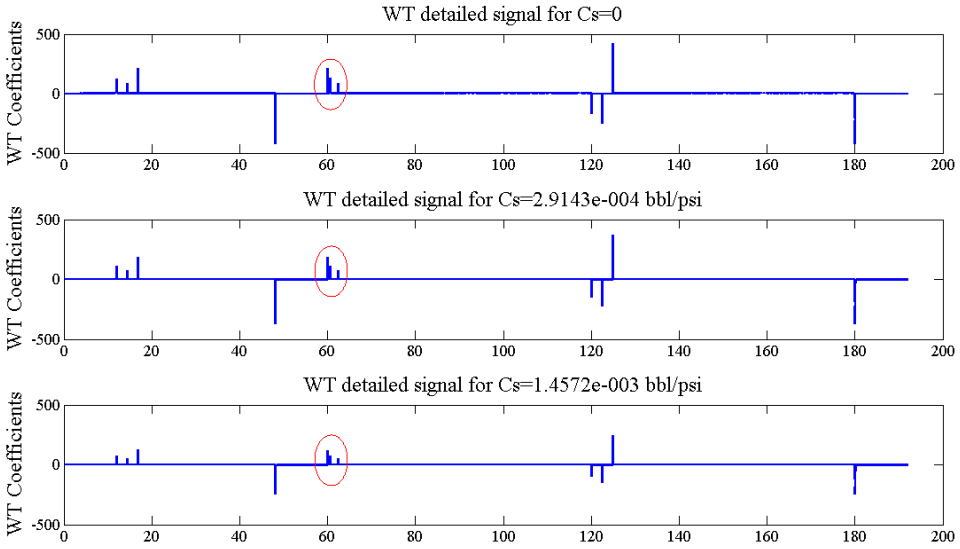

Figure 4-4: WT detailed signal with different wellbore storage coefficient.

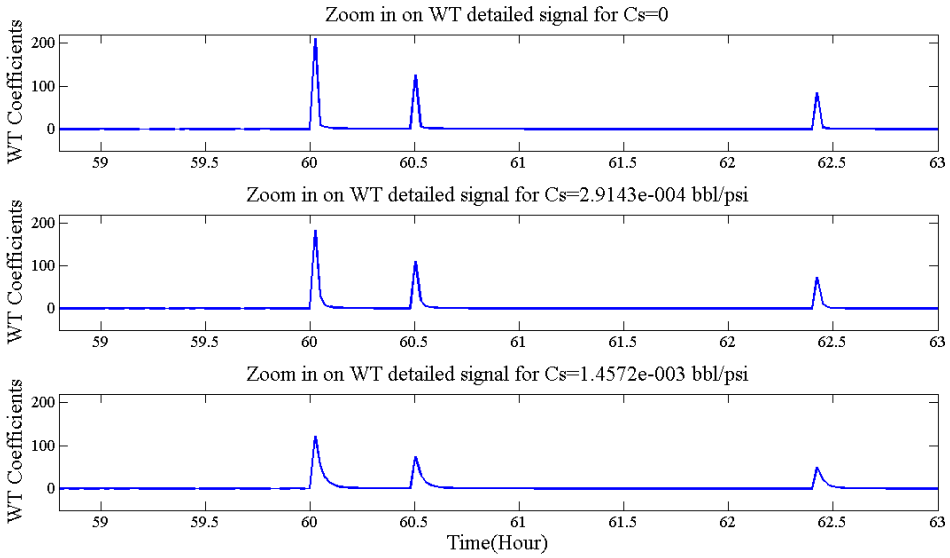

Figure 4-5: Zoom-in of WT detailed signal with different wellbore storage coefficient.

4.3.2.2 Skin factor

In the case of a damaged well, skin is additional pressure drop near well due to well damage. For a simulated well, pressure decline is reduced near the wellbore, and $S < 0$.

Figure 4-6 shows the impulse response function $g(t)$ with different skin factors. For the large skin factor, the impulse response is large, but the declining rate change little compared with the wellbore storage effect. **Figures 4-7 and 4-8** shows the amplitude of WT coefficients is large for the large skin factor, and the time resolution of flow event identification changes little.

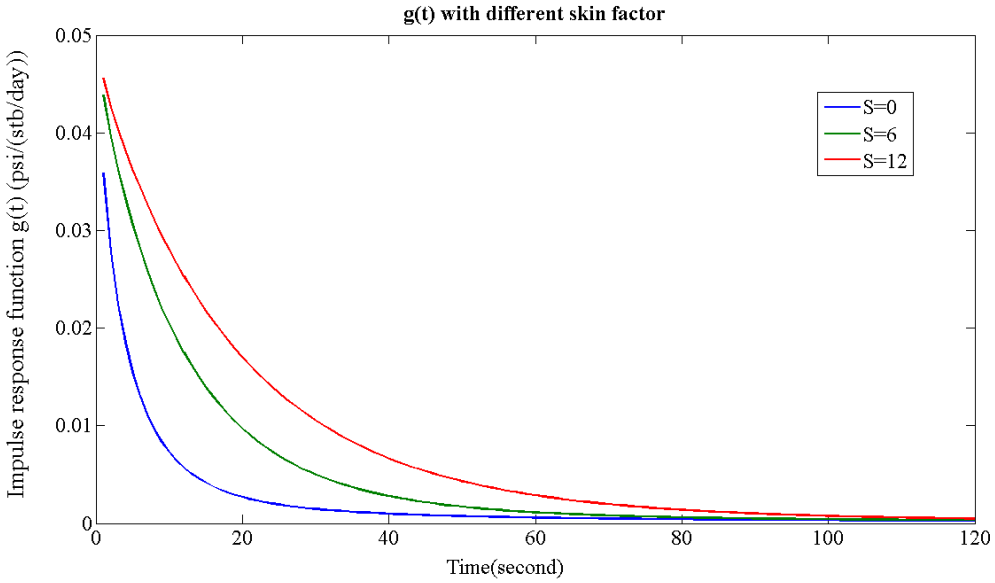

Figure 4-6: The impulse response function $g(t)$ with different skin factor.

Table 4-5: The impulse response function $g(t)$declines with time for different skin factor.

Skin factor	$g(t)$ value at first second (psi/(STB/day))	Percent after 30 seconds	Percent after 1 minute	Percent after 2 minutes
0	0.0359	4.0819%	1.6284%	0.7326%
6	0.0439	11.3703%	2.5594%	0.7425%
12	0.0456	23.1131%	6.2748%	1.0631%

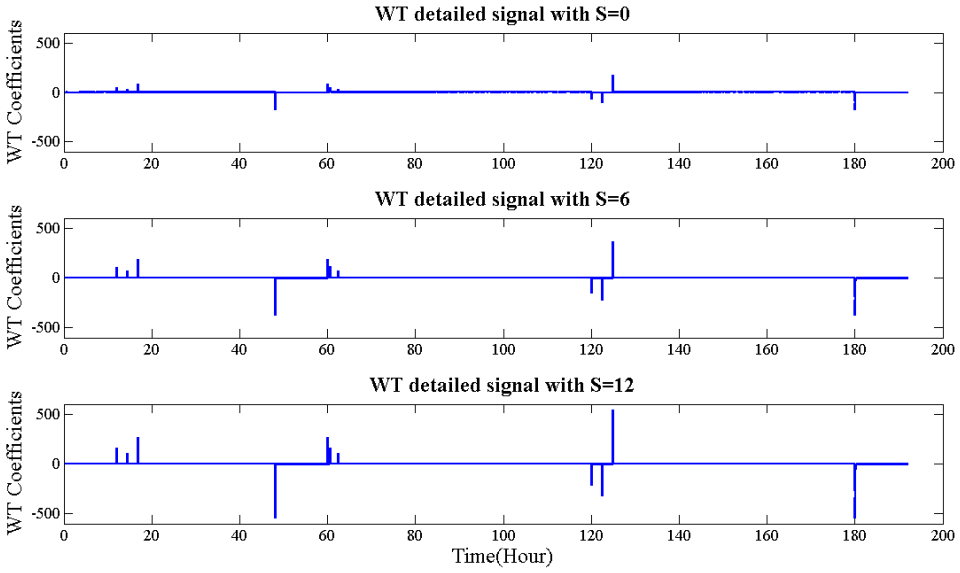

Figure 4-7: WT detailed signal with different skin factor.

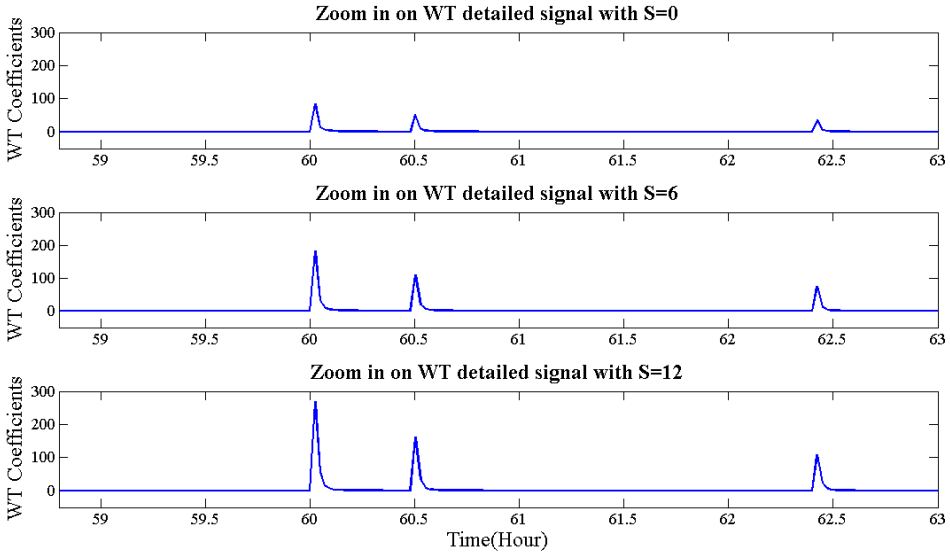

Figure 4-8: Zoom in of WT detailed signal with different skin factor.

4.3.2.3 Flow events happening closely

According to Eq. 4.2, when the time interval of two successive flow events is very small, production history is large enough that not to be neglected. As a result, Eq. 4.3 is not valid, and the amplitude of WT coefficients A is not proportional to flow rate change Δq.

Figure 4-9 shows another simulated flow history from in base case model. The Haar wavelet is selected to process the transient pressure data (**Figure 4-10**). The flow events happen closely at the third day and fifth day. On the third day, three flow events happen successively at the time period 0.01 day (14.4 minutes). On the fifth day, four flow events happen successively at the time period 0.003 day (4.32 minutes).

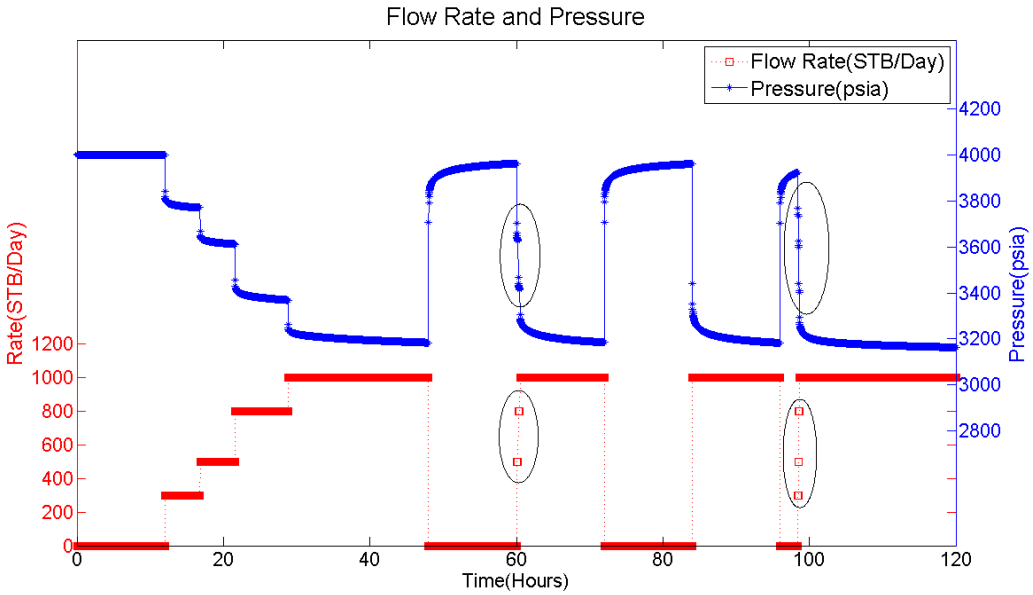

Figure 4-9: Flow history with flow events happened closely.

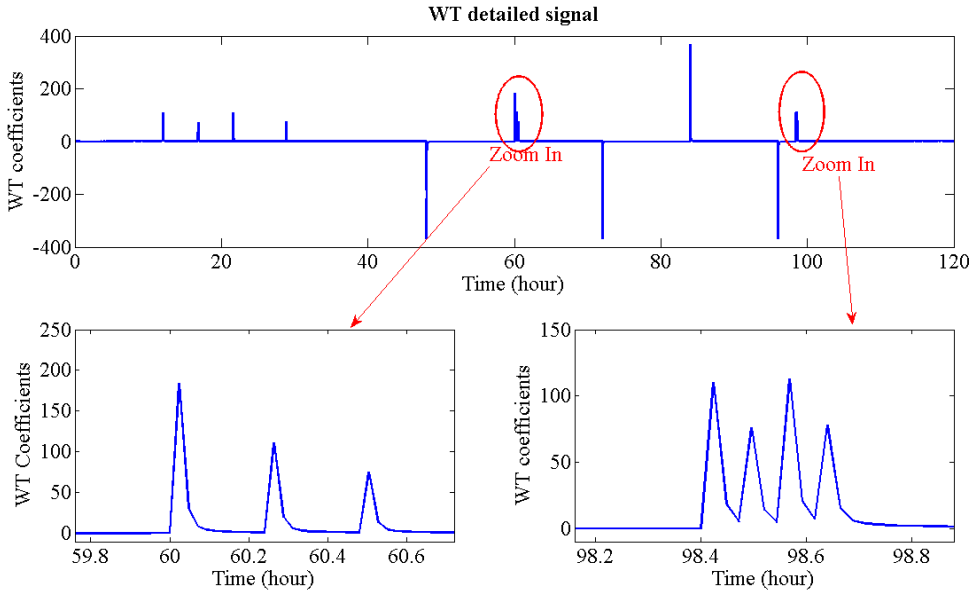

Figure 4-10: WT detailed signal and zoom in on closely happening flow events

The proportional coefficient b of the flow rate change Δq and amplitude of WT coefficients A for each flow event is calculated, as the **Table 4-6** shows. The normal range of proportional coefficient b is 0.368-0.370. When the time period is just 0.01 day, b is 0.372 and 0.375. When the time period is just 0.003 day, b is 0.380 and 0.389. It means the production history will lead to the WT amplitude larger than the normal value. This may cause error in flow rate history reconstruction.

Table 4-6: The proportional coefficients b for every flow event.

Beginning (hour)	Ending (hour)	Time period (hour)	Rate (STB/day) q	Rate change (STB/day) Δq	Amplitude of wavelet transform A	Proportional coefficient $b = A/\Delta q$
0	12	12	0			
12	16.8	4.8	300	300	110.44	0.368
16.8	21.6	4.8	500	200	73.775	0.369
21.6	28.8	7.2	800	300	110.8	0.369
28.8	48	19.2	1000	200	73.999	0.37
48	60	12	0	-1000	-369.61	0.37
60	60.24	0.24	500	500	184.07	0.368
60.24	60.48	0.24	800	300	111.57	0.372
60.48	72	11.52	1000	200	75.015	0.375
72	84	12	0	-1000	-369.55	0.37
84	96	12	1000	1000	368.23	0.368
96	98.4	2.4	0	-1000	-369.45	0.369
98.4	98.472	0.072	300	300	110.28	0.368
98.472	98.544	0.072	500	200	76.045	0.380
98.544	98.616	0.072	800	300	113.17	0.377
98.616	120	21.384	1000	200	77.711	0.389

Fortunately, form Eq. 4.12, the proportional coefficient b also has relationship with time period t_i. The more closely flow events happen, the smaller the time period is t_i. An accurate average proportional coefficient b can be calculated from Eq. 4.12. The reconstructed flow rate is shown as the **Table 4-7**, and the error is still very small even close flow events. The error is in the 1% range. This algorithm has very good error tolerance.

Table 4-7: The errors of calculated flow rate are small.

Beginning (day)	Real rate (STB/day)	Calculated rate (STB/day)	Error (%)
0	0	0	0
12	300	297.6	-0.024
16.8	500	496.4	-0.036
21.6	800	795	-0.05
28.8	1000	994.4	-0.056
48	0	0	0
60	500	494.4	-0.056
60.24	800	795.1	-0.049
60.48	1000	997.3	-0.027
72	0	1.4	0.014
84	1000	993.7	-0.063
96	0	0	0
98.4	300	295.3	-0.047
98.472	500	500.2	0.002
98.544	800	805.2	0.052
98.616	1000	1014.6	0.146

4.3.2.4 Pressure noise

Pressure noise is always with the pressure data measured from pressure gauges. Although noise is recommended to remove before reconstructing flow rate history and pressure transient analysis, the reliable algorithm of rate history reconstruction should have good noise tolerance.

Figure 4-11 shows the pressure data in **Figure 4-1** is added with the artificial noise. The noise is normal distributed with mean 0 and stand deviation 1.

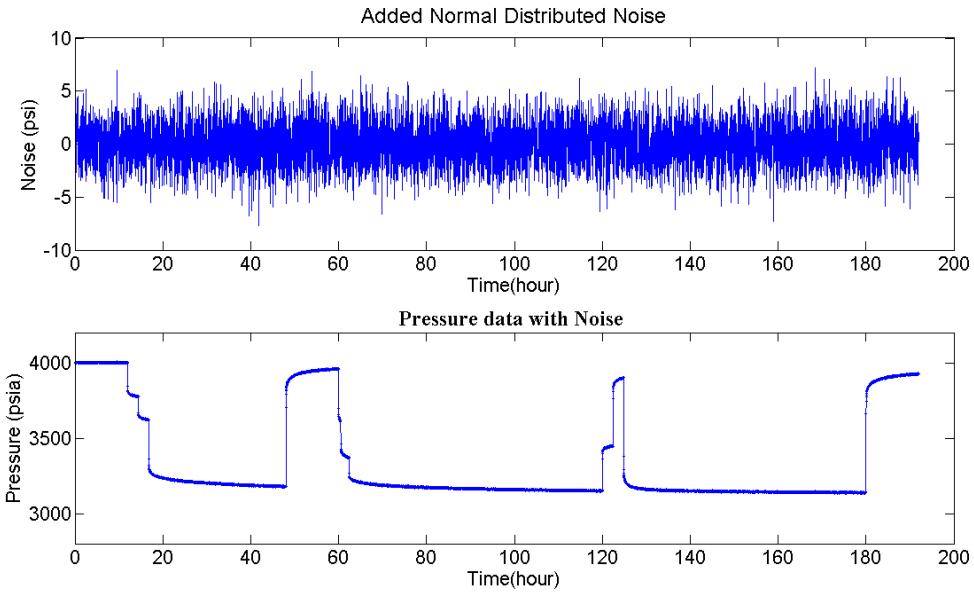

Figure 4-11: Artificial noise is added to the pressure data.

Wavelet Transform is applied to process the noisy pressure data with Haar wavelet, as illustrated in **Figure 4-12**. Noise cause small WT amplitude around 0, and the flow events cause large WT amplitude. Noise threshold can be set to separate the flow events from noise. Therefore, the time and WT amplitude for each flow events can be determined, and flow rate history can be calculated.

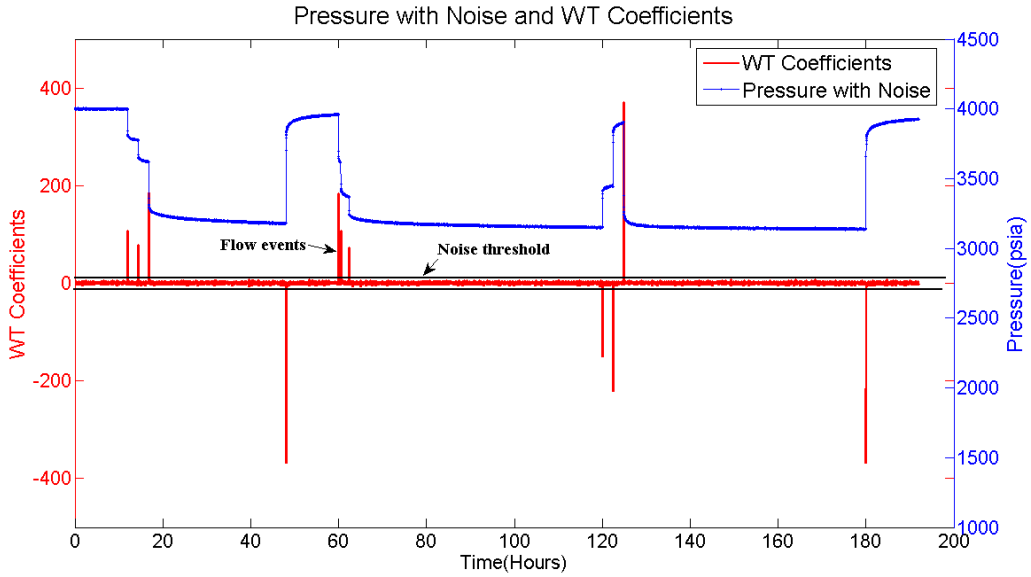

Figure 4-12: Noisy pressure is processed with wavelet transform.

Table 4-8 presents the calculated flow rate from the noisy pressure data, and the error is small and less than 2%, but the error is little high than that in **Table 4-2**, due to noise effect.

As this case illustrates, even there are noise in the pressure data, the calculated rate history is close to the real flow rate. This algorithm of rate calculation has good tolerance of pressure noise.

Table 4-8: The calculated rate history from the noisy pressure data.

Beginning (day)	Period (hour)	Real rate (STB/day)	Calculated rate (STB/day)	Error (%)
0	12	0	0	0
12	14.4	300	294.03	-1.99
14.4	16.8	500	509.28	1.86
16.8	48	1000	1014.8	1.48
48	60	0	7.8227	0
60	60.48	500	506.86	1.37
60.48	62.4	800	801.32	0.17
62.4	120	1000	999.63	-0.04
120	122.4	600	589.22	-1.79
122.4	124.8	0	0	0
124.8	180	1000	993.81	-0.62
180	192	0	0	0

4.4 Flow rate history reconstruction for the case initial flow rate q_1 is unknown

4.4.1 Algorithm development

As Eq. 4.12 and Eq. 4.13 show, the initial flow rate q_1 is an important parameter in this algorithm. Generally, the initial flow rate q_1 is unknown, as the accumulative production may be given on daily, weekly or monthly, or even just a period of production time. Unknown initial flow rate is common but it causes difficulties, as the proportional coefficient b cannot be calculated.

A trial-and-error algorithm is developed here to solve this problem. If there is at least one BU during this time period, this information can be utilized to find the unknown

initial rate q_1 and reconstruct the flow rate history. The workflow is shown in **Figure 4-13**.

Step 1: Define initial rate q_1 range. The range of q_1 can be calculated from Eq. 4.12. As the proportional coefficient b must be positive, the value of $\sum_{i=1}^{n} t_i \sum_{j=1}^{i-1} A_j$ is calculated. If $\sum_{i=1}^{n} t_i \sum_{j=1}^{i-1} A_j > 0$, because the proportional coefficient b is positive, then $Q - q_1 \sum_{i=1}^{n} t_i > 0$, which requires $q_1 < \frac{Q}{\sum_{i=1}^{n} t_i}$. The range of q_1 is $0 < q_1 < \frac{Q}{\sum_{i=1}^{n} t_i}$.

If $\sum_{i=1}^{n} t_i \sum_{j=1}^{i-1} A_j < 0$, then $Q - q_1 \sum_{i=1}^{n} t_i > 0$ which requires $q_1 > \frac{Q}{\sum_{i=1}^{n} t_i}$. The material balance requires $Q \geq q_1 t_1$, which generates $q_1 \leq \frac{Q}{t_1}$. So the range of q_1 is $\frac{Q}{\sum_{i=1}^{n} t_i} < q_1 \leq \frac{Q}{t_1}$.

Step 2: Set initial value of q_1 from the range, and calculate b and flow rate q_i at each time period with Eq. 4.12 and Eq. 4.13.

Step 3: Check whether or not the reconstructed flow rate is reasonable. In BU time period, the flow rate should be zero. If the calculated flow rate in this time period satisfies this requirement, the result is reasonable and the calculation is complete. Otherwise, go to step 4.

Step 4: If the reconstructed flow rate is not reasonable, change the value q_1 and make another calculation until the calculated flow rate is reasonable.

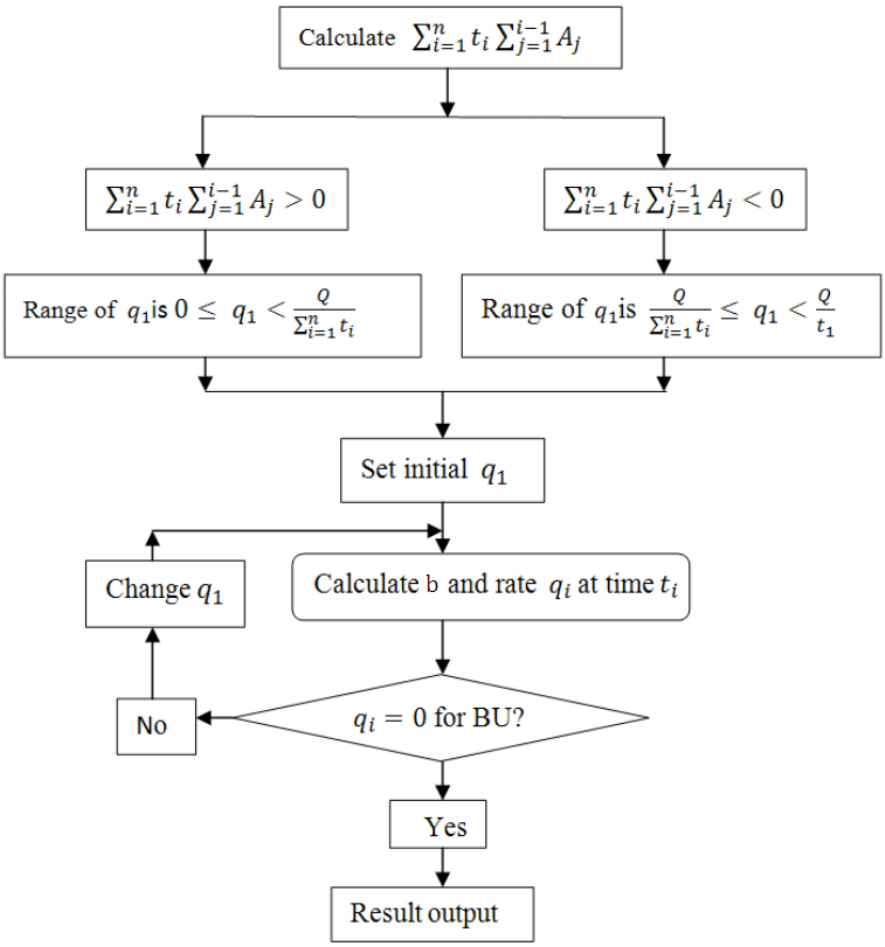

Figure 4-13: The trial-and-error algorithm for flow rate history reconstruction with unknown initial flow rate q_1.

4.4.2 Case study

Figure 4-14 depicts a simulated model of a heterogeneous oil reservoir with a single production well. Some model parameters are shown in **Table 4-9**. Constant skin factor and wellbore storage effect are considered. The grids near the wellbore are refined to reduce the numerical dispersion. A part of flow history is researched, as **Figure 4-15** shows. The pressure data is added with noise. During the production lasting nearly 240 hours, the cumulative production is 8941 STB. The initial flow rate is unknown, but there are two pressure BUs in the pressure data, and indicates the flow rate is zero during these pressure BU time periods. This information will be used to reconstruct flow rate history with the developed algorithm.

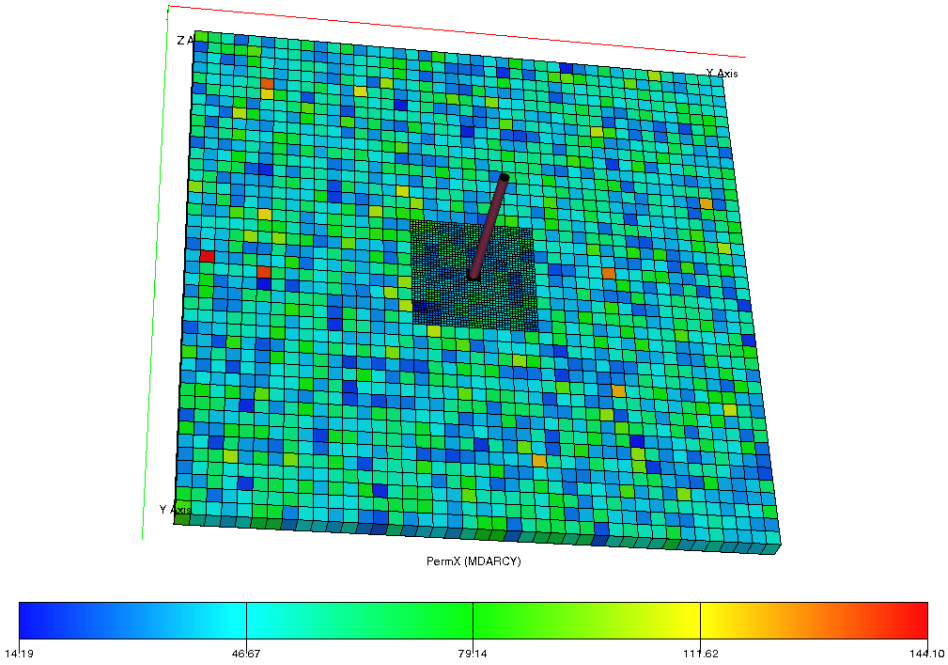

Figure 4-14: A heterogeneous oil reservoir model with a single producer.

Table 4-9: Model parameters in the case study.

Initial field pressure, p_0	4000 psia
Reservoir length, R	4100 ft
Reservoir width, R	4100 ft
Thickness, h	50 ft
Oil formation volume factor, B_o	1.2 rb/STB
Average permeability, k	50 mD
Average porosity, ϕ	0.25
Viscosity, μ_o	1 cp
Oil compressibility, C_o	3e-6 1/psi
rock compressibility, C_f	3e-6 1/psi
Well radius, r_w	0.15 ft
Skin factor, S	6
Well bore storage volume, V_w	1.53e-004 bbl/psi

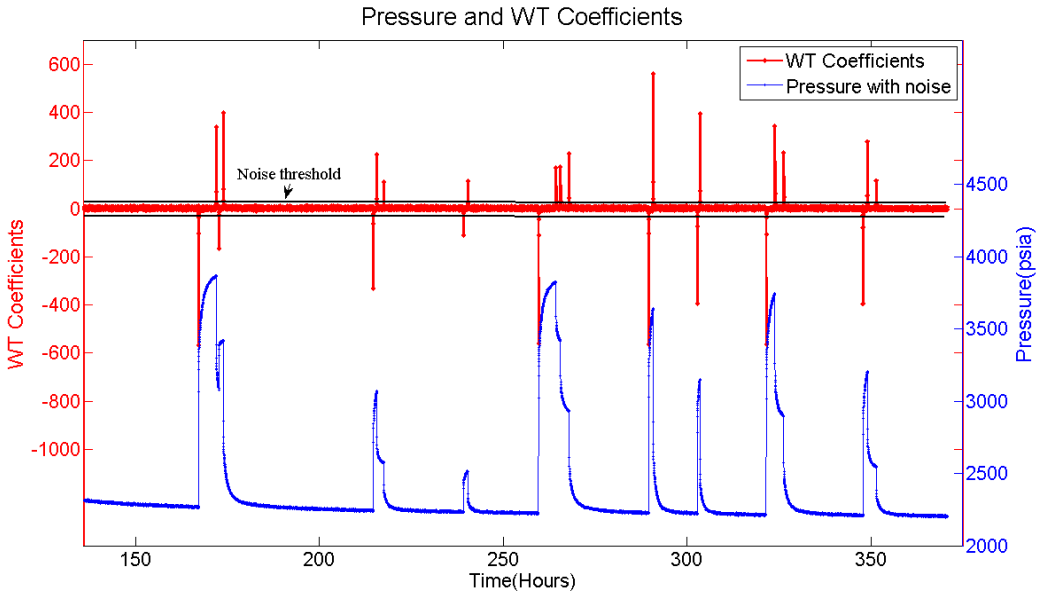

Figure 4-15: The noisy pressure data is processed with WT.

At first, the noisy pressure data is processed with the Haar wavelet. As **Figure 4-1**5 presents, in the detail signal of wavelet transform, noisy threshold can be set to distinguish flow events from the noise. The time of flow events can be accurately identified in the WT detailed signal. With the WT amplitude A_i and time period t_i for each flow event, the rate history can be calculated using the trial-and-error algorithm developed in **Figure 4-13**. The calculation procedures are shown as following.

Step 1: Define q_1 range. As $\sum_{i=1}^{n} t_i \sum_{j=1}^{i-1} A_j = -592.71 < 0$, the range of q_1 is $0 < q_1 < \frac{Q}{\sum_{i=1}^{n} t_i}$. That is $792.71 < q_1 < 3193.2$. Select $q_1 = 792.8$ as the initial value.

Step 2: Calculate b and flow rate q_i. When $q_1 = 792.8$, the average proportional coefficient b can be calculated with Eq. 4.12, and the result is $b = 521.4266$. All flow rates for each flow period are nearly 792 STB/day.

Step 3: Check the result. The result is not reasonable, because it is contrary to the condition that flow rate is zero for pressure BU $q_2 = q_{11} = 0$.

Step 4: Change the value of q_1 by adding 0.1, then $q_1 = 792.9$. Repeat the Step 1, 2 and 3 until the result is reasonable.

The finial reconstructed flow rate is shown in **Table 3-10**.

Table 4-10: The errors of calculated flow rate are nearly less than 5%.

Beginning time (hour)	Ending time (hour)	WT amplitude	Calculated rate (STB/day)	Real rate (STB/day)	Error (100%)
136	167.2		1000.9	1000	0.09
167.2	172	-565.41	0	0	0
172	172.72	337.96	607.67	600	1.28
172.72	173.92	-166.93	312.06	300	4.02
173.92	214.72	394.92	1009	1000	0.9
214.72	215.68	-339.36	403.42	400	0.86
215.68	217.6	223.96	809.14	800	1.14
217.6	239.2	113.22	1014.3	1000	1.43
239.2	240.4	-113.15	799.82	800	-0.02
240.4	259.6	112.6	1003	1000	0.3
259.6	264.4	-565.5	0	0	0
264.4	265.6	168.84	297.6	300	-0.8
265.6	268	169.84	607.17	600	1.20
268	289.6	226.28	1002.2	1000	0.22
289.6	290.8	-565.49	0	0	0
290.8	302.8	561.71	993.71	1000	-0.63
302.8	303.52	-395.92	288.32	300	-3.89
303.52	321.52	392.37	987.1	1000	-1.29
321.52	323.92	-565.52	0	0	0
323.92	326.32	337.45	593.74	600	-1.04
326.32	347.92	226.29	991.99	1000	-0.80
347.92	349.12	-395.94	282.47	300	-5.84
349.12	351.52	280.56	788.2	800	-1.48
351.52	371.13	113.25	986.49	1000	-1.35

4.5 Flow rate history reconstruction for multi-wells

4.5.1 Reconstruction algorithm for multi-wells

In oilfields, it is not possible to equip flow metering devices for each well. The common practice is several wells are connected through manifolds and measured

together with separation equipments. The reconstruction algorithm for multi-wells needs developing to allocate rate for each individual well from total production.

There are m wells measured together, and the proportional coefficient for each well is $b_k (1 \le k \le m)$. To calculated m unknown b_k, there must be n time periods when total productions are measured and $n \ge m$. The total production for each measured time is $Q_i (1 \le i \le n)$. To simplify the problem, assume that the initial rate of each well at each measured time period is known. For i th measured time period, there are l different flow events and expressed by $j (1 \le j \le l)$. The flow rate of k th well at j flow event in i th measured time is expressed by q_{kij} .

$$q_{kij} = q_{ki1} + \sum_{j=1}^{l-1} A_{kij} / b_k \tag{4.17}$$

With the material balance, the total production Q_i during the i th measured time ($1 \le i \le n$) equals the sum of total production of each well during all the flow events time t_{ij} $(1 \le j \le l)$:

$$\sum_{j=1}^{l} q_{1ij}\, t_{2j} + \cdots \sum_{j=1}^{l} q_{kij}\, t_{2j} \ldots + \sum_{j=1}^{l} q_{mij}\, t_{2j} = Q_i \tag{4.18}$$

There are n measured time periods, so n equations can be derived:

$$\begin{cases} \sum_{j=1}^{l} q_{11j}\, t_{1j} + \cdots \sum_{j=1}^{l} q_{k1j}\, t_{1j} \ldots + \sum_{j=1}^{l} q_{m1j}\, t_{1j} = Q_1 \\ \sum_{j=1}^{l} q_{12j}\, t_{2j} + \cdots \sum_{j=1}^{l} q_{k2j}\, t_{2j} \ldots + \sum_{j=1}^{l} q_{m2j}\, t_{2j} = Q_2 \\ \cdots \\ \sum_{j=1}^{l} q_{1ij}\, t_{2j} + \cdots \sum_{j=1}^{l} q_{kij}\, t_{2j} \ldots + \sum_{j=1}^{l} q_{mij}\, t_{2j} = Q_i \\ \cdots \\ \sum_{j=1}^{l} q_{1nj}\, t_{nj} + \cdots \sum_{j=1}^{l} q_{knj}\, t_{nj} \ldots + \sum_{j=1}^{l} q_{mnj}\, t_{nj} = Q_n \end{cases} \tag{4.19}$$

By solving Eq. 4.19, the proportional coefficient $b_k (1 \le k \le m)$for each well can be calculated, and then rate history of each well can be calculated using Eq. 4.17.

4.5.2 Case study

Figure 4-16 shows a heterogeneous reservoir with two producers. There are three layers in the formation and permeability and porosity for each layer are shown in **Table 4-11**. The first and second layer is high-perm, but the permeability for the third layer is low. Other model parameters are shown in **Table 4-12**. Different skin factors and wellbore storage coefficients are considered for two wells and two wells are partially

perforated. For the first well, the first layer is perforated and the second layer is perforated for the second well.

Down-hole pressure of two wells is presented in **Figure 4-17**. The total production of two wells is measured together. In this case, two time periods of total production are measured. In the first 240 hours, the total production is Q_1 =12190 STB, and in another 355.2 hours, the cumulative production of two wells is Q_2 =20900 STB. With the developed multi-well algorithm, detailed flow rate history can be reconstructed from the pressure data and cumulative production.

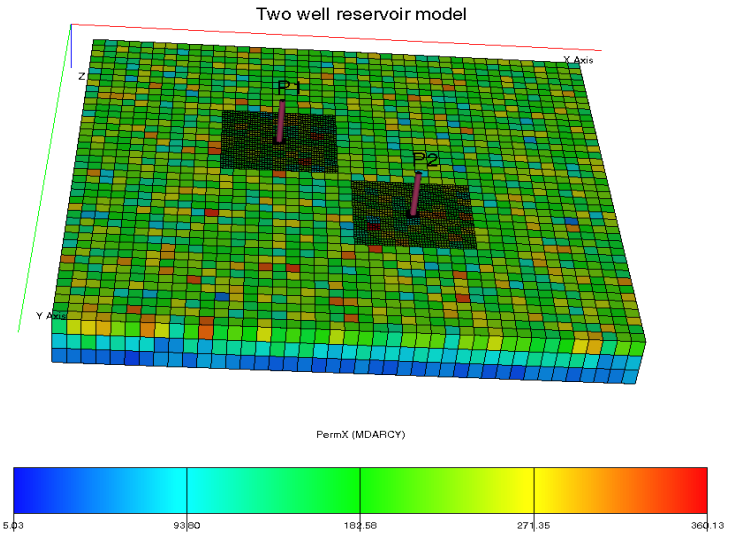

Figure 4-16: A heterogeneous reservoir model with two producers. Total production for two wells is measured.

Table 4-11: The permeability and porosity for different layer.

property	Layer	Direction	Range	Average
Permeability k (mD)	1	X	169.5-234.1	200
		Y	114.2-183.3	150
		Z	12.8-26.5	20
	2	X	81-118.4	100
		Y	63.6-98.7	80
		Z	6.7-13.2	10
	3	X	33.0-66.3	50
		Y	42.3-78.2	60
		Z	1.1-8.7	5
Porosity $\emptyset$	1		0.164-0.234	0.2
	2		0.268-0.335	0.3
	3		0.214-0.283	0.25

Table 4-12: The parameters for the two-well reservoir model.

Initial pressure, p_0	3000 psia
Thickness, h	150 ft
Reservoir length and width, R	4100 ft
Oil formation volume factor, B_o	1.2 rb/STB
Viscosity, μ_o	1.2 cp
Total compressibility, c_t	6e-6 1/psi
Well radius, r_w	r_{w1} =0.125 ft, r_{w2} =0.15 ft
Skin factor, S	$S_1 = 4, S_2 = 1$
Well bore storage, C_s	C_{s1} =1.53e-004 bbl/psi C_{s2} =2.9128e-4 bbl/psi
Perforation	Well 1-First layer Well 2-Second layer

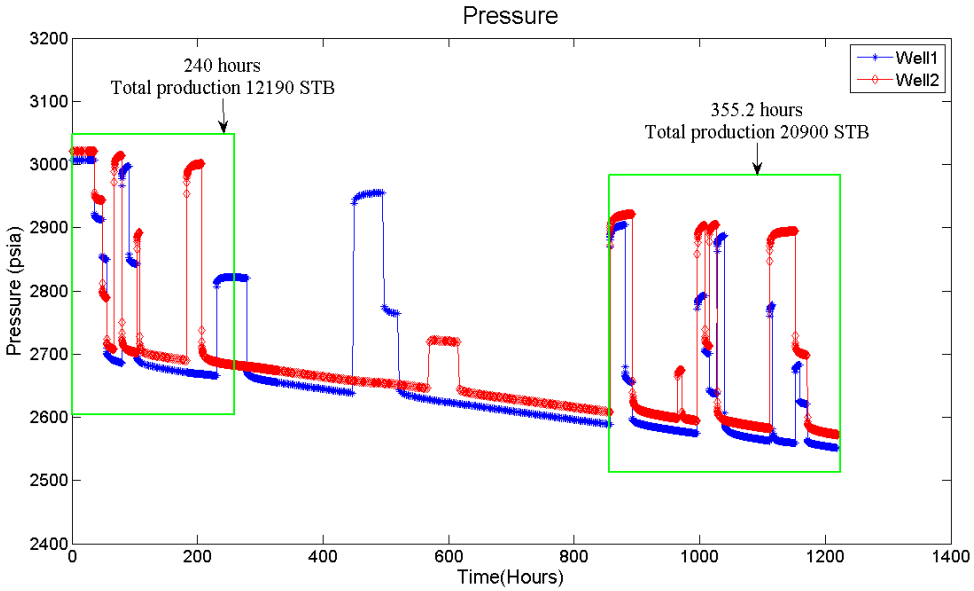

Figure 4-17: Down-hole pressure history for two wells. The total production of two wells is measured together.

The proportional coefficients for two wells are assumed b_1 b_2, and the initial flow rate in two periods of time for two wells is zero, and the Eq. 4.19 can be simplified:

$$\begin{cases} \sum_{j=1}^{l} \sum_{j=1}^{l-1} A_{11j}\, t_{1j} / b_1 + \sum_{j=1}^{l} \sum_{j=1}^{l-1} A_{21j}\, t_{1j} / b_2 = Q_1 \\ \sum_{j=1}^{l} \sum_{j=1}^{l-1} A_{12j}\, t_{2j} / b_1 + \sum_{j=1}^{l} \sum_{j=1}^{l-1} A_{22j}\, t_{2j} / b_2 = Q_2 \end{cases} \tag{4.20}$$

Wavelet is applied to process pressure data to identify flow periods, then A and t can be determined:

$$\begin{cases} 1398.9/b_1 + 1197.3/b_2 = 12190 \\ 2493.4/b_1 + 1941.3/b_2 = 20900 \end{cases} \tag{4.21}$$

The solution of Eq. 4.21 is:

$$\begin{cases} b_1 = 0.1984 \\ b_2 = 0.2330 \end{cases} \tag{4.22}$$

With Eq. 4.18, flow rate history for each well can be calculated, and the result is shown in **Figure 4-18**. The calculated flow rate is very close to the real value used for model simulation.

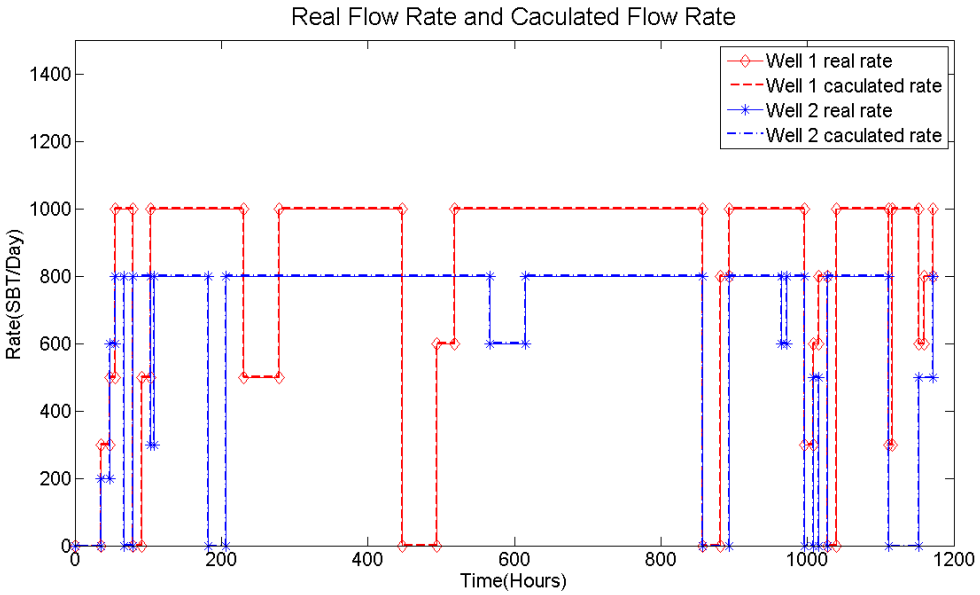

Figure 4-18: The calculated flow rate for two wells is very close to the real flow rate, and the error is less than 1%.

4.6 Flow rate history reconstruction in oil and water two-phase reservoir

During water flooding, water is produced after water breakthrough. Then the flow conditions near the wellbore change from the single oil phase flow to oil and water two-phase flow. Reconstructing flow rate history in two-phase flow condition is much more challenging than that in the single phase flow condition. Flow rate history for each phase needs to be reconstructed. Besides, due to the dynamic changes in relative permeability and phase saturation of each phase, there are high nonlinearities in the reservoir when more than single phase flowing in the porous media. As the developed algorithm of flow rate history reconstruction is based on the linearity assumption, the direct application of the reconstruction algorithm may have some problems, and further discussion and algorithm validation are necessary.

Generally, the produced oil and water are mixed together and transported in the tubing, manifolds and pipeline before they are separated with separation equipments on the surface. The total cumulative production of liquid, oil or water is measured together. To reconstruct flow rate history, the total liquid flow rate $q_t = q_o + q_w$ is calculated at first, and then oil and water flow rate q_o q_w can be calculated with water cut information.

The average proportional coefficient b:

$$b = \frac{\sum_{i=1}^{n} t_i \sum_{j=1}^{i-1} A_j}{Q - q_{t1} \sum_{i=1}^{n} t_i} \tag{4.23}$$

where q_{t1} is initial total flow rate. The total flow rate at time period t_i:

$$q_{ti} = q_{t1} + \sum_{j=1}^{i-1} A_j \Big/ \frac{\sum_{i=1}^{n} t_i \sum_{j=1}^{i-1} A_j}{Q - q_{t1} \sum_{i=1}^{n} t_i} \tag{4.24}$$

Assume the average water cut during this time period is f_w, which can be calculated from cumulative total liquid production Q_t and water production Q_w:

$$f_w = \frac{Q_w}{Q_t} \tag{4.25}$$

The oil flow rate q_{oi} and water flow rate q_{wi} at time period t_i is:

$$q_{oi} = q_{ti}(1 - f_w) \tag{4.26}$$

$$q_{wi} = q_{ti} f_w \tag{4.27}$$

Eq. 4.23 is valid in the linear system. For the oil and water two-phase reservoir, the total mobility near the wellbore should be constant or change little. As a result, the water cut is constant or change little. For the time period when water cut changes a lot, Eq. 4.23 has large errors.

Two different cases are researched, one is constant water cut case, and another is oil and water two-phase reservoir with increasing water cut.

4.6.1 Oil and water two-phase flow with constant water cut case

This case is oil and water two phase reservoir with constant water cut. For the dispersed flow with uniform saturation or oil-water segregated flow, the water cut may be constant during the production. This two type flow mechanisms are show in **Figure 4-19**. For the dispersed flow with uniform saturation, water and oil are assumed to be fully dispersed across the reservoir formation. It is an ideal case and doesn't exist in practice. When gravity force is dominate, complete segregation of oil lying water leads to segregated flow. Besides, for the early water breakthrough in high permeability layer, segregated flow may happen as well.

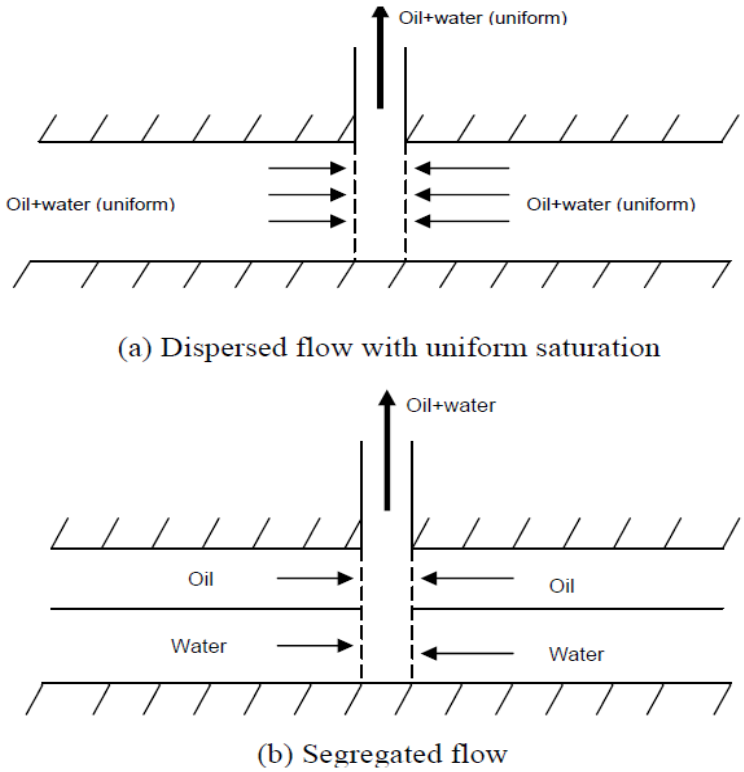

Figure 4-19: Dispersed flow with uniform saturation and segregated flow (from Xu, W. 2010)

A single homogeneous reservoir with segregated flow is modelled with Eclipse, shown as **Figure 4-20**. The bottom may be an aquifer or high permeability layer with early water breakthrough, and the formation is fully perforated. The down-hole flow pressure and water cut history are shown in **Figure 4-21**. The water cut is almost constant except a little variation in the case of flow events. During nearly 300 hours production, the cumulative liquid production is 10435 STB, and 3124.1982 STB water is produced.

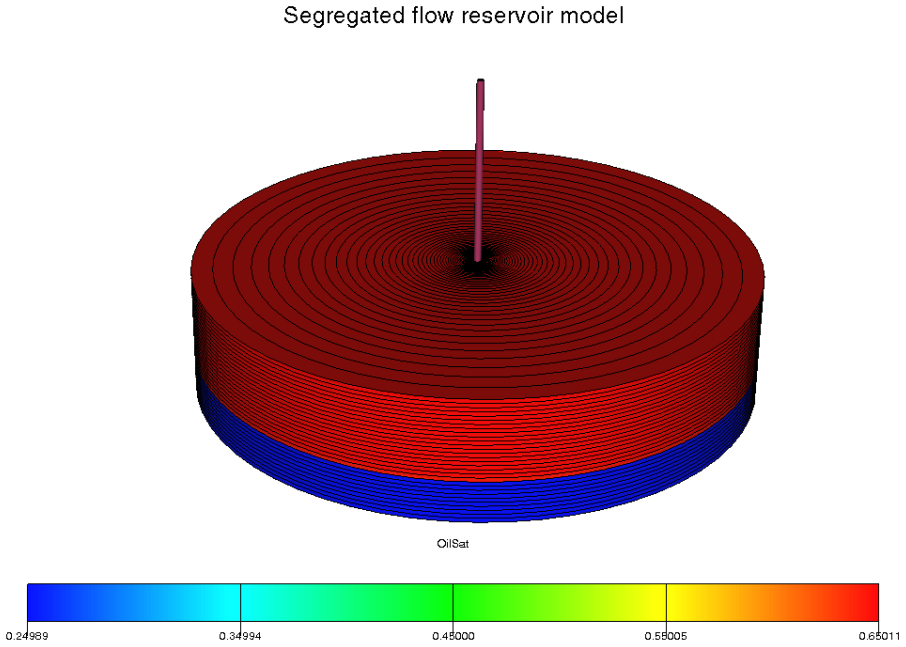

Figure 4-20: The segregated flow reservoir model.

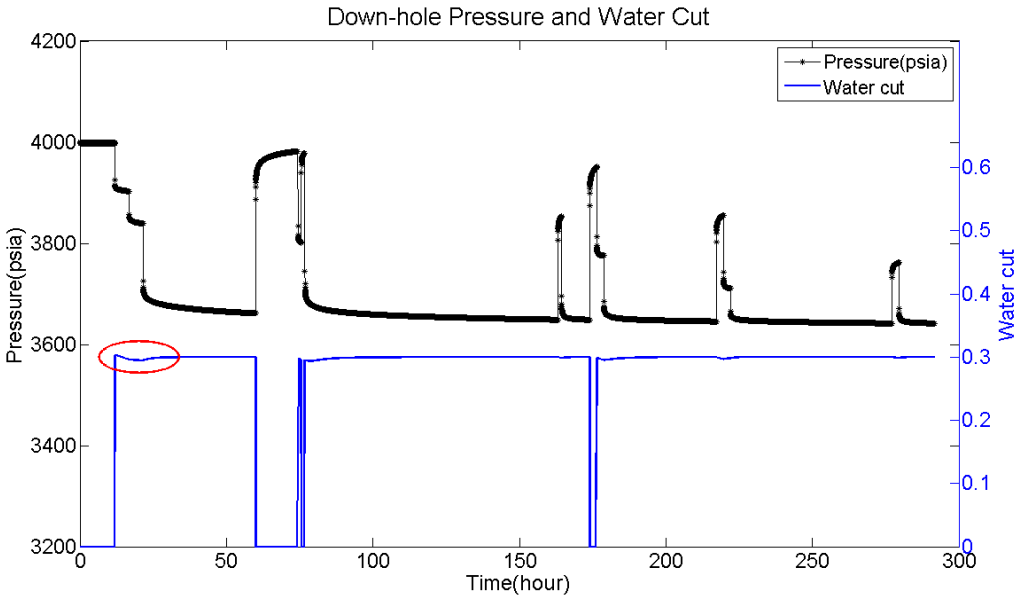

Figure 4-21: Down-hole flow pressure and water cut history in the segregated flow reservoir.

As the water cut changes little during the entire production time, reservoir properties and flow conditions can be assumed to be constant. Then the system can be treated to be linear and total liquid flow rate can be calculated. Firstly, the Haar wavelet is used to process pressure data and flow events are identified, as **Figure 4-22** shows. Then with Eq. 4.23, the average proportional coefficient b can be calculated $b = 0.1761$. After

that, the total liquid flow rate can be calculated using Eq. 4.24, and the result is shown in **Figure 4-23**.

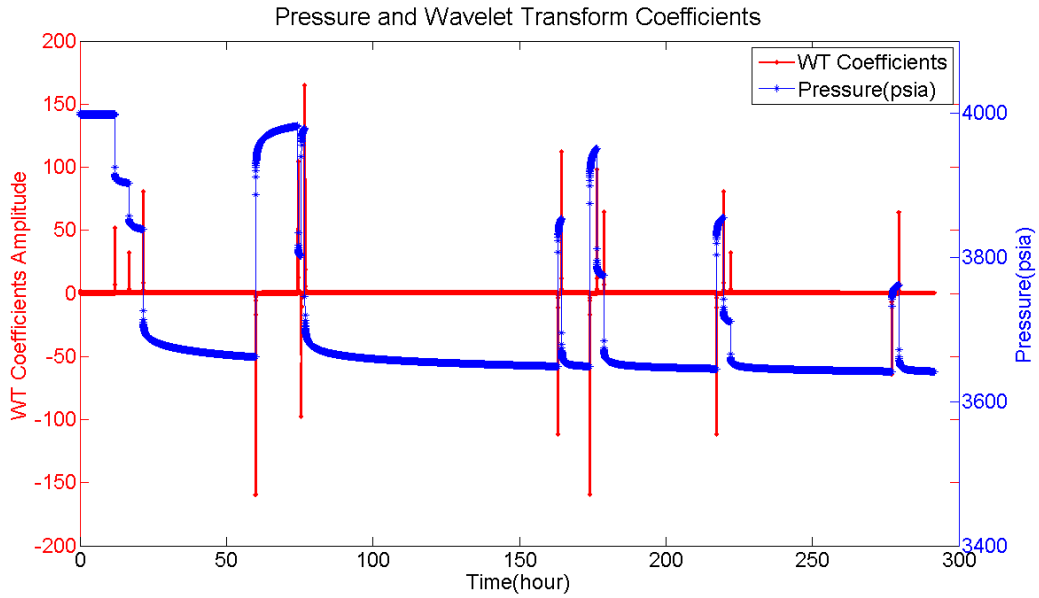

Figure 4-22: The pressure of segregated flow is processed with Haar wavelet.

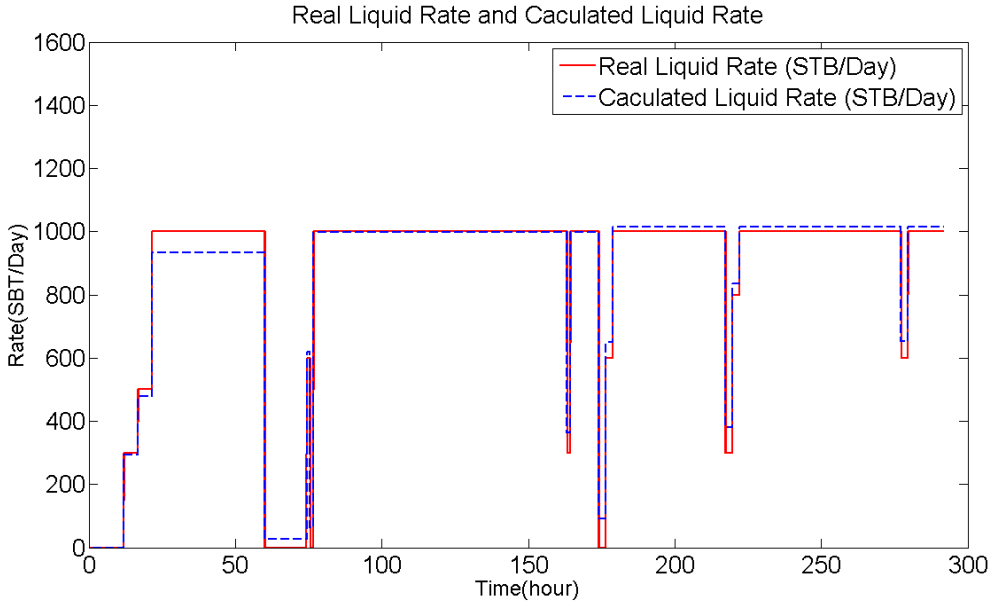

Figure 4-23: The reconstructed total liquid flow rate history.

The average water cut is $f_w = \frac{Q_w}{Q_t} = \frac{3124.1982}{10435} = 0.2994$. With the calculated total liquid flow rate, oil and water flow rate history can be reconstructed using Eq. 4.26 and Eq. 4.27, as shown in **Figure 4-24**.

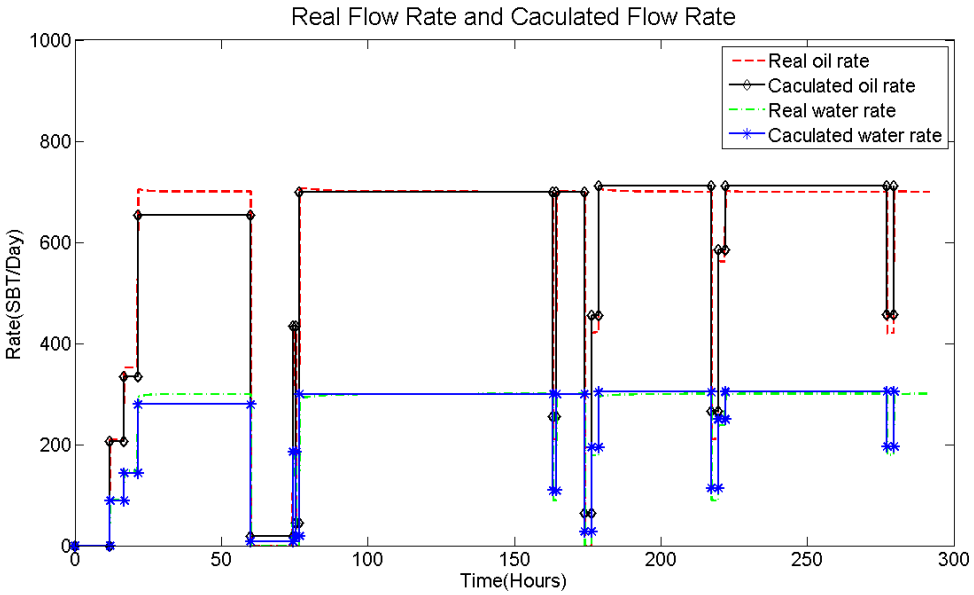

Figure 4-24: The real flow rate and reconstructed flow rate history of oil and water.

The reconstructed oil and water flow rate history is satisfying overall, although the errors are large for the third flow events. This is caused by the variation of water cut at the beginning, and the linear assumption is not valid seriously. The diagnostic result is shown in **Figure 4-25**. URSR A_{urc} is time-varying at the beginning and indicates the total mobility near the wellbore changes, which also leads to water cut variation.

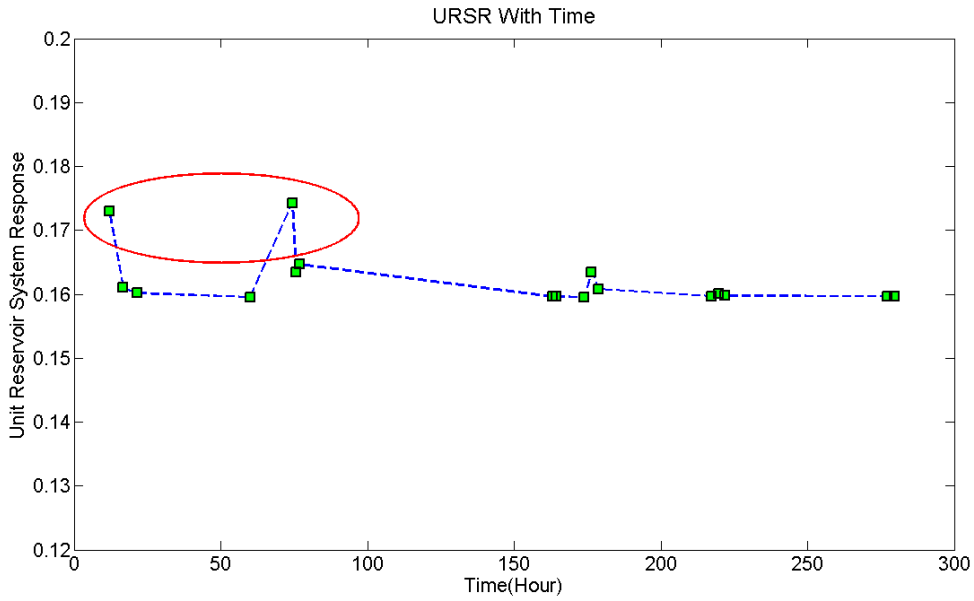

Figure 4-25: Nonlinearity diagnostic result in the segregated flow model.

4.6.2 Oil and water two-phase reservoir with increasing water cut

After water breakthrough, water cut at down-hole will increase with time. As the discussion in **Section 3.4.5**, total mobility of fluids will change correspondingly. The reservoir system is highly nonlinear. Reconstructing flow rate history from the whole pressure data will have large errors. The best practice is dividing the pressure history into different windows, in which the total fluid properties change little and the system can be treated to be linear. Then the reconstruction algorithm is applicable.

The pressure history in **Section 3.4.5** is taken as an example. In the first window, the production time period is one week. Only oil is produced and water cut is almost zero. The cumulative liquid production is 4960 STB. In the second window, 16780 STB cumulative liquid is produced in more than two weeks. The water cut increases from 0.58 to 0.66.

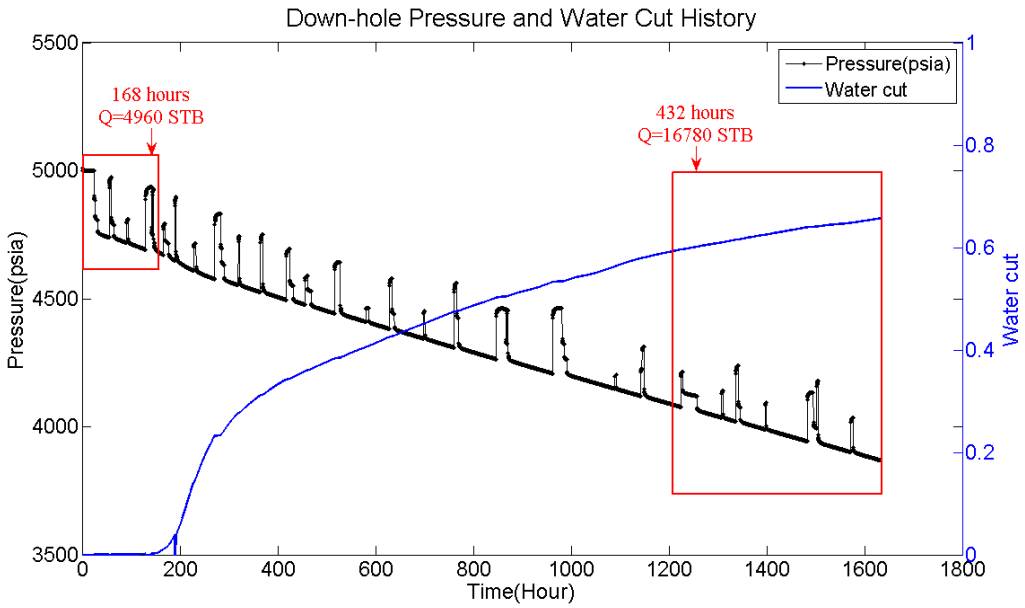

Figure 4-26: Oil and water two-phase reservoir with increasing water cut.

In the first window, as only oil is flowing in the porous media, the reservoir system is linear. The algorithm of flow rate history reconstruction is applicable. The calculated oil flow rate is shown in **Figure 4-27**. The calculated flow rate is almost identical to real rate, and the error is less than 1%.

For the second window, the increasing water cut may cause problems. Fortunately, as the research in the **Section 3.4.5**, the total mobility changes a lot at the time of water breakthrough, and after that, total mobility changes a little during the short time period.

In the second window, the reservoir system can be treated to be linear approximately. With the Haar wavelet processing pressure data (**Figure 4-28**), the developed reconstruction algorithm is used to calculated flow rate history. The total liquid flow rate history is reconstructed at first, as shown in **Figure 4-29**. The errors are very small, and indicate that the linear assumption is correct.

In fact, nonlinearity is very little in the second window, although the water cut is increasing. The nonlinearity diagnostic plot is shown in **Figure 4-30**, and it shows URSR A_{urc} is almost constant. The total water production is $Q_w = 10515.952$ STB, and the average water cut $f_w = \frac{Q_w}{Q_t} = \frac{10515.952}{16780} = 0.6267$. With the average water cut, then oil and water flow rate can be calculated, shown in **Figure 4-31**. The difference between calculated rate and real rate is caused by the average water cut. If real time water cut data is used, the result will be more satisfying, as the error of reconstructed total liquid rate is very small.

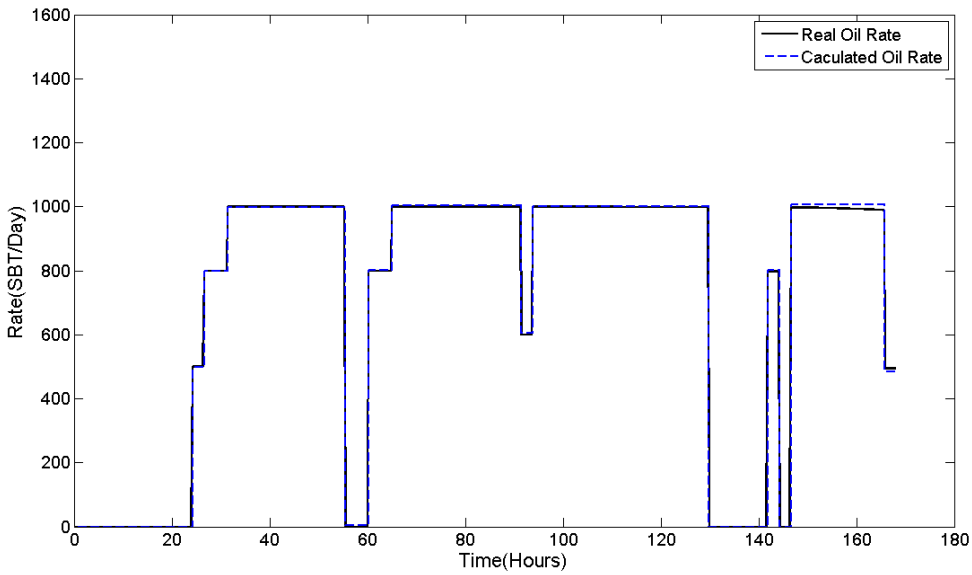

Figure 4-27: The reconstructed oil flow rate history in the first window.

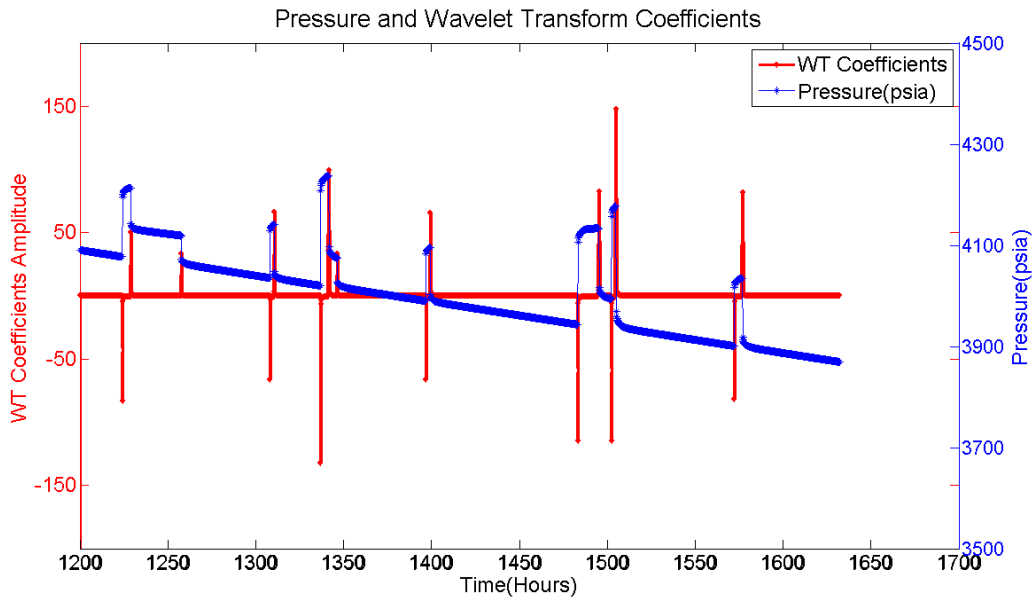

Figure 4-28: Pressure data in the second window is processed by Haar wavelet.

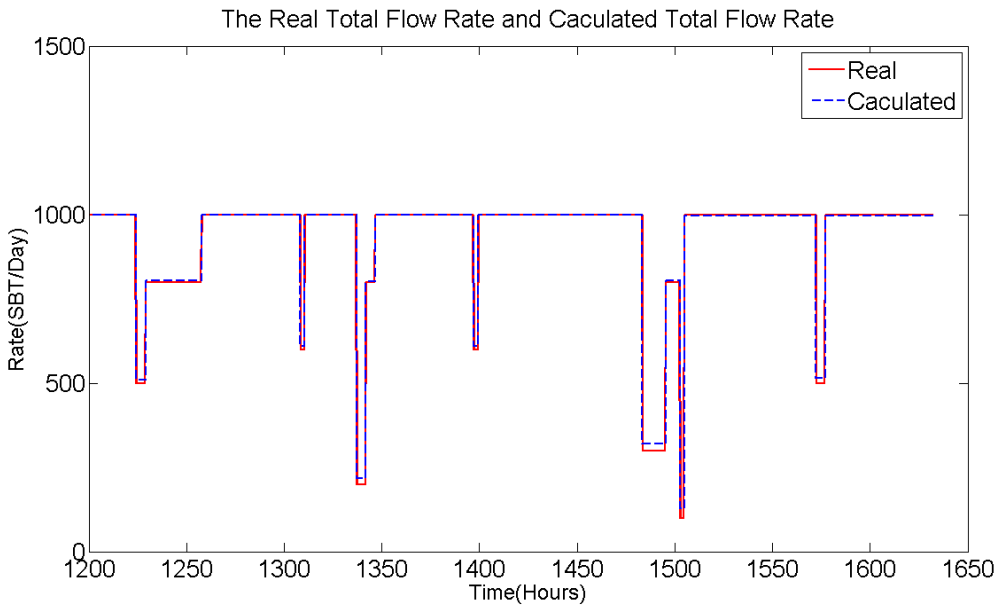

Figure 4-29: The reconstructed total liquid flow rate history.

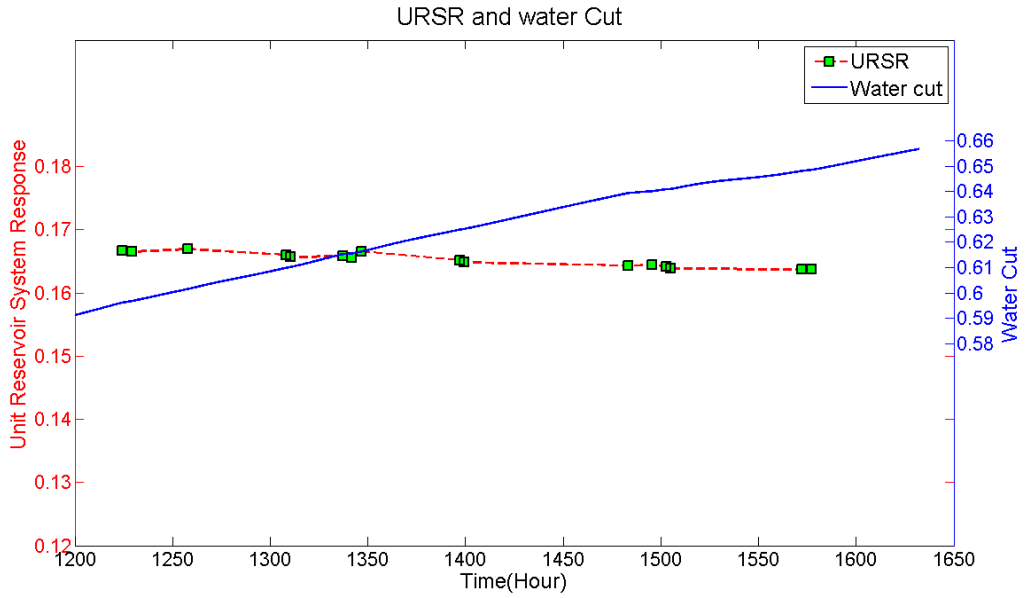

Figure 4-30: The diagnostic result in the second window. URSR A_{urc} is almost constant, and indicates the system can be treated as linear in this time window.

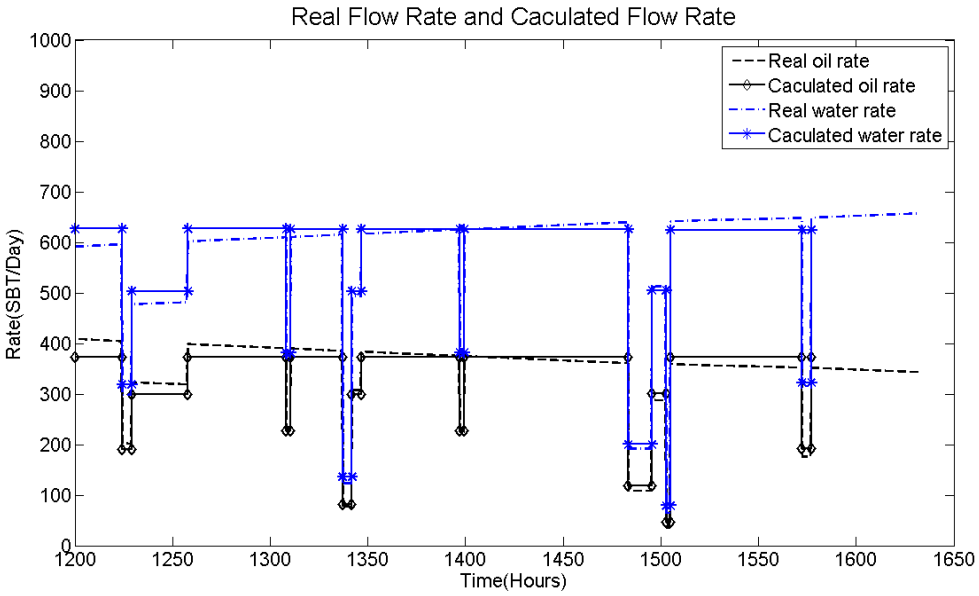

Figure 4-31: The reconstructed oil and water flow rate history in the second window.

When reconstructing flow rate history in oil and water two-phase reservoir with increasing water cut, two kinds of errors may be introduced. The first kind of error is due to nonlinearities which make the linearity assumption is invalid, and the second kind of error is caused by the average water cut data. Nonlinearity brings errors to total liquid flow rate calculation, and the average water cut data will cause errors to the flow rate of each phase.

Besides, around the time of water breakthrough, total mobility changes a lot. High nonlinearity makes flow rate history reconstruction difficult. When selecting time window, the time period of water breakthrough should be avoided.

4.7 Flow rate history reconstruction in gas reservoir and gas condensate reservoir

4.7.1 Real gas reservoir

Flow behaviour of real gas in the porous media is more complex than that of liquid flow system. As the discussion in **Section 3.4.2**, the nonlinearly due to pressure-dependent gas properties has long been recognized as one of the problems in analysing gas well test data.

The compressibility of real gas is the function of pressure:

$$c_g = \frac{1}{p} - \frac{1}{Z}\frac{\partial Z}{\partial p} \tag{4.28}$$

Here z is the real gas deviation factor. For the ideal gas $Z = 1$, and $c_g = \frac{1}{p}$.

Besides, the viscosity of real gas μ is also a function of pressure. As a result, pressure-dependent gas properties make the diffusivity equation governing real gas flow in porous media highly nonlinear and analytical solution is unavailable.

Pseudo-pressure is introduced to partially linearize the diffusivity equation (Al-Hussainy et al. 1966). After linearization, the diffusivity equation is very similar to that of slightly compressible fluids. The definition of pseudo-pressure is:

$$m(p) = 2\int_{p_i}^{p} \frac{p}{\mu(p)z(p)}\,dp \tag{4.29}$$

Here p_i is the reference pressure. Viscosity $\mu(p)$ and deviation factor $z(p)$ must be known as a function of pressure. In field unit, the unit of pseudo-pressure is psia^2/cp.

Normalized pseudo-pressure is introduced to retain unit of pressure, and then the constants of the working equations for a liquid system can be directly used when the gas formation volume is bbl/SCF (Meunier et al. 1987). The definition of normalized pseudo-pressure is:

$$m_n(p) = p_i + (\frac{\mu z}{p})_{p_i} \int_{p_i}^{p} \frac{p}{\mu(p)z(p)} dp \quad (4.30)$$

Normalized pseudo-pressure will be used here, as the linear relationship between the pressure change and rate change can be retained. A case study is presented as follow.

Figure 4-32 depicts a part of pressure history from a gas reservoir. Gas properties are pressure-dependent, as shown in **Table 4-13**. During more than nearly 700 hours production, the cumulative gas production is 1097.5 MMSCF. As the pressure varies from 1500 to 3100 psi, gas compressibility and viscosity change a lot, and the system is nonlinear.

Initially, pressure data is used directly for the flow rate history reconstruction. The average proportional coefficient b is calculated $b = 8.4025$, and the calculated flow rate is shown in **Table 4-14**. Compared with real value, although most of calculated flow rates are satisfying, some error is as high as 7%, which is larger than that in the liquid flow system, which are due to the nonlinearity of pressure-dependent properties.

By contrast, normalized pseudo-pressure is used to linearize the nonlinearity caused by pressure-dependent properties, as shown in **Figure 4-33**. The average proportional coefficient b is $b = 12.3644$. The reconstructed flow rate history is shown in **Table 4-15**. The errors are in 2%, and most is less than 1%. The accuracy is much high than that using pressure directly to calculated flow rate.

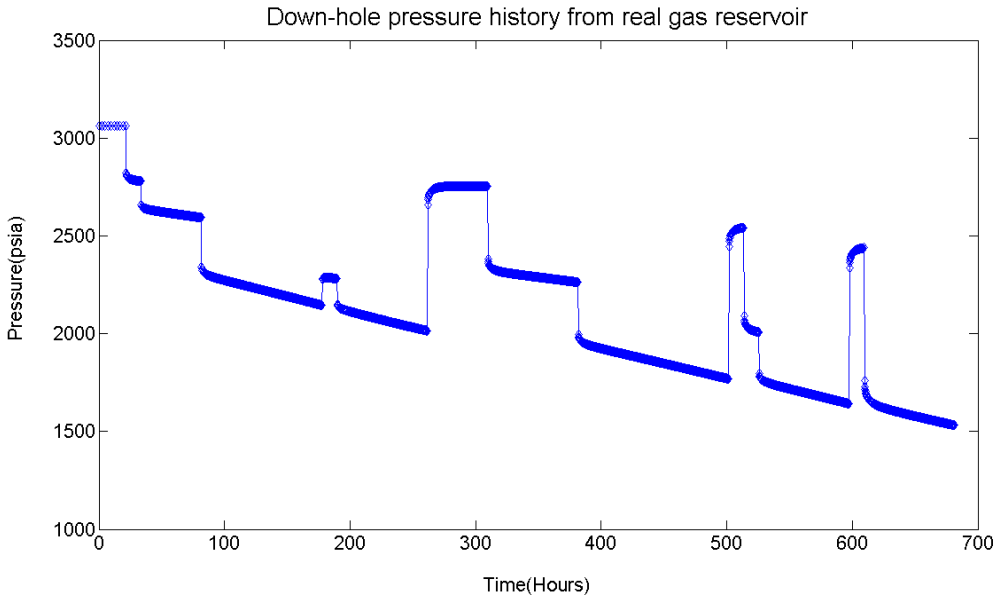

Figure 4-32: Down-hole pressure history from real gas reservoir

Table 4-13: The real gas PVT properties**.**

Pressure (psia)	Deviation factor Z	Viscosity (cp)
0	0.937	0.01286
800	0.882	0.0139
1200	0.832	0.0153
1600	0.794	0.0168
2000	0.77	0.0184
2400	0.763	0.0201
2800	0.775	0.0217
3200	0.797	0.0234
3600	0.827	0.025
4000	0.86	0.0266
4400	0.896	0.02831

Table 4-14: The calculated flow rate with gas pressure data.

Beginning (Hour)	Ending (Hour)	Time period (Hour)	Real rate (MMSCF/D)	Calculated rate (MMSCF/D)	Error (%)
0	21.84	21.84	0	0	0
21.84	33.84	12	20	20.15	-0.77
33.84	81.84	48	30	30.41	-1.35
81.84	177.84	96	50	51.59	-3.18
177.84	189.84	12	40	40.66	-1.64
189.84	261.84	72	50	51.64	-3.27
261.84	309.84	48	0	0	0
309.84	381.84	72	30	28.81	3.96
381.84	501.84	120	50	51.32	-2.63
501.84	513.84	12	0	-5.57	0
513.84	525.84	12	35	32.54	7.02
525.84	597.84	72	50	50.42	-0.84
597.84	609.84	12	0	0	0
609.84	681.6	71.76	50	48.92	2.16

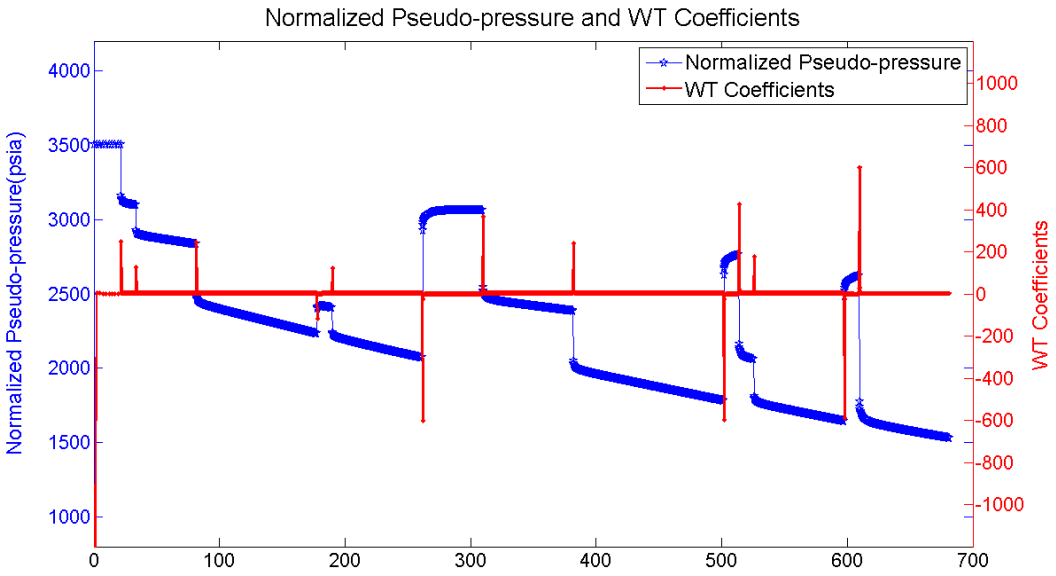

Figure 4-33: Normalized pseudo-pressure and WT

Table 4-15: The flow rate calculation using pseudo-pressure.

Beginning (Hour)	Ending (Hour)	Time period (Hour)	Real rate (MMSCF/D)	Calculated rate (MMSCF/D)	Error (%)
0	21.84	21.84	0	0	0
21.84	33.84	12	20	19.95	-0.27
33.84	81.84	48	30	29.86	-0.45
81.84	177.84	96	50	49.57	-0.87
177.84	189.84	12	40	39.96	-0.11
189.84	261.84	72	50	49.61	-0.78
261.84	309.84	48	0	0.76	-
309.84	381.84	72	30	30.36	1.21
381.84	501.84	120	50	49.71	-0.58
501.84	513.84	12	0	1.30	-
513.84	525.84	12	35	35.6	1.71
525.84	597.84	72	50	49.89	-0.22
597.84	609.84	12	0	1.94	-
609.84	681.6	71.76	50	50.33	0.65

For the gas production with large production rate and low formation permeability, down-hole pressure has large variation range, and as a result, the nonlinearity is high due to large variation of gas properties. Using normalized pseudo-pressure instead of

pressure data can significantly improve the accuracy of reconstructed flow rate history in gas reservoir.

4.7.2 Gas condensate reservoir

The reservoirs with gas condensate are becoming more common as explorations are encountering greater depth, higher pressure and higher temperature. The multi-phase flow conditions near the wellbore and pressure-dependent fluid properties make the system highly nonlinear. Reconstruction flow rate history is challenging.

A part flow history from condensate reservoir is shown in **Figure 4-34**. During more than one month production, the gas oil ratio (GOR) is around 21 MSCF/STB and increases a little. The cumulative gas production is 653MMSCF, and cumulative oil production is 3167.734 STB.

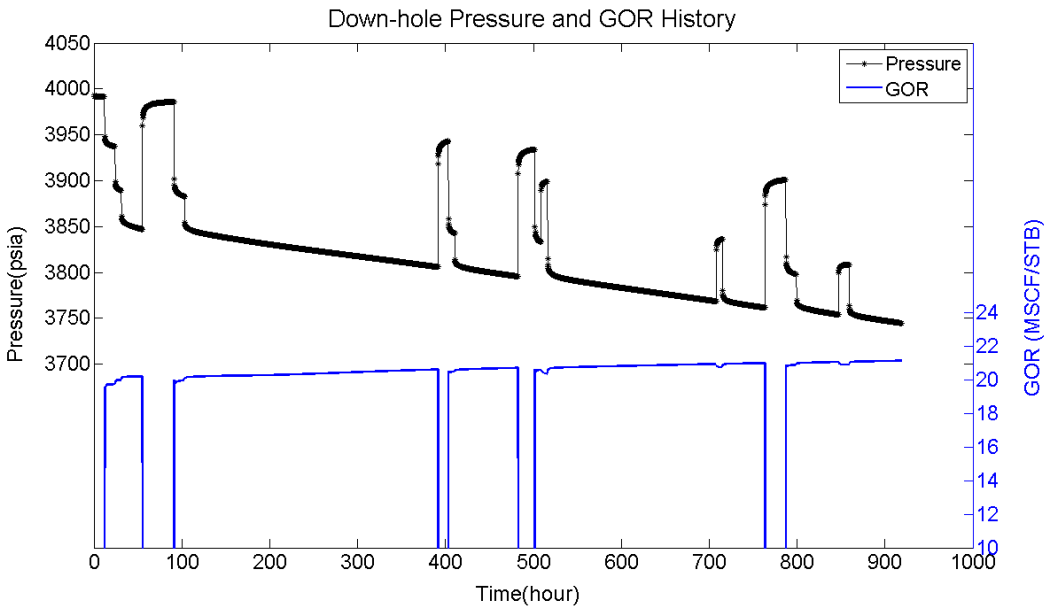

Figure 4-34: The down-hole pressure and GOR history from a gas condensate reservoir.

As the range of down-hole pressure change is small (3750-4000 psi) and the GOR change little, the reservoir system is treated to linear. Wavelet is used to process pressure data, and flow rate history of oil and gas are reconstructed with the developed algorithm. The result is shown in **Figure 4-35**.

The reconstructed flow rate history for oil and gas are stratifying overall. It is due to the low nonlinearity during this short production time. The pressure variation is small, and

flow conditions (such as GOR) can be treated to be constant, therefore the linear assumption is valid.

However, the practice productions are much more complex than this case. During the long-term production, reservoir depletes and down-hole pressure changes a lot. Productivity can be reduced due to accumulation of condensate near the wellbore. As a result, the linear assumption may be not valid under this circumstance, large uncertainties may be introduced.

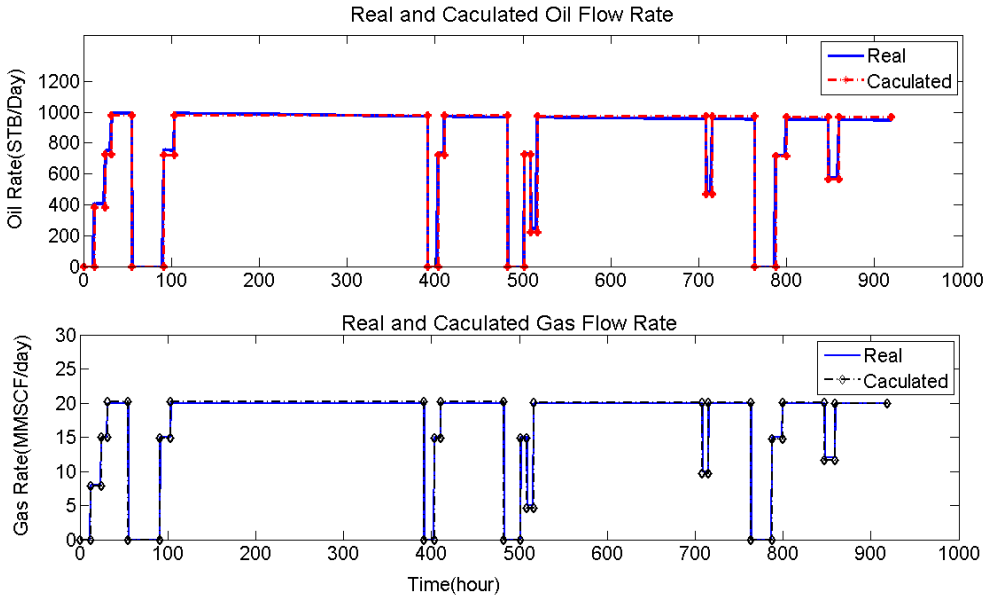

Figure 4-35: The calculated oil and gas rate is near to the real rate.

4.7.3 Gas out of solution

When down-hole pressure drops below the bubble point, dissolved gas will be out of solution. As the discussion in **Section 3.4.4**, the flow conditions near the wellbore change to oil and gas two-phase flowing. The pressure history in **Section 3.4.4** is taken as an example. To simplify the problems, wellbore storage is not considered. Two time windows are selected to reconstruct flow history, shown in **Figure 4-36**.

In the first window, pressure is above the bubble point and only oil is flowing in the porous media. In this one week production, the cumulative gas production is 1650 MSCF and 1110 STB oil is produced. With the developed reconstruction algorithm, the calculated oil and gas flow rate is shown in **Figure 4-37**. The results are close to the real values as the system is linear.

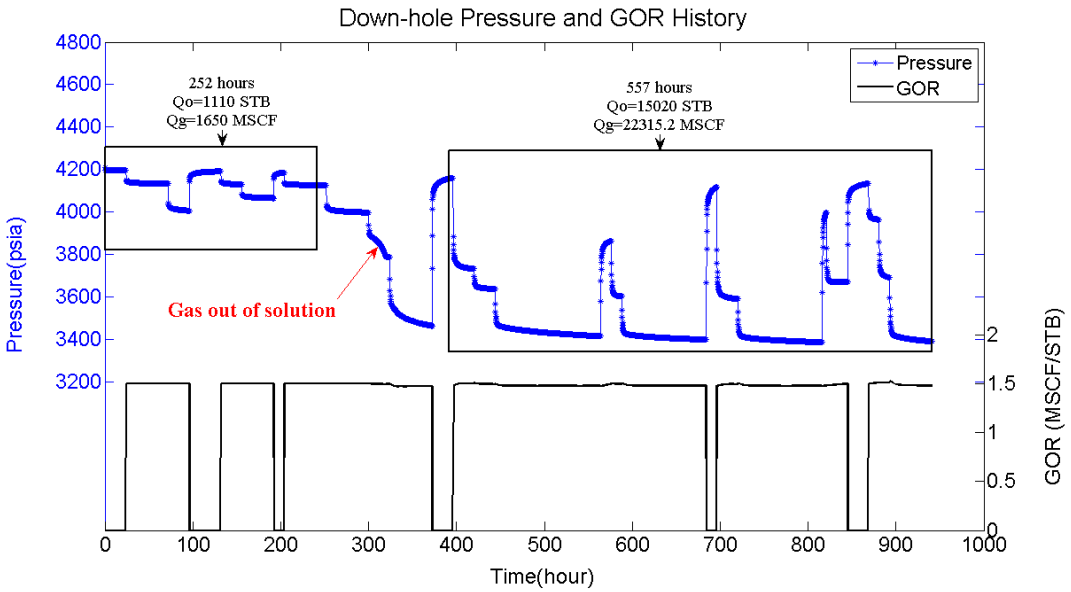

Figure 4-36: Two time windows are selected to reconstruct flow rate history.

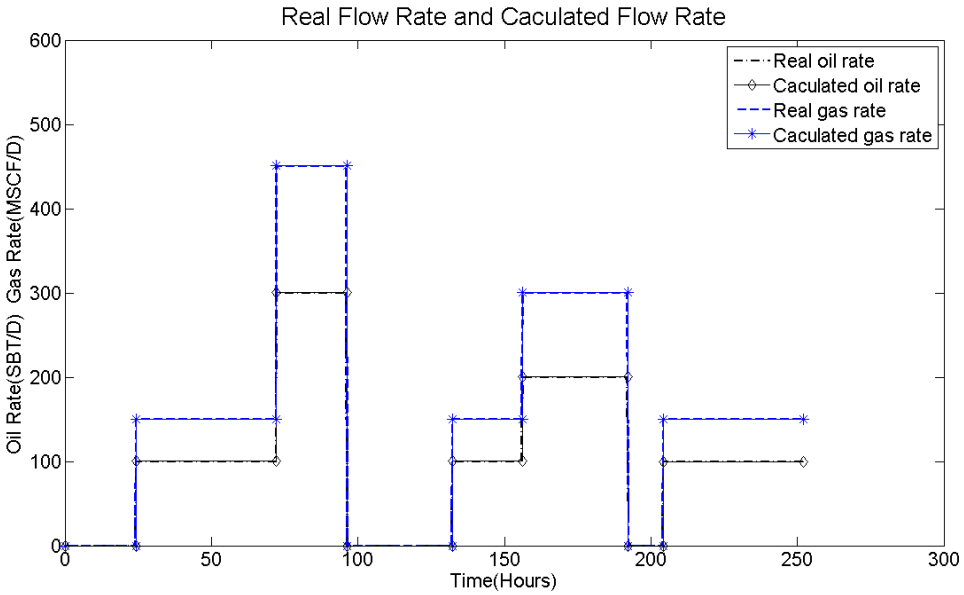

Figure 4-37: The calculated flow rate for gas and oil phase in the first time window.

The second time window is after gas out of solution. During more than two weeks production, 15020 STB oil and 22315.2 MSCF gas are produced. As the nonlinearity is low, the system is approximated to be linear. The calculated flow rate for gas and oil are shown in the **Figure 4-38**. Although the errors are small but they are larger than that in the first time window, due to the nonlinearity caused by pressure-dependent gas properties.

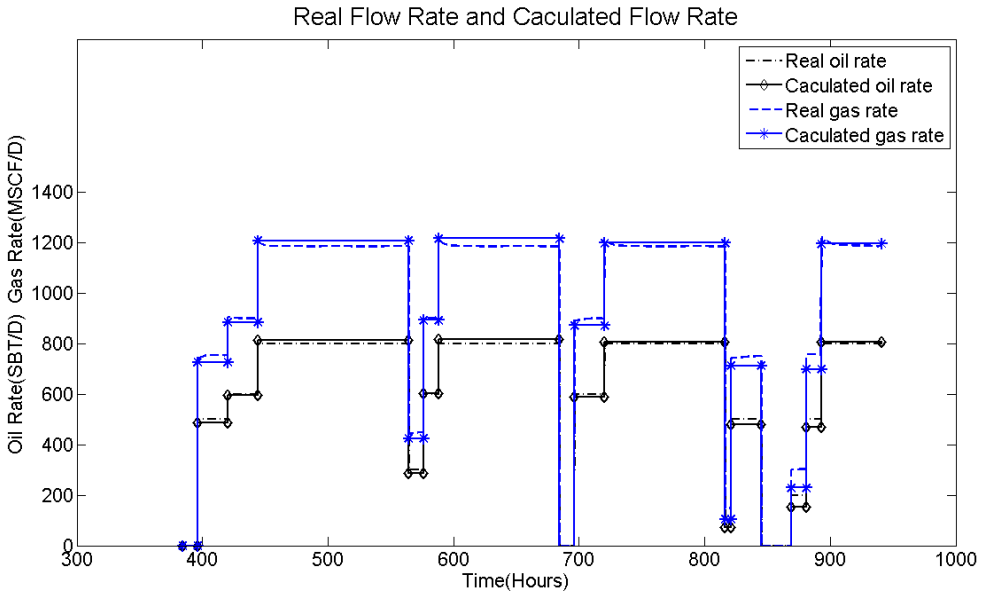

Figure 4-38: The reconstructed flow rate history in the second time window.

However, when wellbore storage effect is considered, the nonlinearity caused by phase segregation is much higher and cannot be neglected. If the system is approximated to be linear, larger errors are introduced, as **Figure 4-39** shows. The errors are very large and the result is unsatisfying. The high nonlinearities make the reconstruction algorithm invalid.

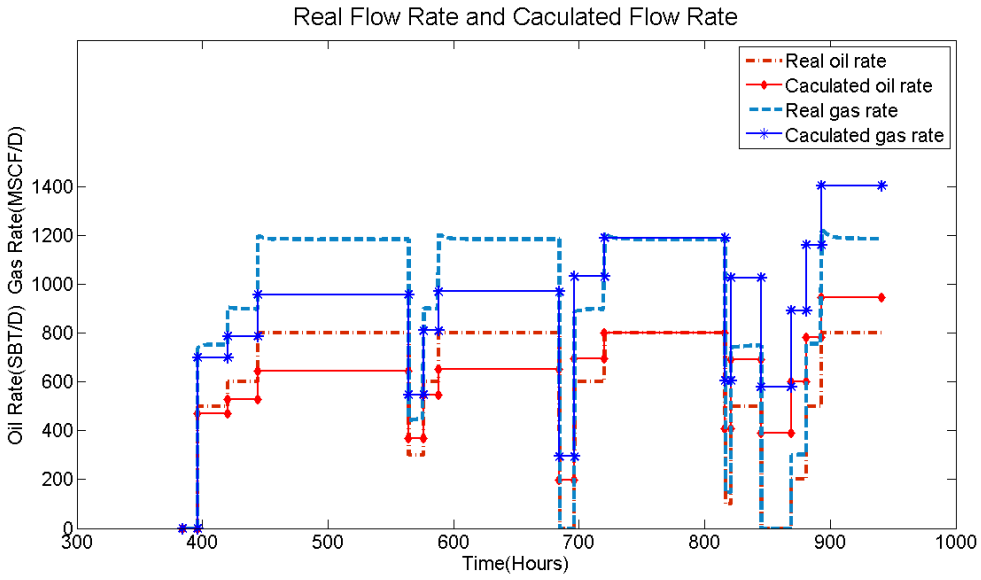

Figure 4-39: The reconstructed flow rate history in the second time window when wellbore storage effect is considered.

Around the time of gas out of solution, the flow conditions change dramatically. During this time periods, flow rate history reconstruction should be avoided due to high nonlinearities.

4.8 Chapter conclusions

In this chapter, a novel method of reconstructing unknown flow rate history method has been proposed. This method is independent of the reservoir model, only the down-hole transient pressure data and cumulative production data are used. This method requires the system is linear, and reservoir properties and flow conditions are constant with time. The effects of skin, wellbore storage, reservoir heterogeneity, well interference, multiphase flow and compressible gas flow have been considered, and therefore this method has the capability for wide applications.

In the process of theory development and case studies, several conclusions can be summarized as following:

1. In the single oil reservoir, in the case of constant skin factor and wellbore storage coefficient, reservoir heterogeneity and production interference, the developed reconstruction algorithm works well. For the flow history with closely happening flow events, the errors of calculated flow rate are small.
2. In the case of unknown initial flow rate, an algorithm based on trial-and-error approach has been developed. The unknown initial rate can be determined and unknown flow rate history can be reconstructed.
3. When the production of several wells are measured together and each well is equipped with pressure gauge, the detailed flow rate history for each well can be calculated with the multi-well reconstruction algorithm.
4. For the reservoir with oil and water two-phase flowing, during the time periods when water-cut is constant or changes little, the nonlinearity is low and unknown flow rate history for each phase can be reconstructed. Two kinds of errors can be introduced. One is due to the nonlinearity and another is caused by the unknown water cut data.
5. For the real-gas reservoir, calculated rate has larger errors than that in liquid systems as gas properties are pressure-dependent. Normalized pseudo-pressure can be applied to overcome the nonlinearity due to pressure-dependent properties. Flow rate history can be reconstructed with high accuracy when the normalized pseudo-pressure is used.
6. When the nonlinearity in the system is very high and cannot be neglected, such as phase segregation effect after dissolved gas out of solution, the calculated flow rates have large errors.

Chapter 5 Sliding Window Technique for Long-term Transient Pressure Analysis and Reservoir Model Calibration

5.1 Introduction

The purposes of nonlinearity diagnostic and unknown rate history reconstruction discussed in the previous chapters are aimed for pressure-transient analysis to obtain reservoir parameters. For the short time traditional well testing, reservoir parameters are assumed to be constant. However, for the long-term PDG pressure data, usually the reservoir-well parameters are time-dependent, as reservoir properties and well conditions may change during the long-term production in field practice.

The nonlinearities due to the changes in reservoir properties and well conditions are common in the long-term transient pressure data. As a result, the linearity assumption is invalid and pressure-transient analysis (PTA) is challenging, as many PTA methods are based on the linearity assumption. Furthermore, reservoir model needs calibration with the new time-dependent reservoir-well parameters.

Analysing the long-term PDG pressure data by one interpretation is very difficult. Sliding window technique is an effective method of analysing the long-term and large quantities of dataset by dividing the whole dataset into series of continuous windows. The piecewise window makes the time span short and pressure data interpretation is possible. More importantly, the reservoir system with nonlinearities can be divided into several linear systems chronologically. In each window, the time span is short and PTA methods based on the linearity assumption are valid. For instance, deconvolution can convert multi-rate pressure into equivalent constant-rate pressure, which can enlarge the radius of investigation significantly. Time-dependent reservoir-well parameters may be derived in each window. New parameters can be used for reservoir model calibration, and in this way reservoir model can be calibrated continuously to match the field performance.

In this chapter, combined with the novel nonlinearity diagnostic method, sliding window technique is introduced for long-term PDG pressure analysis and reservoir model calibration.

5.2 Theory description

5.2.1 Deconvolution

Deconvolution can provide unit constant-rate drawdown response from the variable-rate pressure data. The time interval of test is longer than that of the conventional well test time, and the radius of investigation is extended.

Figure 5-1 presents the pressure and flow rate history from a simulated heterogeneous closed reservoir model. There are several flow events, and one pressure BU lasting for 24 hours can be used for traditional pressure-transient analysis.

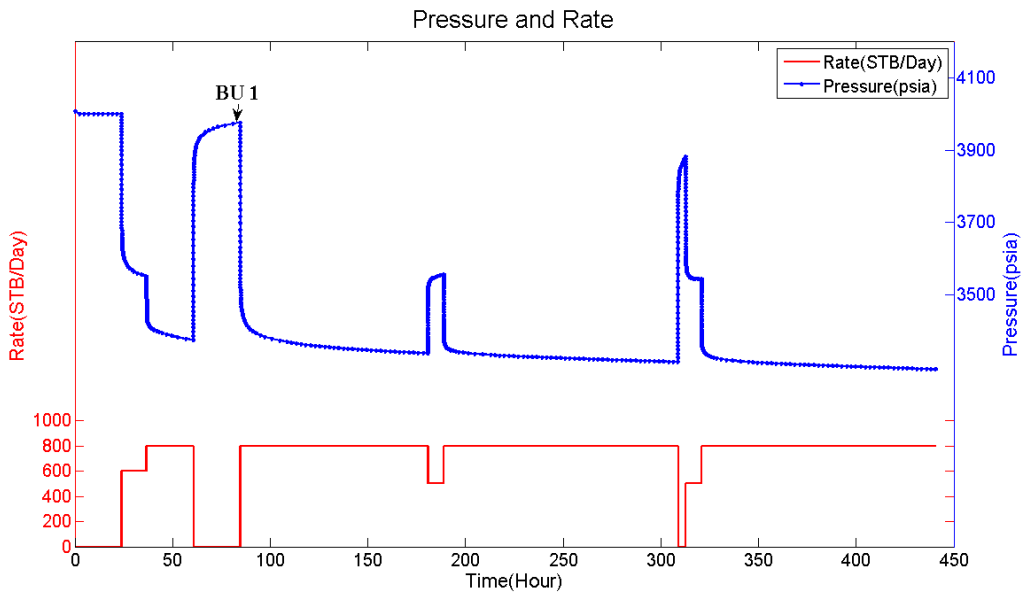

Figure 5-1: The simulated test data from a heterogeneous closed reservoir model.

As shown in **Figure 5-2**, the pressure derivative of pressure BU1 is not long enough to detect the boundary conditions. Deconvolution is used to convert the whole variable-rate pressure into the equivalent constant-rate pressure drawdown response. The deconvolved pressure response is long enough to develop the unit-slop trend characteristic of closed boundaries.

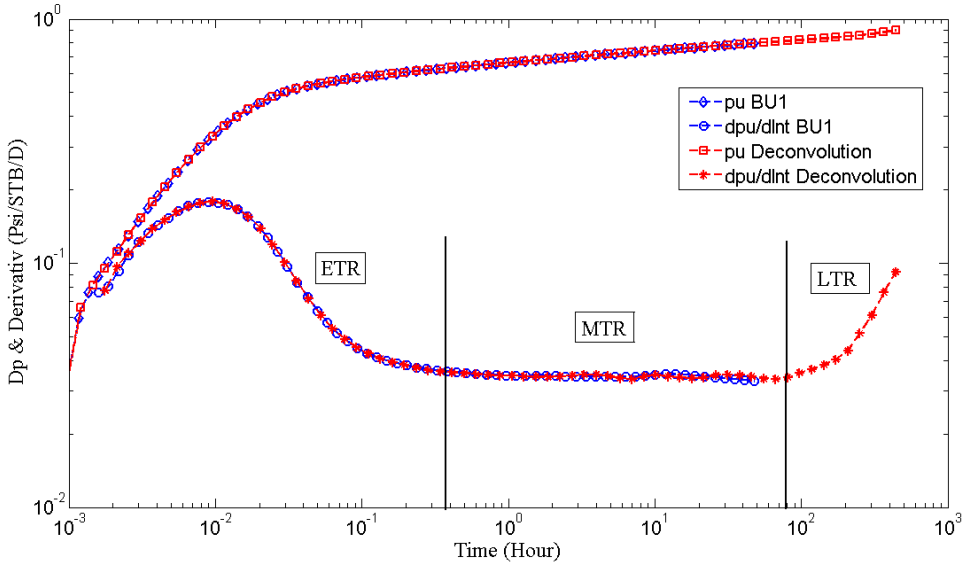

Figure 5-2: Comparison of pressure derivative from PU1 with the response from deconvolution.

Deconvolution is an inverse algorithm of superposition principle and it is only valid under the assumption of linearity. It will fail when there is nonlinearity in the reservoir. In this chapter, deconvolution is used for the demonstration of the nonlinearity diagnostic and window selection for pressure-transient analysis.

5.2.2 Sliding window technique

Sliding window technique is widely applied in signal processing, data mining and etc., especially for long and time-dependent dataset (Luo and Billings 1995, Babcock et al. 2002). The continuous data is divided into a series of time windows, and in each window data is processed separately.

For the long-term pressure data last for thousands of hours, the volume of dataset is too large to analyse by one interpretation. Besides, the reservoir-well properties may change. Therefore, several interpretations with limited pressure length are more reasonable. **Figure 5-3** shows the window technique dividing the long-term pressure data into several short windows.

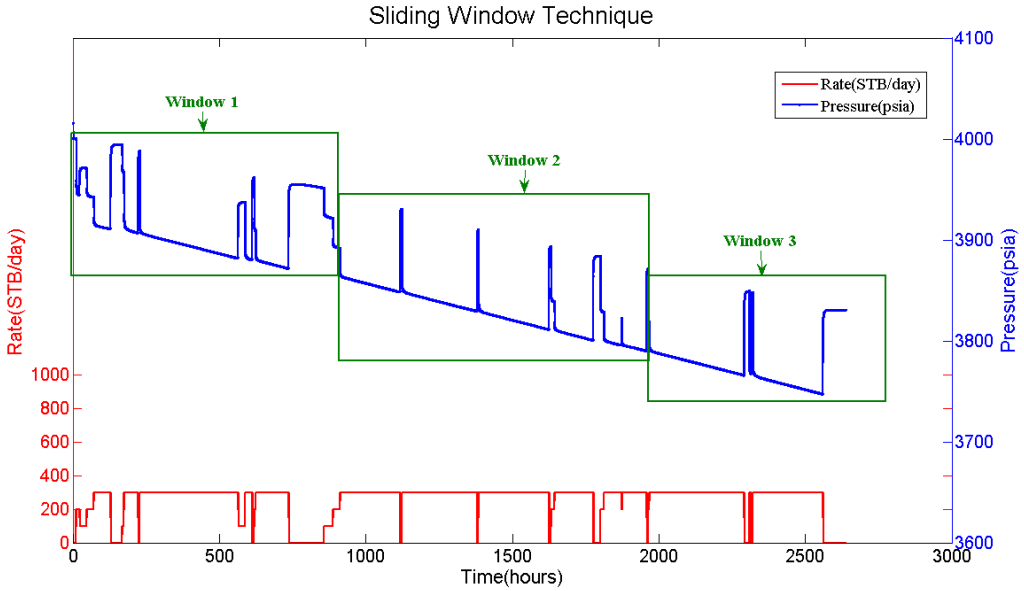

Figure 5-3: Sliding window technique. The pressure data is grouped into different windows, and in each window pressure data is interpreted separately.

Athichanagorn (1999) applied the sliding window technique combined with nonlinear regression to analyse long-term PDG pressure data. In each time window, nonlinear regression is applied to calculate unknown reservoir parameters as well as flow rate. In detail, his method can be summarized into five steps:

1. Select window size and time length.
2. Determine the reservoir model parameters as well as known flow rate by regression method in selected window.
3. Remove the aberrant transients.
4. Update local parameters such as unknown flow rates before moving to subsequent windows.
5. Analyse pressure data in new window.

This method has the potential to solve the problems of long-term and large quantity of PDG pressure analysis, and cope with the problem of nonlinearities due to time-dependent reservoir properties. However, the window selection is unclear and with lots of uncertainties. In Athichanagorn's method, the window size is fixed and only the availability of rate information is considered. The calculated parameters from regression in different windows vary a lot. Some calculated result is shown in **Figure 5-4**. As the figure shows, the change range of calculated value is huge and some values are totally incorrect. Taking the wellbore storage coefficient as an example, some calculated value is even larger than 5 STB/psi, which is unreasonable. The variations of

calculated parameters are not caused by reservoir-well properties change, but mainly due to the instability of regression algorithms. As a result, the calculated parameters are confused and not useful for production monitoring, model calibration.

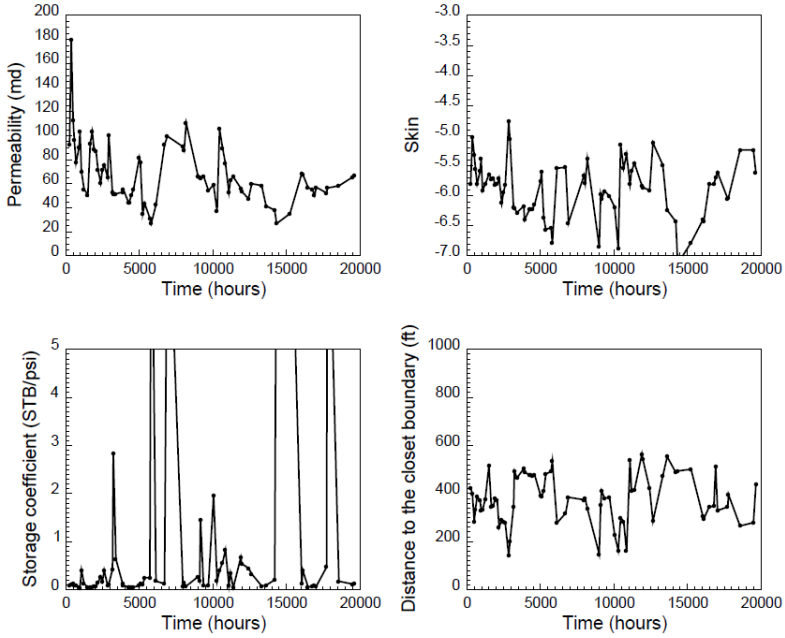

Figure 5-4: Calculated model parameters in different time windows (Athichanagorn 1999).

The better method for window selection is based on changes in reservoir-well properties. With the novel nonlinearity diagnostic method developed in Chapter 3, this problem can be solved. URSR A_{urc} function can evaluate how many changes in reservoir properties and well conditions both qualitatively as well as quantitatively. The large changes in URSR A_{urc} mean high nonlinearities and large changes in reservoir-well properties. The continuous pressure data with little nonlinearities will be grouped into one window. When there are high nonlinearities, time window slides to the subsequent one.

Figure 5-5 shows the workflow of window selection based on the URSR A_{urc} function. Threshold will be set up, when A_{urc} changes more than this threshold, time window will slide to the subsequent one, and reservoir model need calibration with new reservoir-well parameters.

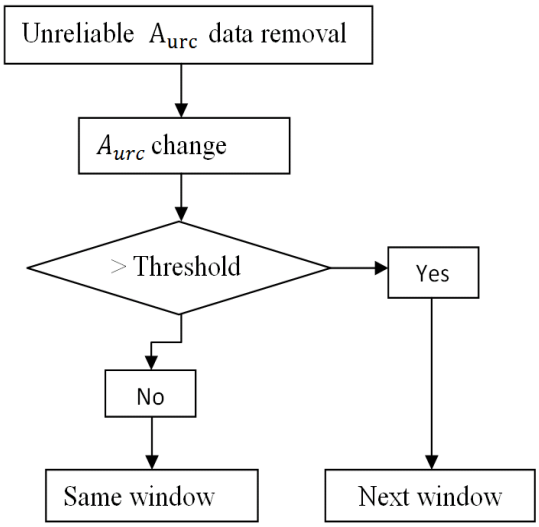

Figure 5-5: The workflow of window selection based on URSR A_{urc} function.

5.2.3 Reservoir model calibration with updating Near Wellbore Model (NWM)

Ideally, the reservoir model should be calibrated continuously with new parameters to match the real field performance and make reliable future forecasting. However, calibrating the full field model (FFM) needs lot of work and also is time-consuming. As the changes in reservoir-well parameters due to long-term production mainly happen near the wellbore, updating the near wellbore model (NWM) is more efficient. After calculation, the size of NWM can be determined and NWM can be extracted from the full field model.

In the near wellbore model, well definitions can be improved and reservoir-well parameters can be updated with new parameters. The grid near the wellbore can be refined, and local grid refinements can reduce numerical dispersions. After that, the NWM can be inserted back to the full field model. The performance of full field model can be improved. The workflow is shown in **Figure 5-6**.

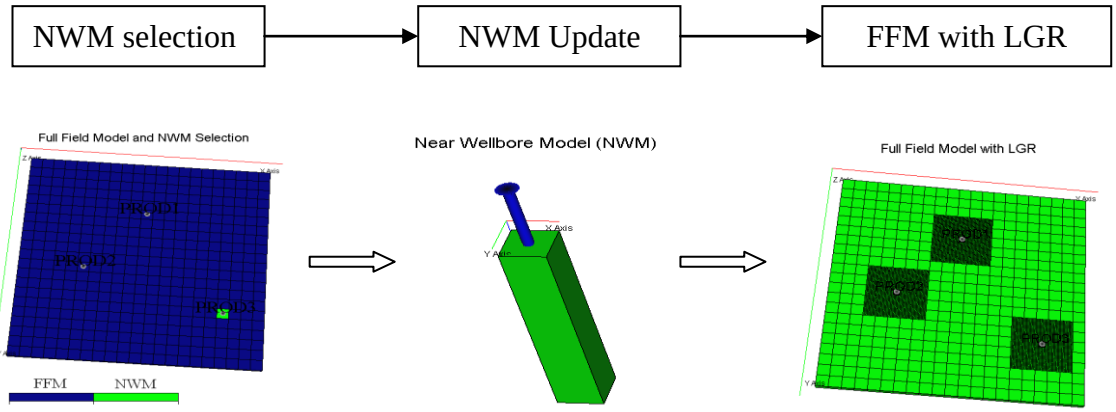

Figure 5-6: Model calibration with updating near wellbore model.

5.3 Analysis of transient pressure with nonlinearity using sliding window technique and deconvolution

5.3.1 Time-dependent skin case

Figure 5-7 shows a part of simulated flow history in a heterogeneous reservoir. After 360 hours production, the well is treated with acidizing and skin factor decreases from 3 to 1.

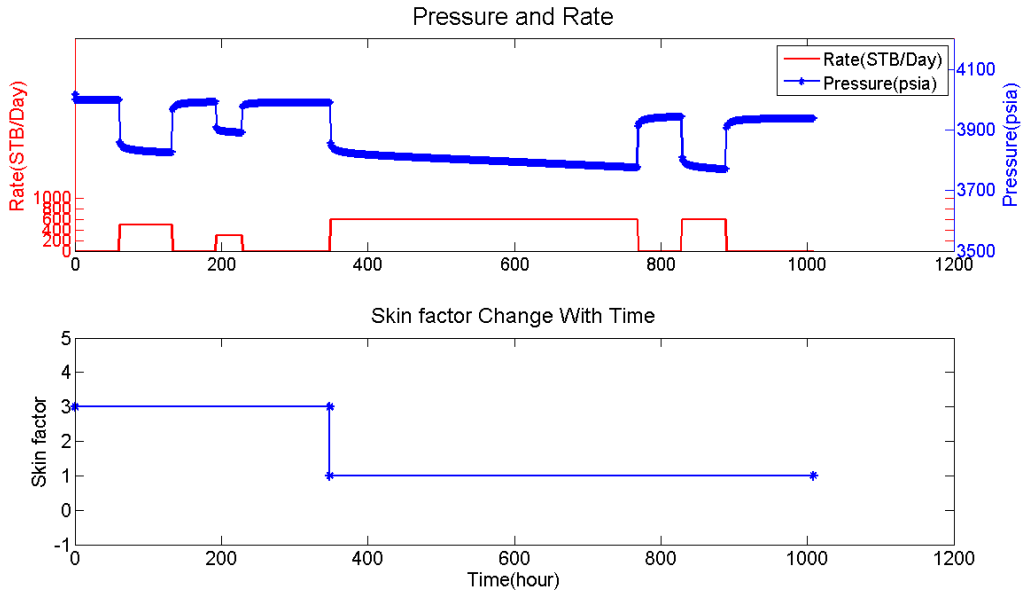

Figure 5-7: The production and skin factor history in a heterogeneous reservoir.

As skin factor is time-dependent, the diffusivity equations governing the fluid flow in the reservoir is nonlinear. As a result, the convolution integral is invalid. Deconvolution algorithm will fail or lead to wrong result. **Figure 5-8** shows the

pressure data for the whole test sequence are processed directly. Although there are no noises in simulated rate and pressure data, deconvolution fails at the late time. The wellbore storage effect and radial flow regime can be detected, but there are large fluctuations at the late time, and boundary condition is unknown.

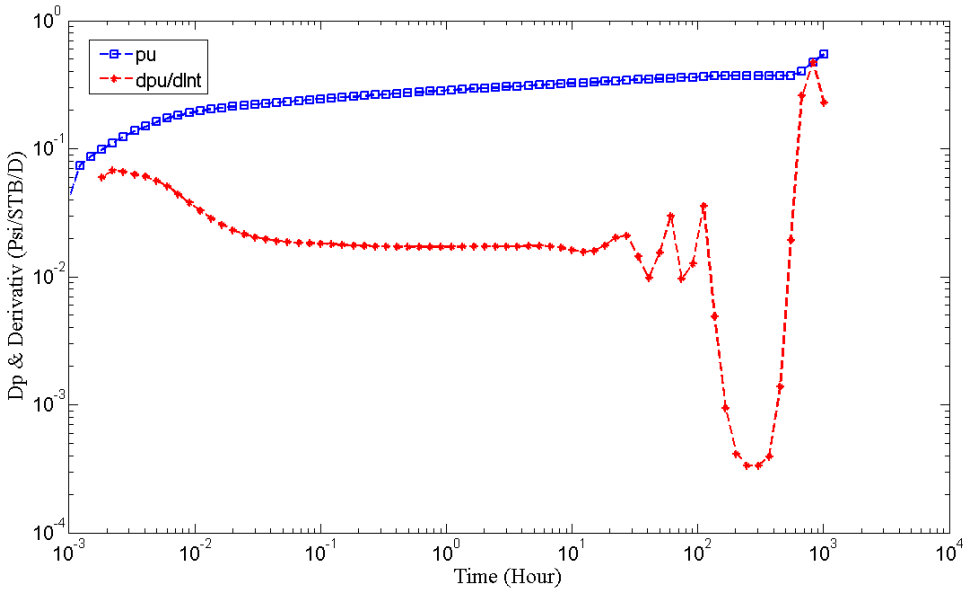

Figure 5-8: Deconvolved response obtained from the whole pressure data in Figure 5-7 with the changing skin factor.

The convolved pressure response obtained from p_u and rate history is shown in **Figure 5-9**. Compared with the real pressure, convolved pressure has large errors. It means that the unit constant-rate pressure p_u cannot match the real pressure response of the reservoir system. The nonlinearity due to time-dependent skin factor makes the deconvoluiton algorithm cannot produce valid result.

To correctly apply deconvolution algorithm, nonlinearities should be diagnosed at first to reduce uncertainties. The Haar wavelet is used for processing pressure data, and the URSR function A_{urc} is calculated to diagnose nonlinearities. In **Figure 5-10**, A_{urc} function is constant initially but decreases to another constant value, indicating that there is nonlinearity in the reservoir system. According to the diagnostic result, time windows can be selected. Sliding window technique is applied to divide the pressure history into two time windows. In this way, the reservoir system is considered to be two linear systems chronologically, and in each time window deconvolution algorithm is valid.

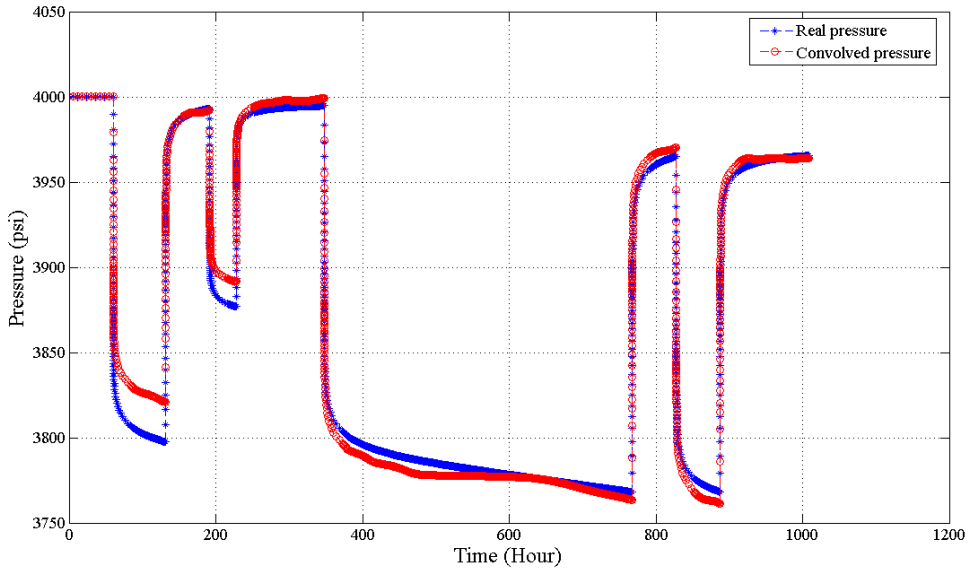

Figure 5-9: The convolved pressure doesn't match the real pressure.

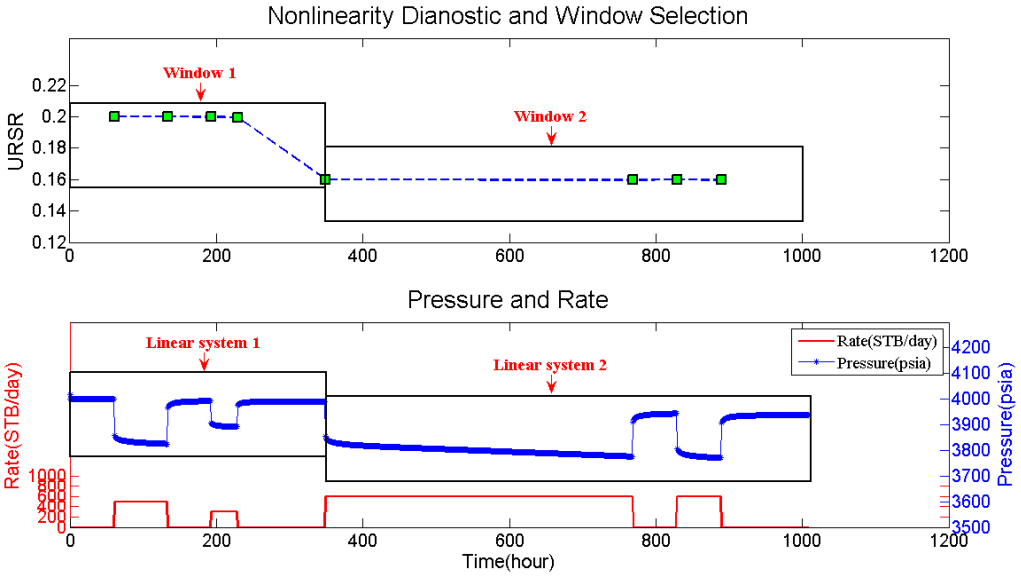

Figure 5-10: Nonlinearity diagnostic and sliding window selection.

Figure 5-11 compares the unit-rate drawdown response derived from the pressure data in two windows. As in each window the reservoir system is linear, deconvolution provides valid results. Deconvolution extends the test time, and the unit slop in p_u derivative in late time regime (LTR) verifies closed boundary conditions. In middle time regime (MTR) and late time regime (LTR), p_u derivative from two windows is coincident but p_u in the second window is lower than p_u in the first window, which means the skin factor decreases during the production time.

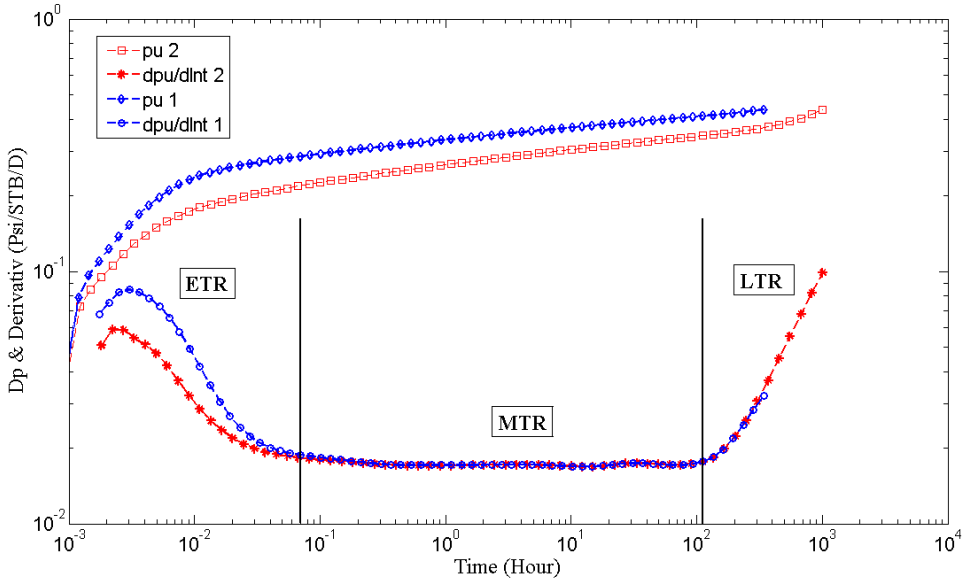

Figure 5-11: Comparison of the drawdown response derived from the deconvolution of pressure data in two time windows.

Figure 5-12 compares the real pressure with the convolved pressure calculated from deconvolution. They are nearly coincident and verify that the pressure response derived from deconvolution can represent the reservoir response.

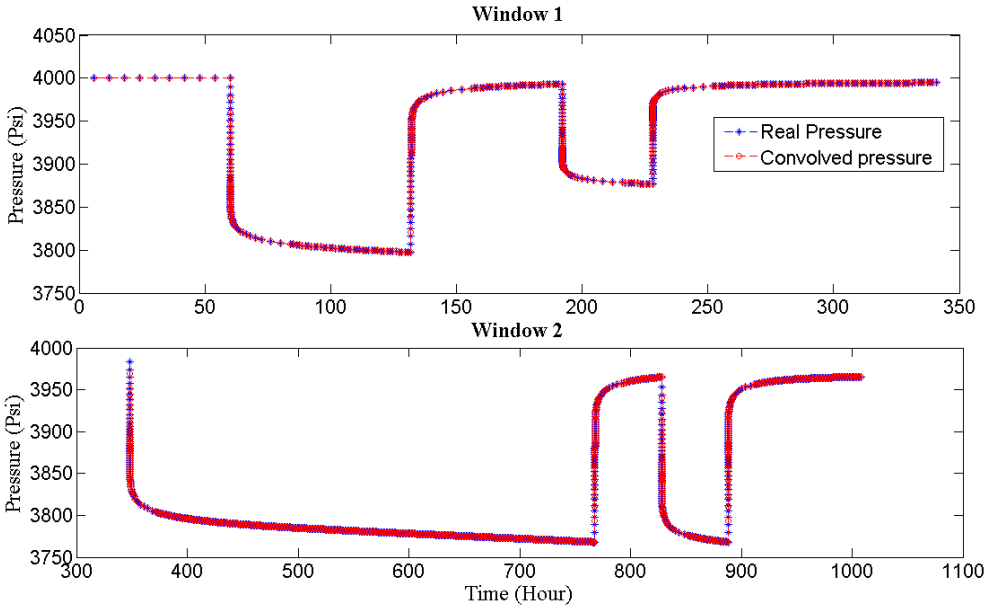

Figure 5-12: Comparison of convolved pressure calculated from deconvolution with the real pressure data in two time windows.

5.3.2 Time-dependent permeability-thickness case

For the reservoirs with poor consolidated formations, permeability-thickness kh may change with time. **Figure 5-13** presents the simulation case with the changing permeability during the production time.

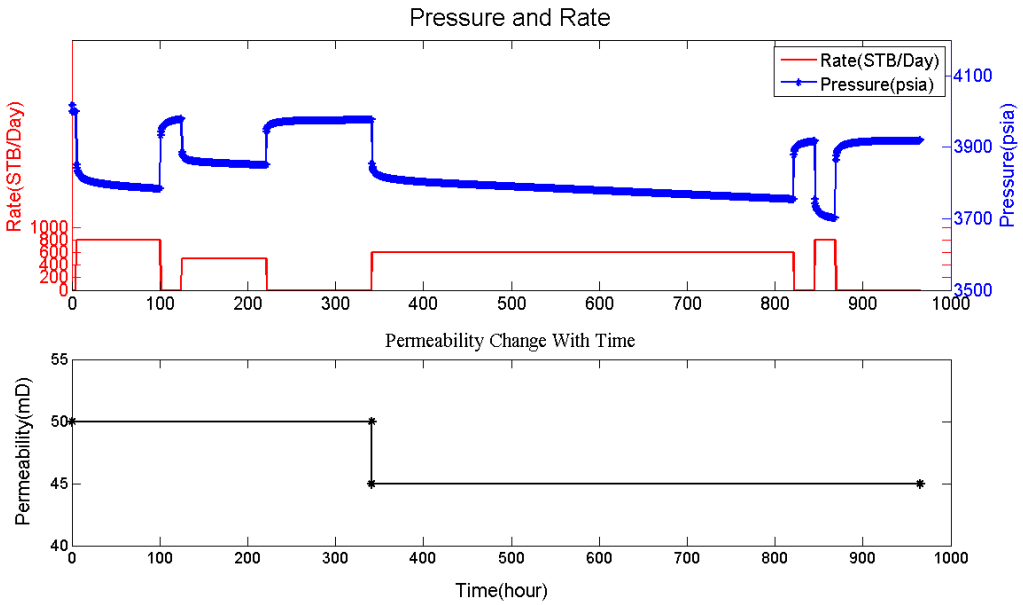

Figure 5-13: Pressure and rate history with changing permeability

In the first 340 hours, the permeability near the wellbore is 50 mD, and after that it declines to 45 mD. The changing permeability causes the reservoir system nonlinear, and deconvolution fails when the whole pressure dataset is processed, as illustrated in **Figure 5-14**. The p_u derivative has a large scattering at late time regime (LTR), and boundary condition cannot be identified. **Figure 5-15** compares the real pressure with the convolved pressure which is calculated from the convolution of derived p_u and rate history. They cannot match with each other due to the changing permeability.

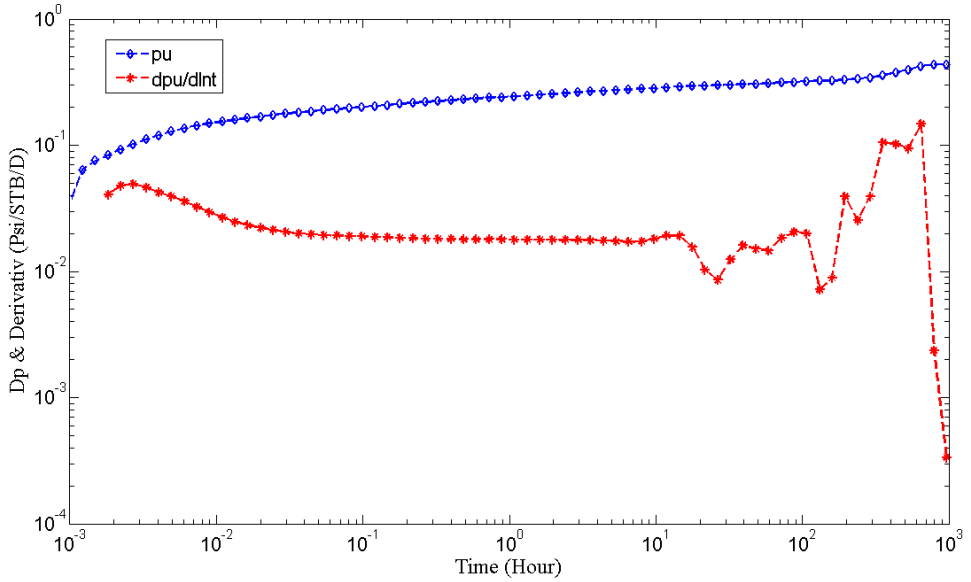

Figure 5-14: Deconvolution of the whole pressure data with changing permeability.

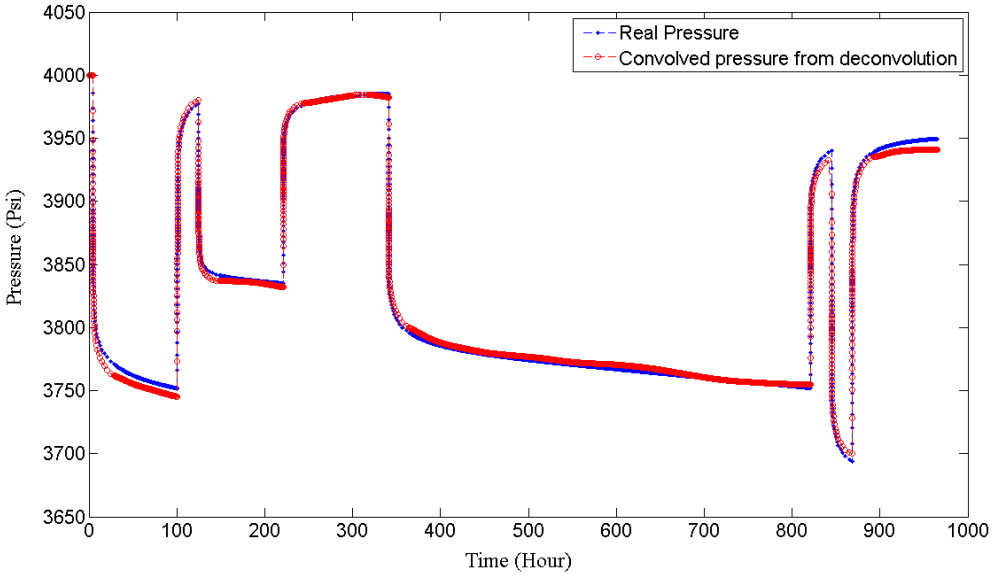

Figure 5-15: The convolved pressure data doesn't match the pressure data due to changing permeability.

Therefore, nonlinearity diagnostic is crucial for deconvolution application. The Haar wavelet is used for processing pressure data, and URSR A_{urc} function is calculated to diagnose nonlinearities. As **Figure 5-16** shows, URSR A_{urc} is constant initially but increases to another constant value. Therefore, two windows can be selected according to the value of URSR A_{urc}. In each time window, URSR A_{urc} is almost constant and system can be treated to be linear. Correspondingly, the pressure data can be grouped into two time windows.

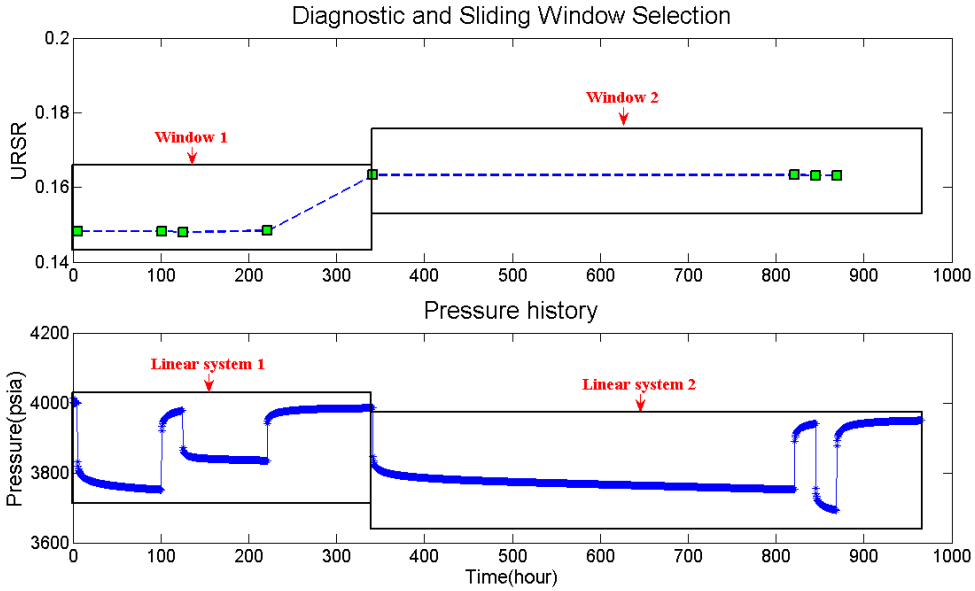

Figure 5-16: Nonlinearity diagnostic result and sliding window selection. The nonlinear system is divided into two linear systems.

In each time window, deconvolution can be applied to convert the variable-rate pressure into unit constant-rate pressure response. **Figure 5-17** compares the unit response p_u and p_u derivative of pressure data in two time windows. In the second time window, unit response p_u and p_u derivative are shift up indicating the decreasing permeability of the formation.

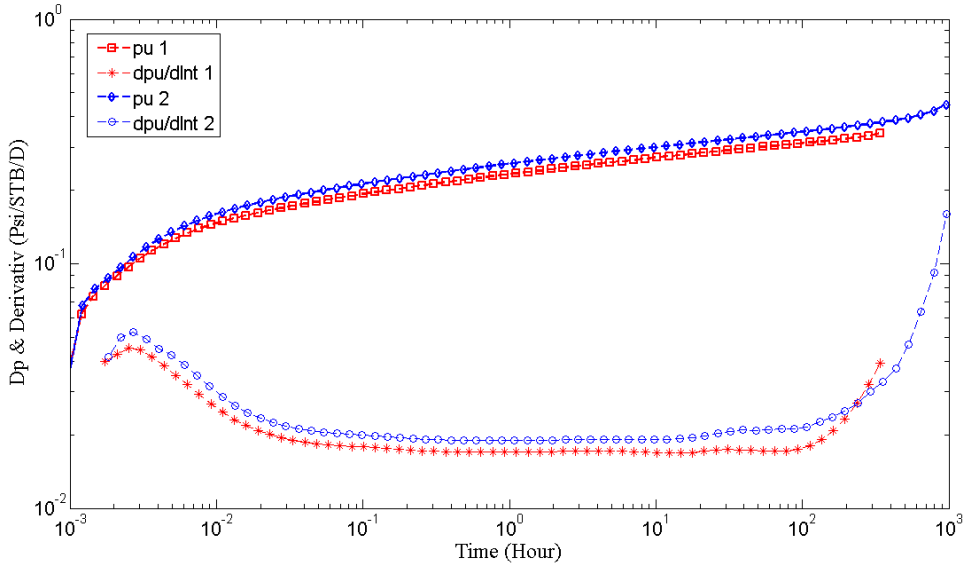

Figure 5-17: Comparison of unit response p_u and p_u derivative in two windows.

5.4 Reservoir model calibration with sliding window technique

In this section, a case of reservoir model calibration with sliding window technique is presented. Initially, nonlinearities are diagnosed from long-term transient pressure data, and pressure data with nonlinearity is analysed with sliding window technique. In each time window time-dependent reservoir-well parameters are interpreted and near wellbore model (NWM) is selected and updated. After that, NWM is put back to the full field model (FFM), and reservoir model can be calibrated.

5.4.1 Reservoir model description

Figure 5-18 shows a heterogeneous oil reservoir model with three production wells, and the initial reservoir properties are shown in **Table 5-1**. The permeability is related log-normal distribution with the range from 10-1000mD, and average is 100mD. The skin factor and wellbore storage effect are considered for each well, and the grids near the wellbore are refined to reduce numerical dispersion. **Figure 5-19** illustrates the production history for three wells which are lasting for nearly four months. Some reservoir-well parameters may change with time during this four months production.

Table 5-1: The parameters for reservoir model

Initial pressure, p_0	4000 psia
Reservoir length, R	6150 ft
Reservoir width, R	6150 ft
Thickness, h	100 ft
Porosity, ϕ	0.27
Average permeability k_h with log normal distribution	100 mD
k_v/k_h	0.1
Oil viscosity, μ_o	1.2 cp
Oil FVF, B_o	1.2 rb/STB
Oil compressibility, C_o	3E-6/psi
Total compressibility, C_t	6.6E-6/psi

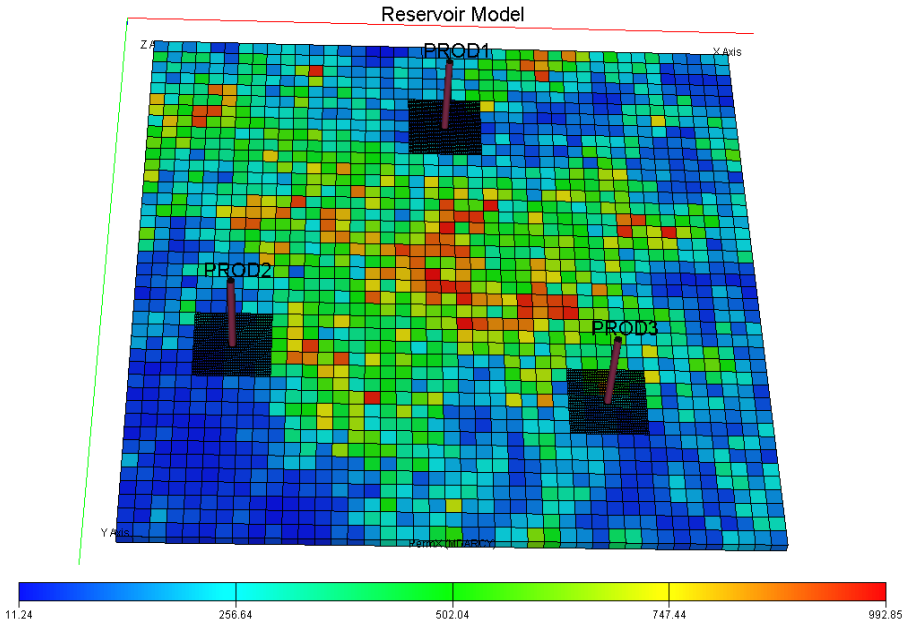

Figure 5-18: Reservoir model for model calibration case study.

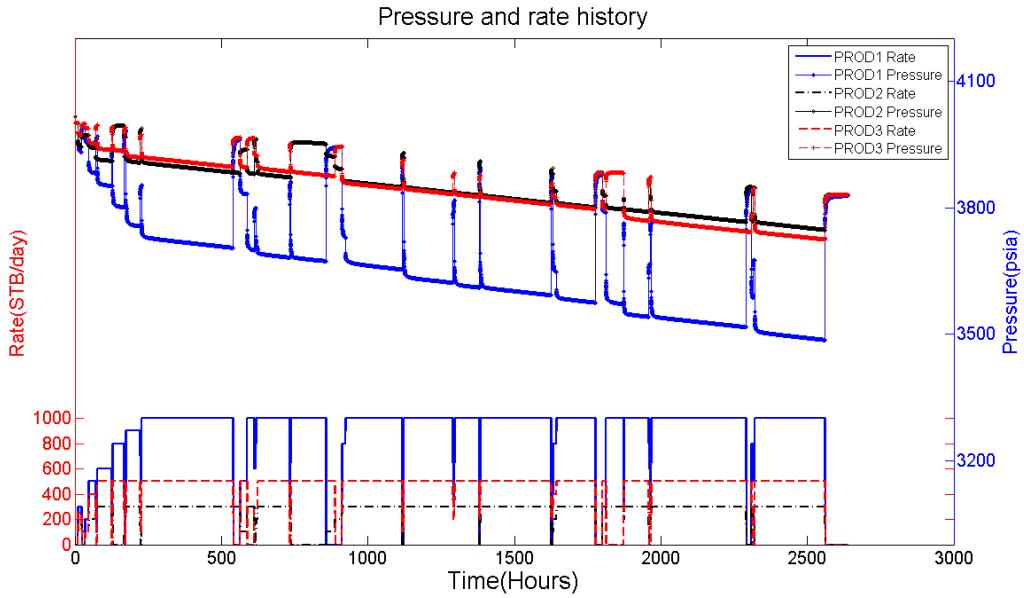

Figure 5-19: Production history for three wells.

5.4.2 Nonlinearity diagnostic with wavelet transform

Figure 5-20 presents that wavelet transform is applied to process pressure data. URSR A_{urc} for three wells is calculated and are shown in **Figure 5-21**. It is a constant value for PROD2 but it changes with time for other two wells, which means there are nonlinearities near PROD1 and PROD3, which are due to the time-dependent reservoir-well parameters.

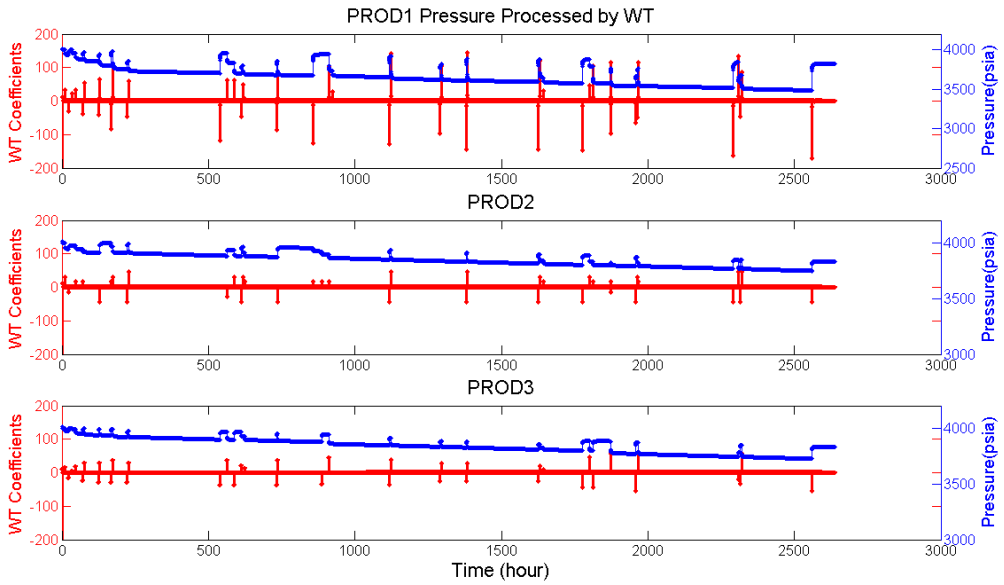

Figure 5-20: WT is applied to process transient pressure data of three wells.

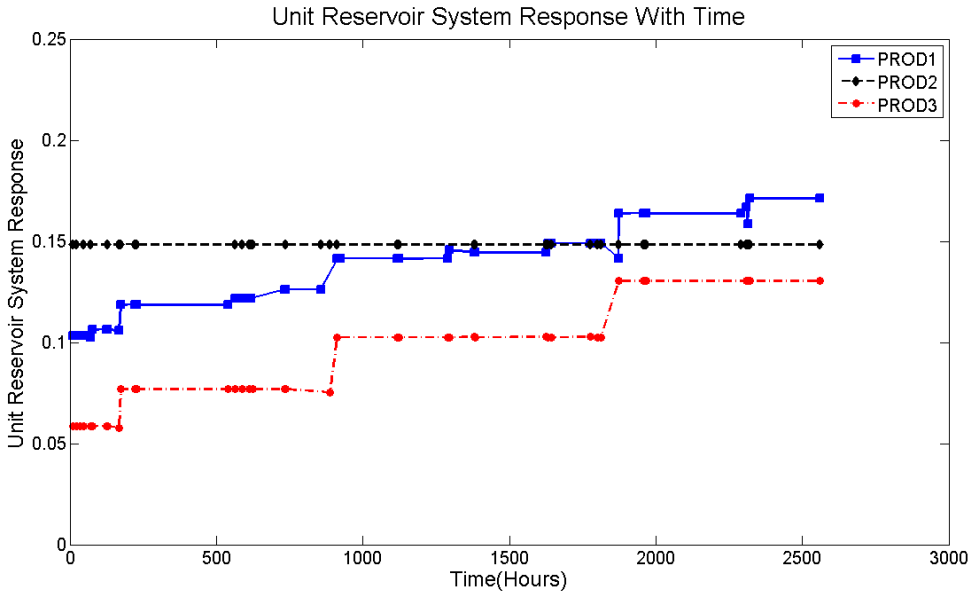

Figure 5-21: URSR A_{urc} for three wells. It is constant for PROD2 well, but it is time-dependent for well1 and well3.

Without model calibration, the model performance cannot match the real pressure, as shown in **Figure 5-22**. With time going on the differences between model performance and real pressure performance become huge, and this will bring large uncertainties for future forecasting. Therefore, for well PROD1 and PROD3, NWM needs update.

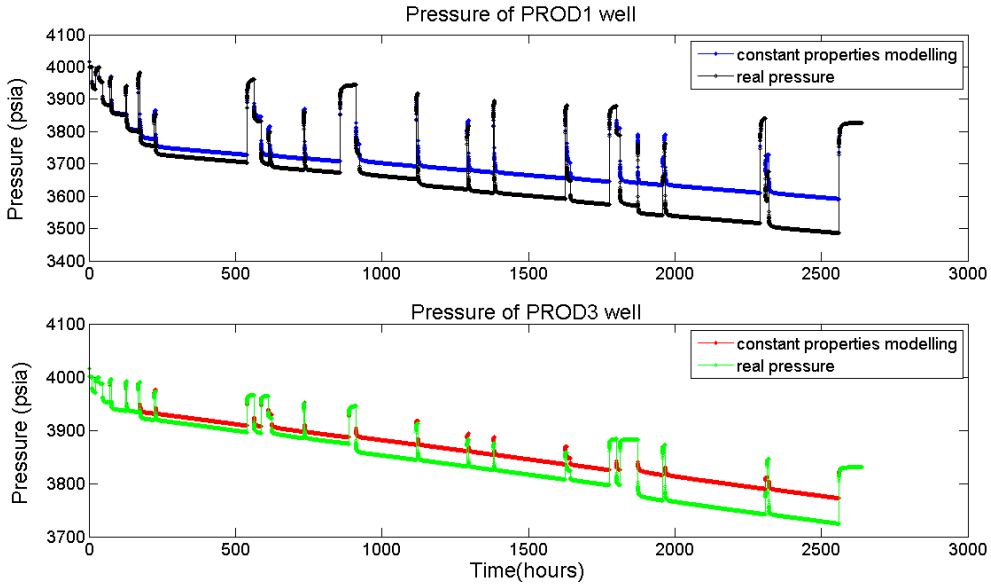

Figure 5-22: The pressure from simulated model with constant reservoir properties cannot match the real pressure performance.

5.4.3 Sliding time window selection

Based on diagnostic result, long-term production history is divided into series of time windows. In the same time window, the nonlinearity is so little than the reservoir-well parameters are treated as constant. **Figure 5-23** shows sliding window selection for PROD1 according to the diagnostic result. Correspondingly, shows the production history of PROD1 is divided into four time windows, as shown in **Figure 5-24**. The window size is same with that in **Figure 5-23**. In each window, one pressure BU is selected for transient pressure analysis to determine new reservoir-well parameters. Similarly, sliding windows are selected for PROD3, shown in **Figures 5-25 and 5-26**.

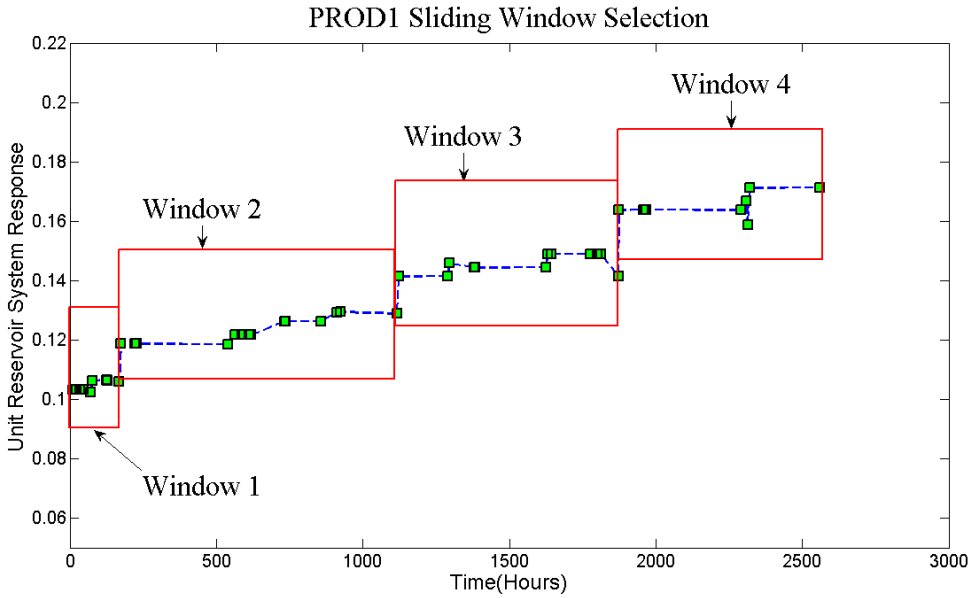

Figure 5-23: The window selection for PROD1 well in URSR A_{urc} function plot

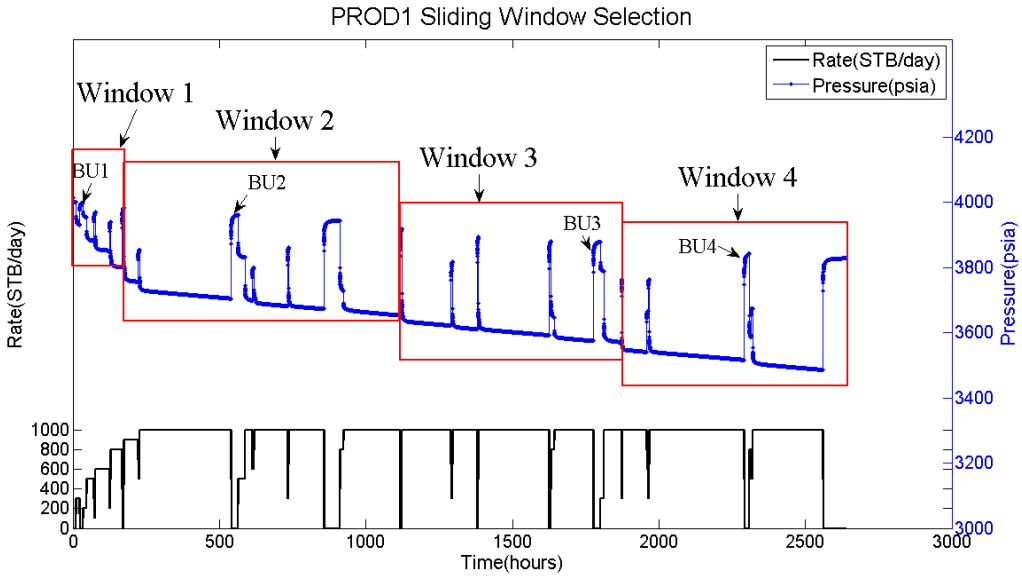

Figure 5-24: The window selection for PROD1 well in pressure history

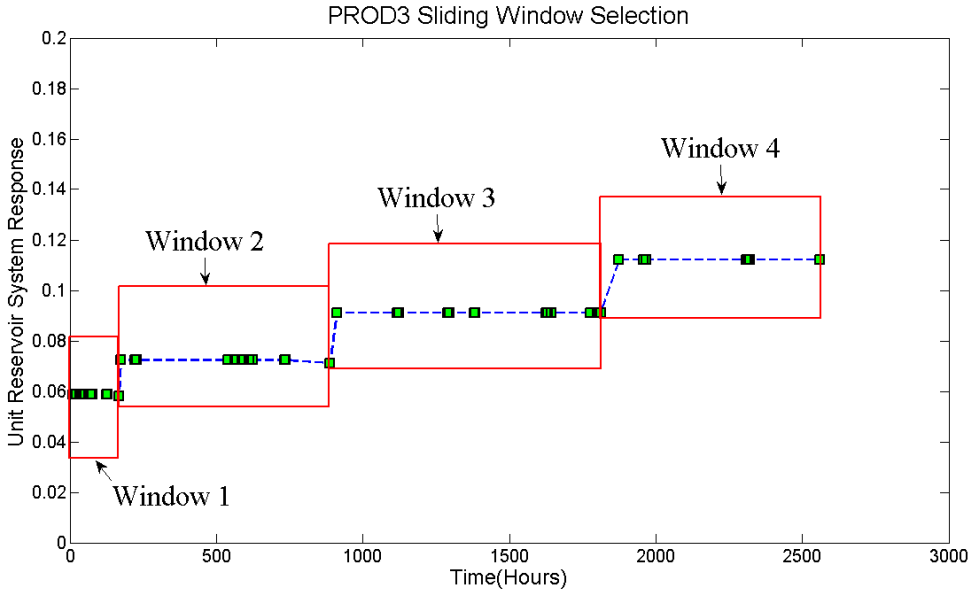

Figure 5-25: The window selection for PROD3 well in URSR A_{urc} function plot

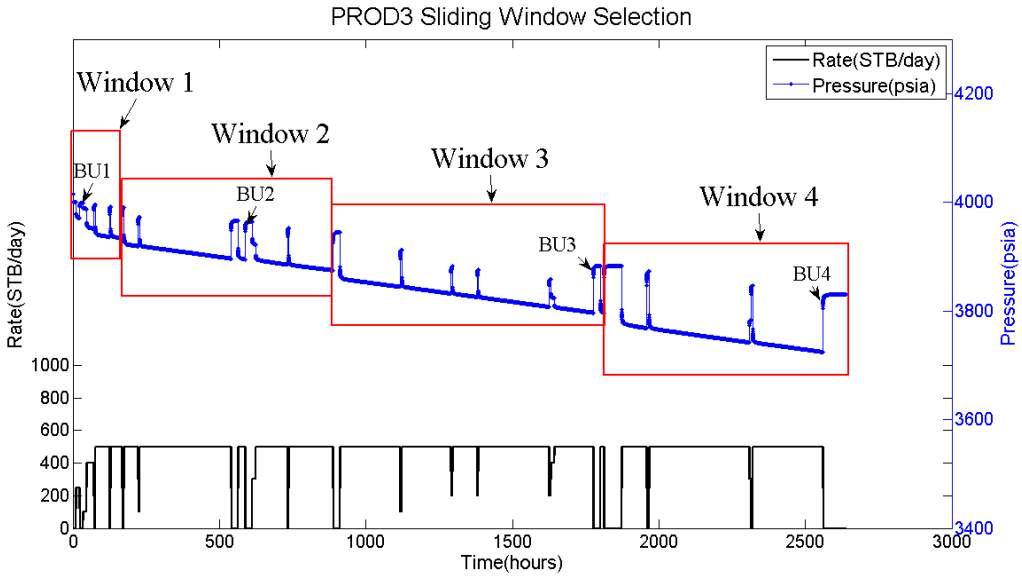

Figure 5-26: The window selection for PROD3 well in pressure history

5.4.4 Pressure-transient analysis for time-dependent parameter interpretation

As the nonlinearity in each time window is little, the reservoir-well parameters can be treated to be constant in each window. With conventional PTA methods, reservoir-well parameters can be interpreted from the selected pressure BU in each time window.

Figure 5-27 shows the pressure BU analysis of PROD1 well in the second time window. **Table 5-2** shows the pressure interpretation results for PROD1 well in four time windows, and skin factor increases from 1.76 to 5.61. Similarly, pressure BU of PROD3 well in each time window is analysed. **Table 5-3** shows the pressure

interpretation results for PROD3 well and permeability around PROD3 wellbore declines from 195.81mD to 98.5 mD, but the skin factor almost is constant. Time-dependent skin factor and permeability cause the reservoir model performance cannot match the real pressure.

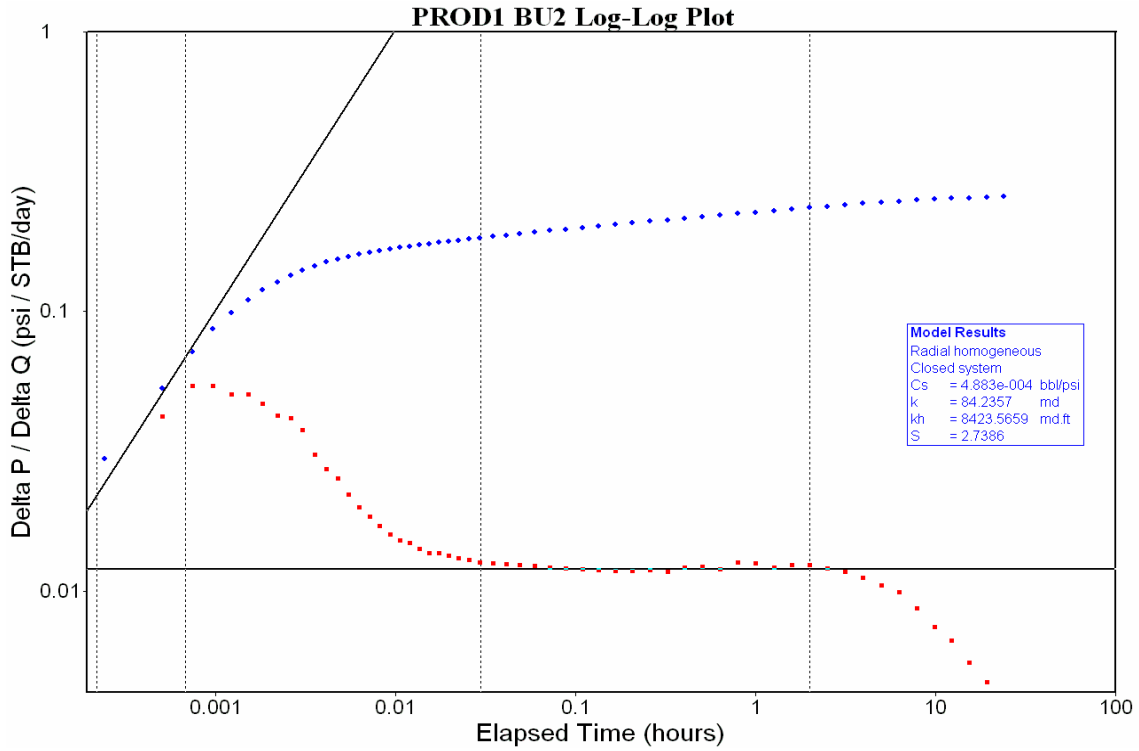

Figure 5-27: Pressure BU of PROD1 well in the second time window is analysed.

Table 5-2: Pressure-transient analysis result in each time window for PROD1

Window index	Window Time Period (hour)	BU well test time period (hour)	Skin factor	Permeability (mD)
1	0-168	24-36	1.76	83.96
2	168-1116	540-564	2.74	83.83
3	1116-1872	1776-1800	4.67	83.92
4	1872-2640	2292-2308.8	5.61	83.67

Table 5-3: Pressure-transient analysis result in each time window for PROD3

Window index	Window Time Period (hour)	BU well test time period (hour)	Skin factor	Permeability (mD)
1	0-168	24-36	2.82	195.81
2	168-888	588-612	2.84	157.11
3	888-1812	1776-1800	2.91	123.7
4	1812-2640	2560.8-2640	2.87	98.5

5.4.5 Near Wellbore Model (NWM) selection and update

PROD1 well can be easily updated with new skin factor, but for PROD3 well, how large area needs updating with the new permeability is unknown. NWM should be calculated before selection. The size of NWM can be calculated with the radius of investigation equation:

$$r_{inv} = 0.029\sqrt{\frac{kt}{\emptyset \mu c_t}} \tag{5.1}$$

As permeability and skin factor are determined in radial flow regime, time t in Eq. 5.1 should be the end time of radial flow, which can be determined in pressure derivative in log-log plot. Taken PROD3 for an example, the size of NWM is calculated in each time window is shown in **Table 5-4**. As the model grid size is 150 ft, only the grid near the wellbore of PROD3 needs update, shown as **Figure 5-28**.

NWM can be updated with time-dependent reservoir-well parameters which changes with different time windows. The interpreted results in **Table 5-2 and 5-3** are used for PROD1 and PROD3 NWM update. After updating, NWM is put back into the FFM with local grid refinement near the well.

Table 5-4: The size of NWM for PROD3 well calculated from the radius of investigation equation.

BU index	End time of radial flow (hour)	Permeability (mD)	Radius of NWM (ft)
1	1.68	195.81	73.42
2	2.04	157.11	72.47
3	2.4	123.7	69.75
4	3.456	98.5	74.69

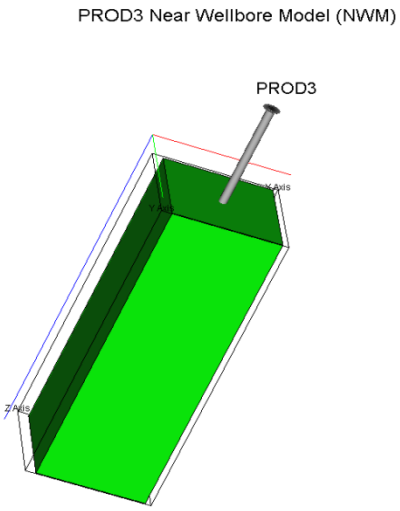

Figure 5-28: Near wellbore model selection for PROD3

The NWM update results for PROD1 and PROD3 are shown as **Figure 5-29**. Compared with constant property modelling, the pressure from updated reservoir model with time-dependent reservoir-well properties varying with different time windows is much more approaching the real pressure performance.

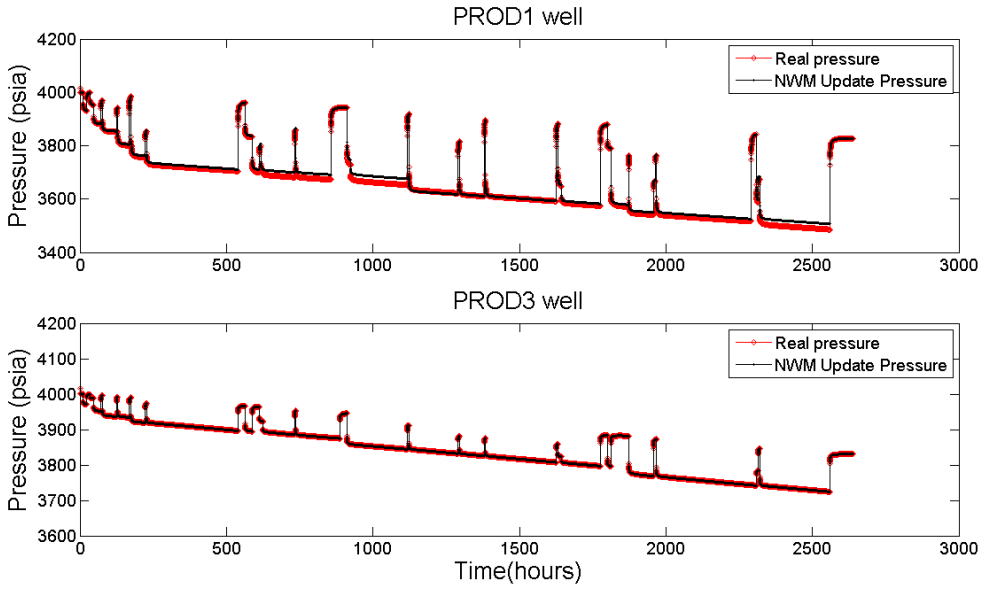

Figure 5-29: The pressure performance after NWM update can match the real pressure of PROD1 and PROD3 well

5.5 Chapter conclusions

In this chapter, combined with the novel nonlinearity diagnostic method, the sliding window technique is proposed for long-term transient pressure analysis and reservoir model calibration. In summary, the following conclusions can be draw:

1. With the novel diagnostic method, sliding window technique is an effective method of analysing the long-term transient pressure data with nonlinearities.
2. The window selection and window size depends on the changes in URSR A_{urc}, which represent the changes of reservoir-well parameters. In each time window, the nonlinearities are little and the system can be treated to be linear.
3. Deconvolution is not recommended to apply to the whole pressure history due to the nonlinearities caused by the changes in reservoir-well properties. In each time window, deconvolution is valid for pressure-transient analysis.
4. The time-dependent parameters can be interpreted from pressure BU in each window, and then can be used for NWM update.
5. The size of the near well model can be determined from the radius of radial flow using the radius of investigation equation.
6. The updated NWM with new parameters can be put back to the FFM. In this way, the reservoir model can be calibrated continuously.

Chapter 6 Field Data Application

6.1 Introduction

In this chapter, the methodologies developed in this thesis are demonstrated with field PDG pressure data. **Figure 6-1** presents the long-term field PDG pressure data from an oil reservoir. The time span of PDG pressure data is very long and it lasts for 10,000 hours. Lots of flow events were recorded, including tens of pressure build-ups. Daily production was measured, but the real-time flow rate history and other reservoir information are unknown.

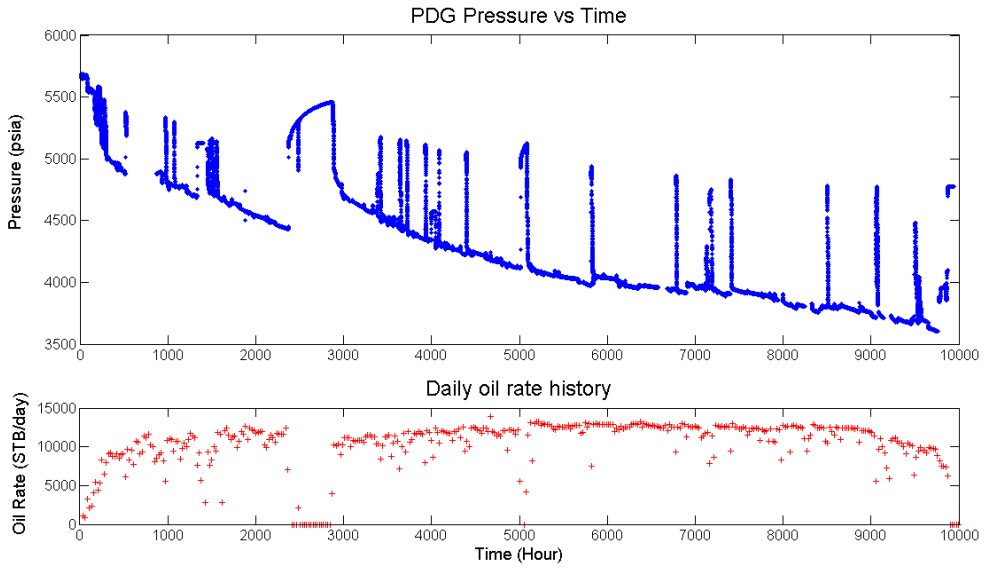

Figure 6-1: PDG pressure data and measured daily rate history from an oil reservoir.

The daily rate history cannot reflect the real-time conditions of the production well, and for pressure-transient analysis the real-time rate history is needed to reduce uncertainties. Besides, the reservoir-well properties around the wellbore may change with the long-term production, which can cause problems for pressure analysis and reservoir modelling.

In this chapter, the field PDG pressure data in **Figure 6-1** is utilized to demonstrate and verify the methods developed in this thesis. Two tasks will be achieved:

1. Reconstruct the real-time rate history from the PDG pressure data.
2. Diagnose the changes in reservoir-well properties around the wellbore using the wavelet frequency diagnostic method to provide guidelines for the reservoir model calibration.

The first task is to demonstrate the method of reconstructing unknown rate history developed in Chapter 4. As the reservoir information is unknown, which means that the reservoir model is unavailable, the model-dependent methods for reconstructing the unknown rate history cannot be applied. The method of rate history calculation developed in Chapter 4 is model-independent, and it can overcome this challenge.

The second task is to demonstrate the method of diagnosing the time-dependent reservoir-well properties developed in Chapter 3 and the sliding window technique for model calibration proposed in Chapter 5. The diagnostic result will be verified with the traditional well testing.

6.2 PDG pressure data processing

As well known that the field PDG pressure data is very noisy, data volume due to high-frequency and long-term data recording is very large. As **Figure 6-1** shows, the data volume of the PDG pressure history in is very large. In the time period of 11.2 hours to the 528 hours, the pressure data was collected every 10 seconds. In the time period of 528 hour to the 873 hour, the pressure data was unavailable due to the gauge failure. After the 873 hour, the pressure was measured every 1 minute until the 9945 hour. The total data number is as large as 625,980.

Figure 6-2 shows the field PDG pressure data in the first 530 hours. The data number during this time period is 145,253. To clearly show the nature of PDG data, the time period between the 246 hour and the 252 hour is zoomed in, and it is clearly shown that how noisy the high-frequency PDG pressure data it is.

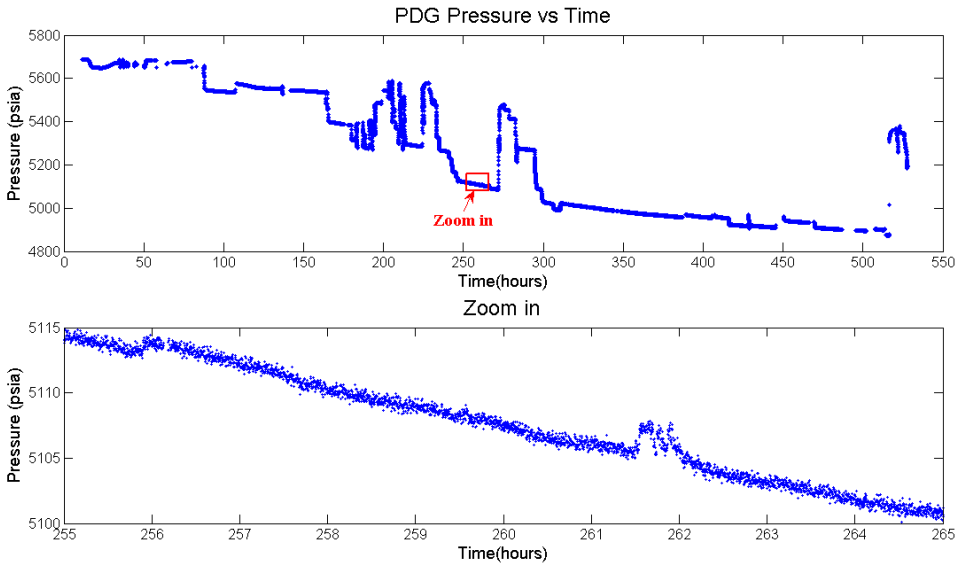

Figure 6-2: The noisy PDG pressure data in the first 530 hours and zoom-in plot.

The noisy and large volume of PDG pressure data is not suitable for rate history reconstruction and pressure-transient analysis. Data pre-processing is an important procedure to remove noise and outliers and reduce the data volume.

Denoising is a good way to avoid noise effect by reducing the fluctuation and scatterings to extract the main feature of the data. Our research has proved wavelet thresholding method is one of the most effective approaches. After wavelet decomposition, small fluctuation in detail signal caused by noise is suppressed, and denoised data can be reconstructed with smoother sub-signals. There are two kinds of thresholding methods: hard thresholding method and soft threshold method. The hard thresholding method is to replace the detailed signal with zero whenever its magnitude is smaller than the threshold λ:

$$d_{j,k}^{hard} = \begin{cases} d_{j,k} & |d_{j,k}| > \lambda \\ 0 & otherwise \end{cases} \tag{6.1}$$

But the denoised signal with hard thresholding method usually contains discontinuities. For the pressure data obtained from permanent down-hole gauge (PDG), the soft thresholding method is recommended by Kikani and He (1998):

$$d_{j,k}^{soft} = \begin{cases} d_{j,k} - \lambda & d_{j,k} > \lambda \\ d_{j,k} + \lambda & d_{j,k} < -\lambda \\ 0 & |d_{j,k}| \leq \lambda \end{cases} \tag{6.2}$$

Athichanagorn et al. (1999) also proposed a hybrid thresholding method. For this method, the soft thresholding method is used in continuous data, and the hard thresholding method is applied to the vicinity of data with discontinuities.

In this thesis, the soft thresholding method is applied. As shown in **Figure 6-3**, the denoised pressure data is more clean and smooth, and the overall trend of the noisy pressure data is kept. Especially the small flow events around the 262 hour, the small fluctuation of pressure data are reserved. To further reduce the data point numbers, the denoised pressure data were further interpolated with the 0.05 hour equal time interval, and the total data number is reduced to 5158. After data pre-processing, the PDG pressure data is more suitable for analysis.

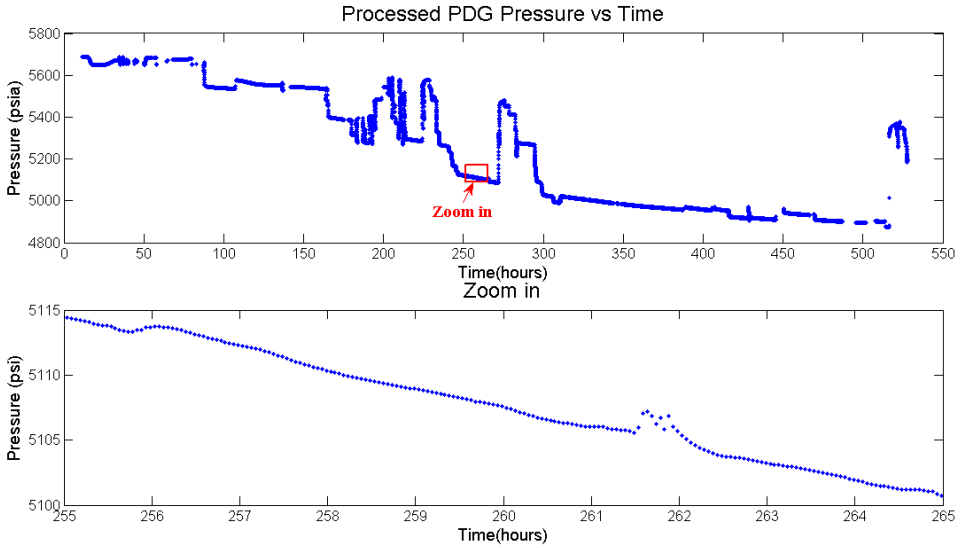

Figure 6-3: Processed PDG pressure data in the first 530 hours and zoom in plot.

6.3 Reconstructing rate history from PDG pressure data

6.3.1 Window selection

As the PDG pressure data is long-term, reconstructing the whole rate history by one process is difficult. Besides, there is high possibility that the reservoir-well properties may change during this long-term production, which will cause the linearity assumption invalid. The better way is dividing the whole PDG pressure history into several time windows with short time span, and in each time window flow rate is calculated.

As shown in **Figure 6-1**, there are nearly 20 build-ups in the PDG pressure history. During pressure build-up time periods, the flow rate is zero. This important information is utilized for window selection. The time period between two build-ups will be

selected as one time window. **Figure 6-4** presents the window selection result in the first 530 hours, and during this time period three windows are selected.

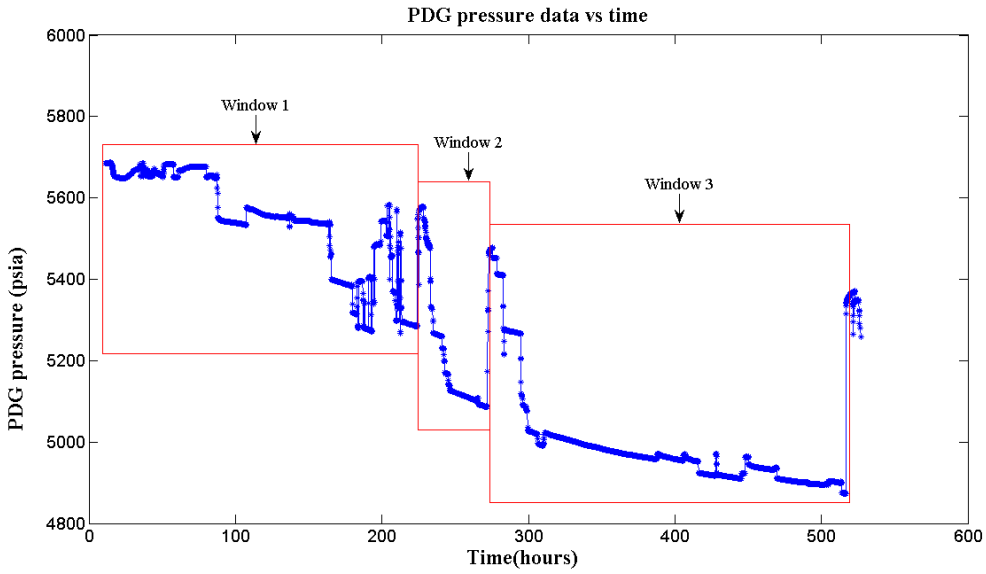

Figure 6-4: The pressure data between two build-ups are selected in one window.

6.3.2 Rate calculation with wavelet transform

The cumulative production for each time window can be calculated from the daily rate. With the cumulative production PDG pressure data in each time window, rate history can be reconstructed using the wavelet-based method developed in Chapter 4.

The pressure data in time window 3 is taken as an example to illustrate the calculation process in detail. Time window 3 covers from the 275 hour to the 518 hour, and the cumulative production can be calculated from daily rate, and it is 86,978 STB. **Figure 6-5** shows the wavelet transform processing the PDG pressure data and the calculated rate history. As the figure shows, flow events can be identified with the amplitude of WT coefficients. For the pressure DD, the WT amplitude is positive and for pressure BU, the WT amplitude is negative.

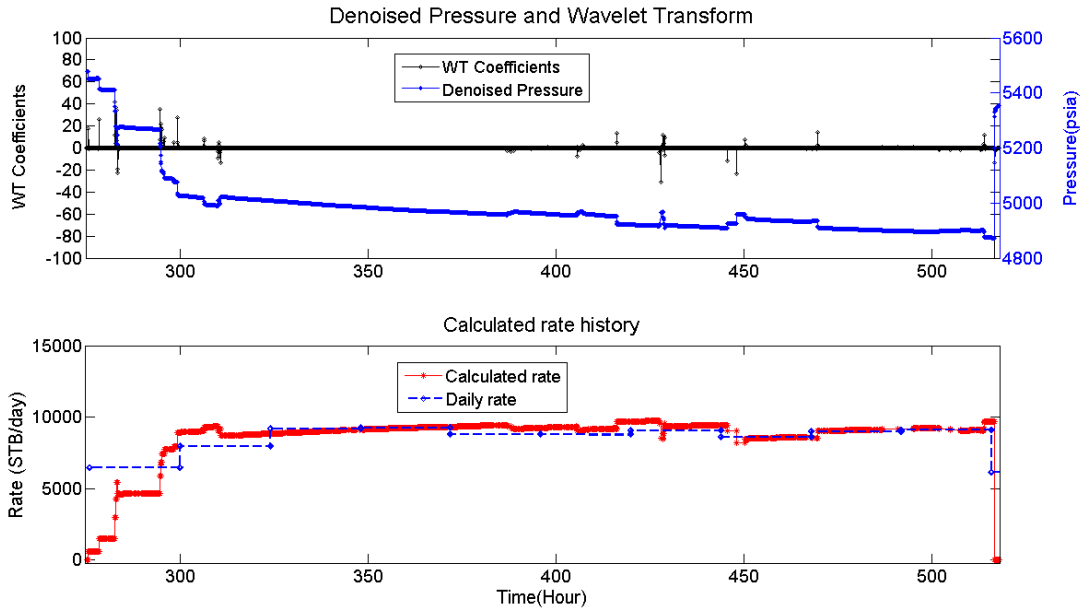

Figure 6-5: The PDG pressure data in window 3 is processed with WT, and rate history is calculated.

The proportional coefficient b between WT amplitude and the change in flow rate can be calculated using the following equation:

$$b = \frac{\sum_{i=1}^{n} t_i \sum_{j=1}^{i-1} A_j}{Q - q_1 \sum_{i=1}^{n} t_i} \tag{6.3}$$

Here cumulative production $Q = 86978$ STB, and initial flow rate is in the build-up period $q_1 = 0$. The calculated average proportional coefficient is $b = 0.030$.

With the calculated b, flow rate q_i at time period t_i can be calculated with the equation:

$$q_i = q_1 + {\sum_{j=1}^{i-1} A_j}\Big/{b} \tag{6.4}$$

As shown in **Figure 6-5,** compared with the measured daily rate history, calculated real-time rate can reflect all the small flow events in detail with high accuracy.

Similarly, the cumulative production during the time window 2 is 13941 STB, and the average proportional coefficient is $b = 0.0292$. The calculated rate history in the time window 2 is shown in **Figure 6-6**. As the figure shows, from the 228 hour to the 252 hour, the daily rate is an average constant value and cannot reflect the real-time flow events. In fact, the rate increased with time from zero to the largest value. The calculated rate history can exactly describe how the rate changes in real-time.

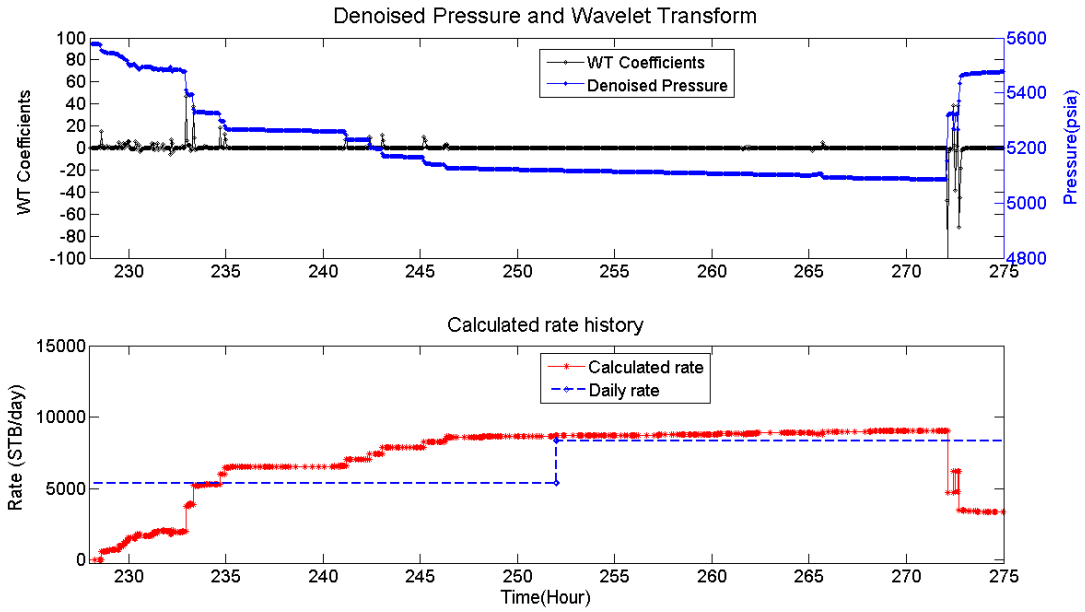

Figure 6-6: Wavelet transform processing pressure data and calculated rate history in window 2.

In the time window 1, the cumulative production is 26342 STB. However, it is challenging that the initial rate q_1 is unknown. According to Eq. 6.3, the proportional coefficient b cannot be calculated. To solve this problem, a trial-and-error algorithm will be used. At first the initial rate q_1 is estimated with one value and then rate history in the time window 1 is calculated and compared with daily rate. If the calculated rate history cannot match the measured daily rate history, the initial rate q_1 will be adjusted until the best matching is performed. In this way the finial initial rate q_1=400 STB/day and the average proportional coefficient is $b = 0.030$.

Figure 6-7 shows the calculated flow rate history in the time window 1. The result is satisfying in the first 200 hours but there are errors after 200 hours. That is due to high frequency changes in pressure, which cause large accumulative errors during this time period.

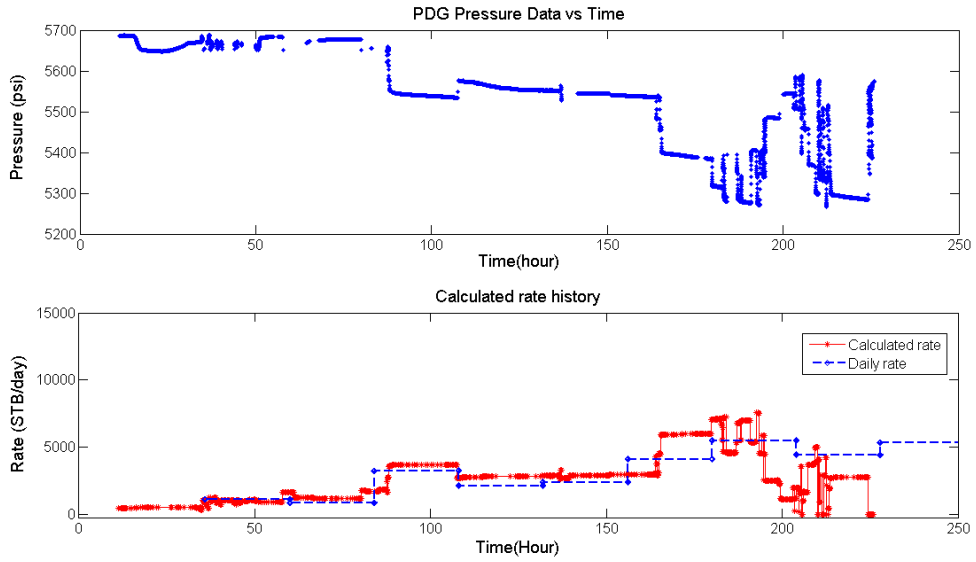

Figure 6-7: Calculated rate history in the window 1 from the 12 hour to the 227 hour.

Figure 6-8 shows the calculated rate history from the 970 hour to the 1070 hour. During this time period, the cumulative production is 41499 STB, and calculated average proportional coefficient is $b = 0.0228$. Overall, the calculation result is good compared with measured daily rate, though that there are pressure data missing around the 1000 hour.

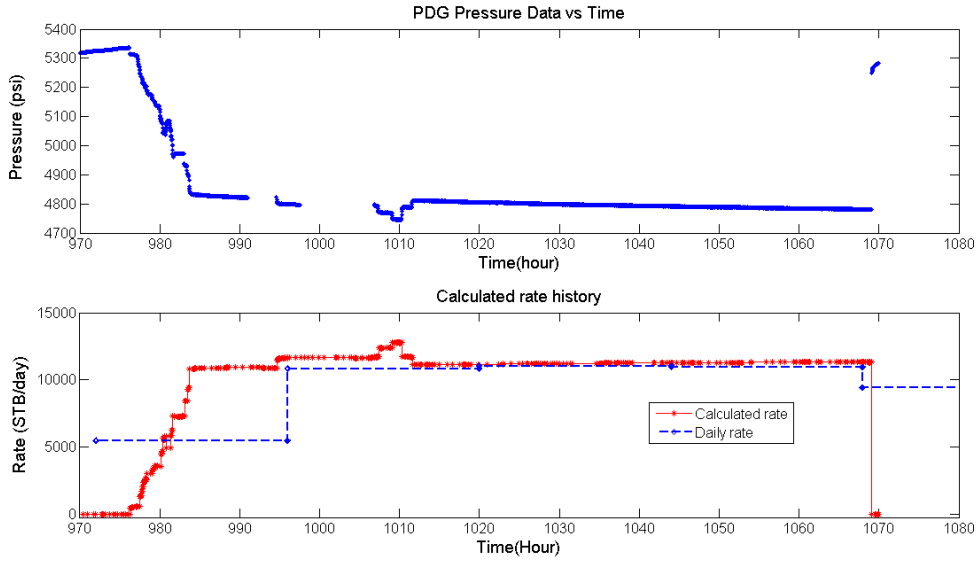

Figure 6-8: Calculated rate history from the 970 hour to the 1070 hour.

Figure 6-9 shows the calculated rate history from the 1070 hour to the 1336 hour. The cumulative production is 114270 STB, and the calculated average proportional coefficient is $b = 0.0272$. As the figure shows, several parts of pressure data are missing, especially the time period around the 1150 hour. Inferred from the measured

daily rate history, the missing data should be pressure build-up due to the decreasing rate. However, this information is covered up by data interpolation, as data interpolation ignores pressure change during this time period.

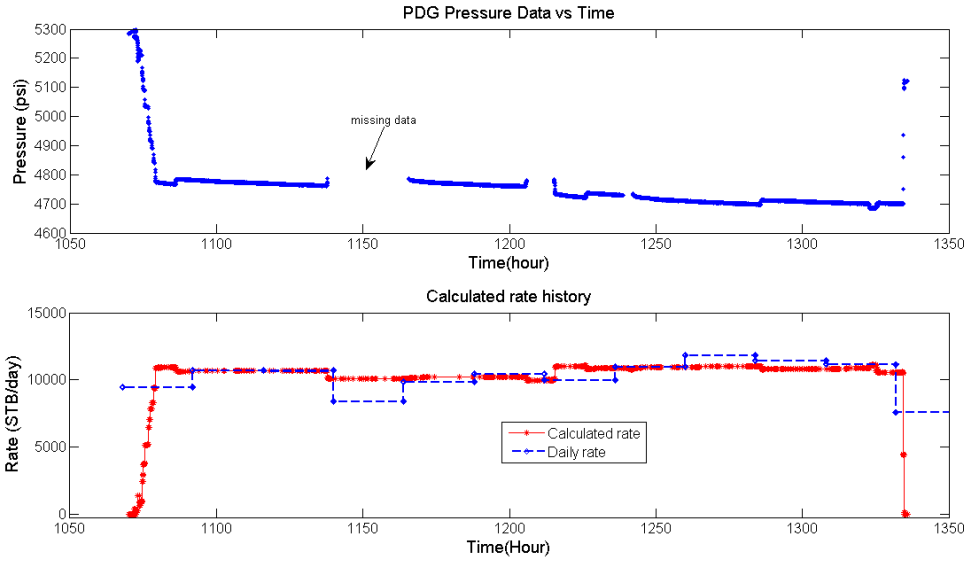

Figure 6-9: Calculated rate history from the 1070 hour to the 1336 hour.

Figure 6-10 presents the calculated rate history from the 1557 hour to the 2375 hour. The calculated result is not as good as that in the above figures, due to the missing pressure data. During the time period around 1630 hour, a pressure build-up data is missing according to the measured daily rate history. As a result, the calculated rate is much larger than the real rate. As the cumulative production is a constant value, the calculated rate during other time period is assigned less production compared with the measured daily rate history.

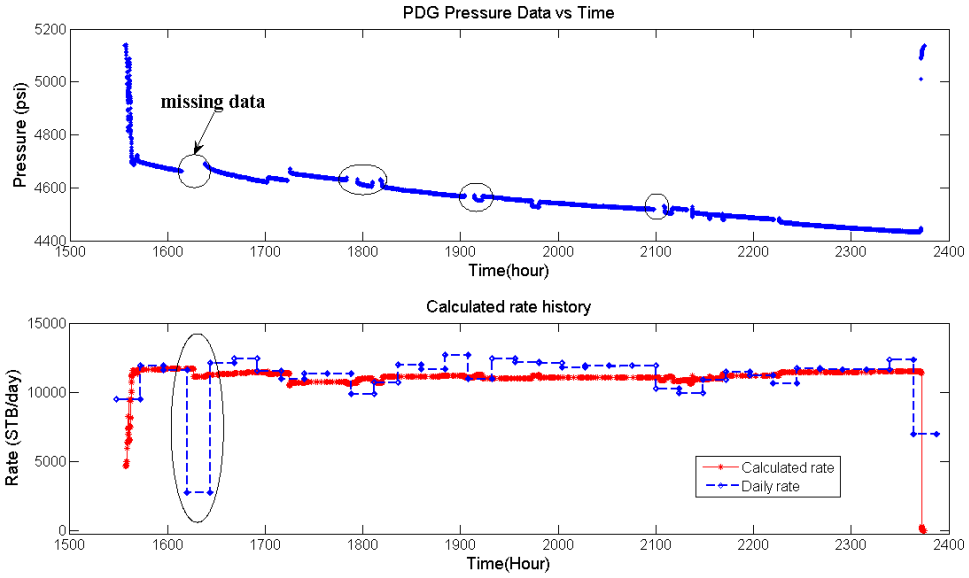

Figure 6-10: Calculated rate history from the 1557 hour to the 2375 hour

Figure 6-11 shows the calculated rate history from the 2500 hour to the 3418 hour. The calculated rate overall matches the measured daily rate history. Around the 3400 hour, the calculated rate is a little larger than the measured daily rate, which is caused by the missing data in pressure drawdown around the 3390 hour.

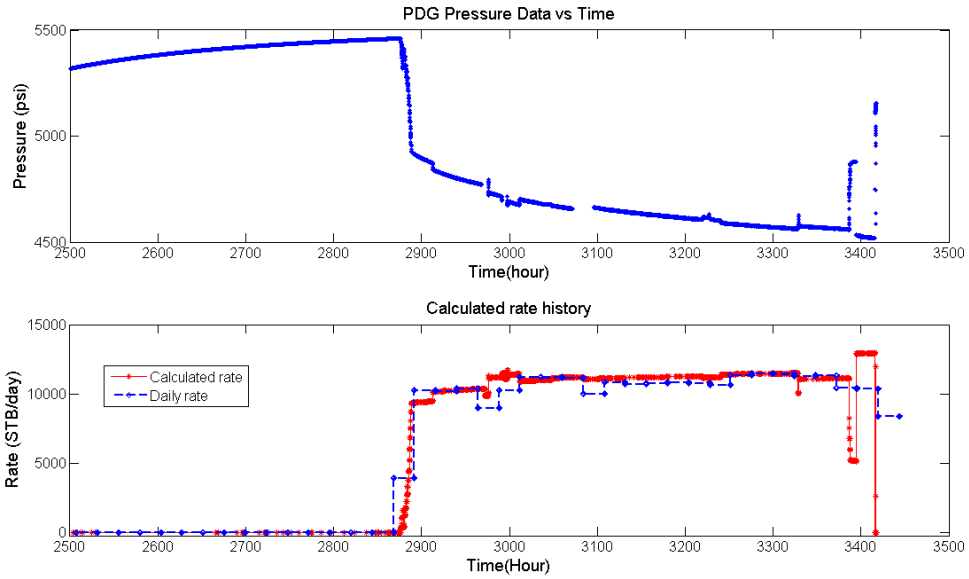

Figure 6-11: Calculated rate history from the 2500 hour to the 3418 hour.

Figure 6-12 presents the calculated rate history from the 3418 hour to the 3619 hour. The calculation result during the 3440 hour to the 3540 hour is good compared with the measured daily rate. However, during other time period the calculated rate have larger error due to the incomplete pressure history.

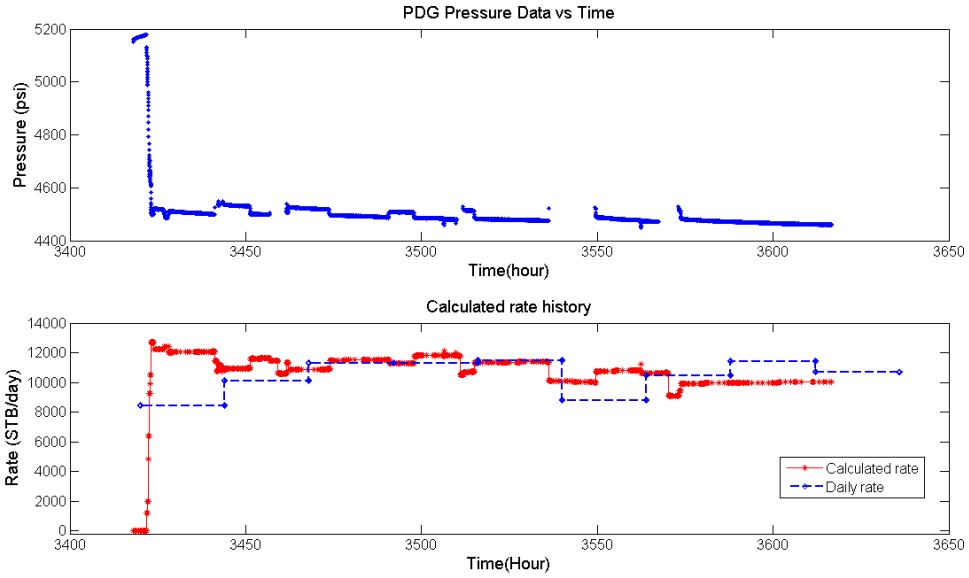

Figure 6-12: Calculated rate history from the 3418 hour to the 3619 hour.

Figure 6-13 shows the rate calculation result from the 3925 hours to the 4000 hours. All the small flow events are identified and calculated with the high accuracy. The result satisfying compared with the measured daily rate.

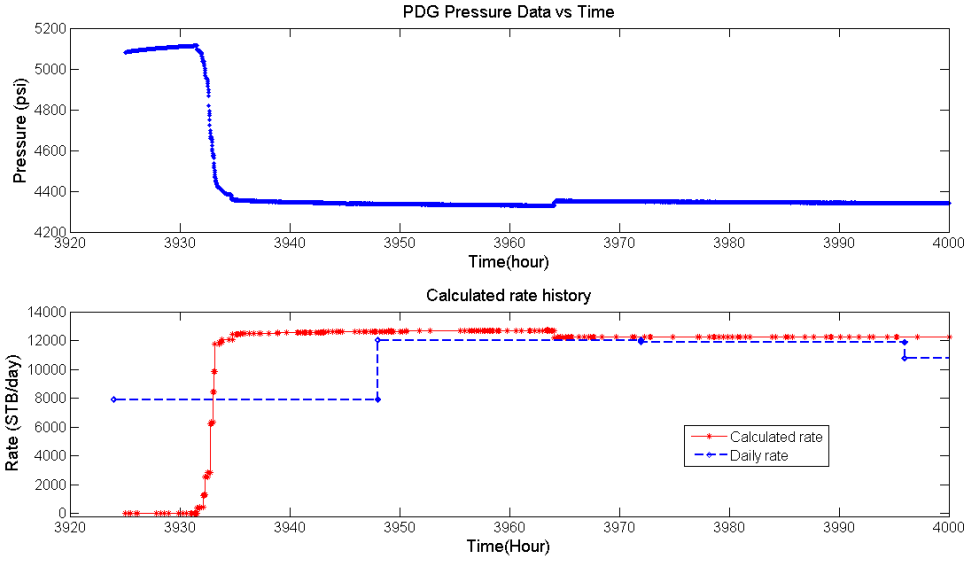

Figure 6-13: Calculated rate history from the 3925 hour to the 4000 hour.

Figure 6-14 shows the calculated rate history from the 4090.19 hour to the 4385 the hour. The calculated rate is good and can match the measured daily rate history, although there are several parts of pressure data are missing.

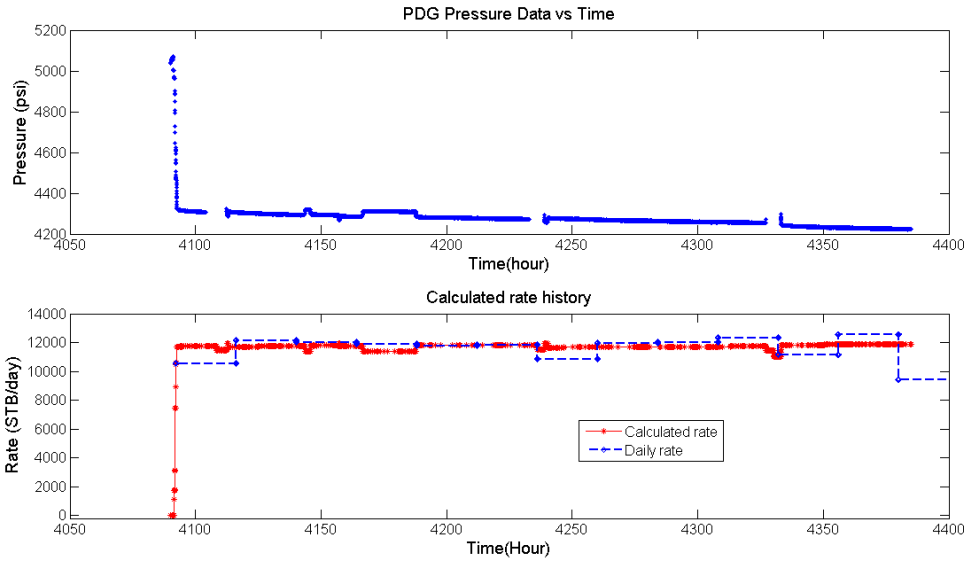

Figure 6-14: Calculated rate history from the 4090.19 hour to the 4385h.

Figure 6-15 shows the calculated rate history from the 4395 hour to the 4995 hour. There are two parts of missing pressure build-up data and during these two time periods the calculated rate is larger than the measured daily rate. In the time period around the 4690 hour, the measured daily rate is much larger than the calculated rate. However, from the point of pressure data, there is no large pressure change which means the measured daily rate at this time is not reliable.

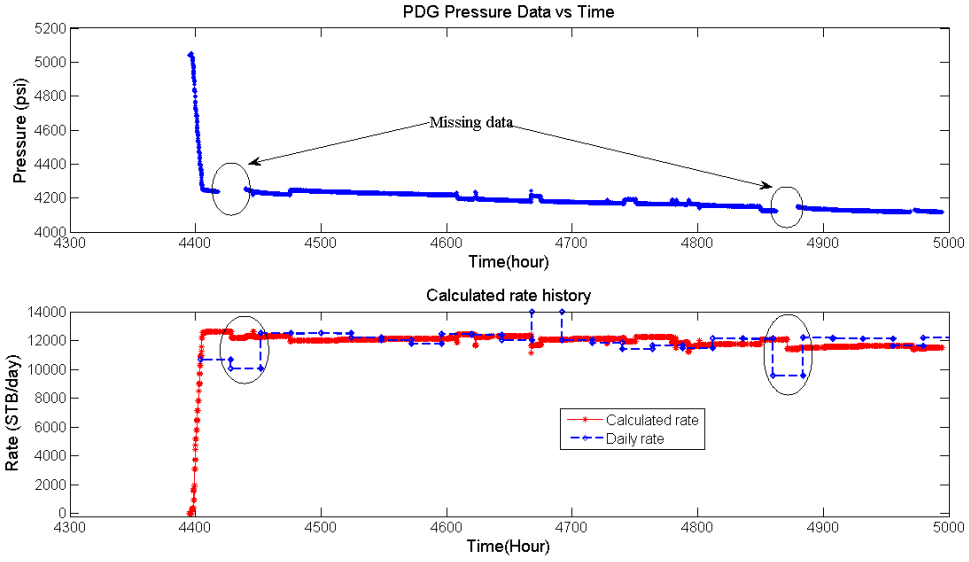

Figure 6-15: Calculated rate history from the 4395 hour to the 4995 hour.

Figure 6-16 shows the calculated rate history from the 5015 hour to the 5785 hour. Except the two parts of missing pressure data, the calculation result is satisfying compared with the measured daily rate history.

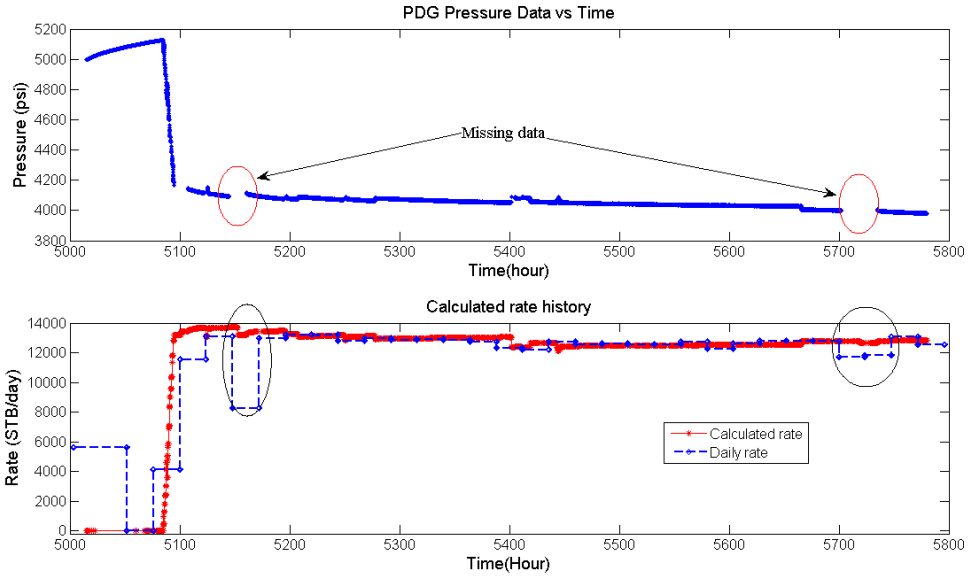

Figure 6-16: Calculated rate history from the 5015 hour to the 5785 hour.

Figure 6-17 shows the calculated rate history from the 5820 hour to the 6710 hour. The calculation result is good during this 1000 hours production time.

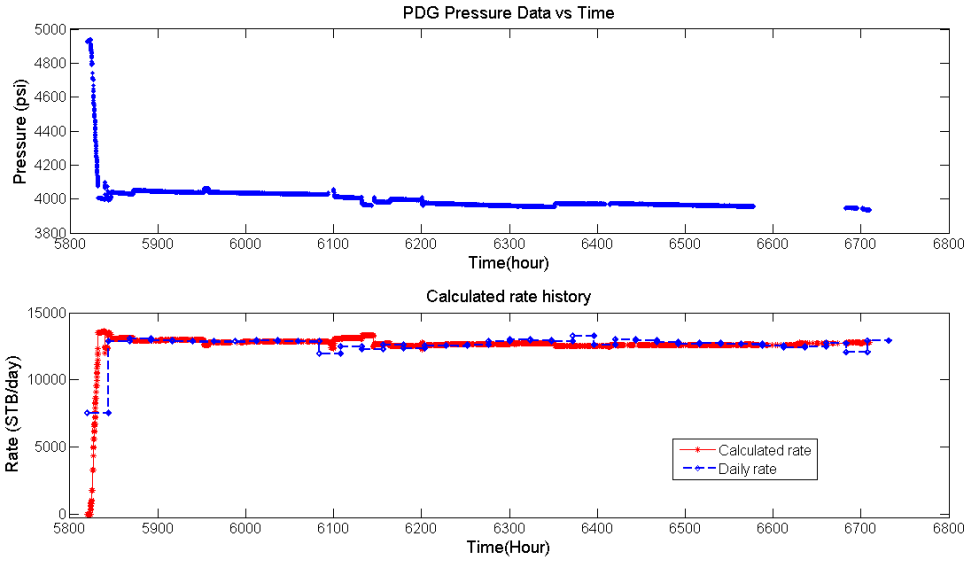

Figure 6-17: Calculated rate history from the 5820 hour to the 6710 hour.

Figure 6-18 shows the calculated rate history from the 6781hour to the 7163 hour. In the time period around the 7140 hour, the measured daily rate is almost constant but the pressure increased strangely. As a result, the rate history calculated from the pressure has errors. This abnormal pressure performance may be caused by the changes in wellbore conditions.

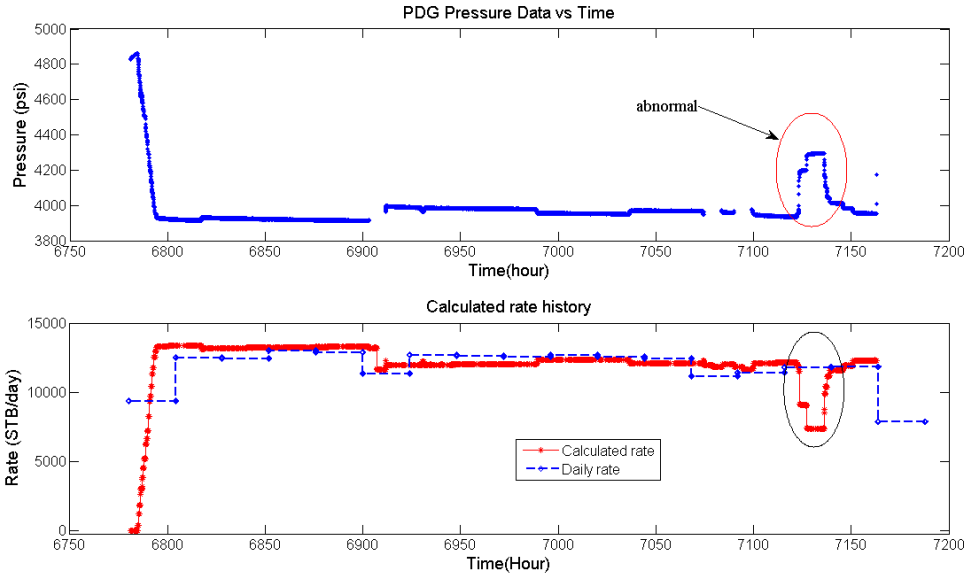

Figure 6-18: Calculated rate history from the 6781 hour to the 7163 hour.

Figure 6-19 shows the calculated rate history from the 7180 hour to the 8400 hour. Many parts of missing pressure data cause errors for rate calculation. These missing data mainly are pressure build-ups, which lead to the calculated value is larger than the real rate.

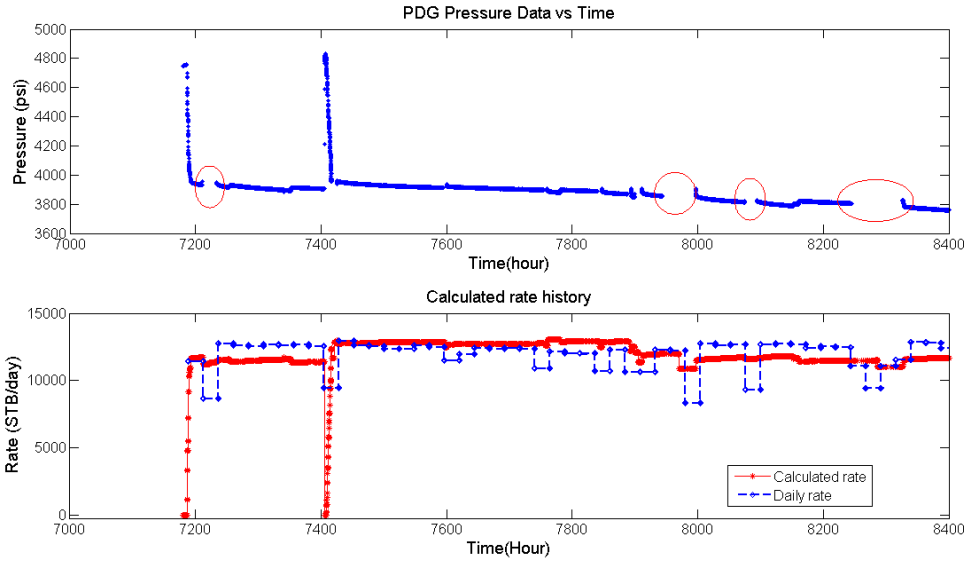

Figure 6-19: Calculated rate history from the 7180 hour to the 8400 hour.

Figure 6-20 shows the calculated rate history from the 8500 hour to the 9040 hour. The calculation result is good during this time period, as the pressure history is complete.

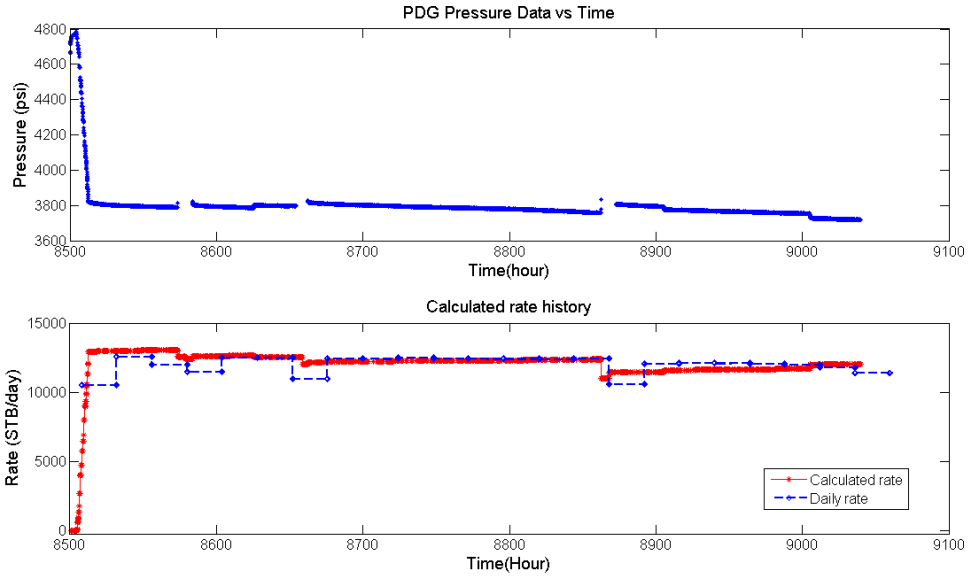

Figure 6-20: Calculated rate history from the 8500 hour to the 9040 hour.

Figure 6-21 shows the calculated rate history from the 9066 hour to the 9400 hour. Around the 9200 hour, pressure data lasting for nearly 80 hours are missing. The calculated rate is much larger than the measured daily rate. Inferred from the daily rate history, the missing pressure data should be increasing with time due to the decreasing rate. In the time period around the 9800 hour, the calculated rate is less than the measured daily rate.

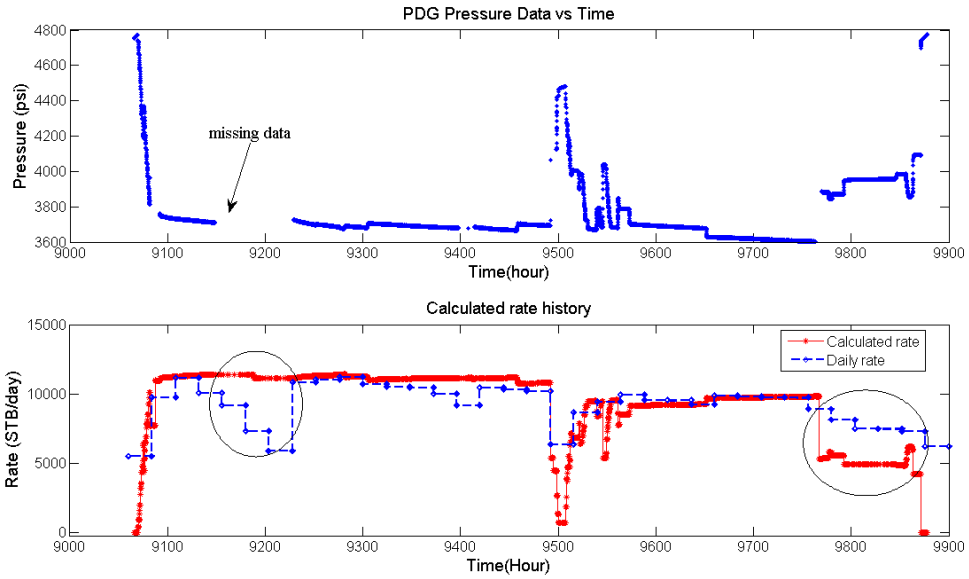

Figure 6-21: Calculated rate history from the 9066 hour to the 9400 hour.

Combining all the calculated rate history in different time windows, the whole rate history reconstructed from the field PDG pressure data is shown in **Figure 6-22**.

Compared with the daily rate, the calculated real-time rate history can reflect the conditions of production well, and reduce uncertainties for pressure-transient analysis.

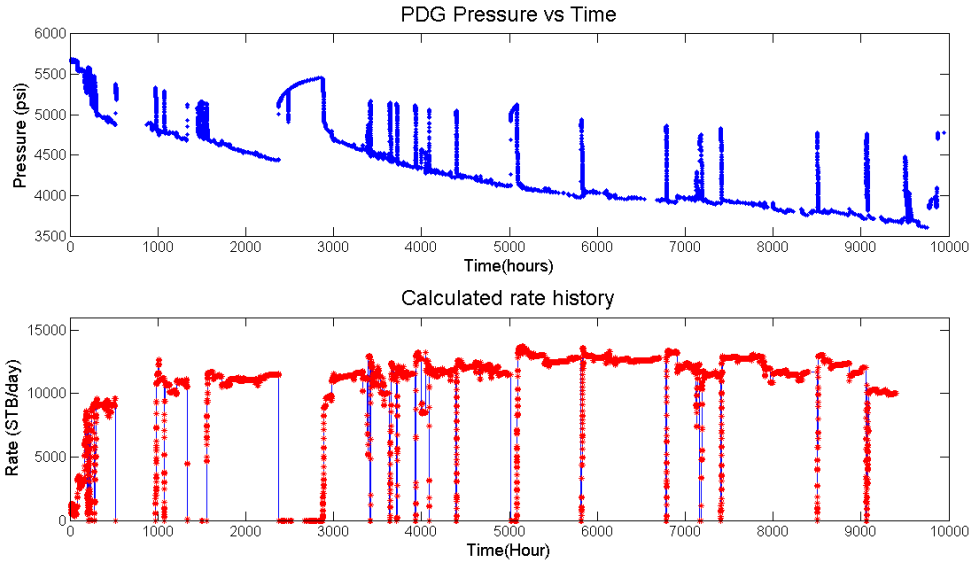

Figure 6-22: The reconstructed whole rate history from PDG pressure data.

6.4 Diagnostic of time-dependent reservoir-well properties

As **Figure 6-1** shows, the production time of the field data is more than one year. During this long-term production, the reservoir properties around the wellbore may change with time. As field studies show, the effective permeability and skin factor may change, due to formation compaction, subsidence and fine migration. These are more common for the unconsolidated deposition reservoirs. Due to that, the reservoir modelling with constant properties may not match the field performance. To make reliable future forecasting, the reservoir model need calibration. When and which reservoir property needs to be determined. At first, the time of model calibration will be determined using the wavelet frequency diagnostic method developed in Chapter 3. Then traditional well test method will be used to verify the diagnostic result and determine which property needs to be updated.

6.4.1 Frequency diagnostic analysis

In the Chapter 3, a novel diagnostic function URSR A_{urc} has been developed and used for diagnosing nonlinearities caused by the changes in reservoir properties, as the following equation shows:

$$A_{urc} \propto \frac{70.6uB}{kh}\left[\ln\Delta t + \ln\frac{k}{\emptyset\mu C_t r_w^2} - 7.43173 + 2S\right] \quad (6.5)$$

The sensitivity study shows that URSR A_{urc} function is sensitive to the changes in skin factor and permeability, and A_{urc} increases with the time for the increasing skin factor and decreasing permeability. In fact, A_{urc} is proportional to the skin factor and inversely proportional to the permeability.

The URSR A_{urc} function is wavelet amplitude caused by unit rate change. However, for this field data real-time rate is unknown and only daily rate is given. The calculated real-time rate in **Figure 6-22** is base on the linearity assumption in each time window. To solve this problem, the average URSR A_{urc} in each time window can be calculated, using the daily rate history. In fact, the average URSR A_{urc} equals the average proportional coefficient b between WT amplitude and the change in flow rate, that is:

$$\overline{A_{urc}} = b = \frac{\sum_{i=1}^{n} t_i \sum_{j=1}^{i-1} A_j}{Q - q_1 \sum_{i=1}^{n} t_i} \quad (6.6)$$

The average proportional coefficient b in each time window is plot with the production time, which is the URSR A_{urc} diagnostic plot, as shown in **Figure 6-23**.

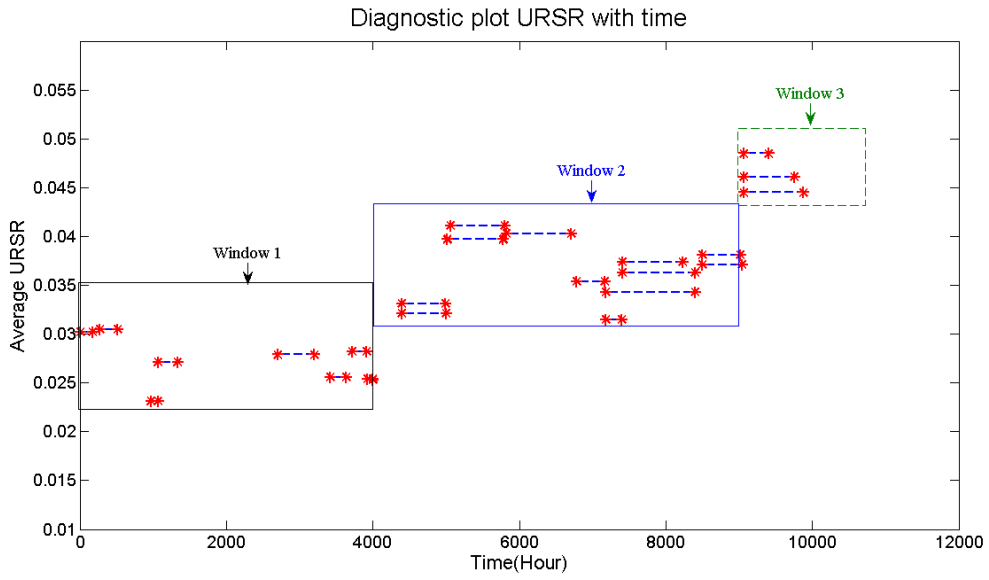

Figure 6-23: The diagnostic function A_{urc} changes with time and three time windows are selected for model calibration.

The general trend of URSR A_{urc} is increasing with the time, which means the reservoir properties around the wellbore changed with production. The conditions of production

well were getting worse, and Production Index (PI) declined with the production time. As a result, reservoir modelling with constant-property cannot match the field performance. Reservoir model/near wellbore model (NWM) needs calibration. Three time windows are selected to calibrate the reservoir model. At first, the changes in reservoir-well properties are little and reservoir model doesn't need calibration. Around the 4000 hour, the diagnostic function A_{urc} increases a lot and reservoir model needs calibration. Around 9000 hours, another model calibration may need, but there are uncertainties as the pressure history in the time window 3 is not long enough. **Figure 6-24** presents window selection for the reservoir model calibration.

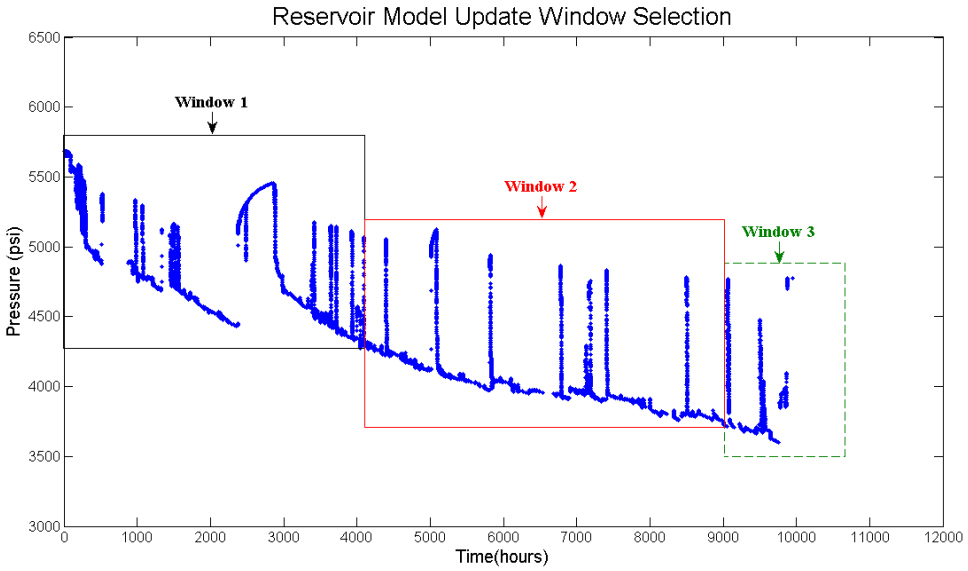

Figure 6-24: The reservoir model needs update around 4000 hours, and another calibration may need around 9000 hours.

6.4.2 Transitional well test analysis

To verify the diagnostic result in **Figure 6-23**, the traditional well testing using pressure build-up analysis is carried out. As the unknown rate history has been reconstructed, the uncertainties of build-up analysis have been reduced a lot. As shown in **Figure 6-25**, several pressure build-ups are selected to analyse. According to the window selection in **Figure 6-24**, three pressure build-ups are in the window 1 and another two pressure build-ups are in the window 2. If the diagnostic result is correct, the reservoir properties derived from different pressure build-ups but in the same time window should be constant or change little. For the pressure build-ups in the different time windows, the derived reservoir properties should change a lot.

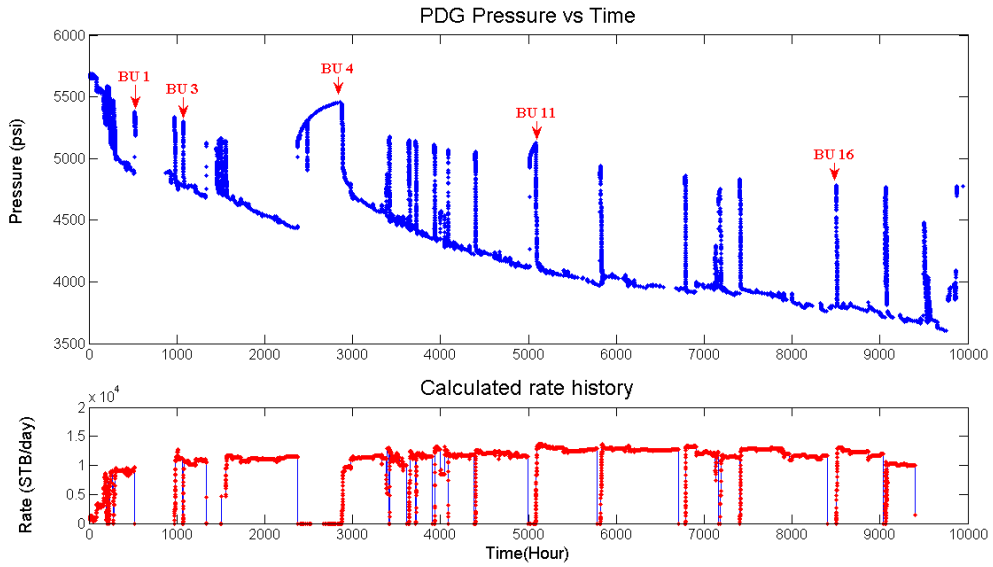

Figure 6-25: Several build-ups are selected to analyse in log-log plot.

Figure 6-26 shows the build-up 1 and 3 are analysed in the log-log plot. Although the data quality is poor for analysis, some reservoir information still can be derived. The pressure derivative lines for two pressure build-ups nearly coincide, but the pressure drop of build-up 3 is less than the pressure drop of build-up 1. It means skin factor of build-up 3 is less than the skin factor of build-up 1. The decreasing skin factor may be caused by the clean up effect at the beginning of the production. At the time of well drilling and perforation, the reservoir formation around the wellbore may be damaged. After the well begins to produce, the fluid flow can remedy the damage and reduce the skin factor. As URSR A_{urc} decreases with the decreasing skin factor, it can explain that the A_{urc} function in **Figure 6-23** decreases a little in the first 1000 hours. Due to the change in skin factor, near wellbore model (NWM) may be updated. At here, as the change in A_{urc} is little and time period of clean up effect is short, reservoir model needn't updated.

Figure 6-27 presents the build-up 4 and build-up 11 are analysed in the same log-log plot. As shown in **Figure 6-24**, build-up 4 is in the time window 1 and build-up 11 is in the time window 2. There should be large changes in reservoir properties according to the diagnostic result in **Figure 6-23**. In **Figure 6-27**, the pressure drop of build-up 11 is much larger than the pressure drop of build-up 4, which shows the skin factor increased a lot. The increasing skin factor may be caused by the formation damage during the long-term production. The increasing skin factor verifies that the diagnostic result is correct.

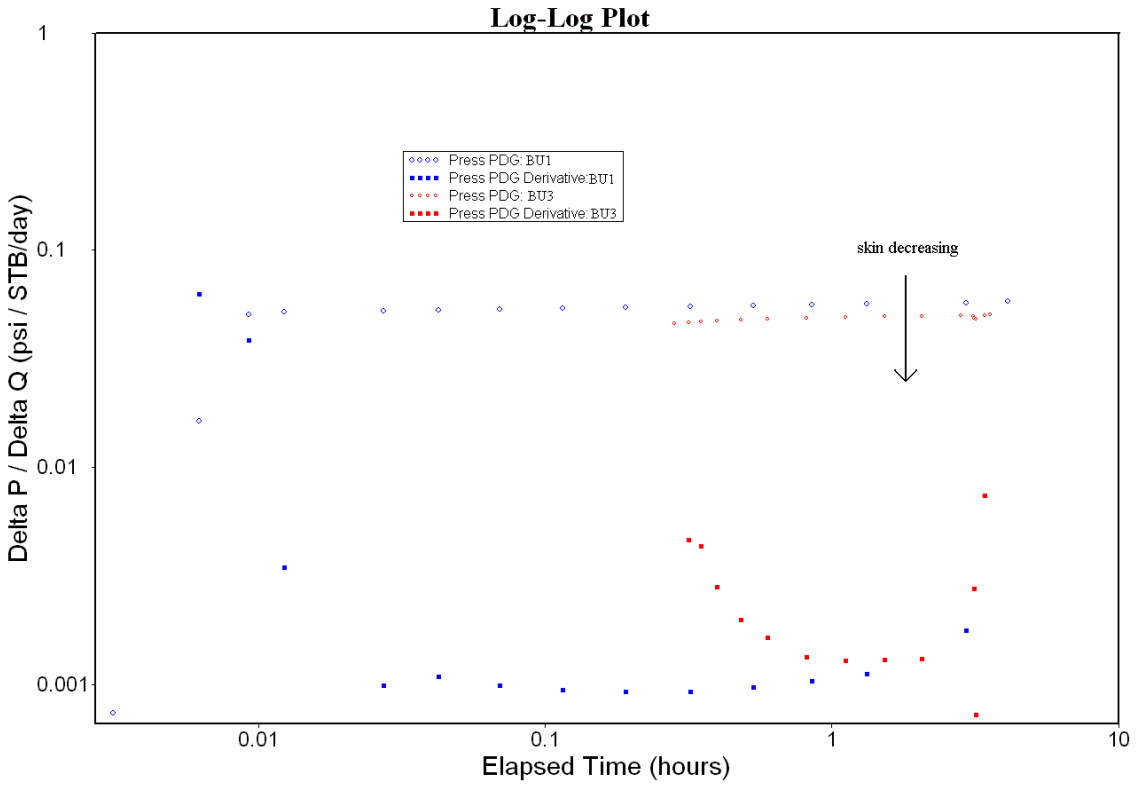

Figure 6-26: Build-up 1 and 3 are analysed in the log-log plot.

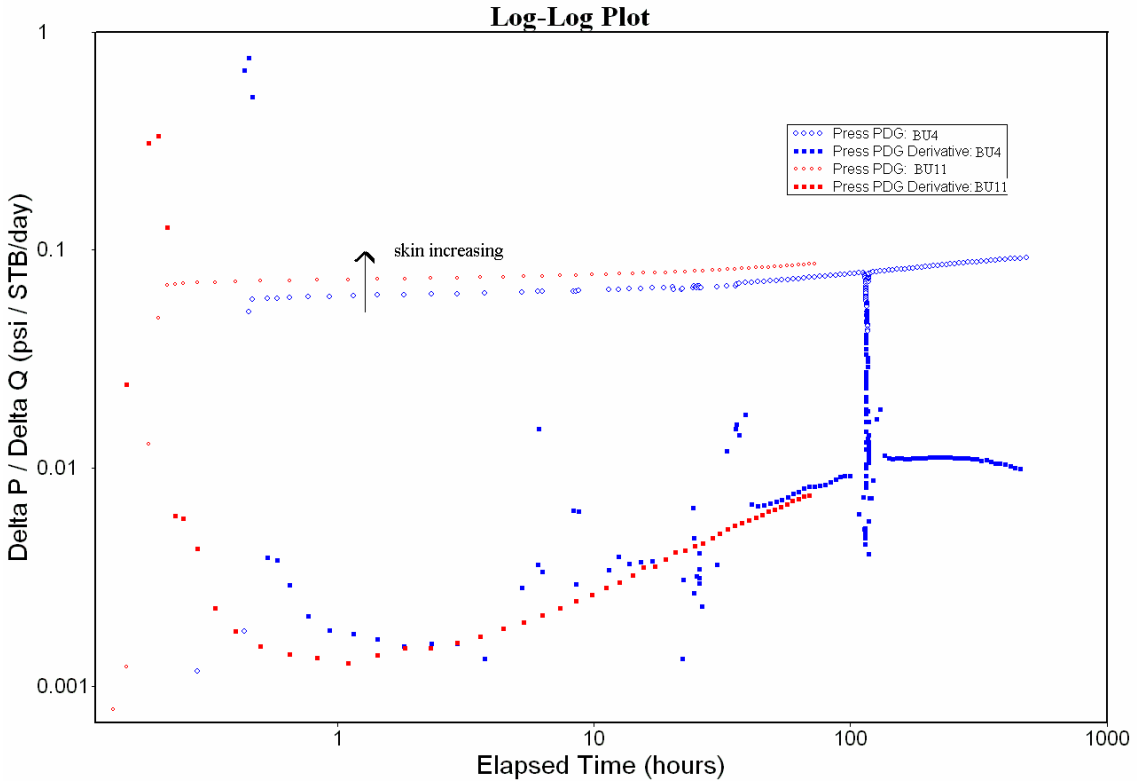

Figure 6-27: Build-up 4 and 11 are analysed in the log-log plot.

Figure 6-28 the build-up 11 and build-up 16 are analysed in the same log-log plot. The lines of pressure drop and pressure derivative for two pressure build-ups coincide, which means the reservoir properties changed little, although the time period between

two build-ups is very long, more than 3500 hours. Therefore, it is reasonable that build-up 11 and build-up 16 is in the same time window and reservoir model needn't update.

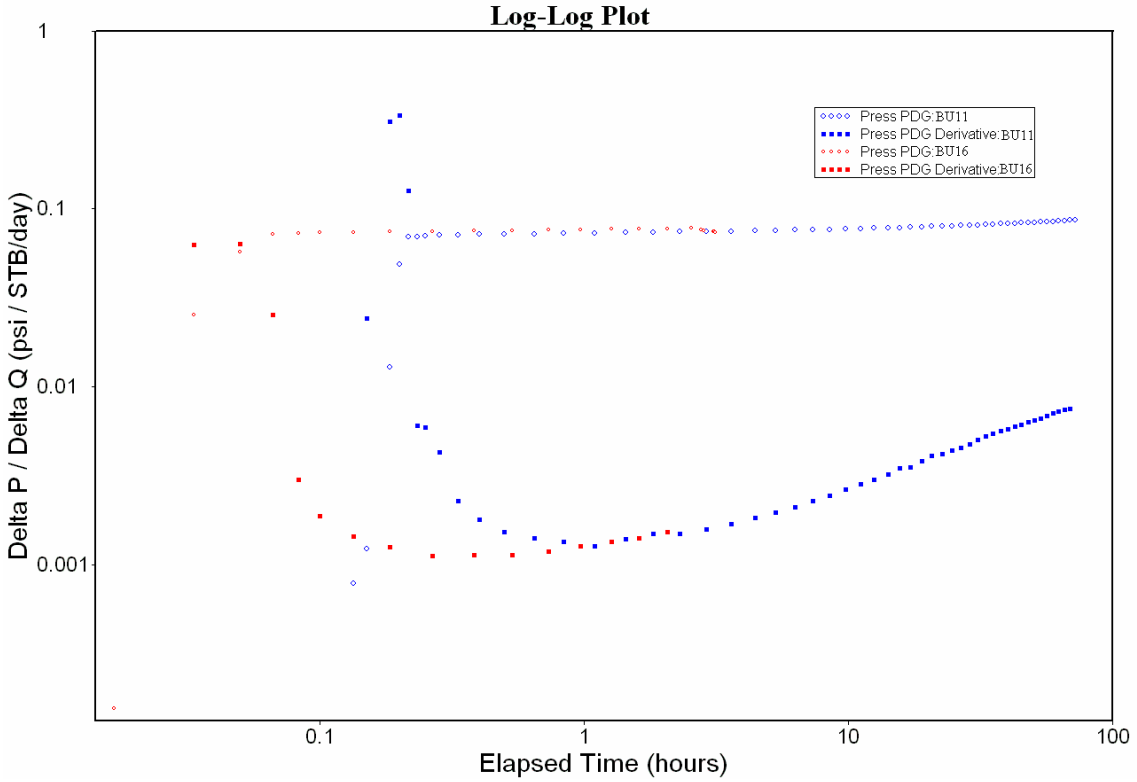

Figure 6-28: Build-up 11 and 16 are analysed in the log-log plot.

The traditional well testing has verified that the diagnostic result in **Figure 6-23** is correct. Based on the diagnostic result, the window selection can provide useful guidelines for model calibration. The time of model calibration can be determined by the change of URSR A_{urc} function. Model update threshold can be set up, when the change of A_{urc} is less than the threshold, reservoir properties change little and reservoir model needn't update. When the change of A_{urc} is larger than the threshold, the reservoir properties change a lot and model calibration is necessary.

As the discussion in Chapter 3, other reservoir behaviours can cause the change in A_{urc} function. For the reservoir with water injection, at the time of water breakthrough the effective permeability will decrease a lot and A_{urc} will increase sharply. Similarly, if the down-hole pressure drops below the bubble-point pressure, total mobility also declines to multi-phase flow. Furthermore, the change in wellbore conditions such as scaling and paraffin wax in the tubing etc. also can cause increasing A_{urc} and declining production index.

6.5 Chapter conclusions

In this chapter, field PDG pressure data is used to demonstrate the algorithms developed in this thesis, including reconstructing unknown rate history and diagnosing time-dependent reservoir properties for reservoir model calibration. Several conclusions can be derived as following:

1. The wavelet-based rate calculation method developed in Chapter 4 can reconstruct unknown rate history from PDG pressure data, and the calculated rate history is very close to the measured rate history. This rate calculation method is model-independent and has wide applications.
2. The field PDG pressure data is very noisy and has very large data volume. Wavelet thresholding method can effectively remove data noise. Besides, sliding window technique can overcome the nonlinear problems and reduce the data volume.
3. Abnormal data and missing data in PDG pressure history can cause calculation errors, especially when the missing pressure data is in transient-state.
4. Time-dependent reservoir properties around the wellbore can be diagnosed with the URSR A_{urc} function. The diagnostic result can provide the useful information when the reservoir model needs calibration.
5. The skin factor may decrease firstly due to the clean up effect, and then increases with the production time due to formation damage. Traditional well testing can verify the diagnostic result and determine which reservoir properties need update.

Chapter 7 Conclusions and Recommendations

This chapter presents the general conclusions drawn from the study work in this thesis and gives the recommendations for the future work based on the current experience.

7.1 General conclusions

In this study, a new methodology of diagnosing and analysing the long-term transient pressure data acquired from permanent down-hole gauge (PDG) has been developed. This methodology includes three categories: (1) diagnostic of nonlinearities from long-term PDG transient pressure data, (2) unknown flow rate history reconstruction, (3) sliding window technique for long-term PDG pressure analysis and reservoir model calibration. The applicability of this methodology has been demonstrated with synthetic data and field PDG data.

For the long-term transient pressure analysis, a novel nonlinearity diagnostic method has been developed. The nonlinearities around the wellbore can be diagnosed both qualitatively as well as quantitatively. The method and results can be summarized as follows:

1. In linear systems, the flow rate and down-hole pressure satisfies superposition principle. Compared with the short-time traditional well testing, nonlinearities are more common in the long-term transient pressure data and they can cause the system nonlinear and superposition principle invalid. The pressure-transient analysis methods based on the linearity assumption such as superposition and deconvolution may fail for applications. Nonlinearity diagnostic and evaluation is a key procedure before pressure-transient analysis.
2. With the Haar wavelet processing transient pressure data, a novel diagnostic function A_{urc} has been developed to diagnose nonlinearities. URSR A_{urc} is the ratio between the amplitude of pressure transform and the change in flow rate. In linear systems, URSR A_{urc} is constant with time. When there is nonlinearity around the wellbore, URSR A_{urc} is time-varying. The large changes in URSR A_{urc} mean high nonlinearities.
3. URSR A_{urc} is more sensitive to the changes in skin factor and (effective) permeability than other reservoir-well parameters.

4. For the gas reservoir, URSR A_{urc} is time-varying due to pressure-dependent gas properties. For the oil reservoir with dissolved gas, URSR A_{urc} is constant before gas out of solution; after that URSR A_{urc} is time varying due to the total mobility change, phase segregation effect and pressure-dependent fluid properties. Similarly, water breakthrough can be detected with the sharply increasing URSR A_{urc}. After water breakthrough URSR A_{urc} changes with the total mobility.
5. URSR A_{urc} can be utilized as a production monitoring tool. Abnormal increasing URSR A_{urc} indicates the reduction in production index (PI) in the production well, and special cautions and remedy responses are needed to optimize the production.
6. A novel workflow of long-term PDG pressure data analysis has been proposed. The nonlinearity diagnostic and evaluation is a crucial procedure before pressure-transient analysis, as it can ensure that suitable PTA methods can be selected and reduce analysis uncertainties.

Unknown flow rate history is reconstructed from PDG pressure and cumulative production data using the wavelet-based method. The important remarks on this method can be summarized as follows:

1. This method is independent of the reservoir model, and based on the linearity assumption that the reservoir-well properties are constant. The skin factor, wellbore storage, reservoir heterogeneity and multi-well interference have no effect on this method.
2. For the real-gas reservoir, calculated rate tends to have larger errors than that in liquid systems as gas properties are pressure-dependent. Normalized pseudo-pressure can be applied to reduce the nonlinearity, and flow rate history can be reconstructed with high accuracy using the normalized pseudo-pressure.
3. For the reservoir with oil and water two-phase flowing, during the time periods when water-cut is constant or changes little, the nonlinearity can be neglected and flow rate history can be reconstructed with small errors. Around the time of water breakthrough, the nonlinearity is high and this method is not recommended for application. The unknown water cut data also brings errors when calculating flow rate history for each phase from the total liquid rate history.

4. For the pressure history with high nonlinearities, such as phase segregation effect after gas of solution, the reconstructed flow rate history has large errors.

Combined with the nonlinearity diagnostic method, sliding window technique has been proposed to analyse the long-term transient pressure data from PDG and calibrate the reservoir model. Conclusions can be drawn as follows:

1. Based on the nonlinearity diagnostic result, the long-term transient pressure history can be divided into a series of time windows. The window selection and window size depends on the changes in URSR A_{urc}. Small changes in URSR A_{urc} mean low nonlinearity and the changes in reservoir-well properties are small, the pressure can be grouped in the same window. When the changes in URSR A_{urc} are high, time window slides to subsequent one.
2. In each time window, the system can be treated as linear. Deconvolution and other PTA methods based on the linear assumption are valid for application. These methods are not recommended to analyse the pressure history with nonlinearity, wrong or misleading analysis result may be derived.
3. When the time window slides to the subsequent one, the reservoir model needs calibration. Time-dependent reservoir properties such as skin factor and permeability can be interpreted from the pressure build-up in each time window. NWM can be selected and updated with new model parameters. Then the updated NWM can be put back to the FFM.

7.2 Recommendations for future work

The following points are recommended for future study:

1. The nonlinearity in the wellbore and the nonlinearity in the reservoir perform differently and have different effects. Diagnosing and distinguishing two kinds of nonlinearities are important for production optimization and model calibration. Temperature data also is measured with PDG and distributed temperature sensor (DTS). PDG temperature data provides temperature information related to the reservoir formation, and DTS temperature data provides the temperature profile along the wellbore. These two kinds of temperature data may be utilized for diagnosing and distinguishing nonlinearities in the reservoir and wellbore.
2. The long-term PDG pressure data may contain interference from other production wells. Although multi-well interference is not nonlinear reservoir

behaviour, analysis of the pressure with interference is difficult. The method for interference diagnostic and analysis needs to be developed.

3. The algorithm of flow rate history reconstruction works well when the nonlinearity in the reservoir system is low or nonlinearity can be linearized with transforms or window technique. When the nonlinearity is very high, such as the phase segregation effect after gas out of solution, the calculated flow rate has large errors. Besides, the missing and abnormal PDG pressure data cause problems for flow rate history reconstruction. These problems may be solved with reservoir modelling.

References

Agarwal, R. G.: "Real Gas Pseudotime-A New Function for Pressure Buildup Analysis of MHF Gas Wells", paper SPE 8279 presented at the SPE Annual Technical Conference and Exhibition, Las Vegas, Sept. 23-26.

Al-Hussainy, R., Ramey, H.J.Jr. and Crawford P.B.: "The Flow of Real Gases in Porous Media", *J. Pet. Tech.,* May, 624-636, 1966a.

Al-Hussainy, R., Ramey, H.J.Jr.: "Application of Real Gas Flow Theory to Well Testing and Deliverability Forecasting", *J. Pet. Tech., May*, 637-642, 1966b.

Anderson, D., and Mattar, L.: "Practical Diagnostics Using Production Data and Flowing Pressures", paper SPE 89939 presented at the SPE Annual Technical Conference and Exhibition held in Houston, Texas, U.S.A., 26-29 September 2004.

Anraku, T., and Horne, R.N: "Discrimination Between Reservoir Models in Well-Test Analysis", *SPE Formation Evaluation*, June 1995, 114-121.

Athichanagorn S., Horne R.N. and Kikani J.: "Processing and Interpretation of Long-term Data from Downhole Pressure Gauges," paper SPE 56419 presented at the 1999 SPE Annual Technical Conference and Exhibition held in Houston, Texas, 3-6 October 1999.

Babcock, B., Babu, S., et al.: "Models and issues in data stream systems", in *Proc. of the 21st ACM SIGACT-SIGMOD-SIGART Symp. on Principles of Database Systems*, pages 1-16, June 2002.

Baker, A., Jeffery, J., Thomas, A. and Unneland, T.: "Permanent Monitoring-Looking at Lifetime Reservoir Dynamics", *Oilfield Review*, No. 4, Vol. 7, winter 1995.

Bergren, F.E., Lagerlef, D.L., and Feldman, S.: "Three-Phase Well-Level Production Allocation at Prudhoe Bay", *SPE Computer Applications*, April 1997, 55-60.

Bezerra, M.F.C., Da Silva, S.F. and Theuveny, B.C.: "Permanent Downhole Gauges: A Key To Optimize Deepsea Production", paper OTC 6991 presented at the 24th Annual OTC in Houston, Texas, May 4-7, 1992.

Bigno, Y, Baillie, J. and Coombes, T.: "The interpretation of Reservoir Pressure Data in the Dunbar Filed (UKCS)", paper SPE 37758 presented at the 1997 Middle East Oil Show held in Bahrain, 15-18 March 1997.

Bourdet, D., Whittle, T.M., Douglas, A.A., and Pirard, Y.M.: "A New Set of Type Curves Simplifies Well Test Analysis", *World oil*, May 1983, 95-96.

Chorneyko, D.M.: "Real-time Reservoir Surveillance Utilizing Permanent Downhole Pressures-An Operator's Experience", paper SPE 103213, presented at the SPE Annual Conference and Exhibition held in San Antonio, Texas, U.S.A., 24-27 September 2006.

Cramer, R., Schotanus, D., Ibrahim, K. and Colbeck, N.: "Improving Allocation and Hydrocarbon Accounting Accuracy Using New Technique", *SPE Economic & Management*, October 2011, 235-240.

Daubechies, I.: "Orthonormal Bases of Compactly Supported Wavelets", *Communications on Pure Applied Mathematics*, XLI, 901-996, 1988.

Duru, O.O. and Horne R.N.: "Modelling Reservoir Temperature Transients and Matching to Permanent Downhole Gauge Data for Reservoir Parameter Estimation," paper SPE 115791 presented at the 2008 SPE Annual Technical Conference and Exhibition held in Denver, Colorado, USA, 21-24 September 2008.

Earlougher, R.C. and Kersch, M.K.: "Field Examples of Automatic Transient Test Analysis", *JPT*, Oct. 1972, 1271-1277.

Flecker, M.J., Thompson, S.J., Mckay, C.S. and Buchwalter, J.L.: "Maximizing Reservoir Production Using New Technologies for permanent Continuous Downhole Sensors", paper OTC 12153, presented at the Offshore Technology Conference held in Houston, Texas, 1-4 May 2000.

Frota, H.M. and Destro, W.: "Reliability Evolution of Permanent Downhole Gauges for Campos Basin Sub Sea Wells: A 10-Year Case Study", paper SPE 102700, presented at the SPE Annual Conference and Exhibition held in San Antonio, Texas, U.S.A., 24-27 September 2006.

Gabor, D.: "Theory of Communications," *Journal of the Institute of Electrical Engineering*, London III (1946) 93, 429-457.

Gringarten, A., Von Schroeter, T., Rolfsvaag, T., and Bruner, J.: "Use of Downhole Permanent Pressure Gauge Data to Diagnose Production Problems in a North Sea Horizontal Well", paper SPE 84470 presented at the SPE Annual Technical Conference and Exhibition held in Denver, Colorado, 5-8 October 2003.

Gringarten, A.: "Analysis of an Extended Well Test to Identify Connectivity Between Adjacent Compartments in a North Sea Reservoir", paper SPE 93988 presented at the SPE Europec/EAGE Annual Conference held in Madrid, Spain, 13-16 June 2005.

Gringarten, A.C.: "From Straight Lines to Deconvolution: The evolution of the State of the Art in Well Test Analysis", *SPE Reservoir Evaluation & Engineering*, February 2008, 41-62.

Gringarten, A.: "Practical Use of Well Test Deconvolution", paper SPE 134534 presented at the SPE Annual Technical Conference and Exhibition held in Florence, Italy, 20-22 September 2010.

Guan, L., Du, Y., Li, L.: "Wavelets in Petroleum Industry: Past, Present and Future", paper SPE 89952 presented at SPE Annual Technical Conference and Exhibition held in Houston, U.S.A., 26-29 September 2004.

Haddad, S. and Proano, E.: "A Method to diagnose Depletion, Skin, kh, and Drive Mechanism Effects Using Reservoir Monitoring Data", paper SPE 90032 presented at SPE Annual Technical Conference and Exhibition held in Houston, Texas, U.S.A., 26-29 September 2004.

Hansen, H.: "Toward the Intelligence Wells", http://www.hansenenergy.biz/activecompletions/The_Long_and_Winding_Road_Towards_The_Intelligent_Completion/Welcome.html

Haugen, O. and Fallet, T.: "Instrumented Oilfields: Downhole Production Allocation by Passive Acoustic Listening", paper SPE 71719 presented at the 2001 SPE Annual Technical Conference and Exhibition held in New Orleans, Louisiana, 30 September-3 October 2001.

Horne, R.N: "Advances in Computer-Aided Well-Test Interpretation", *JPT*, July 1994, 599-606.

Horne, R.N.: "Listen to the Reservoir-Interpreting Data from Permanent Downhole Gauges", *JPT*, Dec. 2007, 78-86.

Houzé, O.: "Pressure-Transient-Analysis Software", *SPE Transient Well Testing Monograph*, 2009.

Houzé, O. and Tauzin, E., and Allain, O.: "New Method to Deconvolve Well-Test Data Under Changing Well Conditions", paper SPE 132478 presented at the SPE Annual Technical Conference and Exhibition held in Florence, Italy, 19-22 September 2010.

Ibrahim, M.: "Optimum Allocation Methodology for Condensate Gas Reservoir", paper SPE 111442 presented at the SPE North Africa Technical Conference and Exhibition held in Marrakech, Morocco, 12-14 March 2008.

Ilk, D., Anderson, D.M., Valko, P.P., and Blasingame, T.A.: "Analysis of Gas-Well Reservoir Performance Data Using B-Spline Deconvolution", paper SPE 100573 presented at the SPE Gas Technology Symposium, Calgary, 15-17 May 2006.

Ilk, D., Anderson D.M., Stotts, G.W.J., Mattar, L. and Blasingame, T.A.: "Production-Data Analysis--Challenges, Pitfalls, Diagnostics", *SPE Reservoir Evaluation & Engineering*, June 2010, 538-55.

Ilk, D., Valko, P.P., and Blasingame, T.A.: "Deconvolution of Variable-Rate Reservoir –Performance Data Using B-Splines", *SPE Reservoir Evaluation & Engineering*, October 2006, 226-247.

Izgec, B., Cribbs, M.E., Pace, S.V., Zhu, D. and Kabir, C.S.: "Placement of Permanent Downhole Pressure Sensors in Reservoir Surveillance", paper SPE 107268, presented at the SPE Europec/EAGE Annual Conference and Exhibition held London, UK Oct. 16-19, 1988

Izgec, B., Hasan A.R., LIN, D. and Kabir, C.S.: "Flow-Rate Estimation From Wellhead-Pressure and –Temperature Data", *SPE Production & Operation* (February 2010) 31-39.

Jalali, Y. and Charron, A.: "A permanent System for Measurement of Downhole Flowrates- North Sea Examples", paper SPE 50670 presented at the 1998 SPE European Petroleum Conference held in the Hague, Netherlands, 20-22 October 1998.

Jansen, F.E. and Kelkar, M.G.: "Upscaling of Reservoir Properties Using Wavelets", paper SPE 39495 presented at India Oil and Gas Conference and Exhibition, New Delhi, India, 17-19 February, 1998.

Khong, C.K.: "Permanent Downhole Gauge Data Interpretation", Master's thesis, Stanford University, Petroleum Engineering, June 2001.

Kikani, J. and He, M.: "Multi-Resolution Analysis of Pressure Transient Data Using Wavelet Methods", paper SPE 48966, presented at the 1998 SPE Annual Technical Conference and Exhibition, New Orleans, U.S.A, 27-30 September, 1998.

Kluth, E.L.E., Varnham, M.P., Clowes, J.R. and Kutlik, R.L.: "Advanced Sensor Infrastructure for Real Time Reservoir Monitoring", paper SPE 65152, presented at the SPE European Petroleum Conference Held in Paris, France, 24-25 October 2000.

Kragas, T.K., Williams, B.A. and Myers, G.A.: "The Optic Oil Field: Deployment and Application of Permanent In-Well Fiber-Optic Sensing Systems for Production and Reservoir Monitoring", paper SPE 71529 presented at the SPE Annual Conference and Exhibition held in New Orleans, 30 September-3 October 2001.

Kragas, T.K., Bostick III, F.X., Mayeu, C., Gysling, D.L. and van der Spek, A.M.: "Downhole Fibre-Optic Flowmeter: Design, Operating Principle, Testing, and Field Installations", *SPE Production & Facilities* (November 2003) 257-268.

Kragas, T.K., Turnbull, B.F. and Francis, M.J.: "Permanent Fiber-Optic Monitoring at Northstar: Pressure/Temperature System and Data Overview", *SPE Production & Facilities*, May 2004, 86-93.

Kuchuk, F.J., Gok, I.M. and Onur, M.: "Decline Curves From Deconvolution of Pressure and Flow-Rate Measurements for Production Optimization and Prediction", paper SPE96002 presented at the SPE Annual Technical Conference and Exhibition held in Dallas, Texas, U.S.A., 9-12 October 2005.

Lee, W.J. and Holditch, S.A.: "Application of Pseudotime to Buildup Test Analysis of Low-Permeability Gas Wells With Long-Duration Well-bore Storage Distortion", *JPT* (Dec. 1982) 2877-87.

Levitan, M.M: "Practical Application of Pressure/Rate Deconvolution to Analysis of Real Well Tests", *SPE Reservoir Evaluation & Engineering,* April 2005, 113-121.

Levitan, M.M, Crawford, G.E. and Hardwick, A.: "Practical Considerations for Pressure-Rate Deconvolution of Well-Test Data", *SPE Journal,* March 2006, 35-47.

Levitan, M.M.: "Deconvolution of Multi-well Test Data", *SPE Journal,* Dec.2007, 420-428.

Li, X.G.: "Processing and Analysis of Transient Data from Permanent Down-hole Gauges (PDG)", Ph. D thesis, Heriot-Watt University, July, 2009.

Li, X., Qiu, M. and Zheng, S.: Integration of Numerical Well Testing and Deconvolution Algorithm for Analysing Permanent Down-hole Gauge (PDG) Data. SPE paper 145324 presented at the SPE Asia Pacific Oil and Gas Conference and Exhibition held in Jakarta, Indonesia, 20-22 September 2011.

Lilley, I.J., Douglas, A.A., Mulr, K.R. and Robinson, E.: "Reservoir Monitoring and Wireline Logging in Subsea Wells", paper SPE 18357 presented at the SPE European Petroleum Conference, London, UK Oct. 16-19, 1988.

Lorentzen, R., Sævareid, O., and Nævdal, G.: "Rate Allocation: Combining Transient Well Flow Modelling and Data Assimilation", paper SPE 135073 presented at the SPE Annual Technical Conference and Exhibition held in Florence, Italy, 19-22 September 2010.

Lu, P., and Horne, R.N.: "A Multiresolution Approach to Reservoir Parameter Estimation Using Wavelet Analysis", paper SPE 62985 presented at SPE Annual Technical Conference and Exhibition held in Dallas, U.S.A., 1-4 October 2000.

Luo, W. and Billings, S.A.: "Adaptive Model Selection and Estimation for Nonlinear Systems Using A Sliding Dada Window", *Signal Processing* (1995), 46, No. 2, 179.

Mallat, S.: "A Theory for Multiresolution Signal Decomposition: The Wavelet Representation", *IEEE Transaction: Pattern Analysis and Machine Intelligence*, 1989, 31,679-693.

Mallat, S.A.: "A Wavelet Tour of Signal Processing", Academic Press, London (1998).

Meunier, D. F. And Kabir, C.S. and Wittmann, M.J.: "Gas Well Test Analysis: Use of Normalized Pseudovariables", *SPE Formation Evaluation, December 1987*, 629-636.

McCracken, M. and Chorneyko, D.: "Rate Allocation Using Permanent Downhole Pressure", paper SPE 1033222, presented at the 2006 SPE Annual Technical Conference and Exhibition held in San Antonio, Texas, 24-27 September 2006.

Morlet, J., Arens, G., Fourgeau, E., and Giard, D.: "Wave Propagation and Sampling Theory-part I: Complex Signal and Scattering in Multilayered Media", *Geophysics*, 47(2), 203-221, 1982.

Moridis, G.J., Nikolaon, M., and You, Y.: "The use of Wavelet Transform in the Solution of Two-Phase Flow Problems", paper SPE 29144, *SPE Journal*, June 1996, 167-177.

Muradov, K.M. and Davies D.R.: "Zonal Rate Allocation in Intelligent wells", paper SPE 121055 presented at the SPE EUROPEC/EAGE Annual Conference and Exhibition held in Amsterdam, the Netherlands, 8-11 Jun 2009.

Nestlerode, W. A.: "The Use of Pressure Data from Permanently Installed Bottom Hole Pressure Gauges", paper SPE 590 presented at the Rocky Mountain Joint Regional Meeting in Denver, Colorado, USA, May 27-28, 1963.

Nyhavn, F., Vassenden, F. and Singstad, P.: "Reservoir Drainage with Downhole Permanent Mentoring and Control System. Real-Time Integration of Dynamic Reservoir Performance Data and Static Reservoir Model Improves Control Decisions", paper SPE 62937 presented at the 2000 SPE Annual Technical Conference and Exhibition held in Dallas, Texas, 1-4 October 2000.

Olsen, S. and Nordtvedt, J.-E.: "Improved Wavelet Filtering and Compression of Production Data," paper SPE 96800, presented at Offshore Europe 2005 held in Aberdeen, Scotland, U.K., 6-9 September 2005a.

Olsen, S. and Nordtvedt, J.-E.: "Automatic Filtering and Monitoring of Real-Time Reservoir and Production Data," paper SPE 96553, presented at the SPE Annual Technical Conference and Exhibition held in Dallas, Texas, U.S.A., 9-12 October 2005b.

Olsen, S. and Nordtvedt, J.-E.: "Experience From the Use of Automatic Well-Test Analysis", paper SPE 102920, presented at the SPE Annual Technical Conference and Exhibition held in San Antonio, Texas, U.S.A., 24-27 October 2006.

Omotosho, R.J.: "Permanent Downhole Sensors in Today's Petroleum Industry", Master thesis, University of Texas at Austin, August, 2004.

Onur, M., Cinar, M., Ilk, D., Blasingame, T.A., and Hegeman, P.S.: "An Investigation of Recent Deconvolution Methods for Well-Test Data Analysis", *SPE Journal*, June 2008, 226-247.

Onur, M. and Reynolds, A.: "Nonlinear Regression: The Information Content of Pressure and Pressure-Derivative Data", *SPE Journal*, Sept. 2002, 243-249.

Ortiz, C.E.P., Aguiar, R.B., and Pires, A.P.: "Wavelet Filtering of Permanent Downhole Gauge Data", paper SPE 123028 presented at the SPE Latin American and Caribbean Petroleum Engineering Conference held in Cartagena, Colombia, 31 May-3 June 2009.

Panda, M.N., Mosher, C.C., and Chopra, A.K.: "Application of Wavelet Transforms to Reservoir-Data Analysis and Scaling", paper SPE 60845, *SPE Journal*, March 2000, 92-101.

Perrine, R.L.: "Analysis of Pressure Build-up Curves", *Drill. and Prod. Prac.*, API, 1956, 482-509.

Queipo, N.V., Verde, A., Goicochea, J. and Romero, D.: "Application of Permanent Downhole Pressure, Temperature, and Flow Rate Measurements for Reservoir Description and Production Optimization: a Taxonomy, Processes, and Benefits", paper SPE 77897 presented at the SPE Asia Pacific Oil & Gas Conference and Exhibition held in Melbourne, Australia, 8-10 October 2002.

Rai, H. and Horne, R.N.: "Analyzing Simultaneous Rate and Pressure Data from Permanent Downhole Gauges," paper SPE 110097, presented at the 2007 SPE Annual

Technical Conference and Exhibition held in Anaheim, California, U.S.A., 11-14 November 2007.

Ribero, P.M., Pires, A.P., Oliveira, E.A.P. and Ferroni, J.G.: "Use of Wavelet Transform in Pressure –Data Treatment," *SPE Production & Operation*, February 2008, 28-31.

Rosa, A.J. and Horne, R.N: "Automated Type-Curve Matching in Well Test Analysis Using Laplace Determination of Parameter Gradients", paper SPE 12131 presented at the SPE Annual Technical Conference and Exhibition, San Francisco, CA, 5-8 October, 1983.

Rosa, A.J. and Horne, R.N: "New Approaches for Robust Nonlinear Parameter Estimation in Automated Well Test Analysis Using the Least Absolute Value Criterion", *SPE Advanced Technology Series*, Vol. 4, No. 1, 21-27, 1996.

Sahni I. and Horne, R.N.: "Multiresoluton Wavelet Analysis for Improved Reservoir Description", paper SPE 87820, *SPE Reservoir Evaluation & Engineering*, February 2005, 53-69.

Shepherd, C.E., Neve, Patrick and Willson, D.C.: "Use and Application of Permanent Downhole Pressure Gauges in the Balmore Field and Satellite Structures", *SPE Production Engineering*, August 1991, 271-276.

Soliman, M.Y., Anshan, J. and Stephenson, S.: "Application of Wavelet Transform to the Analysis of Pressure-Transient Data," paper SPE 83670, *SPE Reservoir Evaluation & Engineering*, April 2007, 89-99.

Sun, K., Konopczynski, M.R., and Ajayi, A.: "Using Downhole Real-Time Data To Estimate Zonal Production in a Commingled-Multiple-Zones Intelligent System", paper SPE 102743 presented at the SPE Annual Technical Conference and Exhibition held in San Antonio, Texas, U.S.A., 24-27 October 2006.

Suzuki, S. and Chorneyko, D.: "Automatic Detection of Pressure-Buildup Intervals From Permanent Down-hole Pressure Data Using Filter Convolution", paper SPE 125240 presented at the SPE Annual Technique Conference and Exhibition held in New Orleans, Louisiana, USA, 4-7 October 2009.

Tibold, M.P., Simonian, S., Chawla, M. and Akbar, M.: "Well Testing With a Permanent Monitoring System", paper SPE 63079 presented at the SPE Annual Technical Conference and Exhibition, Dallas, Texas, 1-4 October 2000.

Udofia, E. Vandenberg, F. Beijer, V. Oguntimehen, G. and Oni, O.: "Advances in Production Allocation: Bonga Field Experience", paper SPE 150450 presented at the SPE Intelligent Energy International held in Utrecht, The Netherlands, 27-29 March 2012.

Unneland, T. and Haugland, T.: "Permanent Downhole Gauges Used in Reservoir Management of Complex North Sea Oil Fields", *SPE Production & Facilities*, August 1994, 195-203.

Unneland, T., Manin, Y. and Kuchuk, F.: "Permanent Gauge Pressure and Rate Measurements for Reservoir Description and Well Monitoring: Filed Cases", *SPE Reservoir Evaluation & Engineering*, June 1998, 224-230.

van Everdingen, A.F. and Hurst, W.: "Application of the Laplace Transform to Flow Problems in Reservoirs", *Trans. AIME* 186, 305-324 (1949).

Van Gisbergen, S.J.C.H.M. and Vandeweijer, A.A.H: "Reliability Analysis of Permanent Downhole Monitoring Systems", *SPE Drilling & Completion*, March 2001, 60-63.

Vibeiti, D., Verga, F. and Delbosco P.: "An Improved Treatment of Long-Term Pressure Data for Capturing Information", *SPE Reservoir Evaluation & Engineering*, August 2007, 359-366.

Von Schroeter, T., Hollaender, F., and Gringarten, A.: "Deconvolution of Well Test Data as a Nonlinear Total least Squares Problems", paper SPE 71574 presented at the SPE Annual Technical Conference and Exhibition held in New Orleans, 30 September-3 October 2001.

Von Schroeter, T., Hollaender, F., and Gringarten, A.: "Analysis of Well Test Data From Permanent Downhole Gauges by Deconvolution", paper SPE 77688 presented at the SPE Annual Technical Conference and Exhibition held in San Antonio, Texas, 29 September-2 October 2002.

Von Schroeter, T., Hollaender, F., and Gringarten, A.: "Deconvolution of Well Test Data as a Nonlinear Total least Squares Problems", *SPE Journal*, December 2004, 375-390.

Wang, F.: "Processing and Analysis of Transient Pressure from Permanent Down-hole Gauges", Ph. D Thesis, Heriot-Watt university, 2010.

Webster, M., Richardson, S., Gabard-cuoq, C., Fitzgerald, J.B. and Stephenson, K.E: "Well Surveillance with a Permanent Downhole Multiphase Flowmeter," *SPE Production & Operation*, August 2006, 388-393.

Xu, W.: "Analysis of Two Phase Transient Pressure from Permanent Down-hole Gauges (PDG)", Ph. D Thesis, Heriot-Watt university, 2010.

Zheng S. and Li X.: "Analyzing Transient Pressure from Permanent Downhole Gauges (PDG) Using Wavelet Method," paper SPE 107521 presented at SPE Europe/EAGE Annual Conference and Exhibition held in London, U.K., 11-14 June 2007.

Zheng S. and Li X.: "Transient Pressure Analysis of 4D Reservoir System Response from Permanent Down-hole Gauge (PDG) for Reservoir Monitoring, Testing and Management", paper SPE 109112 presented at SPE Asian Pacific Oil & Gas Conference and Exhibition held in Jakarta, Indonesia, 30 October-1 November 2007.

Zheng S. and Li X..: "Individual Well Flow Rate Recovery from PDG Transient pressure with Either Assigned Daily Rate or Total Cumulative Production of the Well or Group of Wells through Wavelet Approach," *Journal of Petroleum Science and Engineering* 68 (2009) 277-286.